การหาขนาดของเครื่องกำเนิดไฟฟ้าแบบกระจายชนิดพลังงานแสงอาทิตย์ ในระบบจำหน่ายไฟฟ้า โดยพิจารณาสภาวะแสงอาทิตย์และความผิดเพี้ยนทางฮาร์มอนิก

นายวิชชากร เฮงศรีธวัช

วิทยานิพนธ์นี้เป็นส่วนหนึ่งของการศึกษาตามหลักสูตรปริญญาวิศวกรรมศาสตรดุษฎีบัณฑิต
สาขาวิชาวิศวกรรมไฟฟ้า ภาควิชาวิศวกรรมไฟฟ้า
คณะวิศวกรรมศาสตร์ จุฬาลงกรณ์มหาวิทยาลัย
ปีการศึกษา 2554

SIZING OF PHOTOVOLTAIC DISTRIBUTED GENERATORS IN A DISTRIBUTION SYSTEM WITH CONSIDERATION OF SOLAR RADIATION AND HARMONIC DISTORTION

Mr. Vichakorn Hengsritawat

A Dissertation Submitted in Partial Fulfillment of the Requirements
for the Degree of Doctor of Philosophy Program in Electrical Engineering
Department of Electrical Engineering
Faculty of Engineering
Chulalongkorn University
Academic year 2011

Thesis Title	SIZING OF PHOTOVOLTAIC DISTRIBUTED GENERATORS IN A DISTRIBUTION SYSTEM WITH CONSIDERATION OF SOLAR RADIATION AND HARMONIC DISTORTION
By	Mr. Vichakorn Hengsritawat
Field of Study	Electrical Engineering
Thesis Advisor	Assistant Professor Thavatchai Tayjasanant, Ph.D.

Accepted by the Faculty of Engineering, Chulalongkorn University in Partial Fulfillment of the Requirements for the Doctoral Degree

…….……………………………………Dean of the Faculty of Engineering
(Associate Professor Boonsom Lerdhirunwong, Dr.Ing.)

THESIS COMMITTEE

……………………………………………….. Chairman
(Professor Bundhit Eua-arporn, Ph.D.)

……………………………………….……. Thesis Advisor
(Assistant Professor Thavatchai Tayjasanant, Ph.D.)

……………………………………………….. Examiner
(Assistant Professor Kulyos Audomvongseree, Ph.D.)

……………………………………………….. External Examiner
(Assistant Professor Natthaphob Nimpitiwan, Ph.D.)

……………………………………………….. External Examiner
(Pradit Fuangfoo, Ph.D.)

วิชชากร เฮงศรีธวัช : การหาขนาดของเครื่องกำเนิดไฟฟ้าแบบกระจายชนิดพลังงานแสงอาทิตย์ในระบบจำหน่ายไฟฟ้า โดยพิจารณาสภาวะแสงอาทิตย์และความผิดเพี้ยนทางฮาร์มอนิก (SIZING OF PHOTOVOLTAIC DISTRIBUTED GENERATORS IN A DISTRIBUTION SYSTEM WITH CONSIDERATION OF SOLAR RADIATION AND HARMONIC DISTORTION) อ.ที่ปรึกษาวิทยานิพนธ์หลัก: ผศ.ดร.ธวัชชัย เตชัสอนันต์, 162 หน้า.

วิทยานิพนธ์เล่มนี้นำเสนอวิธีทางความน่าจะเป็น เพื่อหาขนาดที่เหมาะสมของเครื่องกำเนิดไฟฟ้าแบบกระจายชนิดพลังงานแสงอาทิตย์ในระบบจำหน่ายไฟฟ้า โดยพิจารณาถึงสภาวะการกระจายของแสงอาทิตย์และความผิดเพี้ยนทางฮาร์มอนิก ด้วยวิธีการดังกล่าว การจำลองแบบมอนติคาร์โลจะถูกนำมาใช้ในการสุ่มค่าการกระจายแสงอาทิตย์, อุณหภูมิแวดล้อมรวมถึงแรงดันที่สถานีไฟฟ้าย่อย และความต้องการของโหลดในระบบจำหน่ายไฟฟ้า โดยมีวัตถุประสงค์ เพื่อทำให้กำลังไฟฟ้าสูญเสีย จริงเฉลี่ยของระบบมีค่าต่ำสุด ในขณะ ที่เงื่อนไขบังคับทางด้านคุณภาพไฟฟ้า ซึ่งได้แก่ แรงดันไฟฟ้าที่โหนด , กระแสฮาร์มอนิก , ค่าความผิดเพี้ยนแรงดันฮาร์มอนิกรวม และค่าความผิดเพี้ยนความต้องการฮาร์มอนิกรวม ยังคงอยู่ในขอบเขตที่กำหนดตามมาตรฐาน IEC และ IEEE ทั้งนี้ยังได้รวมผลของฮาร์มอนิกที่มีอยู่เดิมในระบบเพื่อ ประเมิน หาขนาดที่เหมาะสมของเครื่องกำเนิดไฟฟ้าแบบกระจายชนิดพลังงานแสงอาทิตย์ด้วย วิทยานิพนธ์เล่มนี้ ยังได้นำเสนอวิธีการวิเคราะห์ด้วยดัชนีเสถียรภาพแรงดันเพื่อ เลือก ตำแหน่งที่เหมาะสมในการติดตั้งเครื่องกำเนิดไฟฟ้าแบบกระจายชนิดพลังงานแสงอาทิตย์ นอกจากนี้ ยังได้มีการศึกษาผลกระทบที่มีต่อการหาขนาดที่เหมาะสมของเครื่องกำเนิดไฟฟ้าแบบกระจายชนิดพลังงานแสงอาทิตย์ จากการใช้แบบจำลองของโหลดและการปรับค่าตัวประกอบกำลัง ในการทำงาน ที่แตกต่างกัน รวมถึง ศึกษาผลกระทบของแบบจำลองของอินเวอร์เตอร์ และ การพิจารณาถึง เครื่องกำเนิดไฟฟ้าแบบกระจายอื่นที่มีอยู่เดิมในระบบจำหน่ายไฟฟ้า วิธีการที่พัฒนาขึ้นสามารถประยุกต์ใช้ได้กับระบบจริง โดยได้ทำการทดสอบกับระบบขนาด 33 บัส และระบบจำหน่ายไฟฟ้าแห่งหนึ่งของประเทศไทยขนาด 51 บัส

ภาควิชา วิศวกรรมไฟฟ้า ลายมือชื่อนิสิต

สาขาวิชา วิศวกรรมไฟฟ้า ลายมือชื่อ อ.ที่ปรึกษาวิทยานิพนธ์หลัก

ปีการศึกษา 2554

4971875421 : MAJOR ELECTRICAL ENGINEERING
KEYWORDS: PHOTOVOLTAIC GENERATION / MONTE CARLO SIMULATION / PROBABILISTIC APPROACH / SOLAR RADIATION / HARMONIC DISTORTION

VICHAKORN HENGSRITAWAT: SIZING OF PHOTOVOLTAIC DISTRIBUTED GENERATORS IN A DISTRIBUTION SYSTEM WITH CONSIDERATION OF SOLAR RADIATION AND HARMONIC DISTORTION. ADVISOR: ASST. PROF. THAVATCHAI TAYJASANANT, Ph. D., 162 pp.

This dissertation presents a probabilistic approach to calculate an optimal size of photovoltaic distributed generators (PV-DGs) in a distribution system with consideration of solar radiation and harmonic distortion. Monte Carlo simulation is applied to predict solar radiations, ambient temperatures, substation voltages and load demands. The formulated objective function is to minimize average real power loss, while power quality constraints i.e., node voltage, harmonic current, total harmonic distortion voltage and total demand distortion are kept within the limits complied with IEC and IEEE standards. Existing background harmonics are included in an evaluation of the optimal size of PV-DG. In addition, static voltage stability index analysis is proposed to select a proper location of PV-DG installation in a distribution system. Furthermore, impacts of static load models and power factor control on optimal PV-DG sizing as well as effects of PV inverter modeling and existing DGs in a distribution system are taken into account. The developed method can be applied to actual systems and was tested with a 33-Bus test system and an actual 51-Bus radial distribution system in Thailand.

Department : Electrical Engineering	Student's Signature ....
Field of Study : Electrical Engineering	Advisor's Signature ....
Academic Year : 2011	

ACKNOWLEDGEMENTS

First, I would like to give a special thank to my advisor, Assistant Professor Dr. Thavatchai Tayjasanant, for his advice, suggestions, encouragement and support throughout the development of this dissertation as well as my study program.

Second, I would like to thank chairman and examination committee for their valuable suggestions and useful recommendations. I would like also thank Sripatum University (SPU) to award me a scholarship for entire my study as well as Dr. Jakpetch Matharatch from the Provincial Electricity Authority of Thailand (PEA) for the measurement data at PV farm of Solar Power Company.

Finally, my special thanks to my family, my wife and my daughter for their love, patience, inspiration, support and understanding in past years. This research is dedicated to them.

Contents

CHAPTER PAGE

CHAPTER PAGE

List of Tables

List of Figures

FIGRURE PAGE

FIGRURE PAGE

FIGRURE PAGE

FIGRURE PAGE

FIGRURE PAGE

FIGRURE PAGE

Nomenclatures

BH	Background Harmonic
CdTe	Cadmium Tellluride
CIGS	Copper, Indium, Gallium and Selenide
CPV	Concentrated Photovoltaic System
CSP	Concentrating Solar Power
CV	Constant Voltage
CP	Constant Power Load
CI	Constant Current Load
CZ	Constant Impedance Load
DEDE	Department of Alternative Energy Development and Efficiency
DG	Distributed Generation
DLF	Deterministic Load Flow
DNO	Distribution Network Operator
FF	Fill Factor
GA	Genetic Algorithm
GFCI	Ground Fault Circuit Interrupter
IC	Incremental Conductance Method
IEA	International Energy Agency
LDC	Line Drop Compensator
LTC	Load-Tap-Changing
MPPT	Maximum Power Point Tracking
NOCT	Normal Operating Cell Temperature
PCU	Power Conditioning Unit
PCC	Point of Common Coupling
PDP	Power Development Plan
PEA	Provincial Electricity Authority
PF	Power Factor
PLF	Probabilistic Load Flow
PWM	Pulse Width Modulation
PV	Photovoltaic

PV-DG	Photovoltaic Distributed Generator
P&O	Perturb and Observe
RE	Renewable Energy
SPP	Small Power Producer
STC	Standard Test Condition
TDD	Total Demand Distortion
THD	Total Harmonic Distortion
THDi	Total Harmonic Distortion Current
THDv	Total Harmonic Distortion Voltage
VSI	Voltage Stability Index
VSPP	Very Small Power Producer

CHAPTER I

INTRODUCTION

1.1 Overview of World's PV Generation

At this time, fossil fuel is the main energy supplier of the worldwide economy. However, using in long time of it as being a major cause of environmental problems and it is necessary to look for alternative resources in power generation. Besides, the increasing demand for energy in a distribution system can create problems such as voltage drop, poor reliability, low power quality, losses increasing and grid instability, etc. Distributed generations (DGs) are a one way to solve this problem and it has continuously been introduced and promoted around the world. Presently, the necessity of producing more energy combined with the interest in clean technologies using renewable energy such as solar, wind, biomass and biogas, etc.

According to the IEEE standard 1547-2003 [1], DG is by definition that which is of limited size roughly 10 MVA or less. Generally, DG produces electricity close to customer loads and can run on fossil fuels, renewable energy resources or waste heat. DG can be categorized into three types according to their generation technologies as shown in Table1.1. These technologies are entering a period of rapid expansion and commercialization. In fact, studies have predicted that DG may account for up to 20% of all new generations going online by the year 2010 [2].

Among the renewable energy sources, hydropower and wind energy have the largest utilization. In countries with hydropower potential, small hydro turbines are used at the distribution level to sustain the utility network in dispersed or remote locations. The wind power potential in many countries around the world has led to a large interest and fast development of wind turbine technology [3].

Table 1.1 DG's category according to generation technologies

Type	Application	Operating Mode
Synchronous	Geothermal, Ocean, Internal combustion engine, Combined cycle, Combustion turbine	Capacitive PF
Induction	Wind turbine	Inductive PF
Inverter-based	Photovoltaic, Micro turbine, Fuel cells	Unity PF

Another renewable energy technology that gains acceptance as a way of maintaining and improving living standard without harming the environment is the photovoltaic (PV) technology. The number of PV installations is mainly depending on the government policy and utility companies that support programs on grid-connected PV system [4-5].

From the studied information in [6], the International Energy Agency (IEA) says that there are ambitious plans for the global development of the solar energy industry and the encouraging progress seen in 2009, over 90% of the world's 192 countries have yet to undertake large-scale deployment projects. However, just eight countries accounted for 89% of the world's total installed PV generating capacity of 15 GW in 2008. The IEA has set 2020 targets of 200 GW of global installed capacity for PV and 148 GW for concentrated solar power (CSP), with both figures targeted to soar by 2030. The IEA suggests one key to progress towards a strong policy regime. However, it should be considering such regimes consist of Feed-in Tariffs (FiT) alone or something wider-reaching. Furthermore, beyond government policy, the other key areas for action must be addressed.

From the annual review in 2008 [7], which presents basic statistical data about the majority of large-scale photovoltaic power plants (>=200 kWp) worldwide currently in operation. It shows that the past year was characterized by several projects of MW-range PV power plants, and it was also the year with the highest market growth related to large-scale PV systems ever. Not only in Spain, where progress is abundantly clear, but in some other countries the cumulative installed power increased significantly. In the European Union progress was, among others, observed in Italy, the Czech Republic and France; the German market decreased slightly, but due to the market explosion in Spain the installed power from 2008 still reached the level of the previous year.

This report's database includes more than 1,900 large-scale PV power plants (put into service in 2008 or earlier), each with peak power of 200 kWp or more as shown in Figure 1.1. The amount of large-scale PV plants sorted by country is shown in Figure 1.2. More than 500 large-scale PV plants are located in Germany, more than 370 are in USA and more than 750 are in Spain. The cumulative power of all these PV power plants is more than 3.6 G Wp and average plant power output is slightly more than 1.8 MWp as shown in Figure1.3.

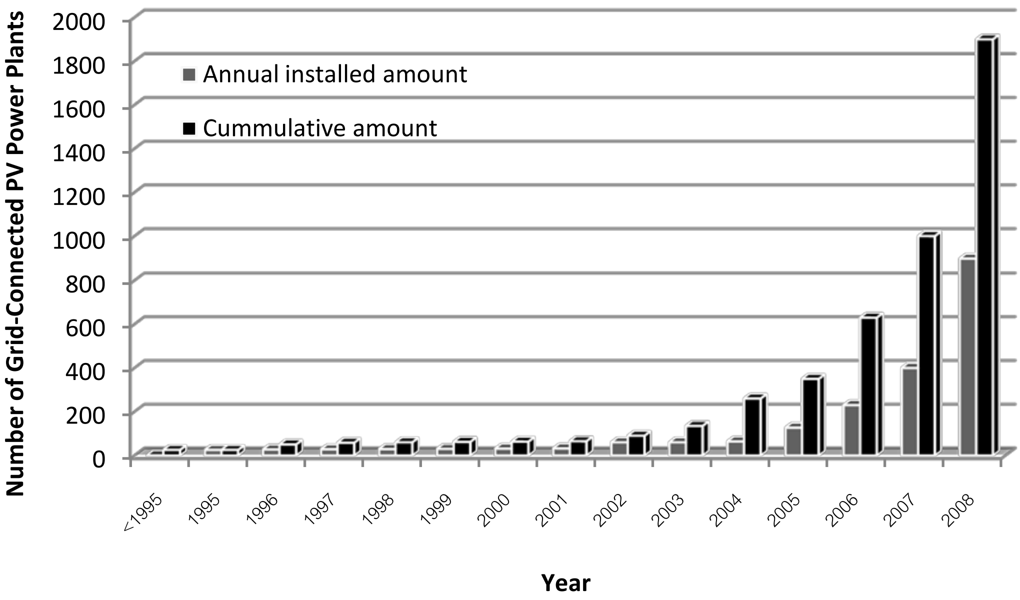

Figure 1.1 Annual installed and cumulative amount of large-scale grid-connected PV power plants in the period from 1995 to 2008

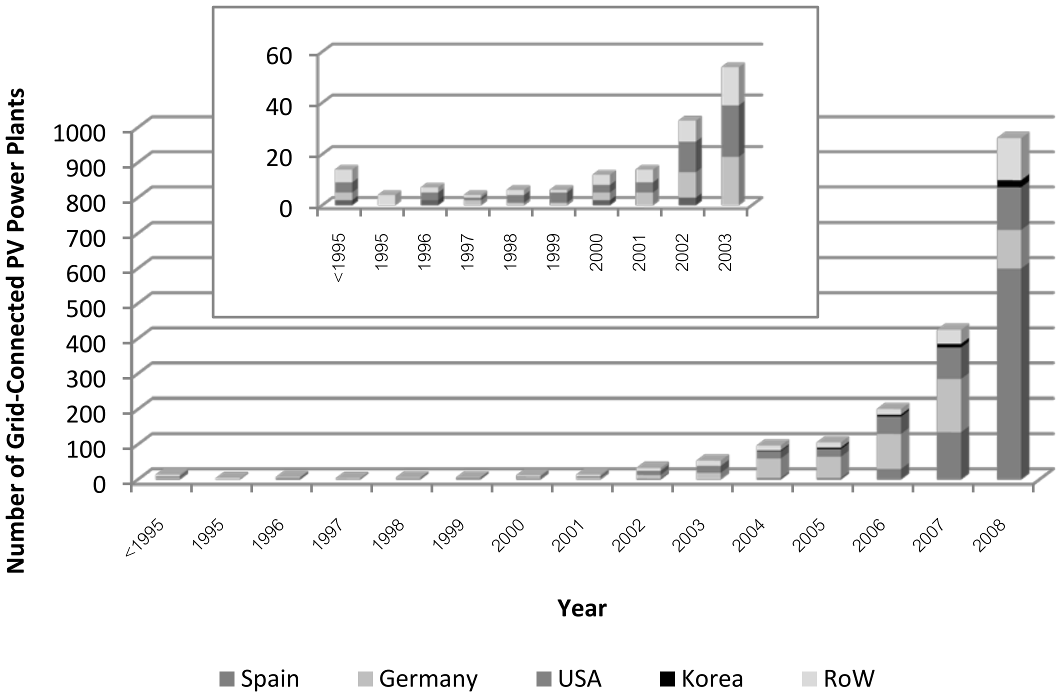

Figure 1.2 Amount of large-scale grid-connected PV power plants put into service annually in the period from 1995 to 2008 (sort by country)

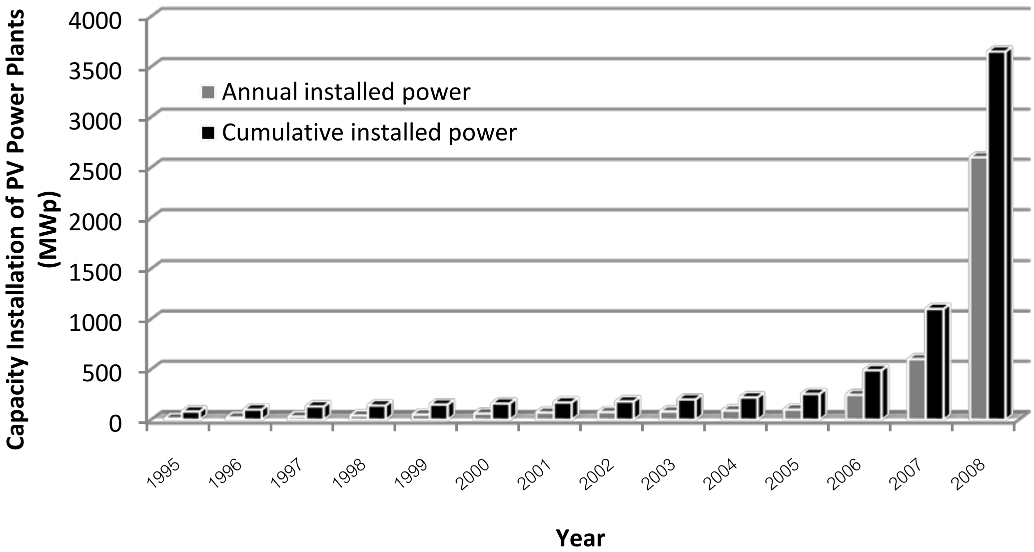

Figure 1.3 Large-scale PV power plants – annual and cumulative installed power output capacity worldwide in the period from 1995 to 2008

In 2008, more than 1,000 large-scale PV plants were constructed and put into service worldwide. In Spain more than 590 large-scale PV plants were put into service, more than 120 for each Germany and the USA. Among other countries it is worth mentioning Belgium and Czech Republic where several large-scale roof-mounted (Belgium) and ground-mounted (Czech Republic) PV plants were constructed. Regarding large-scale PV power plants Korea took on a leading role in Asia. Several MW-range power plants were put into service in Korea last year. Europe is by far the most advanced region with more than 800 large-scale PV plants put into service in 2008. In Europe more than 1500 large-scale PV power plants are currently operating, followed by the USA with about 400 PV plants.

1.2 Solar PV Technologies Overview

There are two major solar PV technologies convert from sunlight directly and indirectly into electricity energy.

1.2.1 Solar Converting Directly Technology [8]

This solar PV technology converts solar energy into useful energy forms by directly absorbing solar photons, particles of light that act as individual units of energy, and either converting part of the energy to electricity (as in a PV cell) or storing part of the energy in a chemical reaction.

In the world of this PV solar power technology, there are several types of semiconductor technologies currently in use for PV solar panels. However, two types based on the thickness of the semiconductor have become the most widely adopted namely crystalline silicon and thin film [9]. Conventional crystalline silicon solar cell is relatively speaking very thick of 200-500 μm where "thin" means something like 1-10 μm.

1.2.1.1 Crystalline Silicon

Crystalline silicon panels are constructed by first putting a single slice of silicon through a series of processing steps, creating one solar cell. These cells are then assembled together in multiples to make a solar panel. Crystalline silicon, also called wafer silicon, is the oldest and the most widely used material in commercial solar panels. There are two main types of crystalline silicon panels as follows:

- Monocrystalline Silicon

Monocrystalline (also called single crystal) panels use solar cells that are cut from a piece of silicon grown from a single, uniform crystal as shown in Figure 1.4. Monocrystalline panels are among the most efficient yet most expensive on the market. They require the highest purity silicon and the most involved manufacturing processes.

Figure 1.4 Monocrystalline silicon PV panel

- Multicrystalline Silicon

Multicrystalline (also called polycrystalline) panels use solar cells that are cut from multifaceted silicon crystals as shown in Figure 1.5. They are less uniform in appearance than monocrystalline cells, resembling pieces of shattered glass. These are the most common solar panels on the market, being less expensive than monocrystalline silicon. They are also less efficient, though the performance gap has begun to close in recent years.

Figure 1.5 Multicrystalline silicon PV panel

1.2.1.2 Thin Film

Thin film solar panels are made by placing thin layers of semiconductor material onto various surfaces, usually on glass. The term *thin film* refers to the amount of semiconductor material used. It is applied in a thin film to a surface structure, such as a sheet of glass. Contrary to popular belief, most thin film panels are not flexible. Overall, thin film solar panels offer the lowest manufacturing costs and are becoming more prevalent in the industry. There are three main types of thin film used.

- Cadmium Telluride (CdTe)

CdTe is a semiconductor compound formed from cadmium and tellurium. CdTe solar panels are manufactured on glass as shown in Figure 1.6. They are the most common type of thin film solar panel on the market and the most cost-effective to manufacture. CdTe panels perform significantly better in high temperatures and in low-light conditions.

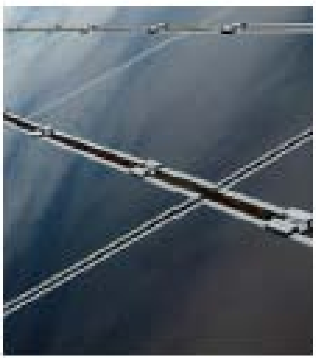

Figure 1.6 Cadmium Telluride PV panel

- Amorphous Silicon

Amorphous silicon is the non-crystalline form of silicon and was the first thin film material to yield a commercial product, first used in consumer items such as calculators. It can be deposited in thin layers onto a variety of surfaces and offers lower costs than traditional crystalline silicon, though it is less efficient at converting sunlight into electricity. Amorphous silicon PV panel is shown in Figure 1.7.

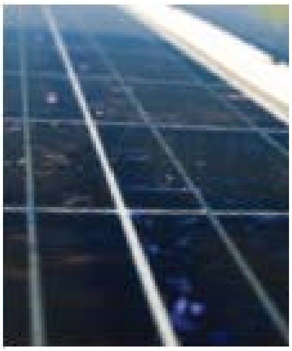

Figure 1.7 Amorphous Silicon PV panel

- Copper, Indium, Gallium and Selenide (CIGS)

CIGS is a compound semiconductor that can be deposited onto many different materials. CIGS has only recently become available for small commercial applications and is considered a developing PV technology. CIGS PV panel is shown in Figure 1.8.

Figure 1.8 CIGS PV panel

At present, CdTe solar panels technology are chose come first for solar application because of its superior energy output characteristic across real-world conditions, its low cost volume production benefits and its superior environmental performance. CdTe has lower temperature-related loss than crystalline silicon due to a lower temperature coefficient. It also provides superior energy output in low, indirect and diffuse light conditions, producing more electricity on cloudy days.

1.2.1.3 Concentrated Photovoltaic System (CPV) [10]

Concentrated PV system is a technology to increase the efficiency of the cells by concentrate sunlight on solar cells. The PV cells in a CPV system are built into concentrating collectors that use a lens or mirrors to focus the sunlight onto the cells as shown in Figure 1.9. CPV systems must track the sun to keep the light focused on the PV cells. The primary advantages of CPV system are high efficiency, low system cost and low capital investment to facilitate rapid scale-up, it means that the systems can use less expensive semiconducting PV material to achieve a specified electrical out put. However, reliability is an important technical challenge for this emerging technological approach. Because of the systems are generally require highly sophisticated tracking devices.

Figure 1.9 Concentrated photovoltaic system

1.2.2 Solar Converting Indirectly Technology [11]

This technology uses mirrors to concentrate the sunlight energy and convert it into thermal energy to create steam to drive a turbine of the generator that generates electrical power. This technology is well known as Concentrating Solar Power (CSP) technology.

Generally, CSP plants generate electric power by using mirrors to concentrate the sun's energy and convert it into high temperature heat. That heat is then channeled through a conventional generator. The plants consist of two parts, one that collects solar energy and converts it to heat and then another that converts the heat energy to electricity. CSP technology utilizes three alternative technological approaches such as trough systems, power tower systems and dish/engine systems. All CSP technological approaches require large areas for solar radiation collection when used to produce electricity at commercial area.

1.2.2.1 Trough Systems

Trough systems use large U-shaped (parabolic) reflectors (focusing mirrors) that have oil filled pipes running along their center or focal point. The mirrored reflectors are tilted toward the sun and focus sunlight on the pipes to heat the oil inside to as much as 750ºF. The hot oil is then used to boil water, which makes steam to run conventional steam turbines and generators. The schematic diagram and parabolic trough system are shown in Figure 1.10.

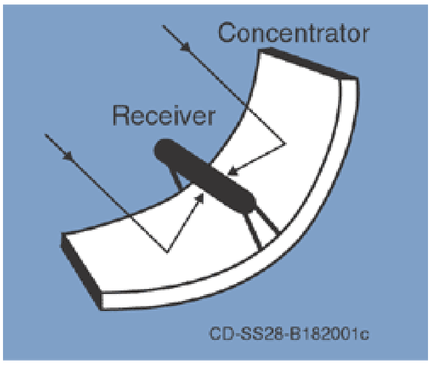

Figure 1.10 Schematic diagram of parabolic trough system

1.2.2.2 Power Tower Systems

Power tower systems also called central receivers, use many large, flat heliostats (mirrors) to track the sun and focus its rays onto a receiver. As shown in Figure 1.11, the receiver sits on top of a tall tower in which concentrated sunlight heats a fluid as hot as 1,050ºF. The hot fluid can be used immediately to make steam for electricity generation or stored for later use. That means electricity can be produced during periods of peak needed on cloudy days or even several hours after sunset.

Figure 1.11 Schematic diagram of power tower system

1.2.2.3 Dish Engine Systems

Dish engine systems use mirrored dishes to focus and concentrate sunlight onto a receiver. As shown in Figure 1.12, the receiver is mounted at the focal point of the dish. To capture the maximum amount of solar energy, the dish assembly tracks the sun across the sky. The receiver is integrated into a high efficiency external combustion engine. The engine has thin tubes containing hydrogen or helium gas that runs along the outside of the engine's four piston cylinders and open into the cylinders. As concentrated sunlight falls on the receiver, it heats the gas in the tubes to very high temperatures, which causes hot gas to expand inside the cylinders. The expanding gas drives the pistons. The pistons turn a crankshaft, which drives an electric generator. The receiver, engine and generator comprise a single, integrated assembly mounted at the focus of the mirrored dish.

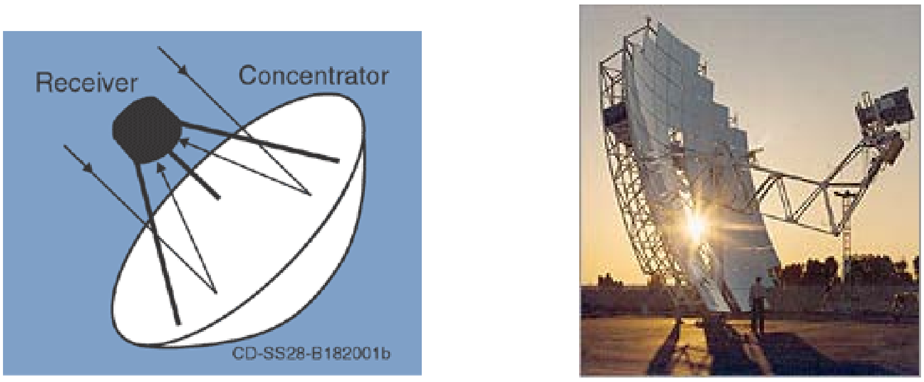

Figure 1.12 Schematic diagram of solar dish engine system

1.3 PV Generation System in Thailand

From Thailand's energy situation in 2010 report [12], it shows that Thailand imports variety forms of energy which worth many millions Baths as shown in Figure 1.13. Actually, Thailand's consumption of energy has been increasing every year in forms of gas, oil, coal and electricity. The energy crisis in the past few years has caused energy price rising up and affected economic development countrywide. Therefore, in order to lower an import of some energy, the Ministry of Energy has come up with a policy to develop the renewable energy (RE) for a fifteen years period (2008-2022) by the Thailand Power Development Plan 2010 (PDP 2010) [13]. The objective of the plan is to increase the portfolio of renewable energy to 20.3% of the final energy consumption in 2022. At the end of the plan, the portion of renewable energy in power generation shall be 2.4% or 5,608 MW from 1.4% at present as shown in Figure 1.14.

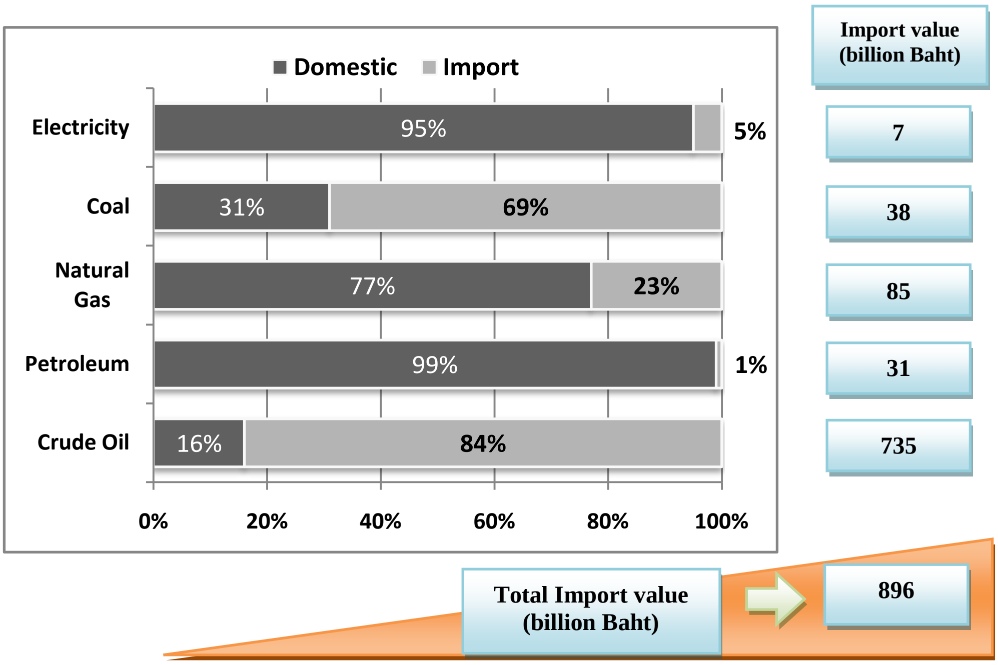

Figure 1.13 Proportion of domestic and import energy of Thailand in 2010

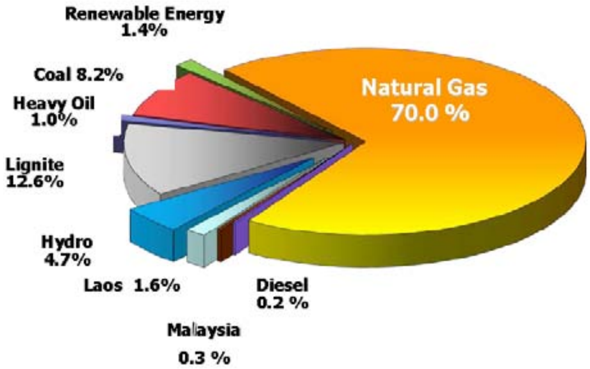

Figure 1.14 Energy source portion of power generation of Thailand in 2010

Furthermore, from the study of Silapakorn University and Department of Alternative Energy Development and Efficiency (DEDE) found that the average solar radiation potential of Thailand is about 18.2 MJ/m^2-day or 5.06 kWh/m^2-day, which is a very good potential. However, the solar radiation potential of the areas in Thailand (as shown in Figure 1.15) can be classified into three groups as follows [14]:

- *<u>The high potential area</u>*: average solar radiation about 19-20 MJ/m^2-day or 5.28-5.56 kWh/m^2-day which covers 14.3% of the total area
- *<u>The medium potential area</u>*: average solar radiation about 18-19 MJ/m^2-day or 5-5.28 kWh/m^2-day which covers 50.2% of the total area
- *<u>The low potential area</u>*: average solar radiation less than 18 MJ/m^2-day or 5 kWh/m^2-day which covers 35.5% of the total area

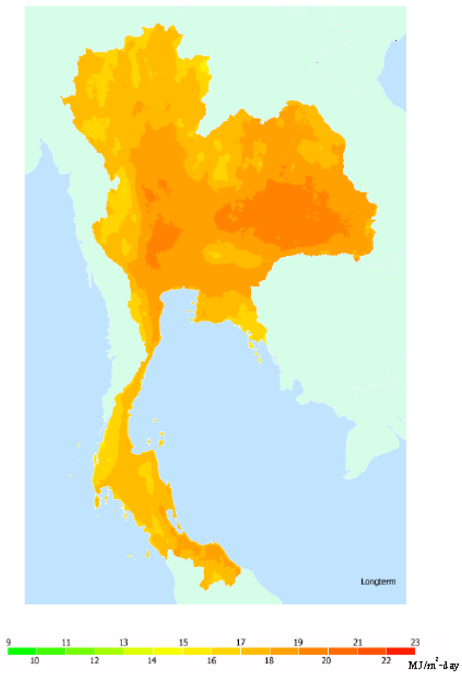

Figure 1.15 Yearly average solar radiation potential of the areas in Thailand

From Figure 1.15, the highest average solar radiation zone is on the north eastern area and some area of the central of Thailand. The percentage of the area which classified by average solar radiation levels is shown in Figure 1.16, while the yearly average solar radiation of the whole country is 18 MJ/m^2-day.

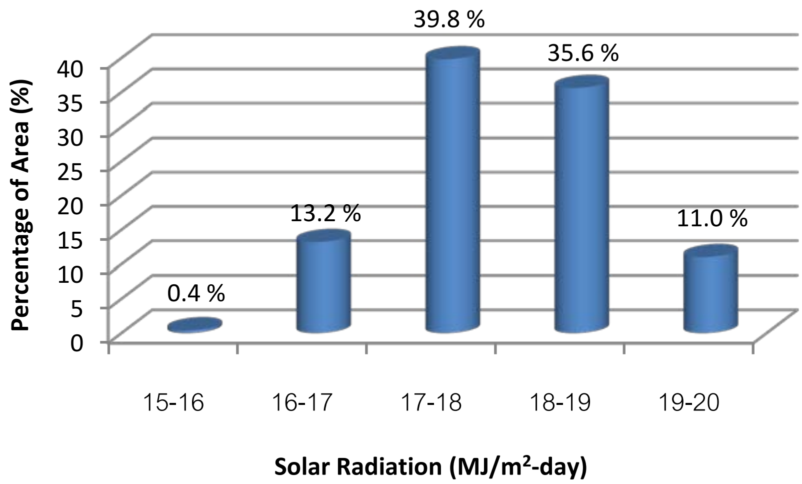

Figure 1.16 Percentage of area classified by average solar radiation levels of Thailand

Therefore, from this information, it shows that the solar potential in Thailand is very important. And it should not be overlooked because the solar energy resource in Thailand is enough for the future. Table 1.2 shows the renewable potential and target plan of Thailand. Note from Table 1.2 that the solar energy potential to produce electricity energy is 50,000 MW, which is the highest compared with other energy resources. However, the existing electricity power produced by solar energy is just only 32 MW. This is because the capital investment cost of PV technology is still expensive compared with other technologies, although PV technology has been continually reduced at the present.

However, in order to encourage to produce more electricity power by solar energy, the Ministry of Energy of Thailand has promoted the adder rate of 8 Bth/kWh for small power producers (SPPs) or very small power producers (VSPPs). This rate is also using solar energy technology (called the concentrating solar power, CSP) to produce the thermal energy and then to produce the electricity power as shown in Table 1.3.

Table1.2 Some of renewable potential and target plan of Thailand

Electricity Power Produced by	***Potential*** (MW)	***Existing*** (MW)	***2008-2011*** (MW)	***2012-2016*** (MW)	***2017-2022*** (MW)
Solar	50,000	32	55	95	500
Wind Energy	1,600	1	115	375	800
Hydro Power	700	56	165	281	324
Biomass	4,400	1,610	2,800	3,220	3,700
Biogas	190	46	60	90	120
Municipal Solid Waste	400	5	78	130	160
Hydrogen	-	-	0	0	3.5
Total	**57,290**	**1,750**	**3,273**	**4,191**	**5,608**

Table1.3 Adder rate for SPPs and VSPPs using renewable energy of Thailand

Type of power source of power plant	***Old adder*** (Bth/kWh)	***New adder*** (Bth/kWh)	***Adder special plus*** (Bth/kWh)	***Adder special plus for Yala, Pattani, Naratiwas*** (Bth/kWh)	***Given adder duration*** (years)
1.Biomass					
-Installed capacity <= 1 MW	0.30	0.50	1.00	1.00	7
-Installed capacity > 1 MW	0.30	0.30	1.00	1.00	7
2.Biogas					
-Installed capacity <= 1 MW	0.30	0.50	1.00	1.00	7
-Installed capacity > 1 MW	0.30	0.30	1.00	1.00	7
3.Waste					
-AD and Land fill	2.50	2.50	1.00	1.00	7
-Thermal process	2.50	3.50	1.00	1.00	7
4.Wind energy					
-Installed capacity <= 50 kW	3.50	4.50	1.50	1.50	10
-Installed capacity > 50 kW	3.50	3.50	1.50	1.50	10
5.Micro water turbine					
-Installed capacity 50kW-<200kW	0.40	0.80	1.00	1.00	7
-Installed capacity < 50kW	0.80	1.50	1.00	1.00	7
6.Solar energy (PV,CSP, etc.)	***8.00***	***8.00***	***1.50***	***1.50***	***10***

From the PV capacity installation report of Thailand [15], the DEDE has PV projects around the country with capacity 3,510.5 kW since 1983 to 2010.

However, the PV generation system that was installed in Thailand can be separated into a stand-alone system (off-grid) and grid-connected system. The total capacity of the PV generation system of Thailand in 2010 is 49.21 MW as shown in Figure 1.17, which are 29.65 MW of stand-alone and 19.56 MW of grid-connected system. This installed capacity can classify by the solar application system as shown in Figure 1.18. It shows that the solar energy is the most applied source to produce the electricity as 26.8 MW or 54.4% of total capacity.

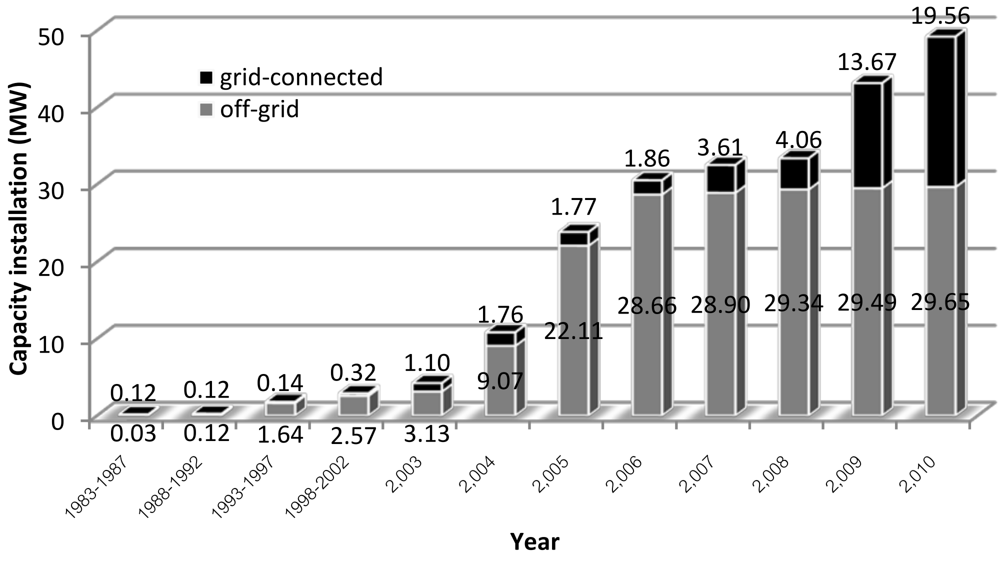

Figure 1.17 PV installation capacity since 1983-2010 of Thailand

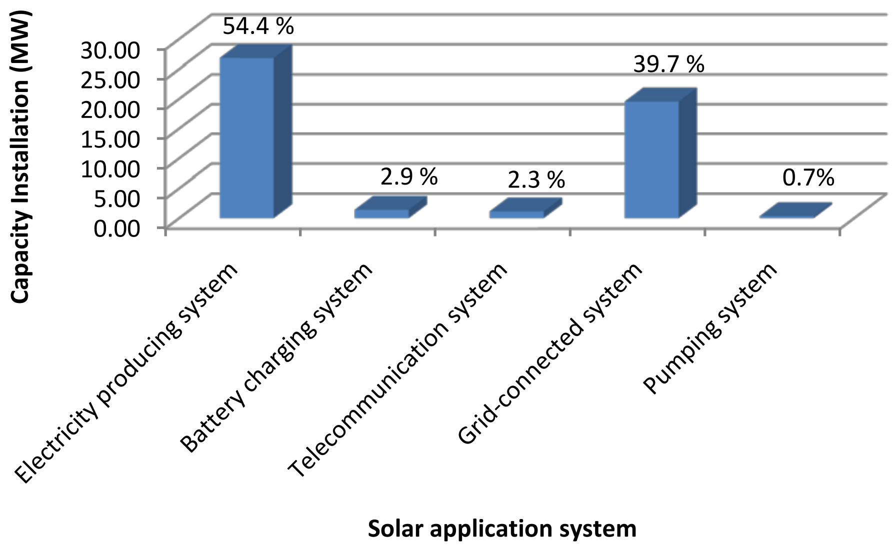

Figure 1.18 Installation capacity of solar application system since 1983-2010 of Thailand

1.4 Motivation

Generally, distribution systems are the radial type systems, which can be found in rural or suburban areas, are normally designed to operate without any generation sources connected to the grid. The interconnection of any generation sources on the distribution system can be variously impact on the power flow, voltage regulations at customer load and utility equipments. These impacts may be caused the system operation in either positively or negatively depending on the distribution system operating characteristics and the DG characteristics [2]. There are some positive impacts which are the system benefits as follows:

- Voltage support and improved power quality.
- Loss reduction in some cases [16].
- Peak shaving.
- Transmission and distribution capacity release.
- Deferment of new or upgraded T&D infrastructure.
- Improved utility system reliability.

Achieving the above benefits is in practice much more difficult than often realized. DG sources must be reliable, dispatchable of the proper size, and at the proper locations. Therefore, without proper planning and analysis, DGs can have negative impacts to the distribution system as follows:

- Large penetration level of DG may deteriorate system operation, system security and system dynamic performance.
- Conventional distribution systems need adequate protection in order to accommodate exchange of power.
- Signaling for dispatch of resources becomes extremely complicated.
- Connection and revenue contracts are difficult to establish.
- Safety concerns with energy generated from multiple sources.

Since DGs have advantages and disadvantages as mentioned above also many DGs will not be utility owned or will be variable energy sources such as solar and wind. There is no guarantee that these conditions will be satisfied and that the full system support benefits will be realized. Thus, DG interconnection policy should take into account how to maximize the desired benefits.

The PV generation is one type of inverter-based DGs that will become more widespread at this time and the future due to anticipated cost reductions in PV technology and installation. PV systems are expected to play a promising role as a clean power electricity source in meeting future electricity demands. However, the integration of PV systems into power networks can cause both benefits and drawbacks depending on locations, operating modes and allowable sizes [17-19]. Since, the PV system is interfaced to the distribution system through a pulse width modulated (PWM) inverter, which is the main source of harmonic current. They may create the associated injection of harmonic currents into the distribution system lead to malfunction of harmonic-sensitive equipment if the injection of harmonic currents is allowed to reach excessive levels [20]. Therefore, with the growing penetration of inverter-based DGs especially photovoltaic distributed generation (PV-DG). There should be more concerns about technical constrains and existing regulation by the Distribution Network Operators (DNO) in order to assess the impact of PV system on the electric power quality and limit their integration.

In system planning and design aspect, there are some of the issue concerns of utilities when PV-DGs are interconnected to the grid as follows:

- Harmonic distortion
- Power fluctuation
- Voltage regulation

1.4.1 Harmonic distortion [21]

From a harmonic modeling standpoint, inverter-based DG units can be viewed as a nonlinear load injecting harmonic current into the distribution feeder [22]. This could result in an unacceptable level of total harmonic distortion (THD).

THD can be applying to both current and voltage which are defined as the ratio of the rms value of harmonics and the rms value of the fundamental. THD of currents (THDi) varies from a few percent to more than 100%. THD of voltage (THDv) is usually less than 5%. However, THDv below 5% is widely considered to be acceptable, but values above 10% are unacceptable and will cause problems for sensitive equipment and loads.

It is widely recognized that the presence of nonlinear components of power systems manifests in the appearance of harmonics [23]. The presence of harmonics in a power system is undesirable for a number of reasons, some of which are:

- Harmonics increase power losses in both utility and customer equipment.
- Sometimes harmonics may provoke malfunctioning of sensitive load or control equipment.
- Harmonics having significant magnitudes can cause a reduction of lifetime of motors, transformers, capacitor banks and some other equipment.
- A harmonic resonance problem with shunt capacitor can be occurred in some condition. And it produces large spikes of current and voltage on the system which cause the operation of protective devices or the failure of equipment.

Power electronic devices, as used for PV inverter, may cause a harmonic's problems. The magnitude and the order of harmonic currents injected by dc/ac inverters depend on the technology of the inverter and mode of its operation. For example, a forced-commutated inverter with pulse-width-modulation operated in the linear range, will introduce only harmonics in the range of high frequencies, i.e., at and/or around multiples of the carrier frequency [24].

Many papers studied power quality problems in harmonic aspect associated with a large number of distributed grid-connected PV system on a distribution network [25-29]. The main objective of these papers is to analyze the observed phenomena of harmonic interference of large populations of these inverters. From the results of these papers, it indicates that the increasing of grid-connected PV systems can cause the harmonic distortion problem due to high penetration of PV system.

1.4.2 Power fluctuations

At a large scale, the uncertainty characteristic of power output of PV systems can affect the power quality and reliability. Since, the power generated from PV systems will be fluctuating all the time depending on climate conditions and geographic location. In the future, if a large number of PV systems are connected to the grids, the fluctuation of PV power output may cause the problems such as voltage fluctuation and large frequency deviation in electric power system operation [30-35]. Therefore, for the high penetration of PV systems interconnection to the grids without reduction of the reliability and power quality of utility power systems, suitable measures should be applied to the PV systems side.

Battery storage is the one device which can be used to reduce the PV power output fluctuation. There are several studies which investigations aimed at improving the performance of PV systems equipped with batteries [36-41]. However, using the energy storage device increases the capital cost, as it needs maintenance.

Therefore, in order to assess the power quality of a distribution system under normal operating conditions with high penetration of PV-DGs and without batteries, electrical characteristics of the current injection into the distribution network are necessary to be understood thoroughly. Generally, the power system analysis under normal operation is based on a deterministic load flow calculation. However, the solar energy sources of PV-DG units are often uncontrollable and thus introduce uncertain factors into the distribution system. As a result, the PV output power injection into the distribution system is fluctuating throughout the year [34].

As mentioned above, the combination of many uncertain factors may be make the difficulty and complicated to assess a distribution system performance under normal operating conditions through a deterministic approach. Therefore, a probabilistic approach is necessary in order to assess the system power quality, which these uncertain factors are taking into account, e.g. power losses, voltage regulation, power fluctuation and harmonic distortion.

1.4.3 Voltage regulation

Generally, load-tap-changing (LTC) transformers at substations, supplementary line regulators on feeders, and switched capacitors on feeders are used to regulate the voltage of a radial distribution system. Through the application of these devices, the voltages at a customer load point are kept within the acceptable limit. In practice, the voltage regulation is normally based on radial power flows from the substation to the load points. Interconnection of DG introduces meshed power flows, which may be interfering with the system voltage regulation. The following regulation problems may occur [2]:

- *Low voltage caused by DG just downstream of a regulator with line-drop compensation*

If a DG is connected to downstream of a voltage regulator or LTC transformer, which is using considerable line drop compensation as shown in Figure 1.19. Then the regulation controls will be unable to properly measure feeder demand. Fig.1.19 demonstrates that the improper voltage profiles may occur under with and without DG. In case of with DG, the voltage is reduced because the DG decreases the observed load at the line drop compensator (LDC) control. In this case, the regulator confuses into setting a voltage lower than is required to maintain adequate service levels at the end of the feeder.

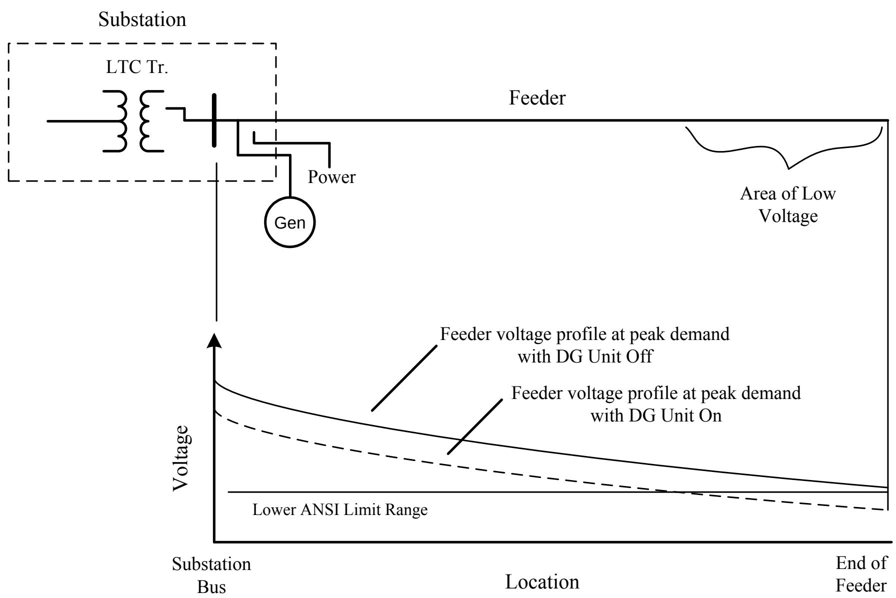

Fig. 1.19 Case of DG unit interfering with voltage regulation on a distribution feeder

- *High voltage due to DG*

DG may also result in high voltage at some electric customers. It can be seen that high penetration of DGs may cause reverse power flow to the substation. For this case, the voltage can increase along the feeder. In some locations where the primary voltage is already high and the load is low, the rise in voltage can be enough to push the voltage over the acceptable limit [21].

Furthermore, the problem of high voltage may occur from the uncertainty of power fluctuation due to both PV-DG as mentioned above and load demand. If PV-DG does not operate in coordinate with the local load, they might increase the variations between the maximum and minimum voltage level. As the minimum voltage level could remain in a high load with a low PV-DG power situation, but the maximum voltage level could increase in low load with full PV-DG production.

- *Interaction with regulating equipment*

Some DGs use feedback to control voltage, but this way interacts negatively to the utility regulation equipment. There may be undesirable cycling of regulation devices and noticeable power quality impacts under such conditions. In case of intermittent power output of PV-DG, this may change the system voltage or current flows enough to cause a regulator tap change or an operation of a switched capacitor [21].

As mentioned all above, it can be seen that there is some interesting issues concern with PV-DG included harmonic distortion, power fluctuation and difficulty of voltage regulation. The installation of PV-DG into a distribution system can cause both benefits and drawbacks depending on locations, operating modes and allowable sizes.

Therefore, this dissertation proposes the sizing of photovoltaic distributed generators in a distribution system with consideration of solar radiation and harmonic distortion. The objective is to maximize the power produced by PV-DG installation and minimize system losses, while the voltage profile as well as harmonic current, total harmonic voltage distortion (THDv) and total demand distortion (TDD) at the point of common coupling (PCC) are kept at an acceptable limit.

The probabilistic approach is applied to solve the problem because distribution utilities deliver electric energy to their customers within an appropriate range to maximize customer satisfaction and to reduce system losses. In the presence of PV-DG, it is difficult to regulate voltage since the PV system is a type of random generation. That is dependent of the environmental conditions namely the voltage variation of PV-DG at the PCC as a function of solar radiation level [42-43]. So, it is impossible to achieve a realistic evaluation of where and when an overvoltage can happen in a distribution system during an investigate a period of time by simply using a deterministic load flow (DLF) analysis, which is based on the mean values or expected values of customer loads and generations as inputs to solve a problem. For this reason, a probabilistic load flow (PLF) analysis is employed to ensure that the solution will be effective for the acceptable voltage deviation.

1.5 Literature Reviews

1.5.1 Literature Review on Optimal DG Sizing and Location

Generally, DG is an electric power source connected directly to a distribution network or customer site. Since DG can be installed close to anyplace, which is required the advantages of DG in terms of efficiency and losses, investment, reliability and power quality. However, interconnection of DG can create some technical problems such as difficulty of voltage regulation, over a thermal limit and exceeded harmonic distortion, etc. The severity of this problem depends on size, location, number and operating mode of DG. Therefore, several papers studied how to determine optimal size and location of DG, which is based on the synchronous type, in a distribution network with consideration of technical constraints as mentioned above.

Authors in [44] and [45] proposed technique to minimize power losses in a distribution feeder by optimizing DG model in terms of size, location and operating point of DG. Sensitivity analysis for power losses in terms of DG size and DG operating point was also performed in these papers. The proposed technique has been developed with considering the load characteristic with constant impedance and constant current models. Test results indicated that real power loss can be reduced with a DG of optimal size, located at an optimal place in the feeder.

DGs in [46] are treated as mobile reactive compensators, which can be connected as a kind of reactive compensation equipment to improve voltage stability. A quantitative index is proposed to evaluate the voltage stability of load nodes to decide the optimal DG location. The optimal penetration level of DG at optimal location is then calculated by Primal-Dual Interior Point Method. The optimal calculation realizes the highest voltage eligible ratio and minimum power loss by adjusting the reactive power output of DG in a precondition of system security. The simulation results show the best location and penetration level of DG for voltage stability in the test system.

A multi-objective approach for optimal location and sizing to maximize the penetration of DG in a distribution network is proposed in [47]. The proposed optimization procedure is an evolutionary multi-objective algorithm based on the genetic algorithm (GA) with the ε-constrained technique. The goal of this methodology is to maximize the benefits of the presence of DGs and limit the network performance deterioration because DG is not connected at optimal locations.

Reference [48] proposed Ant Colony Optimization (ACO) based algorithm for DG sources allocation and sizing in distribution systems. The objective is defined as minimization of DG investment cost and total operation cost of the system subject to a set of constraints such as capacity of feeder, voltage limit and total DG capacity limitation.

The optimal DG number and sizing formulated as a NonLinear Programming (NLP) problem has been proposed in [49]. The major objective is improving the voltage profiles of distribution networks using multiple DG sources. The constraints of this paper are the nodal complex voltage and DG power factors. Further, the static load models as constant power, constant current and constant impedance are investigated.

In [50], the optimization of DG units and shunt capacitors for economic operation of distribution systems was proposed. The minimization of overall investment cost with the integration of DG units and shunt capacitors is assessed with the consideration of supply quality, reliability and energy loss. A new planning methodology by using Particle Swarm Optimization (PSO) is proposed to minimize the overall cost for optimal sizing and location of DG units and shunt capacitors.

The effect of the variation of loads with voltage and frequency for optimal allocation of DG in terms of location and size is addressed in [51]. The objective is to minimize the real power loss and to maintain the voltage within specified limits at buses using genetic algorithms in a distribution network. However, an evaluation of frequency on analysis under certain assumptions regarding frequency has been made within the permissible range 0.98 pu to 1.02 pu.

The paper in [52] presents an approach by using the genetic algorithm for optimal allocation of single and multiple DGs in terms of location and size to minimize an average of locational charges for unit active power at buses. It means that the bus with maximum locational charge may be chosen as optimal location. The voltage at buses within specified limits is considered as the constraint. The static load models as constant power, constant current and constant impedance were considered.

The paper in [53] proposed the selection of optimal location and size of multiple DGs by using Kalman filter algorithm. The selection of optimal locations of multiple DGs was considered from total power loss in a steady-state operation. Thereafter, the optimal sizes are determined by using the Kalman filter algorithm. The objective is to minimize the total power loss of system. The merit of this algorithm is that it took the only few samples from a large-scale power system with many data samples and therefore, it reduced the computational requirement dramatically during the optimization process.

The optimal DG sizing problem in [54] is tackled by the Sequential Quadratic Programming deterministic technique. The DG modeling is separated into two types, which are treated as a PV bus and PQ bus. The objective function is minimizing real power losses with consideration of the thermal network restrictions and the bus complex voltage constraints. Furthermore, the impact of both the DG modeling and the static load response to voltage upon the optimal DG size were studied.

A multi-objective placement and penetration level of DGs were examined in [55]. By concerning both technical and economical parameters of a power system using genetic algorithm combined with Multi-Attribute Decision Making (MADM) method. The technical parameter including total losses, buses voltage profile, line capacity limits and total reactive power flow were considered. The approach consists of GA for determining the best generation configurations of system by considering technical parameters that are included in the fitness function, and MADM techniques for ranking the selected plans regard to technical and economical attributes.

A combination of genetic algorithm and simulated annealing is presented in [56] for optimal DG allocation in distribution networks. The objective is to minimize distribution power losses for a fixed number of DGs and a specific total capacity of DGs. The constraints are buses voltage magnitude and line current capacity limits. Through this algorithm, a significant improvement in the optimization goal is achieved.

From [44-56], methods, objective function, parameter constraints and load models for optimal sizing and location of DG based on the synchronous type in a distribution system can be summarized as shown in Table 1.4. Among the methods for optimal DG sizing and location, the genetic algorithm is the most popular method.

Table 1.4 Summary of the methodologies for optimal DG sizing and location

Methodologies	**Objective functions**	**Constraints**	**Load models**
- Genetic algorithm (GA) - Nonlinear programming - Sequential quadratic programming - Particle swarm optimization - Ant colony optimization - Combination of GA and Simulated annealing - Combination of GA and MADM - Kalman filter algorithm	- min (real power loss) - min (voltage variation) - min (investment and operating cost)	- Bus voltages - Thermal limits - DG capacity	- Constant power - Constant current - Constant impedance

1.5.2 Literature Review on Optimal PV-DG Sizing

The methodologies as shown in Table 1.4, however, are used for optimal synchronous-based DG sizing and location, which all are based on a deterministic approach. There are many techniques presented in both stand-alone and grid-connected systems through deterministic and probabilistic approaches. In order to determine a PV-DG size and assess a distribution system performance under normal operating conditions.

In order to determine PV-DG size based on a probabilistic approach, an analysis of a stand-alone PV system on output of PV systems and load demands were studied in [57]. Reliability indices in terms of loss of load hours (LOLH), energy losses and total cost of investment are the main factors for evaluating the optimal operation of stand-alone PV scheme. Solar radiation and load demand in [57] were modeled as stochastic variables using historical data and experimentation, respectively.

In [58], authors presented several techniques to design a stand-alone PV system. Three probabilistic methods (i.e., fixed days of battery backup and recharge, loss of load probability (LOLP) and Markov Chain modeling) were proposed. The LOLP technique has been suggested as the most reliable because it provided a detailed view of the system performance to design the PV system among all proposed techniques.

In [59], authors proposed the sizing procedure for stand-alone and grid-connected PV systems. It was based on an analytical method and sized not only PV arrays but also batteries and inverters. The analytical sizing method could be categorized into three types, which are based on loads and irradiation, available areas and LOLP. The objective was not to minimize system cost mathematically, but to give an optimal design at the practical level on the basis of experimental knowledge.

In [60], authors proposed a probabilistic approach to design a grid-connected PV system in low voltage feeder. The proposed method determined the optimum PV rating with a voltage constraint at the specified connecting point.

At present, inverter-based DG can perform functions other than supplying real power. The innovation and improvements in electronic devices allow using DG to improve power quality in the grid [61]. For this reason, specific planning tools for optimal placement and sizing of DG should be adopted to consider the multiple and contrasting goals that the DNO strives to achieve [62].

Furthermore, in case of PV-DG, the uncontrollable of solar energy sources can introduce uncertain factors into a distribution system such as voltage fluctuation as mentioned in section 1.4. Therefore, it is necessary to obtain an effective method for optimal PV-DG sizing and location. To cope with this, a probabilistic approach is an alternative for solving the problem.

However, most research works related to optimal PV-DG sizing normally do not consider the power quality constraints i.e., harmonic currents from PV-DG, total harmonic distortion due to PV-DG as well as background harmonic condition. Furthermore, the PV model in relevant papers is mostly using an approximate model which ac power output of PV system is assumed to be linearly proportional to solar radiation. And they do not mention about optimal location of PV-DG installation.

1.6 Objectives and Scope of Works

Objectives of this dissertation can be described as follows:

- To obtain an optimal size of single and multiple PV-DGs in a distribution system with consideration of solar radiation and harmonic distortion.
- To propose the steady state voltage stability index method for determining the proper locations of PV-DG as utility planning and design aspect.
- To compare PV-DG sizing between consideration with and without system background harmonics.
- To assess power quality impacts on a distribution system under normal operating conditions with installation of PV-DG units.
- To study an impact of static load models and power factor control on the optimal sizing of PV-DG.
- To study an effect of PV inverter models and existing DGs in a distribution system on the optimal PV-DG sizing.

Scope of the research can be summarized as follows:

- The proposed technique is based on a probabilistic approach, i.e., Monte Carlo simulation.
- The PV model in this research is based on Sharp 80Wp, NE-80E2E solar module, which is polycrystalline silicon material type. The maximum power (80W) is defined at 1000 W/m^2 solar radiation and 25ºC cell temperature under standard test conditions (STC).

- The PV model is integrated with the simplified perturb and observe (P&O) maximum power point tracking (MPPT) technique to automatically find the maximum power output under a given solar radiation and ambient temperature, which are based on real statistical data.
- The substation voltage and load demand are assumed to be a random variable with a normal distribution function.
- The protection coordination is not considered in this research.
- The coordination of voltage regulation equipments with PV-DGs is not considered.
- PV-DGs are considered without batteries storage.
- A distribution system is assumed to be balanced.
- The background harmonics are taking into account to determine the optimal size of PV-DG.
- Other types of DGs, such as synchronous and induction generation, are allowed with various locations, operating modes and sizes to incorporate with the optimal PV-DG sizing.
- In order to evaluate the harmonic distortion levels in a distribution system, the PV-DG is modeled as a harmonic current source based on statistical harmonic current spectra from measurements of a PV farm.
- The steady state voltage stability index (VSI) method is used to determine the proper locations for placing a PV-DG.
- The objective function of the proposed method is to:
    - Minimize average system real power loss

  Subjected to the technical constraints as follows:

    - Node voltage limited as $1 \pm 0.05 \ pu$

      or $0.95 \ pu \leq V_i \leq 1.05 \ pu$
    - Harmonic currents at each order (up to 33^{rd}) should not exceed the limits, which are based on IEC 61727 standard [63].
    - Total harmonic voltage distortion (THD_v) at PCC should not exceed 5%, which is based on IEEE 519-1992 standard [64].

  - Total demand distortion (TDD) at PCC should not exceed 5%, which is based on IEC 61727 standard.
- An actual PEA 51-bus radial distribution system in Thailand and a 33-bus system are used for test cases of the proposed method.

1.7 Synopsis of Chapters

The material in this dissertation is organized as follows:

Chapter 1 presents world's PV generation overview, solar PV technologies and PV generation in Thailand. The literature reviews of related research are also addressed. The motivation, objective, scope of work and research approach are also mentioned.

Chapter 2 presents models of grid-connected PV system components. The statistical models of solar radiation and ambient temperature are proposed. The probabilistic load model, PV model, MPPT and PV inverter model are also addressed.

Chapter 3 presents the steady state voltage stability index method to determine the proper PV-DG installation location.

Chapter 4 presents the modified Newton method to calculate power flow in a radial distribution system. The harmonic modeling and calculation are also presented.

Chapter 5 proposes the algorithm of PV-DG sizing technique and problem formulation. The numerical results of several study cases are also investigated.

Chapter 6 presents contributions of the dissertation, conclusion and future works.

CHAPTER II
MODELING OF SYSTEM COMPONENTS

2.1 Grid-Connected Photovoltaic Systems

PV power systems have made a successful transition from small stand-alone sites to large grid-connected systems. The utility interconnection brings a new dimension to the renewable power economy by pooling the temporal excess or the shortfall in the renewable power with the connecting grid that generates base-load power using conventional fuels. Generally, the grid supplies power to the site loads when needed or absorbs the excess power from the site when available. A kilowatt-hour meter is used to measure the power delivered to the grid and another is used to measure the power drawn from the grid.

As shown in Figure 2.1 [9], the principal components in a single phase grid-connected, PV system side consists of the array itself with two leads from each string sent to a combiner box that includes blocking diodes, individual fuses for each string and usually a lightning surge arrestor. Two wires from the combiner box deliver dc power to a fused array disconnected switch, which allows the PVs to be completely isolated from the system. The inverter sends ac power through a breaker to the utility service panel. Additional components not shown include the maximum power point tracker (MPPT), a ground-fault circuit interrupter (GFCI) that shuts the system down if any currents flow to ground and circuitry to disconnect the PV system from the grid if the utility loses power. The inverter, some of the fuses and switches, the MPPT, GFCI and other power management devices are usually integrated into a single power conditioning unit (PCU). Figure 2.2 shows the simplified schematic diagram of the grid-connected PV systems included PV generator, PCU and step-up transformer.

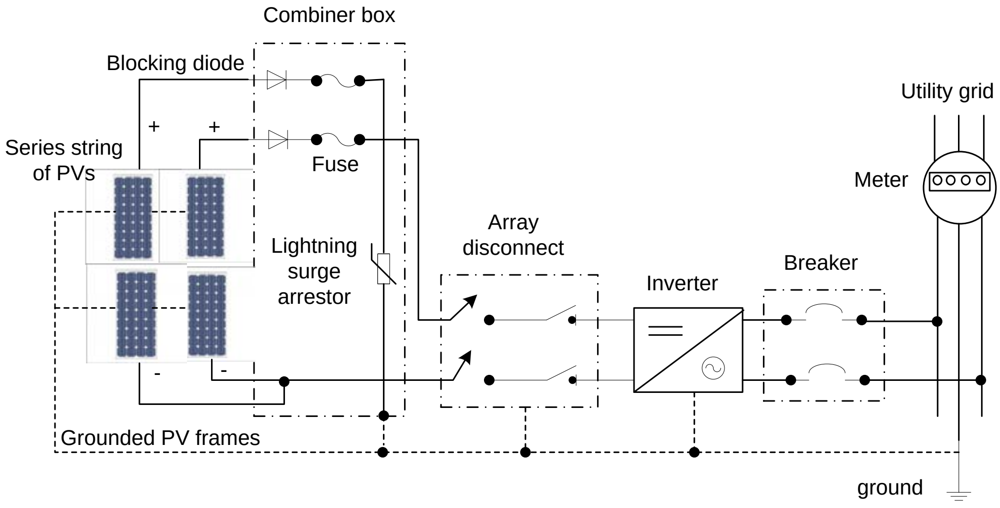

Figure 2.1 Principal components in a single phase grid-connected PV systems

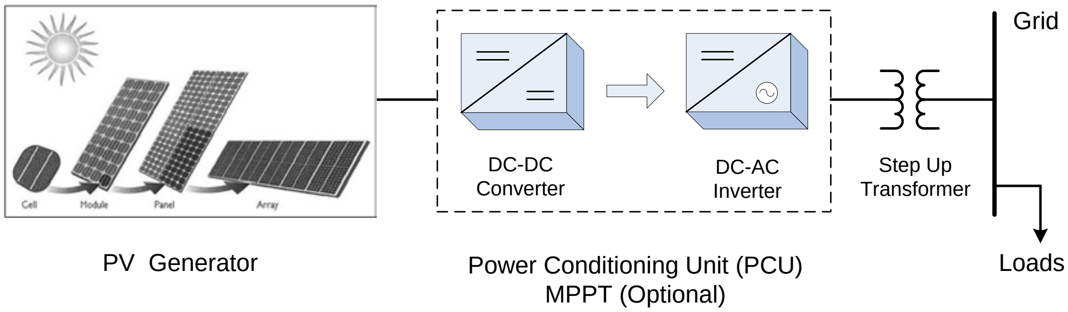

Figure 2.2 Simplified schematic diagram of grid-connected PV systems

For large-scale grid-connected PV systems, a PV generator consists of a typical connection group of PV strings, of which the type of connection is not considered in this dissertation. The MPPT is integrated into the PCU which sends the maximum power through a step-up transformer to the grid. In power quality aspect, a large amount of converted power from DC to AC side can cause the harmonic problem. This depends on typical inverter topologies and operating point, which depends on power produced by PV generator under a solar radiation condition.

2.2 Solar Radiation and Ambient Temperature Modeling

To analyze PV systems, we need to know how much sunlight is available. A fairly straightforward set of equations can be used to predict where the sun is in the sky at any time of a day for any location on earth as well as solar intensity (or insolation which incident solar radiation) on a clear day. To determine average daily solar radiation under the combination of clear and cloudy conditions that exist at any site long-term measurements of sunlight hitting a horizontal surface is required.

2.2.1 Statistical Model of Solar Radiation

In this dissertation, hourly solar radiation is modeled as a statistical model based on data measured from a study area. Hourly variations of solar radiation were collected in one year. Figure 2.3 shows the example of hourly variations of solar radiation in Chiang Mai during 6.00 am to 6.00 pm on January to December 2007 (see Appendix A for complete data). The SI unit for solar radiation is watt per square meter (W/m^2).

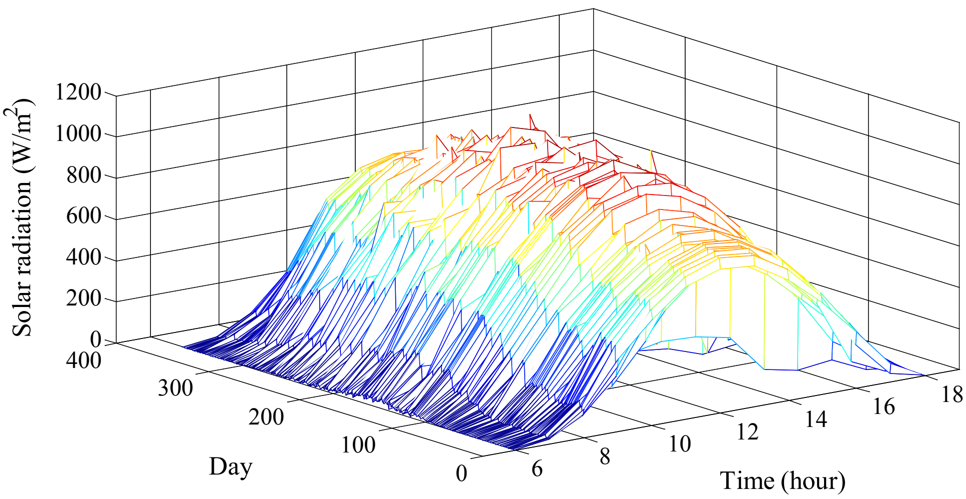

Figure 2.3 Hourly variations of solar radiation in Chiang Mai during 6.00 am-6.00 pm on Jan-Dec 2007

From the measurements, in this case, the probability density of solar radiation may not be able to accurately model as a conventional distribution function e.g., Weibull, Gamma, Exponential, etc. Hence the solar radiation is modeled as a stochastic variable from historical measurement data, as shown in Figure 2.4.

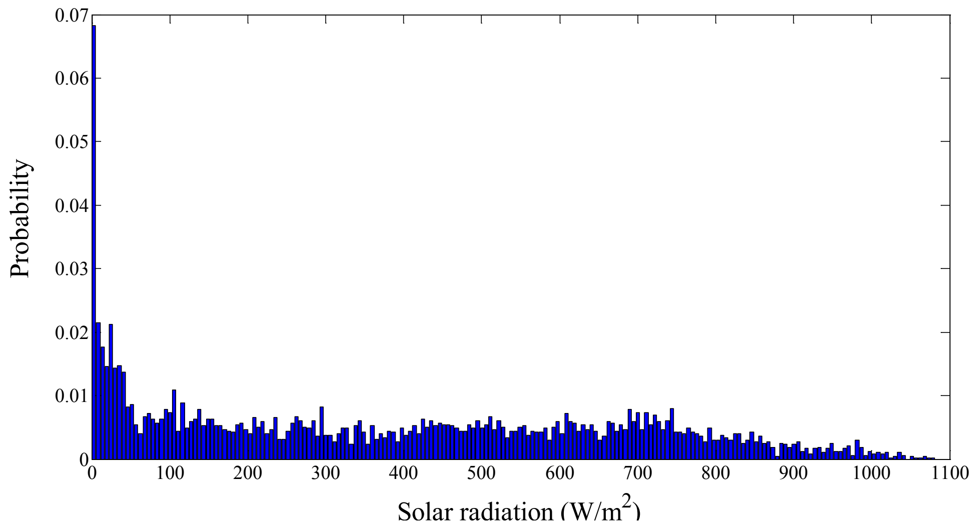

Figure 2.4 Probability density of solar radiation corresponding to Figure 2.3

2.2.2 Statistical Model of Ambient Temperature

Generally, the operating temperature is not considered in PV system analyzing. Because the temperature has a few effect on the PV system output power. Thus, in PV model, the power output of PV system is approximately proportional to solar radiation. However, the power output of PV system can be changed around 10% (constant solar radiation) when the ambient temperature is varied from the minimum to maximum values, based on measurement data, by simulation. Therefore, in this dissertation, the temperature effect is included in the PV model.

Similarly to solar radiation, hourly variations of ambient temperature are modeled as a statistical model based on data measured from the same area and time (see Appendix A for complete data). Figure 2.5 shows the hourly variations of ambient temperature (degree) in Chiang Mai during 6.00 am to 6.00 pm on January to December 2007.

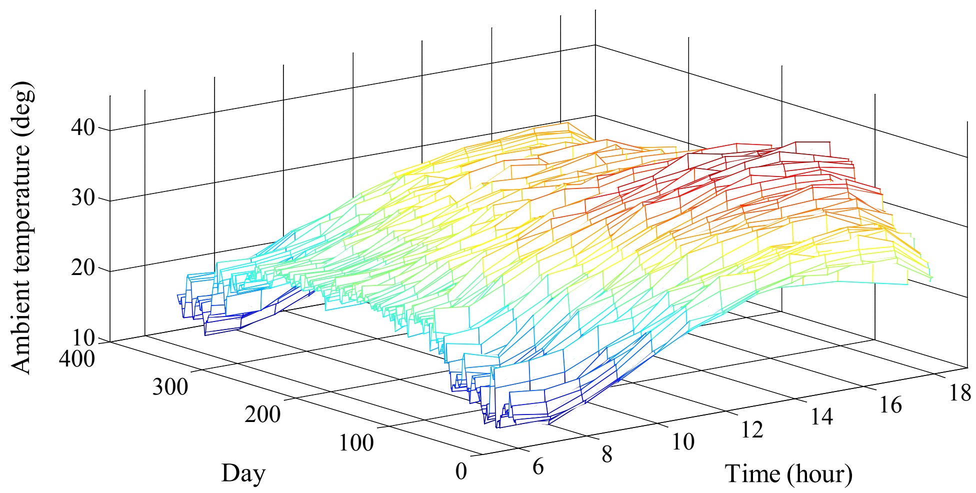

Figure 2.5 Hourly variations of ambient temperature in Chiang Mai during 6.00 am-6.00 pm on Jan-Dec 2007

From Figure 2.5, the ambient temperature can be modeled as a Weibull distribution function, as shown in Figure 2.6. The probability density function of a Weibull random variable x is [65]

$$f(x) = \frac{\beta}{\alpha^{\beta}} x^{\beta-1} \exp\left[-\left(\frac{x}{\alpha}\right)^{\beta}\right] \tag{2.1}$$

where $0 \le x < \infty$, $\beta > 0$ is the *shape parameter* and $\alpha > 0$ is the *scale parameter* of the distribution. The cumulative probability distribution function is

$$F(x) = 1 - \exp\left[-\left(\frac{x}{\alpha}\right)^{\beta}\right] \tag{2.2}$$

By the inverse transform method

give $$U = F(x) = 1 - \exp\left[-\left(\frac{x}{\alpha}\right)^{\beta}\right] \tag{2.3}$$

so $$X = \alpha\left[-\ln(1-U)\right]^{1/\beta} \tag{2.4}$$

where U is a uniformly distributed random variate between [0,1]. Since 1-U is also a uniformly distributed random variate between [0,1], Equation (2.4) becomes

$$X = \alpha(-\ln U)^{1/\beta} \tag{2.5}$$

where the values of α is 29.2763 and β is 6.5052 from the curve fitting.

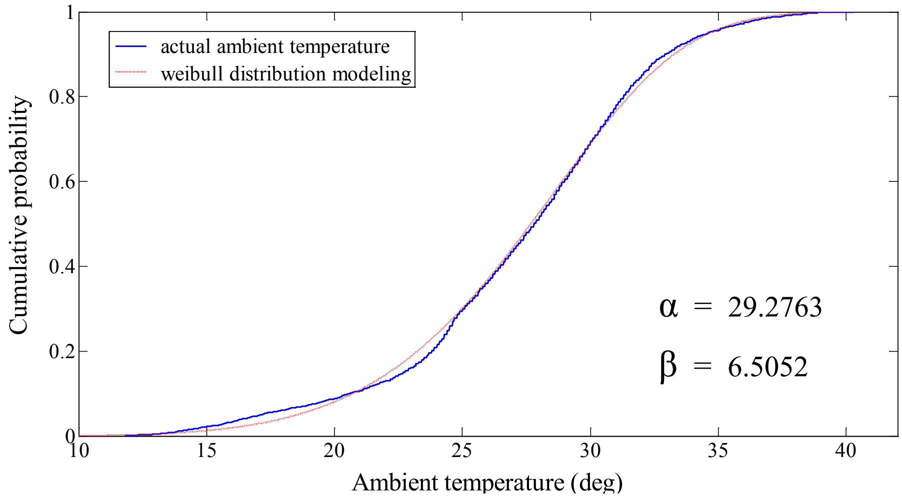

Figure 2.6 Cumulative probability of ambient temperature corresponding to Figure 2.5

2.3 Photovoltaic Modeling

For this research work, a model of moderate complexity was used [66]. The PV model included temperature dependence of the photo-current (I_{ph}) and the saturation current of the diode (I_0). A series resistance (R_s) was included, but not a shunt resistance. A single shunt diode was used with the diode quality factor set to achieve the best curve match. This model is a simplified version of the two diode model presented by Gow and Manning [67]. The simplified equivalent circuit of a PV cell is shown in Figure 2.7.

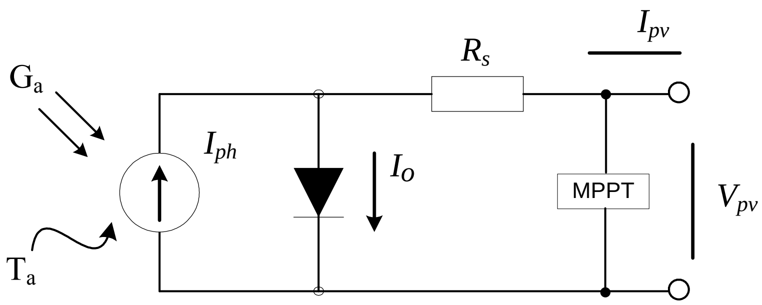

Figure 2.7 Simplified equivalent circuit of the PV cell model

Furthermore, PV model in this dissertation is integrated with maximum power point tracker as will be described in next section. Accuracy and complexity can be introduced to the model by adding in turn

- Temperature dependence of the diode saturation current I_0
- Temperature dependence of the photo current I_{ph}
- Series resistance R_s, which gives a more accurate shape between the maximum power point and the open circuit voltage
- Either allowing the diode quality factor to become a variable parameter, instead of being fixed at either 1 or 2

From the corresponding statistical model, random solar radiation (G_a) and ambient temperature (T_a) are generated by Monte Carlo simulation. These data are required to evaluate the I-V characteristic of PV model. The voltage output of the PV cell is represented by Equation (2.6), which is a function of the photocurrent mainly determined by load current and depended on the solar irradiation level and cell temperature during the operation.

$$V_{pv} = (AkT_c / q)\ln(I_{ph} + I_0 - I_{pv} / I_0) - I_{pv}R_s \tag{2.6}$$

Equation (2.6) can be rewritten as

$$I_{pv} = I_{ph} - I_0(e^{\frac{q(V_{pv}+I_{pv}R_s)}{AkT_c}} - 1) \tag{2.7}$$

The equations which describe the I-V characteristic of PV model are as follows:

$$I_{ph} = I_{ph(T_1)}\left[1 + K_0(T_c - T_1)\right] \tag{2.8}$$

$$I_{ph(T_1)} = G_a\left(I_{sc(stc)} / G_{a(stc)}\right) \tag{2.9}$$

$$K_0 = \left(I_{sc(T_2)} - I_{sc(T_1)}\right) / (T_2 - T_1) \tag{2.10}$$

$$I_0 = I_{0(T_1)}\left(\frac{T_c}{T_1}\right)^{3/A} \times e^{-\frac{qV_g}{Ak}\left(\frac{1}{T_c}-\frac{1}{T_1}\right)} \tag{2.11}$$

$$I_{0(T_1)} = I_{sc(T_1)} / (e^{\frac{qV_{oc(T_1)}}{AkT_1}} - 1) \tag{2.12}$$

where I_{ph} is temperature dependence of the photo-current (A)

I_0 is temperature dependence of the diode saturation current (A)

I_{pv} is cell output current (A)

V_{pv} is cell output voltage (V)

V_{oc} is cell open circuit voltage (V)

V_g is band gap voltage (V)

R_s is series resistance of cell (Ω)

q is electron charge (coulomb)

k is Boltzmann constant (J/K)

A is diode quality factor

T_c is cell operating temperature (ºC)

G_a is operating solar radiation (W/m^2)

$G_{a(stc)}$ is solar radiation at Standard Test Condition, STC, (1000 W/m^2)

T_1 is reference cell temperature at condition-1, normally refer at STC (25ºC)

T_2 is reference cell temperature at condition-2 (ºC)

$I_{sc(stc)}$ is short circuit current per cell at STC (A)

$I_{sc(T_2)}$ is short circuit current per cell at T_2 (A)

The photo-current is directly proportional to solar radiation. When short circuit occurs in the cell, negligible current can flows in the diode. Hence, the proportionality constant in Equation (2.9) is set so the rated short circuit current is delivered under rated solar radiation. The relationship between the photo-current and temperature is linear as shown in Equation (2.8) and is deduced by noting the change of photo-current with the change of temperature as follow by Equation (2.10).

When the cell is not illuminated, the relationship between the cell's terminal voltage and current is given by the Shockley equation. When the cell is open circuited and illuminated, the photo-current flows entirely in the diode. The I-V curve is offset from the origin by the photo generated current as follow by Equation (2.7). For the value of the saturation current at 25 ºC is calculated using the open-circuit voltage and short-circuit current at this temperature as follow by Equation (2.12). The relationship of diode saturation current to temperature is more complex, but fortunately it contains no variables requiring evaluation as follow by Equation (2.11).

The value of diode quality factor is depending on the material type of photovoltaic cell, it takes a value between 1 and 2. Generally, the value of diode quality factor $A = 2$ for crystalline silicon and $A < 2$ for amorphous silicon PV cell.

Therefore, the value of 2 is used as typical in normal operation of the model validation for the Sharp 80Wp PV module, which is a crystalline silicon material.

For the series resistance (R_s) of PV cell, it can be obtained using the only manufacturer supplied data for the PV modules at Standard Test Conditions (STC), such as open-circuit voltage, short-circuit current and maximum power. The equations which used to evaluate the value of the series resistance are given by the expression [68-69]:

$$R_s = \left[1 - \frac{FF}{FF_0}\right] \times \left[\frac{V_{oc(stc)}}{I_{sc(stc)}}\right] \tag{2.13}$$

$$FF = P_{\max}^{C} \Big/ \left[V_{oc(stc)} \times I_{sc(stc)}\right] \tag{2.14}$$

$$FF_0 = \left[V_{oc(nom)} - \ln(V_{oc(nom)} + 0.72)\right] \Big/ \left[V_{oc(nom)} + 1\right] \tag{2.15}$$

$$V_{oc(nom)} = V_{oc(stc)} \big/ V_t \tag{2.16}$$

$$V_t = AkT_c \big/ q \tag{2.17}$$

$$P_{\max}^{C} = P_{\max(stc)}^{M} \big/ (N_{sm} \times N_{pm}) \tag{2.18}$$

$$V_{oc(stc)} = V_{oc(stc)}^{M} \big/ N_{sm} \tag{2.19}$$

$$I_{sc(stc)} = I_{sc(stc)}^{M} \big/ N_{pm} \tag{2.20}$$

where $V_{oc(stc)}$ is cell open circuit voltage at STC (V)

$V_{oc(stc)}^{M}$ is module open circuit voltage at STC (V)

V_t is cell thermal voltage (V)

$I_{sc(stc)}^{M}$ is module short circuit current at STC (A)

P_{max}^{C} is cell maximum power (W)

$P_{\max(stc)}^{M}$ is module maximum power at STC (W)

FF is fill factor

N_{sm} is number of series cells in each cell parallel branches

N_{pm} is number of cell parallel branches in module

Normally, cells are grouped in to "modules", which are encapsulated with various ma terials to protect the c ells a nd the e lectrical c onnectors f rom the environment. T he m anufacturers s upply P V c ells i n m odules, c onsisting of N_{pm} parallel branches, each with N_{sm} solar cells in series, as shown in Figure 2.8 [69].

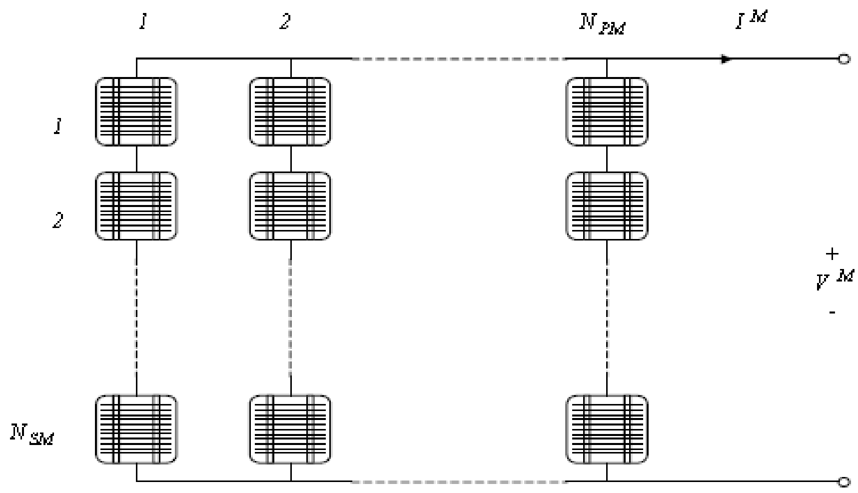

Figure 2.8 PV module consists of N_{pm} parallel branches, each of N_{sm} cells in series

In order to develop the model of PV module, the cell output voltage (V_{pv}) is then multiplied by the number of the cells connected in series N_{sm} to calculate the full module voltage (V^M), they all have the same voltage in each parallel branches. In the s ame w ay, t he c ell out put c urrent (I_{pv}) is t hen m ultiplied b y t he num ber of branches c onnected in parallel N_{pm} to obt ain the f ull m odule c urrent (I^M), they a ll carry the same current in series each branches.

The m odules i n a P V s ystem ar e t ypically conn ected in "arrays". Figure 2.9 illustrates the case of an array with M_p parallel branches each with M_s modules in series [69]. The a pplied voltage a t th e a rray's te rminal is de noted b y V^A, w hile t he total c urrent of t he a rray is de noted b y E quation (2.21). If it is a ssumed that the modules are identical and the ambient solar radiation is the same on all the modules, then the array's current is Equation (2.22).

$$I^A = \sum_{i=1}^{M_p} I_i \tag{2.21}$$

$$I^A = M_p \times I^M \tag{2.22}$$

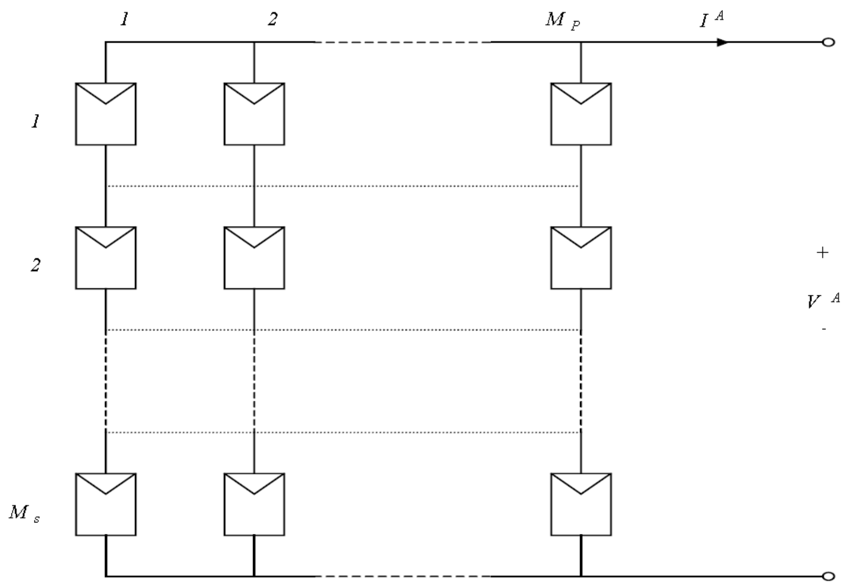

Figure 2.9 PV array consists of M_p parallel branches, each with M_s modules in series

In this dissertation, the PV arrays are modeled based on a connection group of Sharp 80Wp PV modules to obtain the rated size of PV-DG. The rated power of PV-DG is defined as peak power output, when solar radiation is 1000 W/m^2 and cell temperature is 25° C. However, a type of connection of PV modules is not considered in this work.

Since the working temperature of the PV cells (T_c) depends exclusively on the solar radiation (G_a) and on the ambient temperature (T_a). To help the researcher account for changes in cell performance with temperature, manufacturers often provide an indicator called the NOCT, which stands for Normal Operating Cell Temperature. The NOCT is cell temperature in a module when ambient is 20ºC, solar radiation is 800 W/m^2 and wind speed is 1 m/s. The value of NOCT for modules currently on the market varies from about 42 to 46 ºC. However, in this dissertation, the value of NOCT is 42ºC from testing. To account for other ambient conditions, the following expression may be used [68]:

$$T_c = T_a + G_a \left[\frac{NOCT - 20°C}{800\ W/m^2} \right] \tag{2.23}$$

where T_c is cell temperature (ºC)

T_a is ambient temperature (ºC)

G_a is solar radiation (W/m^2)

2.3.1 PV Model Implementation in Matlab/Simulink

This section shows how the mathematical model of PV module described in section 2.3 works by implemented in Matlab/Simulink. The mathematical model of PV module can be represented in Simulink implementation as shown in Figure 2.10. The input of PV module is an operating solar radiation G_a and ambient temperature T_a. The major part of structure is Matlab function blocks, which each contains necessary equations listed in previous section, as follows from Equations (2.7) to (2.20), to calculate the cell current I_{pv}. Then I-V and P-V curve can be established by changing the terminal output cell voltage V_{pv}.

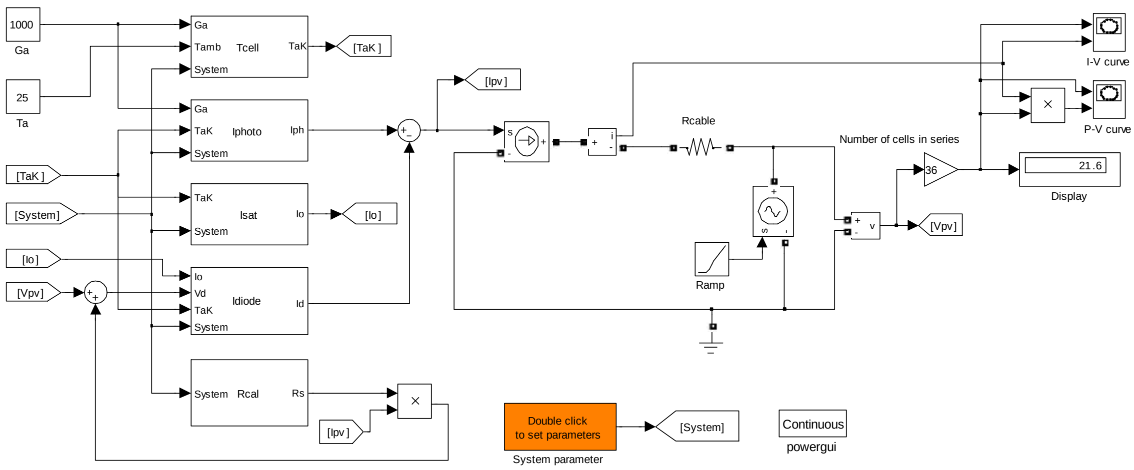

Figure 2.10 PV module model implementation in Simulink

A PV module of Sharp 80Wp is used to examine on PV model implementation. The electrical characteristics of Sharp 80Wp under STC (T_c = 25ºC, G_a = 1000 W/m^2) as given in Table 2.1, which the specification sheet can be found in Appendix B. The current and power versus voltage of PV module provided by manufacturer is shown in Figure 2.11.

Table 2.1 The key specifications of the Sharp 80 Wp PV module at STC (1000 W/m^2 solar radiation, 25ºC cell temperature)

Electrical Characteristic		
Open-circuit voltage	(V_{oc})	21.3 V
Short-circuit current	(I_{sc})	5.31 A
Voltage at max power	(V_m)	17.1 V
Current at max power	(I_m)	4.67 A
Maximum power	(P_m)	80 W

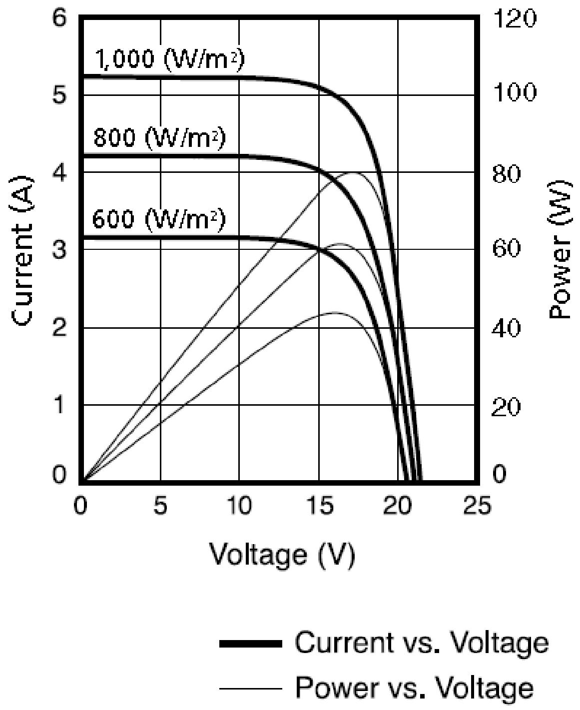

Figure 2.11 Current and power versus voltage characteristics of Sharp 80Wp PV module provided by manufacturer (T_c = 25ºC)

In or der to compare s imulation results w ith the e lectrical characteristic provided b y m anufacturer. T he out put c urrent a nd pow er r elated to voltage are simulated for va rious s olar r adiation l evels a s 600, 800 a nd 1000 W /m^2, while cel l temperature i s f ixed a t 25ºC. T he s imulation r esults of c urrent a nd pow er ve rsus voltage characteristics are shown in Figures 2.12 and 2.13 respectively.

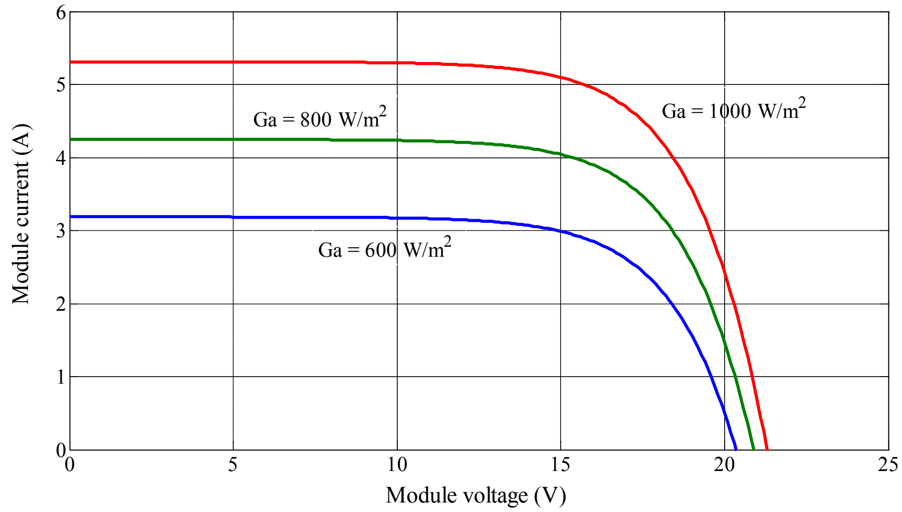

Figure 2.12 I-V characteristics of Sharp 80Wp PV module by simulation (T_c = 25ºC)

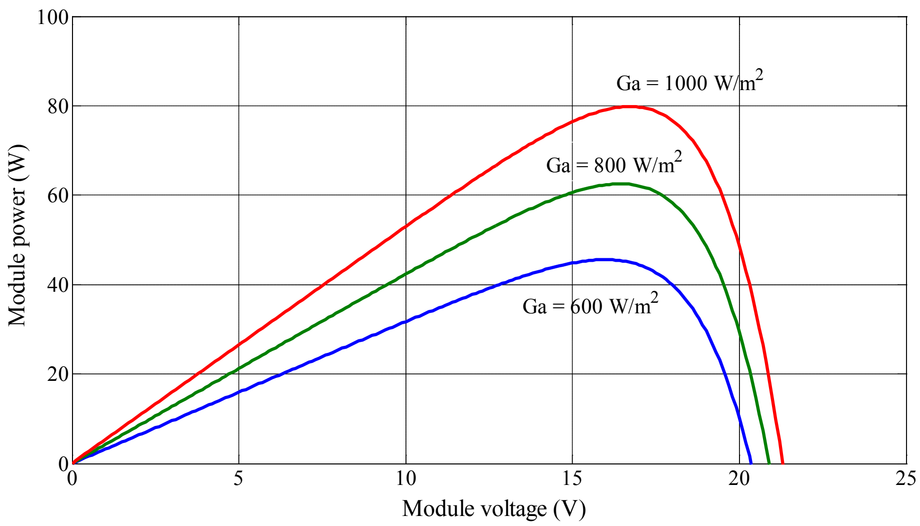

Figure 2.13 P-V characteristics of Sharp 80Wp PV module by simulation (T_c = 25ºC)

Note from Figures 2.12 and 2.13 that the results show good correspondence to the model. Table 2.2 summarizes the values of various parameters used in PV model.

Table 2.2 Summary of PV model parameters values

Parameters	***Values***
Band gap voltage , V_g	1.12 V (for crystalline silicon)
Electron charge , q	$1.6e^{-19}$ Coulomb
Boltzmann constant , k	$1.38e^{-23}$ J/K
Diode quality factor , A	2 (for crystalline silicon)
Cell temperature at STC , T_1	25ºC
Cell temperature at condition-2 , T_2	75ºC
Short circuit current at STC , $I_{sc(stc)}$	5.31 A (T_1)
Short circuit current at T_2 , $I_{sc(T_2)}$	5.47 A (3% increase of $I_{sc(stc)}$)
Series resistance , R_s	0.0132 Ω/cell
Number of series cells , N_{sm}	36
Number of parallel branches , N_{pm}	1
NOCT	42ºC

2.3.2 PV Model Validation

This section shows the results of Sharp 80 Wp PV module model validation using real data from measurement of solar radiation. Pyranometer was directly connected to the portable PV module tester (I-V checker/MP-140), as shown in Figure 2.14. Ambient temperature was recorded by a thermocouple sensor. The data measured of solar radiation and ambient temperature is shown in Figures 2.15 and 2.16 respectively. All of this is measured in one of a cloudy day on 21 October 2008.

Figure 2.14 PV module tester (I-V Checker/MP-140), EKO Instruments Co., Ltd.

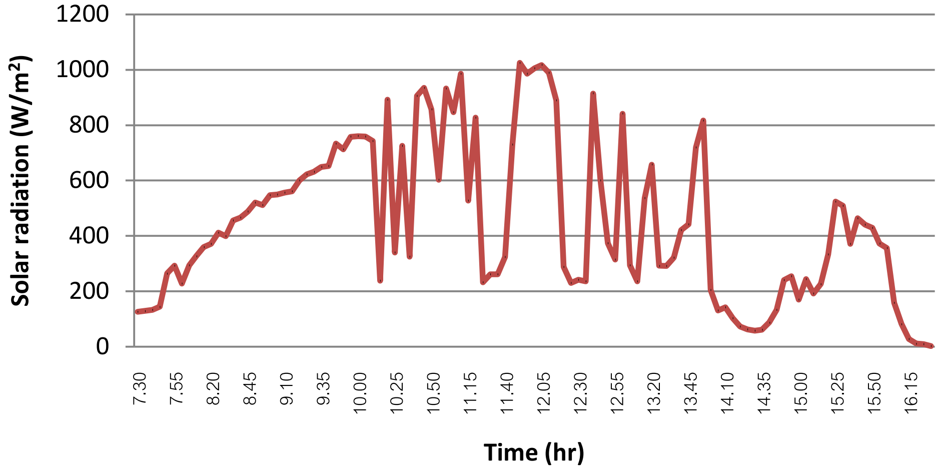

Figure 2.15 Data measured in time series of the solar radiation

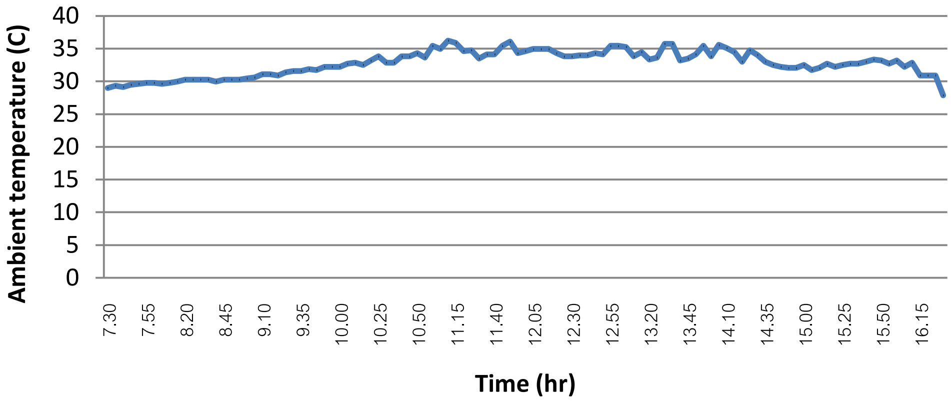

Figure 2.16 Data measured in time series of the ambient temperature

The model validation is done by comparing between results which obtained by I-V checker and simulation results obtained by Matlab/Simulink. In order to validate the model, three different levels of solar radiation are considered. Table 2.3 shows the specified values of high, medium and low solar radiation levels and ambient temperatures corresponding to a certain solar radiation.

Table 2.3 Solar radiation levels and corresponded ambient temperatures

Level	*Solar radiation (W/m^2)*	*Ambient temperature (°C)*	*Time (hr)*
High	1025.3	36.04	11.50
Medium	600.6	30.91	09.20
Low	205.1	33.80	14.00

Various out puts such as I_{sc}, V_{oc}, P_m, etc., are compared between t he simulation results and the measurements on three levels of solar radiation, as shown in Table 2.4. A good agreement of the results can be seen although it has a small error. From Table 2.4, it indicates that the error of the fill factor (FF) is less than 5% for all solar r adiation l evels. F urthermore, i t s hows t hat t he e rror of a ll pa rameters is l ess than 5% except at low solar radiation. The I-V curve which obtained by I-V checker and simulation on high, medium and low solar radiation are shown in Figures 2.17 to 2.22 respectively.

Table 2.4 Output comparison between the simulation results and the measurements on different solar radiation

Level	***High solar radiation***			***Medium solar radiation***			***Low solar radiation***		
Output	Measured	Simulated	% Error	Measured	Simulated	% Error	Measured	Simulated	% Error
I_{sc} (A)	5.619	5.572	**0.83**	3.149	3.232	**2.64**	1.101	1.099	**0.23**
V_{oc} (V)	19.18	18.51	**3.49**	19.51	18.66	**4.36**	17.50	17.18	**1.83**
P_m (W)	69.66	67.38	**3.27**	42.55	40.52	**4.77**	13.50	12.58	**6.81**
I_m (A)	4.979	4.847	**2.65**	2.842	2.834	**0.29**	0.969	0.960	**0.93**
V_m (A)	13.99	13.90	**0.64**	14.97	14.30	**4.48**	13.93	13.10	**5.96**
FF	0.6465	0.6533	**1.05**	0.6925	0.6718	**2.99**	0.7011	0.666	**4.96**

Note. *Fill factor (FF) is the ratio of the P_m and the product of I_{sc} and V_{oc} as given in Equation (2.14)*

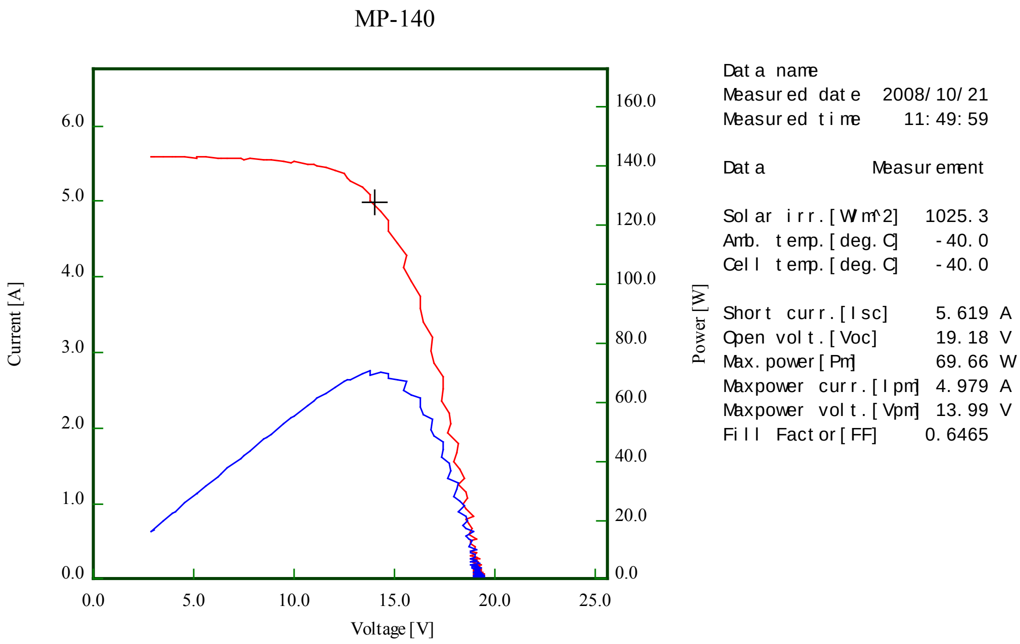

Figure 2.17 I-V characteristic curve from I-V checker at high solar radiation

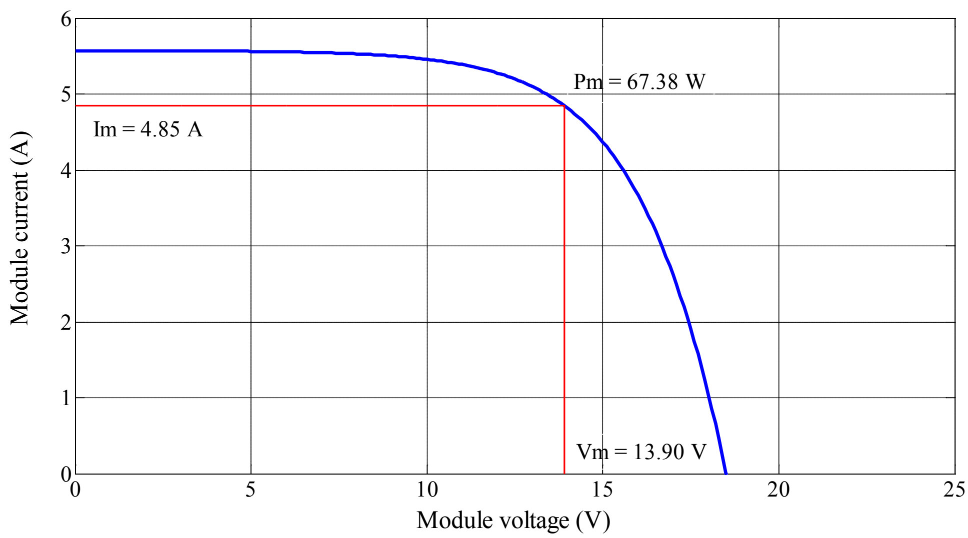

Figure 2.18 I-V characteristic curve from simulation at high solar radiation

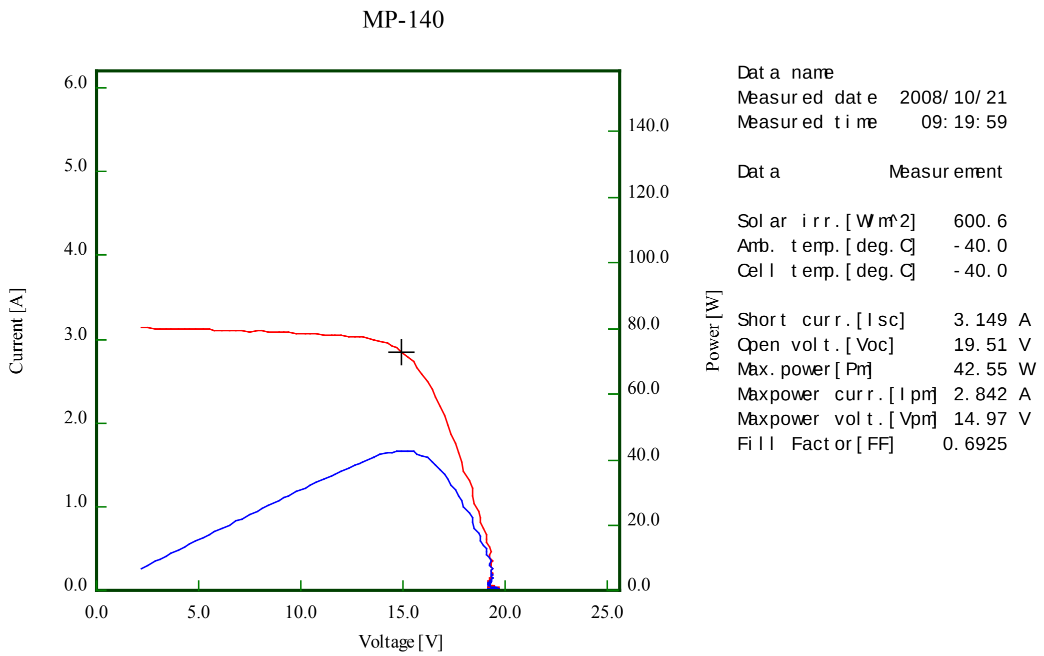

Figure 2.19 I-V characteristic curve from I-V checker at medium solar radiation

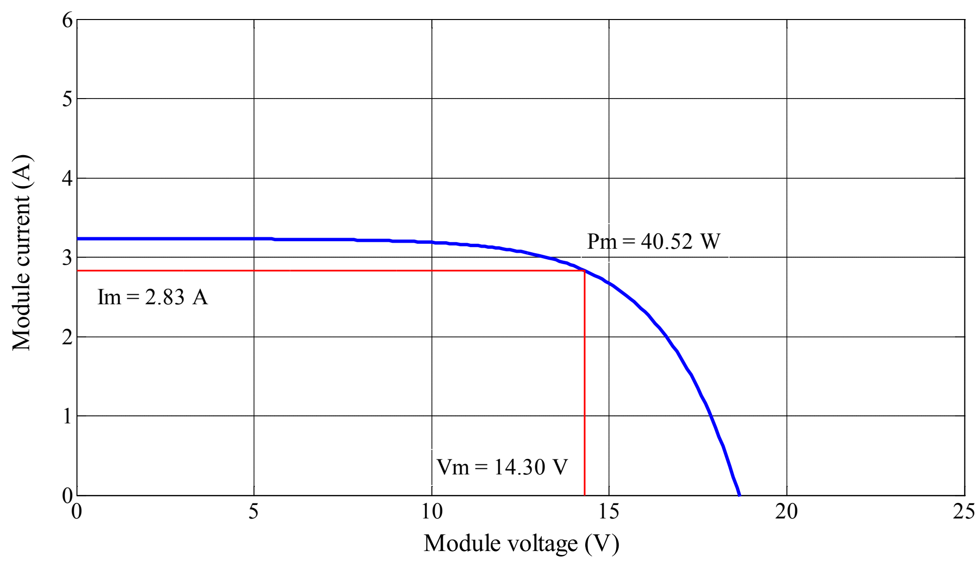

Figure 2.20 I-V characteristic curve from simulation at medium solar radiation

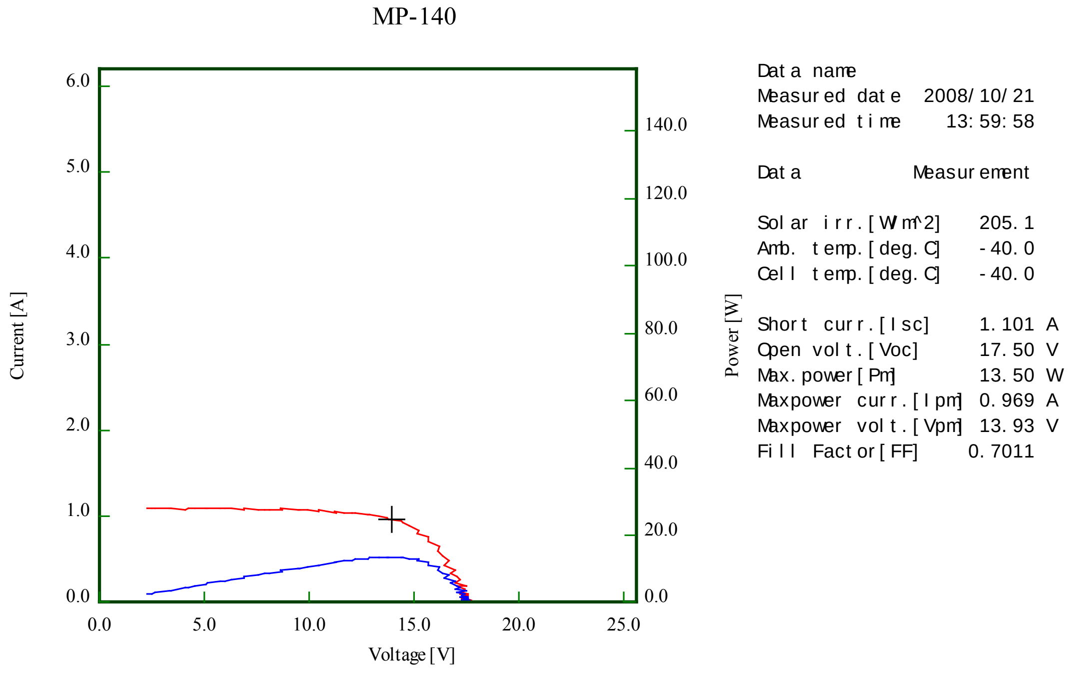

Figure 2.21 I-V characteristic curve from I-V checker at low solar radiation

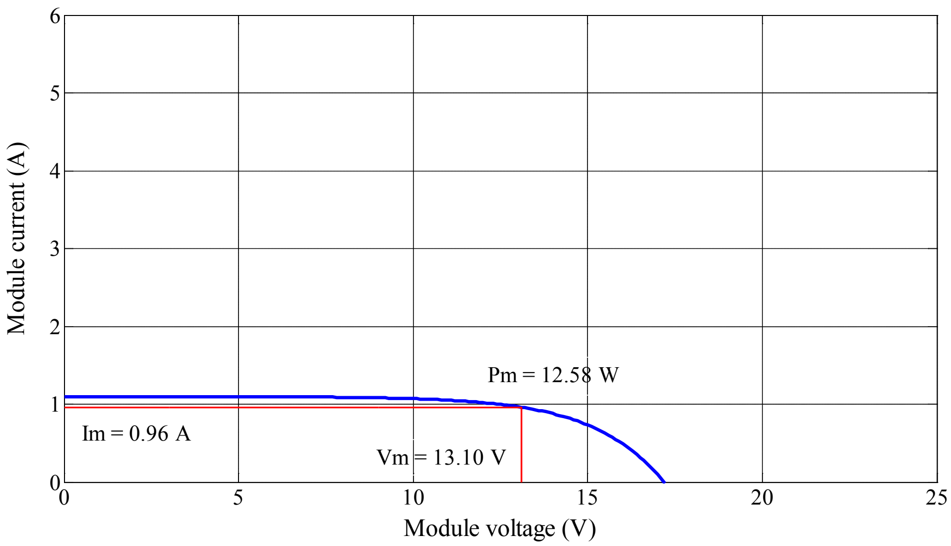

Figure 2.22 I-V characteristic curve from simulation at low solar radiation

2.3.3 Maximum Power Point Tracking (MPPT)

The maximum power point tracking of a PV array is usually an essential part of a PV system to draw peak power from the solar array in order to maximize the produced energy to DC-DC converter, as a part of PCU in Figure 2.2. Many MPPT methods have been developed and implemented. The methods vary in complexity, sensors required, convergence speed, cost, range of effectiveness, implementation hardware, popularity, and in other respects. They range from the almost obvious (but not necessarily ineffective) to the most creative (not necessarily most effective).

In fact, so many methods have been developed like, Perturb and Observe Method (P&O), Incremental Conductance Method (IC), Sliding Mode Control Method that are widely used for MPPT system in PV, and other method like, Constant Voltage (CV), Short-current Pulse Method, Open Voltage Method, Fuzzy Logic Control, Neutral Network, and other unpopular method is also used in different field of MPPT [70-72].

Therefore, it has become difficult to adequately determine which method, newly proposed or existing is most appropriate for a given PV system. However, the simplified P&O MPPT technique is used in this dissertation.

The P&O algorithms operate by periodically perturbing (i.e. incrementing or decrementing) the array terminal voltage and comparing the PV output power with that of the previous perturbation cycle. If the PV array operating voltage changes and power increases ($dP/dV > 0$), the control system moves the PV array operating point in that direction; otherwise the operating point is moved in the opposite direction. In the next perturbation cycle the algorithm continues in the same way [70].

Generally, classic P&O method is widely used, the perturbations of the PV operating point have a fixed magnitude. In an analysis, the magnitude of perturbation is 0.37% of V_{oc} of PV array. The algorithm of the classic P&O is shown in Figure 2.23.

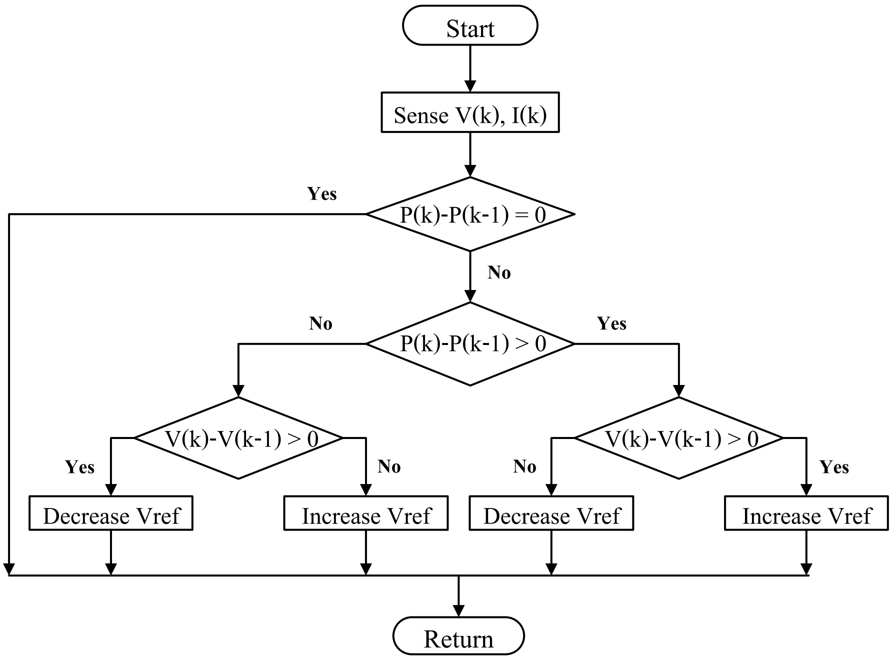

Figure 2.23 Flow chart of classic P&O technique

2.4 PV Inverter Modeling

Since, PV systems are interfaced to a distribution system through a PWM-based inverter, which is one of the main harmonic sources. These harmonic sources may create problems to vicinity equipment depending on their harmonic order, amplitudes and system characteristic. Unfortunately, there is no standard harmonic waveform of inverter-based DG since the harmonic injection from inverter-based DG depends on the design of individual manufacture.

Therefore, the PV-DG is modeled as a harmonic current source at the point of common coupling (PCC). The harmonic current spectra of PV-DG were collected from measurements of a 6 MWp PV farm on May 2010 in Nakhon Ratchasima province, north-eastern region of Thailand. The system schematic diagram of the PV farm is shown in Figure 2.24.

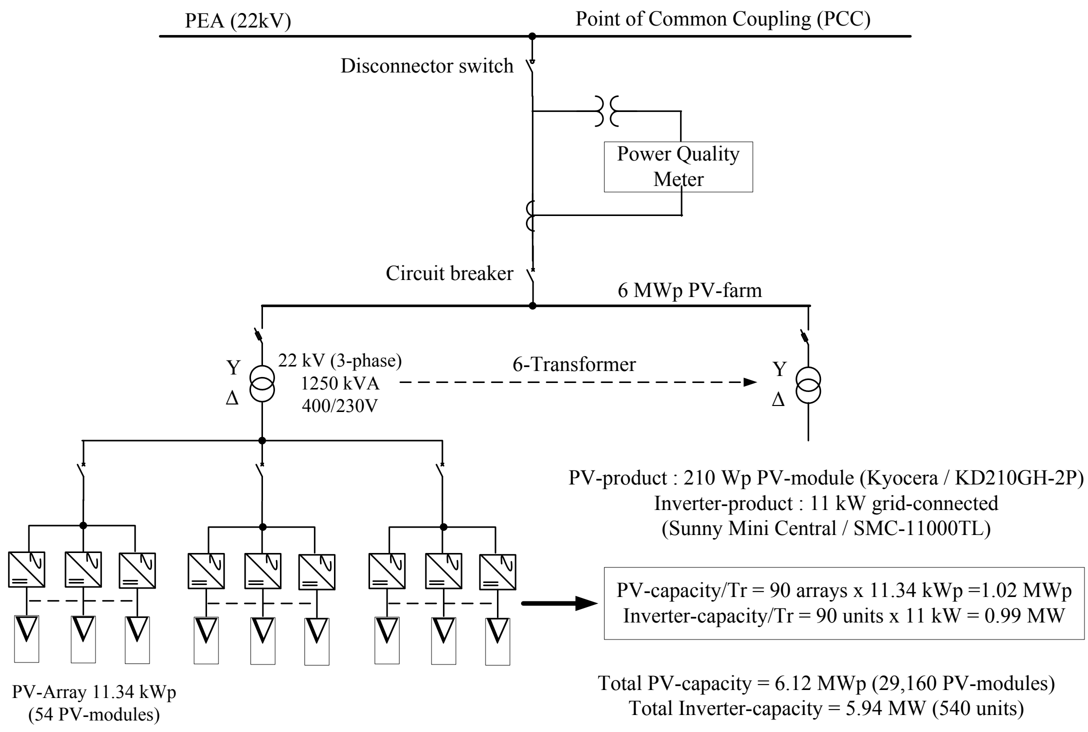

Figure 2.24 System schematic diagram of the PV farm

Harmonic current measurements are based on 540 units of 11 kW Sunny Mini C entral S MC-11000TL g rid-connected i nverter. Maximum i nverter out put current and total harmonic current distortion (THDi) at various solar radiation levels are shown in Figure 2.25.

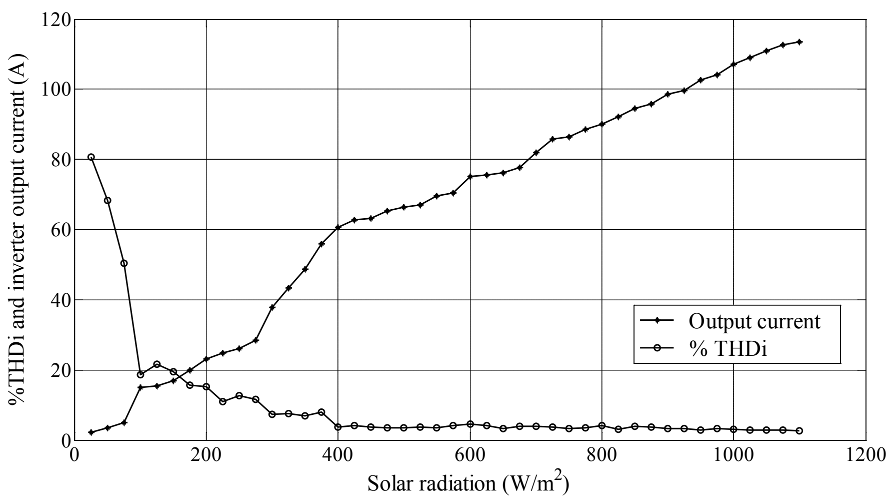

Figure 2.25 Maximum inverter output current and %THDi at various solar radiations

From Figure 2.25, it indicates that the THDi and output current of the inverter varied proportionally to the solar radiation. Furthermore, from the relationship of %THDi and solar radiation, nonlinearity of the inverter becomes large at low solar radiation. Under such conditions, the large amount of harmonics will be injected to a distribution system. Although, the magnitudes of harmonic currents are small at low solar radiation, but the % THDi is large. This may deteriorate the electrical power quality of systems, if the large number of PV-DGs is interconnected to a distribution system. In this dissertation, only harmonic current magnitudes are considered for worse-case study.

Figures 2.26 to 2.28 show some of harmonic spectrum up to 33rd order at PCC of the PV farm corresponding to solar radiation at 200, 600 and 1 000 W/m^2, respectively. The typical harmonic current in percent of fundamental (50 Hz) can be seen in Table 2.5.

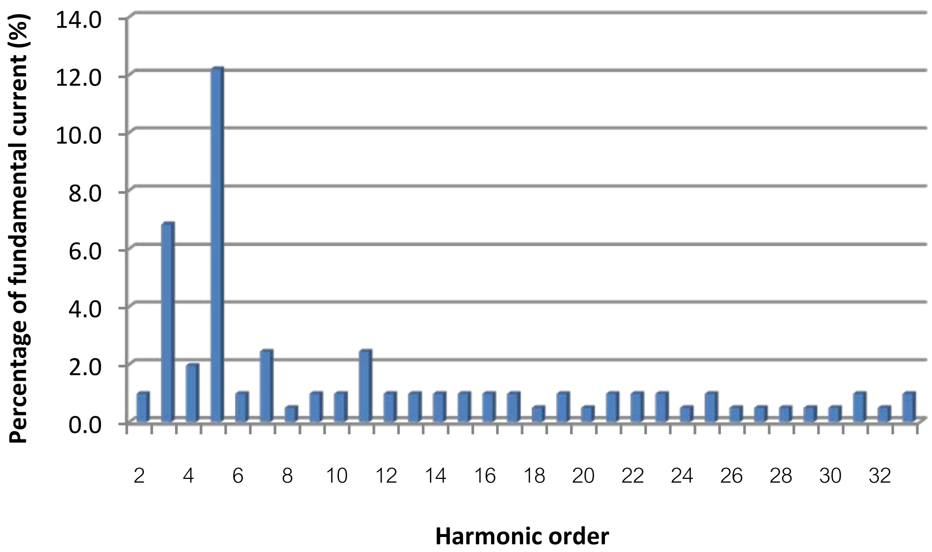

Figure 2.26 Harmonic current spectrum at PCC of the PV farm corresponding to 200 W/m^2 solar radiation

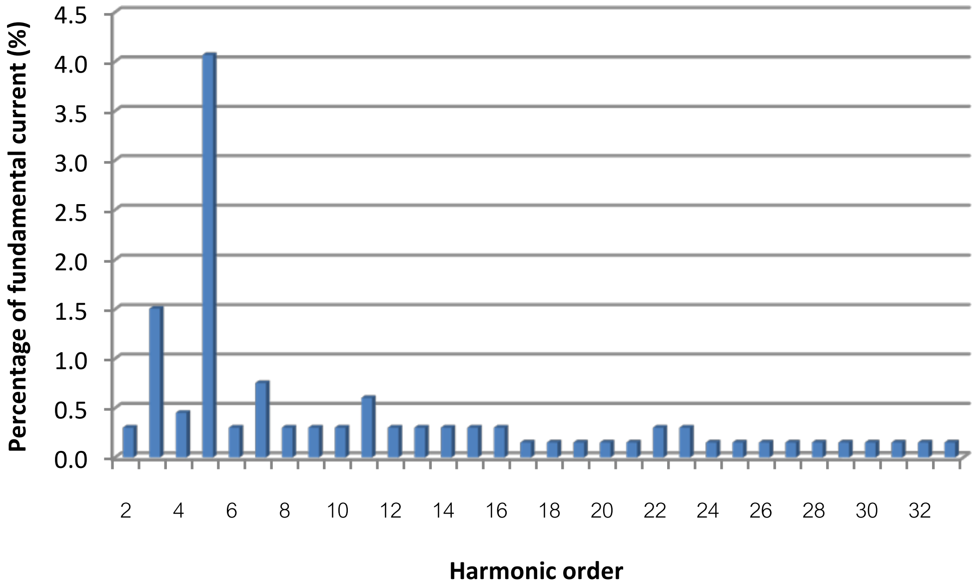

Figure 2.27 Harmonic current spectrum at PCC of the PV farm corresponding to 600 W/m^2 solar radiation

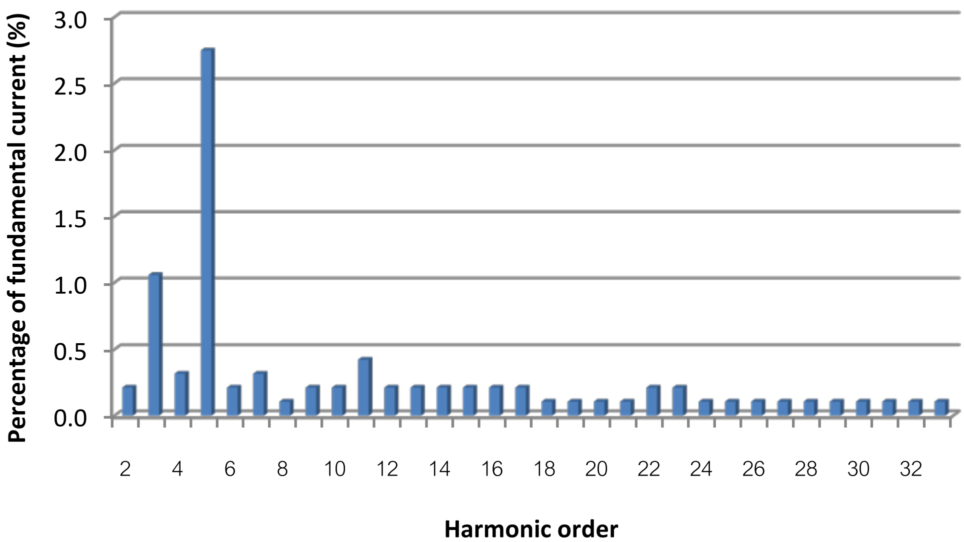

Figure 2.28 Harmonic current spectrum at PCC of the PV farm corresponding to 1000 W/m^2 solar radiation

Table 2.5 Typical harmonic current in percent of fundamental corresponding to solar radiation

Harmonic order	***Typical harmonic current in percent of fundamental (%)***		
	200 W/m^2	600 W/m^2	1000 W/m^2
2	0.976	0.301	0.211
3	6.829	1.506	1.057
4	1.951	0.452	0.317
5	12.195	4.066	2.748
6	0.976	0.301	0.211
7	2.439	0.753	0.317
8	0.488	0.301	0.106
9	0.976	0.301	0.211
10	0.976	0.301	0.211
11	2.439	0.602	0.423
12	0.976	0.301	0.211
13	0.976	0.301	0.211
14	0.976	0.301	0.211
15	0.976	0.301	0.211
16	0.976	0.301	0.211
17	0.976	0.151	0.211
18	0.488	0.151	0.106
19	0.976	0.151	0.106
20	0.488	0.151	0.106
21	0.976	0.151	0.106
22	0.976	0.301	0.211
23	0.976	0.301	0.211
24	0.488	0.151	0.106
25	0.976	0.151	0.106
26	0.488	0.151	0.106
27	0.488	0.151	0.106
28	0.488	0.151	0.106
29	0.488	0.151	0.106
30	0.488	0.151	0.106
31	0.976	0.151	0.106
32	0.488	0.151	0.106
33	0.976	0.151	0.106

In practical, interconnections of small PV-DGs may not result in violation of the power quality standard. However, with the existent of background harmonics and the increase of penetration level, PV-DGs may create harmonic currents which bring to excessive levels of total harmonic voltage distortion (THDv) at PCC. Therefore, prior to interconnect PV-DGs, utilities should consider several technical constraints to avoid the power quality impacts from PV-DGs. Background harmonics modeling will be mentioned in Chapter 4 on harmonic calculations section.

2.5 Substation and Load Modeling

Since, in order to find the optimal size of PV-DG without considering uncertainties of load and substation voltage may be questionable. Therefore, in probabilistic load flows process, load demand and substation voltage are assumed to be a random variable with a normal distribution.

2.5.1 Probabilistic Load Models

In this work, all loads are correlated and follow the same probability density function of load demands (L_d) as given by:

$$f(L_d) = \frac{1}{\sigma\sqrt{2\pi}} \exp - \frac{(L_d - \overline{L}_d)^2}{2\sigma^2} \tag{2.24}$$

where $\overline{L}_d$ is the mean value of load demand

σ is the standard deviation, which set to 10% in this dissertation

Generally, the classical constant power load model is typically used in power flow studies of a distribution system. However, the actual load of a distribution system cannot just be modeled using constant power model. The use of constant current, constant impedance or a composite of all these load models are required to accurately represent the load. Therefore, three static load models are investigated to study the impact of load model on optimal PV-DG sizing. Probability density function of all static load models follows normal distribution in Equation (2.24). These types of loads are typically categorized as follows [73]:

- *Constant Power Load Model (CP)* :

  The active and reactive powers do not vary with voltage magnitude changes.
- *Constant Current Load Model (CI)* :

  The active and reactive powers are directly proportional to the voltage magnitude.
- *Constant Impedance Load Model (CZ)* :

  The active and reactive powers are proportional to the square of voltage magnitude.

The active and reactive power characteristics of three static load models are given by:

$$P = P_0\left[a_p + b_p\left(\frac{|V|}{|V_0|}\right) + c_p\left(\frac{|V|}{|V_0|}\right)^2\right] \tag{2.25}$$

$$Q = Q_0\left[a_q + b_q\left(\frac{|V|}{|V_0|}\right) + c_q\left(\frac{|V|}{|V_0|}\right)^2\right] \tag{2.26}$$

where P_0 and Q_0 are active and reactive powers consumed at a reference voltage V_0, respectively. Constant coefficients depend on the type of load that is being represented, e.g.,

for CP model $a_p = a_q = 1, b_p = b_q = c_p = c_q = 0$
for CI model $b_p = b_q = 1, a_p = a_q = c_p = c_q = 0$
for CZ model $c_p = c_q = 1, a_p = a_q = b_p = b_q = 0$

Figure 2.29 illustrates an example of active power probability density function at a load point with a normal distribution, which $\bar{L}_d$ is 145 kW, and σ is 10%.

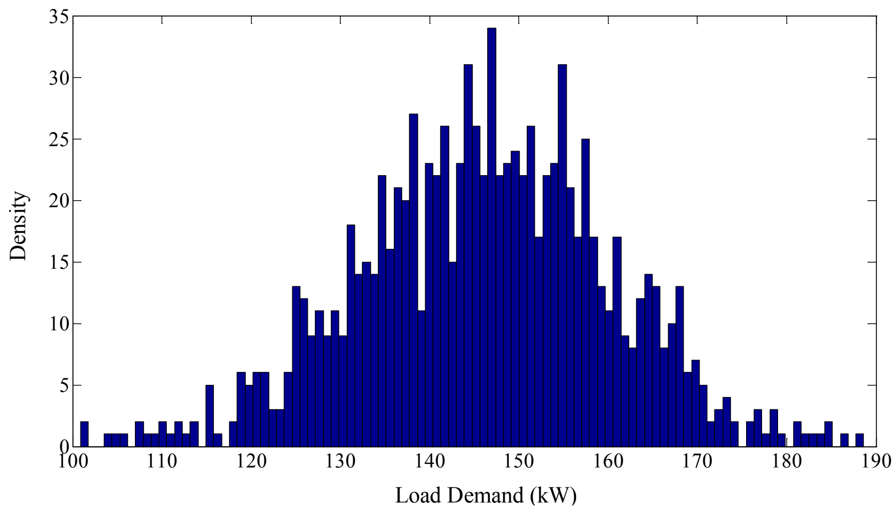

Figure 2.29 Probability density function of a load point with a normal distribution

2.5.2 Probabilistic Substation Voltage Model

Similarly to load models, substation voltage (V_S) is assumed to be a random variable with normal distribution. But the standard deviation of substation voltage is set to 1.5% to cover in 0.95 pu to 1.05 pu range of mean value ($\bar{V}_S$), which is assumed to be 1.0 pu. The probability density function of substation voltage illustrates in Figure 2.30 and it can be expressed mathematically as follow:

$$f(V_s) = \frac{1}{\sigma\sqrt{2\pi}} \exp - \frac{(V_s - \bar{V}_s)^2}{2\sigma^2} \tag{2.27}$$

where $\bar{V}_s$ is the mean value of substation voltage

σ is the standard deviation, which set to 1.5% in this dissertation

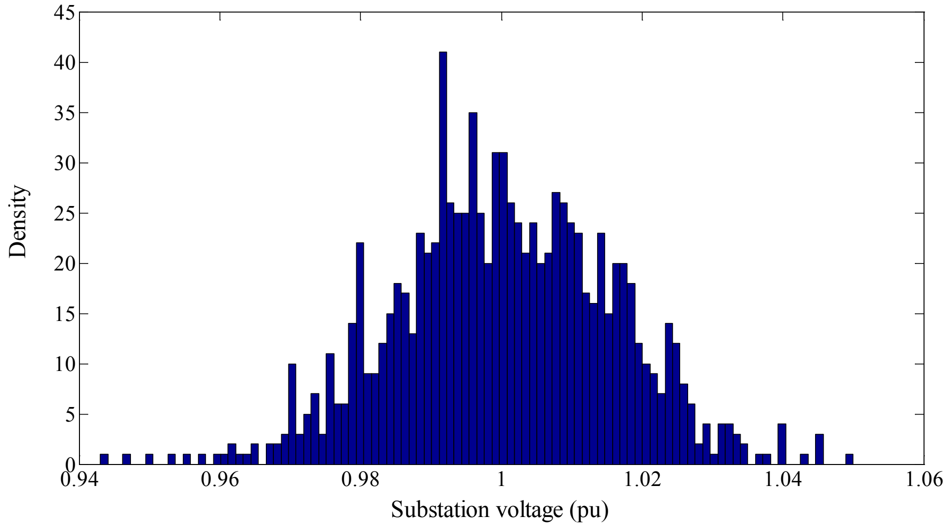

Figure 2.30 Probability density function of substation voltage with a normal distribution

CHAPTER III
A VOLTAGE STABILITY INDEX FOR RADIAL DISTRIBUTION NETWORKS

3.1 Introduction

In practice, utilities cannot assign the PV-DGs installation location to be connected to the feeder because it mainly depends on customers who own the PV systems. However, for planning aspect, this chapter presents a voltage stability index (VSI) for identifying the most sensitive bus to the voltage collapse in a radial distribution network for selecting the proper PV-DG located.

With an increased loading and exploitation of the existing power structure, the probability of occurrence of voltage collapse is significantly greater than before and the identification of the nodes which are prone to the voltage fluctuations has attracted more attention for the transmission and as well as the distribution systems. The main causes of voltage instability are as follows:

- The load on transmission line is too high
- The voltage sources are too far from the load centers
- The voltage sources are too low
- There is insufficient load reactive compensation

For operating a power system in a safe and secure manner, all insecure operating states must be identified well in advance to facilitate corrective measures to overcome the threat of possible voltage collapse [74].

3.2 Voltage Stability Index Methodology [75]

For deriving the voltage stability index of radial distribution networks, we need to consider a simple two-node system as shown in Figure 3.1.

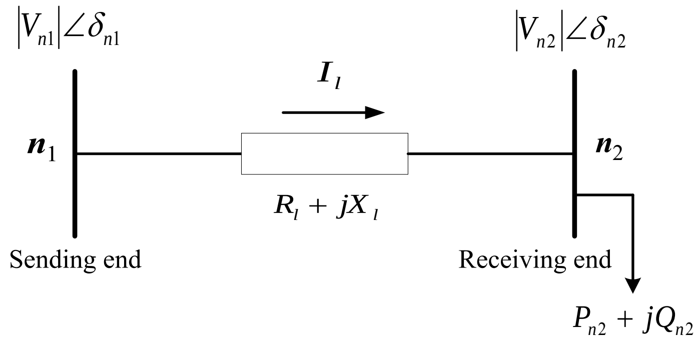

Figure 3.1 Simple two-node system

From Figure 3.1, the following equations can be written:

$$I_l = \frac{|V_{n1}|\angle\delta_{n1} - |V_{n2}|\angle\delta_{n2}}{R_l + jX_l} \tag{3.1}$$

and
$$I_l = \frac{P_{n2} - jQ_{n2}}{V_{n2}^*} \tag{3.2}$$

where l is branch number

n_1 is branch end node

n_2 is receiving end node

I_l is current of branch l

V_{n1} is voltage of node n_1

V_{n2} is voltage of node n_2

P_{n2} is total active power load fed through node n_2

Q_{n2} is total reactive power load fed through node n_2

From Equations (3.1) and (3.2), we obtain:

$$\frac{|V_{n1}|\angle\delta_{n1} - |V_{n2}|\angle\delta_{n2}}{R_l + jX_l} = \frac{P_{n2} - jQ_{n2}}{V_{n2}^*} \tag{3.3}$$

therefore
$$|V_{n1}||V_{n2}|\angle(\delta_{n1} - \delta_{n2}) - |V_{n2}|^2 = (P_{n2} - jQ_{n2})(R_l + jX_l) \tag{3.4}$$

and

$$|V_{n1}||V_{n2}|\cos(\delta_{n1} - \delta_{n2}) - |V_{n2}|^2 + j|V_{n1}||V_{n2}|\sin(\delta_{n1} - \delta_{n2})$$
$$= (P_{n2}R_l + Q_{n2}X_l) + j(P_{n2}X_l - Q_{n2}R_l) \tag{3.5}$$

Separating real and imaginary parts of Equation (3.5), we obtain:

$$|V_{n1}||V_{n2}|\cos(\delta_{n1}-\delta_{n2})-|V_{n2}|^2 = P_{n2}R_l + Q_{n2}X_l \tag{3.6}$$

therefore
$$|V_{n1}||V_{n2}|\cos(\delta_{n1}-\delta_{n2}) = |V_{n2}|^2 + P_{n2}R_l + Q_{n2}X_l \tag{3.7}$$

and
$$|V_{n1}||V_{n2}|\sin(\delta_{n1}-\delta_{n2}) = P_{n2}X_l - Q_{n2}R_l \tag{3.8}$$

Squaring and adding Equations (3.7) and (3.8), we obtain:

$$|V_{n1}|^2|V_{n2}|^2 = \left(|V_{n2}|^2 + P_{n2}R_l + Q_{n2}X_l\right)^2 + \left(P_{n2}X_l - Q_{n2}R_l\right)^2 \tag{3.9}$$

From algebraic formula:

$$(a+b+c)^2 = a^2 + b^2 + c^2 + 2(ab+bc+ac) \tag{3.10}$$

We can rearrange Equation (3.9) to

$$|V_{n2}|^4 + 2\left(P_{n2}R_l + Q_{n2}X_l - 0.5|V_{n1}|^2\right)|V_{n2}|^2 + \left(R_l^2 + X_l^2\right)\left(P_{n2}^2 + Q_{n2}^2\right) = 0 \tag{3.11}$$

or
$$|V_{n2}|^4 - \left(|V_{n1}|^2 - 2P_{n2}R_l - 2Q_{n2}X_l\right)|V_{n2}|^2 + \left(P_{n2}^2 + Q_{n2}^2\right)\left(R_l^2 + X_l^2\right) = 0 \tag{3.12}$$

Equation (3.12) has a straightforward solution and does not depend on the phase angle, which simplifies the problem formulation. In a distribution system, the voltage angle is not so important because the variation of voltage angle from the substation to the tail-end of a distribution feeder is only few degrees [76].

Let
$$b_l = \left(|V_{n1}|^2 - 2P_{n2}R_l - 2Q_{n2}X_l\right) \tag{3.13}$$

and
$$c_l = \left(P_{n2}^2 + Q_{n2}^2\right)\left(R_l^2 + X_l^2\right) \tag{3.14}$$

From Equations (3.12) to (3.14), we get

$$|V_{n2}|^4 - b_l|V_{n2}|^2 + c_l = 0 \tag{3.15}$$

From Equation (3.15), it is seen that the receiving end voltage $|V_{n2}|$ has four solutions follow to a given formulation:

$$|V_{n2}| = \pm\sqrt{\frac{-b \pm \sqrt{b^2 - 4ac}}{2a}} \tag{3.16}$$

and these solutions are:

1. $0.707\sqrt{b_l - \sqrt{b_l^2 - 4c_l}}$

2. $-0.707\sqrt{b_l - \sqrt{b_l^2 - 4c_l}}$

3. $-0.707\sqrt{b_l + \sqrt{b_l^2 - 4c_l}}$

4. $0.707\sqrt{b_l + \sqrt{b_l^2 - 4c_l}}$

Now, for realistic data, when *P, Q, R, X* and *V* are expressed in per unit, b_l is always positive because the term $2\{P_{n2}R_l + Q_{n2}X_l\}$ is very small as compared to $|V_{n1}|^2$ and also the term $4c_l$ is very small as compared to b_l^2. Therefore, $\sqrt{b_l^2 - 4c_l}$ is nearly equal to b_l and hence the first two solutions of $|V_{n2}|$ are nearly equal to zero and not feasible. The third solution is negative and so not feasible. The fourth solution of $|V_{n2}|$ is positive and feasible. Therefore, the solution of Equation (3.15) is unique.

That is
$$|V_{n2}| = 0.707\sqrt{b_l + \sqrt{b_l^2 - 4c_l}} \tag{3.17}$$

From Equation (3.17), it is seen that a feasible load flow solution of radial distribution networks will exist if:

$$b_l^2 - 4c_l \geq 0 \tag{3.18}$$

Thus, from Equations (3.13), (3.14) and (3.18), we get

$$\left(|V_{n1}|^2 - 2P_{n2}R_l - 2Q_{n2}X_l\right)^2 - 4\left(P_{n2}^2 + Q_{n2}^2\right)\left(R_l^2 + X_l^2\right) \geq 0 \tag{3.19}$$

After simplification we get

$$|V_{n1}|^4 - 4\left(P_{n2}X_l - Q_{n2}R_l\right)^2 - 4\left(P_{n2}R_l + Q_{n2}X_l\right)|V_{n1}|^2 \geq 0 \tag{3.20}$$

Let

$$VSI(n_2) = |V_{n1}|^4 - 4\left(P_{n2}X_l - Q_{n2}R_l\right)^2 - 4\left(P_{n2}R_l + Q_{n2}X_l\right)|V_{n1}|^2 \tag{3.21}$$

where $VSI(n_2)$ is voltage stability index of node n_2 , for stable operation of the radial distribution networks, $VSI(n_2) \geq 0$ for $n_2 = 2,3,....,N_b$

By using this voltage stability index, one can measure the level of stability of radial distribution networks and thereby appropriate action may be taken if the index indicates a poor level of stability.

Actually, P_{n2} and Q_{n2} are sum of the active and reactive power loads of all the nodes beyond node n_2 plus the active and reactive power load of node n_2 itself plus the sum of the active and reactive power losses of all the branches beyond node n_2.

After load flow calculation, when the load was increased gradually, the voltages of all nodes are known, the branch currents are known. Therefore, P_{n2} and Q_{n2} for $n_2 = 2,3,....,N_b$ can easily be calculated using Equation (3.2) and hence one can easily calculate the voltage stability index of each node. The node at which the value of the stability index is minimum, is more sensitive to the voltage collapse and more candidate to install PV-DG.

In this dissertation, load flow analysis was achieved by using the load flow algorithm given in Chapter 4 in which each nodes power is multiplied by a load factor as [74]:

$$S = \lambda\ S_b \tag{3.22}$$

where λ is load factor and S_b is base load

The critical bus identified by evaluating bus voltage magnitudes just before the load flow diverges. Divergence is assumed when the iteration number of the load flow algorithm reaches to 200. The algorithm of voltage stability index calculation can be summarized as seen the flow chart in Figure 3.2.

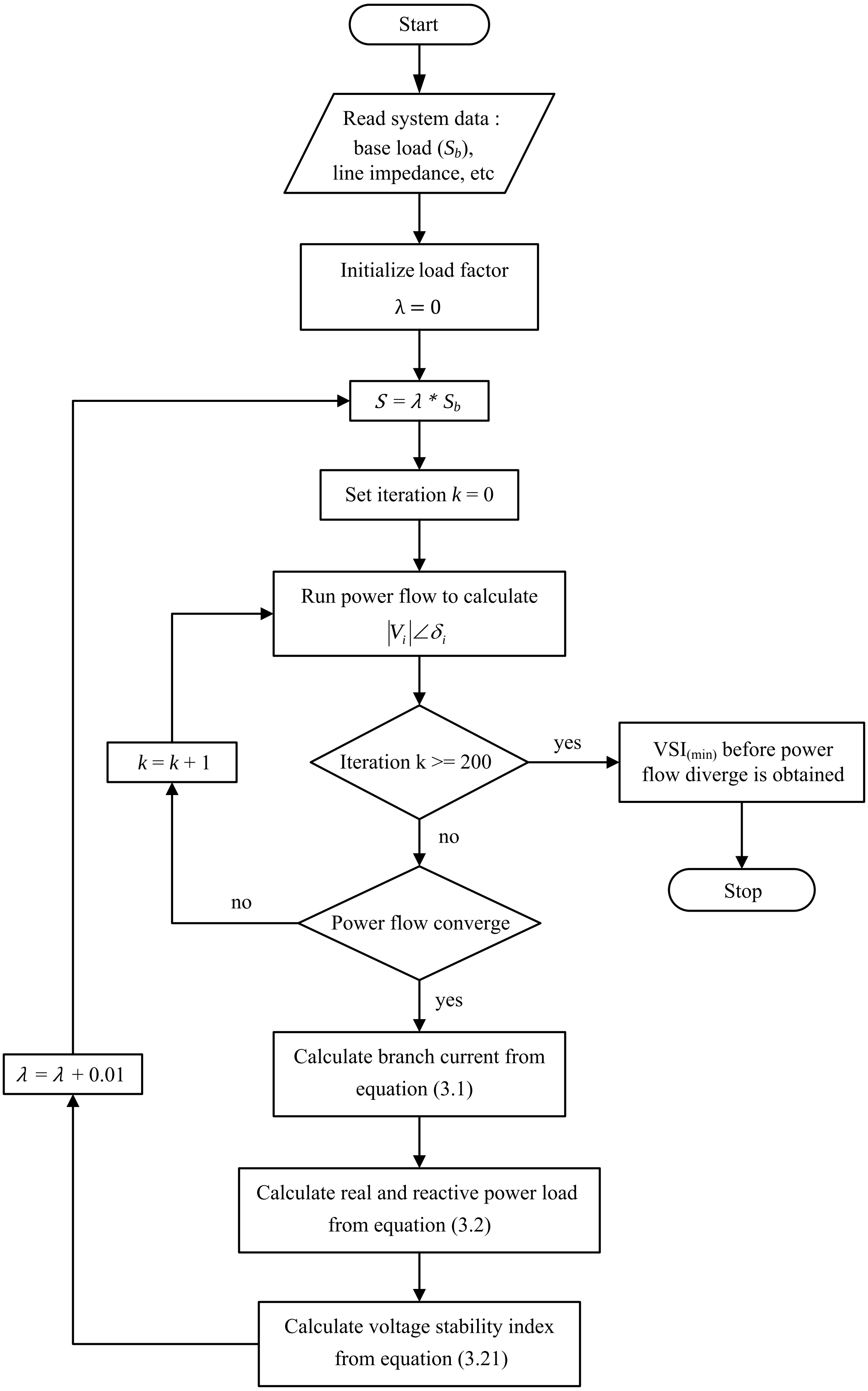

Figure 3.2 Flow chart of voltage stability index calculation

3.3 Test Results of Voltage Stability Index Calculation

To demonstrate the methodology of the voltage stability index (VSI), this section presents a 15-bus radial distribution system from [77] for VSI calculation. The single-line diagram of the 15-bus test system is shown in Figure 3.3. Line and load data of this system are given in Table 3.1.

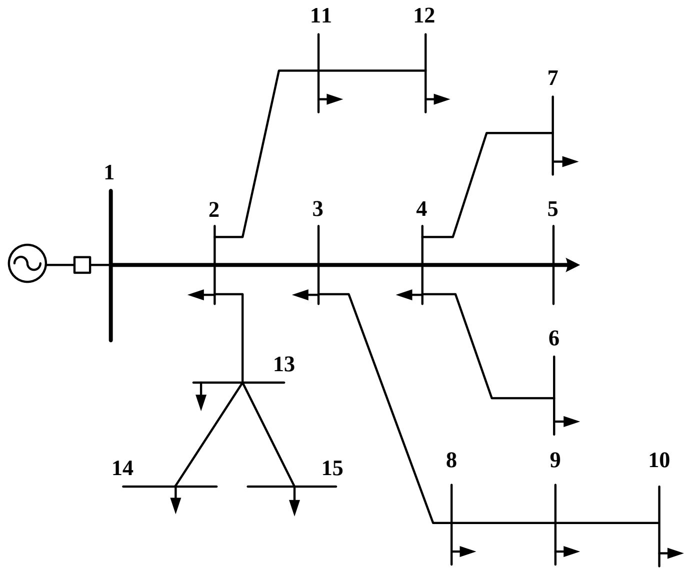

Figure 3.3 Single-line diagram of the 15-bus radial distribution system

Table 3.1 Line data and load data of the 15-bus radial distribution system

Branch	***Line impedance (ohm)***		***Load demand (kW/kVar)***	
	R	***X***	P_L	Q_L
1 – 2	1.35309	1.32349	44.10	44.99
2 – 3	1.17024	1.14464	70.00	71.41
3 – 4	0.84111	0.82271	140.00	142.82
4 – 5	1.52348	1.02760	44.10	44.99
4 – 6	1.19702	0.80740	140.00	142.82
4 – 7	2.23081	1.50470	70.00	71.41
3 – 8	1.79553	1.21110	140.00	142.82
8 – 9	2.44845	1.65150	70.00	71.41
9 – 10	2.01317	1.35790	44.10	44.99
2 – 11	2.01317	1.35790	70.00	71.41
11- 12	1.68671	1.13770	44.10	44.99
2 – 13	2.55727	1.72490	140.00	142.82
13 – 14	1.08820	0.73400	140.00	142.82
13 – 15	1.25143	0.84410	70.00	71.41

Total base load = 1.226 MW, 1.251 MVar

For this simulation, a different magnitude substation voltages $(|V_s|)$ and different static load models of constant power (CP), constant current (CI) and constant impedance (CZ) are considered. Table 3.2 shows bus stability indices and its minimum bus voltage for different load models and substation voltage 1.0 pu of the 15-bus test system.

Table 3.2 Bus stability indices for different load models of the 15-bus test system ($|V_s| = 1.0 \ pu$)

Bus No.	***CP model***		***CI model***		***CZ model***	
	VSI	**$\|V_{min}\|$ pu**	**VSI**	**$\|V_{min}\|$ pu**	**VSI**	**$\|V_{min}\|$ pu**
2	0.2042	0.7259	0.3259	0.7854	0.4841	0.8479
3	0.0936	0.5737	0.1991	0.6768	0.3505	0.7731
4	0.0679	0.5140	0.1600	0.6339	0.3048	0.7436
5	0.0644	0.5038	0.1541	0.6266	0.2975	0.7385
6	0.0563	0.4879	0.1434	0.6156	0.2855	0.7311
7	0.0572	0.4897	0.1446	0.6169	0.2868	0.7319
8	0.0600	0.5004	0.1523	0.6268	0.2971	0.7391
9	0.0411	0.4528	0.1257	0.5963	0.2663	0.7187
10	0.0365	0.4374	0.1183	0.5866	0.2572	0.7122
11	0.2407	0.7009	0.3334	0.7603	0.4707	0.8285
12	0.2302	0.6927	0.3200	0.7522	0.4572	0.8223
13	0.1310	0.6126	0.2139	0.6873	0.3590	0.7774
14	0.1234	0.5930	0.2021	0.6707	0.3431	0.7655
15	0.1308	0.6015	0.2109	0.6778	0.3523	0.7705

From Table 3.2, when the load is increased gradually, it founds that the minimum value of voltage stability index is occurring at bus-10 for all types of load models. It is also observed that bus 10 has the minimum voltage.

Table 3.3 shows critical bus index value and its bus voltage of the 15-bus test system for different substation voltage and different static load models. The system loads are increased from zero to the critical loading point by multiplying each node active and reactive power by a load factor lambda (λ) as 0.01 times of its previous value in each step for all loads. Note from Table 3.3 that, for all loading conditions, minimum stability index value is observed of the bus 10.

Table 3.3 Critical bus stability index value for different types of load and substation voltage

Load model	*Substation voltage (pu)*	*Critical loading condition*	
		$VSI_{min} = VSI_{10}$	$\|V_{min}\|$ pu
CP	0.95	0.0296	0.4152
	1.00	0.0365	0.4374
	1.05	0.0433	0.4566
CI	0.95	0.1151	0.5825
	1.00	0.1183	0.5866
	1.05	0.1730	0.6450
CZ	0.95	0.2104	0.6773
	1.00	0.2582	0.7129
	1.05	0.3139	0.7485

Figures 3.4 and 3.5 show the variations of the critical bus index value at bus-10 and its bus voltages with the increase of the system loads for different load models, substation voltage 1.0 pu. Points A, B and C indicate the critical loading point beyond which a small increment of load causes the voltage collapse.

From Figures 3.4 and 3.5, it is seen that the critical bus index value decrease with the increase of the system load, and it closes to zero when system's total power closes to the critical loading point. From the each loading conditions, it is observed that the critical bus indices are always at the minimum. Moreover, it is also observed that the different load models cause only different stability index value and bus voltage magnitudes, it does not affect the critical bus number of the test system.

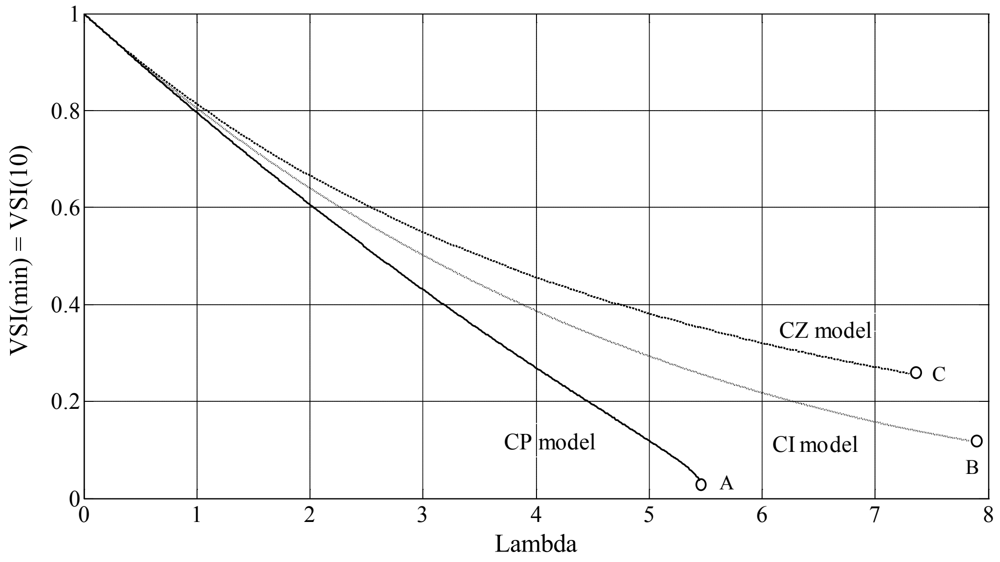

Figure 3.4 Variation of critical bus stability index value with system load for different static load models

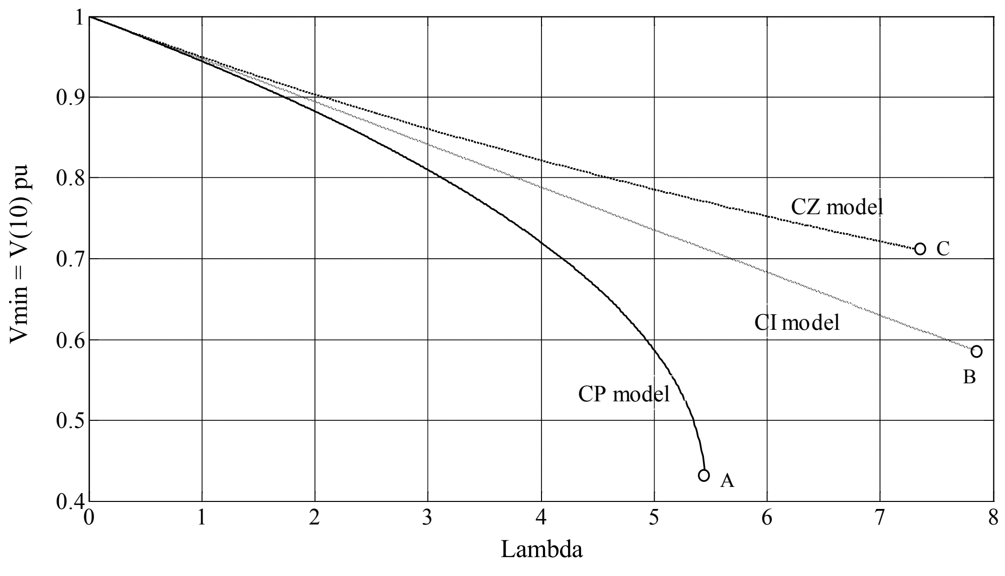

Figure 3.5 Variation of critical minimum bus voltage with system load for different static load models

Similarly, Figures 3.6 and 3.7 show the variations of the critical bus index value at bus-10 and its bus voltages with the increase of the system loads for different substation voltage, constant power load model. Points A, B and C indicate the critical loading point beyond which a small increment of load causes the voltage collapse.

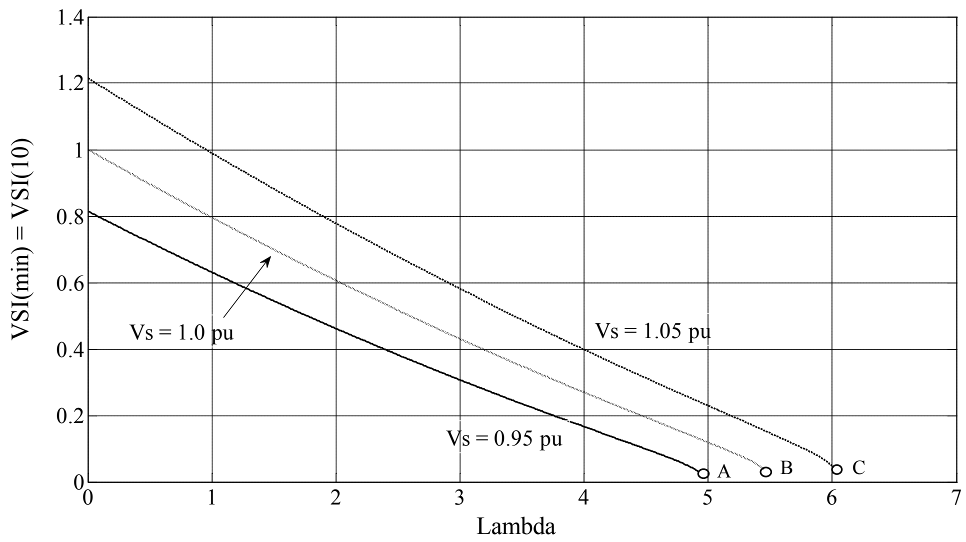

Figure 3.6 Variation of critical bus stability index value with system load for different substation voltages

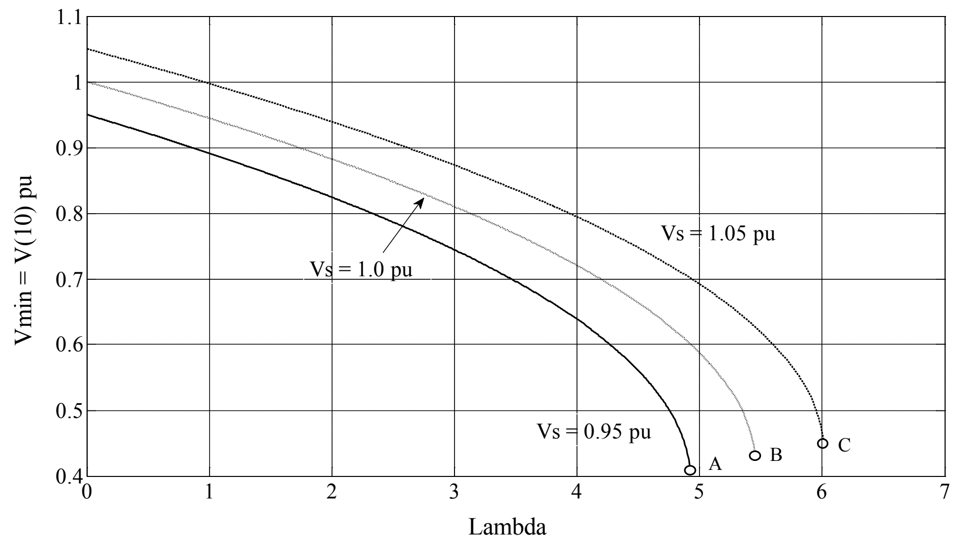

Figure 3.7 Variation of critical minimum bus voltage with system load for different substation voltages

From simulation results, in this case, it can summarize that the stability index and consequently, the voltage are minimum for constant power load and maximum for constant impedance load and that for constant current load is in between these two, as seen in Table 3.3.

Finally, if we have a planning to install PV-DG in this system, the most candidate bus is bus-10 based on the voltage stability index.

CHAPTER IV

RADIAL DISTRIBUTION SYSTEM POWER FLOW AND HARMONIC CALCULATION

4.1 Introduction

In practical, configurations of a distribution system have been high r/x ratio (ill-condition) which deteriorates the diagonal dominance of the Jacobian matrix. Therefore, the conventional Newton's power flow method may be divergence in some case. Therefore, this chapter presents a modified Newton method from [78] to solve the problem. Furthermore, harmonic modeling and harmonic calculation in a distribution system are mentioned.

A modified Newton method is utilized to solve the power flow for a radial distribution system without reducing the problem size, yet still capable of achieving robust convergence and high efficiency. This method is derived a Newton formulation where the Jacobian matrix is in UDU^T form, where U is a constant upper triangular matrix depending solely on system topology and D is a block diagonal matrix resulting from the radial structure and special properties of the distribution system.

With this formulation, the conventional Newton algorithm of forming the Jacobian matrix, LU factorization and forward back substitution can be replaced by back/forward sweeps on radial feeders with equivalent impedances.

4.2 The Modified Newton Method

In conventional Newton method [79], the equation to solve power flow problem for $\Delta\theta$ and ΔV is expressed in Equation (4.1).

$$\begin{bmatrix} H & N \\ J & L \end{bmatrix} \begin{bmatrix} \Delta\theta \\ \Delta V / V \end{bmatrix} = \begin{bmatrix} \Delta P \\ \Delta Q \end{bmatrix} \tag{4.1}$$

where

$$H_{ij} = -V_i V_j \left(G_{ij} \sin\theta_{ij} - B_{ij} \cos\theta_{ij} \right) \qquad j \neq i \tag{4.2}$$

$$H_{ii} = V_i \sum_{j \in i, j \neq i} V_j \left(G_{ij} \sin\theta_{ij} - B_{ij} \cos\theta_{ij} \right) \tag{4.3}$$

$$N_{ij} = -V_i V_j \left(G_{ij} \cos\theta_{ij} + B_{ij} \sin\theta_{ij} \right) \qquad j \neq i \tag{4.4}$$

$$N_{ii} = -V_i \sum_{j \in i, j \neq i} V_j \left(G_{ij} \cos\theta_{ij} + B_{ij} \sin\theta_{ij} \right) - 2V_i^2 G_{ii} \tag{4.5}$$

$$J_{ij} = V_i V_j \left(G_{ij} \cos\theta_{ij} + B_{ij} \sin\theta_{ij} \right) \qquad j \neq i \tag{4.6}$$

$$J_{ii} = -V_i \sum_{j \in i, j \neq i} V_j \left(G_{ij} \cos\theta_{ij} + B_{ij} \sin\theta_{ij} \right) \tag{4.7}$$

$$L_{ij} = -V_i V_j \left(G_{ij} \sin\theta_{ij} - B_{ij} \cos\theta_{ij} \right) \qquad j \neq i \tag{4.8}$$

$$L_{ii} = -V_i \sum_{j \in i, j \neq i} V_j \left(G_{ij} \sin\theta_{ij} - B_{ij} \cos\theta_{ij} \right) + 2V_i^2 B_{ii} \tag{4.9}$$

Term $G_{ij} + jB_{ij}$ is the entry of nodal admittance matrix. Under assumption the voltage difference between two adjacent nodes is small $(\sin\theta_{ij} \approx 0)$ as well as term $G_{ii} + jB_{ii} = -\sum_{j \in i, j \neq i} \left(G_{ij} + jB_{ij} \right)$. Thus the Jacobian matrix can be approximated as:

$$H_{ij} \approx V_i V_j B_{ij} \cos\theta_{ij} \qquad j \neq i \tag{4.10}$$

$$H_{ii} \approx -V_i \sum_{j \in i, j \neq i} V_j B_{ij} \cos\theta_{ij} \tag{4.11}$$

$$N_{ij} \approx -V_i V_j G_{ij} \cos\theta_{ij} \qquad j \neq i \tag{4.12}$$

$$N_{ii} \approx V_i \sum_{j \in i, j \neq i} V_j G_{ij} \cos\theta_{ij} \tag{4.13}$$

$$J_{ij} \approx V_i V_j G_{ij} \cos\theta_{ij} \qquad j \neq i \tag{4.14}$$

$$J_{ii} \approx -V_i \sum_{j \in i, j \neq i} V_j G_{ij} \cos\theta_{ij} \tag{4.15}$$

$$L_{ij} \approx V_i V_j B_{ij} \cos\theta_{ij} \qquad j \neq i \tag{4.16}$$

$$L_{ii} \approx -V_i \sum_{j \in i, j \neq i} V_j B_{ij} \cos\theta_{ij} \tag{4.17}$$

Equations (4.10) to (4.17) show that matrices H, N, J and L all have the same properties (symmetry, sparsity pattern) as the Nodal Admittance Matrix, hence they can be formed as:

$$H = L = A_{n-1} D_B A_{n-1}^T \tag{4.18}$$

$$J = -N = A_{n-1} D_G A_{n-1}^T \tag{4.19}$$

where D_B and D_G are diagonal matrices with diagonal entries to be:

$$D_B = V_i V_j B_{ij} \cos\theta_{ij} \tag{4.20}$$

$$D_G = V_i V_j G_{ij} \cos\theta_{ij} \tag{4.21}$$

and A_{n-1} is node to branch incidence matrix, defined as:

$$A_{ij} = \begin{cases} 1, & \textit{if brance } j \textit{ is directed away from node } i \\ -1, & \textit{if brance } j \textit{ is directed towards node } i \\ 0, & \textit{if brance } j \textit{ is not incident to node } i \end{cases}$$

For a radial distribution system with n nodes and without shunt branches, the num ber of br anches i s n -1. Also b y know ing t he noda l vol tage at one node , assuming it is the first node for convenience. Hence, there are remaining n-1 unknown nodal voltages and we obtain matrix A_{n-1} is a square matrix, which its dimension is (n-1) $\times$(n-1).

Furthermore, if nodes and branches are ordered appropriately, A_{n-1} is an upper triangular matrix with all diagonal entries to be 1 and all non-zero off-diagonal entries to be -1. One way to achieve such an A_{n-1} is ordering branches by layers away from t he r oot node (source node o r r eference node) as s een in Figure 4.1. T he direction of each branch i s t owards t he r oot nod e. T he node or dering i s pr oceeded simultaneously with the branch ordering. Note from Figure 4.1 t hat the branch from side node number is the same as the branch number. And the node to branch incident matrix of it is given in Equation (4.22).

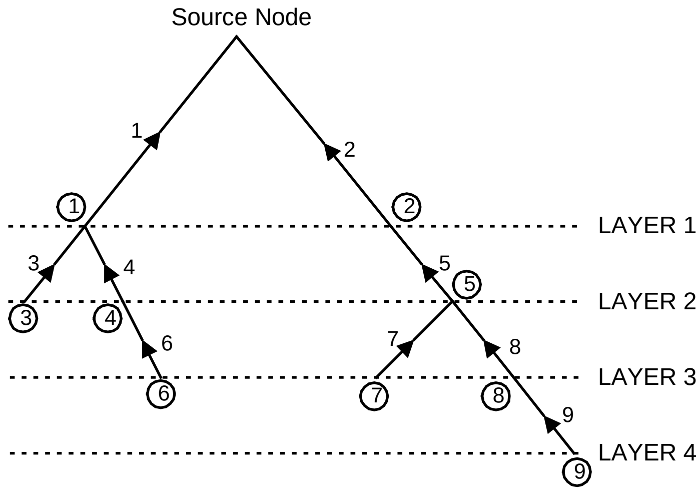

Figure 4.1 A simple radial distribution system with 10-nodes and 9-branches

$$A_{n-1} = \begin{bmatrix} 1 & 0 & -1 & -1 & 0 & 0 & 0 & 0 & 0 \\ & 1 & 0 & 0 & -1 & 0 & 0 & 0 & 0 \\ & & 1 & 0 & 0 & 0 & 0 & 0 & 0 \\ & & & 1 & 0 & -1 & 0 & 0 & 0 \\ & & & & 1 & 0 & -1 & -1 & 0 \\ & & & & & 1 & 0 & 0 & 0 \\ & & & & & & 1 & 0 & 0 \\ & & & & & & & 1 & -1 \\ & & & & & & & & 1 \end{bmatrix} \tag{4.22}$$

From Equations (4.18) and (4.19), thus Equation (4.1) can be rewritten as:

$$\begin{bmatrix} A_{n-1} & \\ & A_{n-1} \end{bmatrix} \begin{bmatrix} D_B & -D_G \\ D_G & D_B \end{bmatrix} \begin{bmatrix} A_{n-1}^T & \\ & A_{n-1}^T \end{bmatrix} \begin{bmatrix} \Delta\theta \\ \Delta V/V \end{bmatrix} = \begin{bmatrix} \Delta P \\ \Delta Q \end{bmatrix} \tag{4.23}$$

ΔP and ΔQ are vector of real and reactive node power mismatches respectively, which can be expressed as:

$$\Delta P_i = P_{i(scheduled)} - P_{i(cal)} \qquad i \neq reference\ node \tag{4.24}$$

$$= [P_{i(gen)} - P_{i(load)}] - P_{i(cal)}$$

$$\Delta Q_i = Q_{i(scheduled)} - Q_{i(cal)} \qquad i \neq reference\ node \tag{4.25}$$

$$= [Q_{i(gen)} - Q_{i(load)}] - Q_{i(cal)}$$

where

ΔP_i and ΔQ_i are vector of real and reactive node power mismatches at node *i*

$P_{i(gen)}$ and $Q_{i(gen)}$ are real and reactive node power generation at node *i*

$P_{i(load)}$ and $Q_{i(load)}$ are real and reactive node power load at node *i*

$P_{i(cal)}$ and $Q_{i(cal)}$ are net real and reactive node power load at node *i*

The expression for the net real and reactive node power, $P_{i(cal)}$ and $Q_{i(cal)}$ are

$$P_{i(cal)} = V_i \sum_{j=1}^{n} V_j \left[G_{ij} \cos\theta_{ij} + B_{ij} \sin\theta_{ij} \right] \tag{4.26}$$

$$Q_{i(cal)} = V_i \sum_{j=1}^{n} V_j \left[G_{ij} \sin\theta_{ij} - B_{ij} \cos\theta_{ij} \right] \tag{4.27}$$

where

V_i , V_j are voltage magnitude at node *i* and *j*

θ_i , θ_j are voltage phase angle at node *i* and *j*

G_{ij} , B_{ij} are elements of bus admittance matrix $\left[Y_{bus} \right]$

$\theta_{ij} = \theta_i - \theta_j$

$Y_{ij} = G_{ij} + jB_{ij}$

It has been shown that the Jacobian matrix can be formed as the product of three square matrices in Equations (4.23). Next will showing the Equation (4.23) can be solved by back/forward sweeps. Let's define:

$$E = \Delta\theta + j\,\Delta V/V \tag{4.28}$$

$$S = \Delta P + j\Delta Q \tag{4.29}$$

$$W = D_B + jD_G \tag{4.30}$$

then equation (4.23) can be written as

$$A_{n-1}\, W\, A_{n-1}^{T}\, E = S \tag{4.31}$$

or

$$A_{n-1}\, S_L = S \tag{4.32}$$

$$W\, A_{n-1}^{T}\, E = S_L \tag{4.33}$$

where Equation (4.32) is the back sweep and Equation (4.33) is the forward sweep.

To solve E in Equation (4.33) in forward sweep ($A_{n-1}^{T}E = W^{-1}S_L$), the diagonal matrix W can be inverted for each line. The diagonal in W^{-1} is denoted as the equivalent line impedance:

$$Z_{eq,ij} = R_{eq,ij} + jX_{eq,ij} \tag{4.34}$$

where

$$R_{eq,ij} = \frac{X_{ij}}{V_i V_j \cos\theta_{ij}} \tag{4.35}$$

$$X_{eq,ij} = \frac{R_{ij}}{V_i V_j \cos\theta_{ij}} \tag{4.36}$$

R_{ij} and X_{ij} are resistance and reactance of line *i-j* respectively. The Diagonal matrix W^{-1} is a square matrix, which its dimension is (n-1) $\times$(n-1).

In order to find the power flow solution, the power flow process has finished when power mismatch of both real and reactive power should be corresponding to:

$$\max\left|\Delta P^k\right| \ and \ \max\left|\Delta Q^k\right| \le \varepsilon \tag{4.37}$$

where

$\max\left|\Delta P^k\right|$ is maximum real power mismatch for any iteration k

$\max\left|\Delta Q^k\right|$ is maximum reactive power mismatch for any iteration k

ε is power mismatch tolerance which set to 10^{-5}

4.2.1 Loss Equations From System Data

Generally, the system real and reactive power loss can be derived into two sets of loss equations i.e., loss equations in terms of Y_{bus} and I_{bus}, and loss equations in terms of Z_{bus} and V_{bus}. The following two sets of loss equations are derived in exactly the same manner, which results in the identical forms for partial derivative equations.

In this dissertation, loss equations in term of Z_{bus} and V_{bus} is used to obtain system real power loss in probabilistic power flow calculation. However, the derivation of two sets of loss equations can be found in [80]. The loss equations in term of Z_{bus} and V_{bus} can be expressed by:

$$P_L = \sum_{i=1}^{N_b}\sum_{k=1}^{N_b}\left[(P_iP_k + Q_iQ_k)\alpha_{ik} + (P_iQ_k - Q_iP_k)\beta_{ik}\right] \quad (4.38)$$

and

$$Q_L = \sum_{i=1}^{N_b}\sum_{k=1}^{N_b}\left[(P_iP_k + Q_iQ_k)\tau_{ik} + (P_iQ_k - Q_iP_k)\theta_{ik}\right] \quad (4.39)$$

by defined

$$\alpha_{ik} = \frac{R_{ik}}{V_iV_k}\cos\delta_{ik} \quad (4.40)$$

$$\beta_{ik} = \frac{-R_{ik}}{V_iV_k}\sin\delta_{ik} \quad (4.41)$$

$$\tau_{ik} = \frac{X_{ik}}{V_iV_k}\cos\delta_{ik} \quad (4.42)$$

$$\theta_{ik} = \frac{-X_{ik}}{V_iV_k}\sin\delta_{ik} \quad (4.43)$$

where P_L, Q_L are system real and reactive power losses

P_i, Q_i are real and reactive power load at bus i

R_{ik}, X_{ik} are resistance and reactance of branch $i-k$

V_i is voltage magnitude at bus i

δ_{ik} is different in voltage phase angle of bus i,k and $\delta_{ik} = \delta_i - \delta_k$

N_b is total number of buses

4.2.2 The Modified Newton Method Calculation Steps

The flow chart of radial distribution system power flow algorithm is shown in Figure 4.2. And the calculation step of modified Newton method based on backward and forward sweeps can be summarized as follows:

(1) Read the radial system data and form bus admittance matrix $[Y_{bus}]$.

(2) Order branches by layers away from the reference node to construct the node to branch incidence matrix $[A_{n-1}]$.

(3) Initialize all node voltage and set iteration $k = 0$

(4) Calculate net real and reactive node power load $P_{i(cal)}$ and $Q_{i(cal)}$ from Equations (4.26) and (4.27).

(5) Calculate power mismatch ΔP_i and ΔQ_i from Equations (4.24) and (4.25).

(6) Test for convergence from Equation (4.37). If power flow converge, the solution is obtained but if not go to step (7).

(7) Calculate S_L in backward sweep from Equation (4.32).

(8) Calculate equivalent line impedance $Z_{eq,ij}$ from Equation (4.34).

(9) Calculate E in forward sweep from Equation (4.33) to find out $\Delta\theta$ and ΔV

(10) Update the adopted node voltage to

$$\theta_i^{(k+1)} = \theta_i^{(k)} + \ real(E_i)$$

$$V_i^{(k+1)} = V_i^{(k)} + \ [imag(E_i) \times V_i^{(k)}]$$

(11) Set new iteration $k = k + 1$ and repeat to step (4) by using new node voltage.

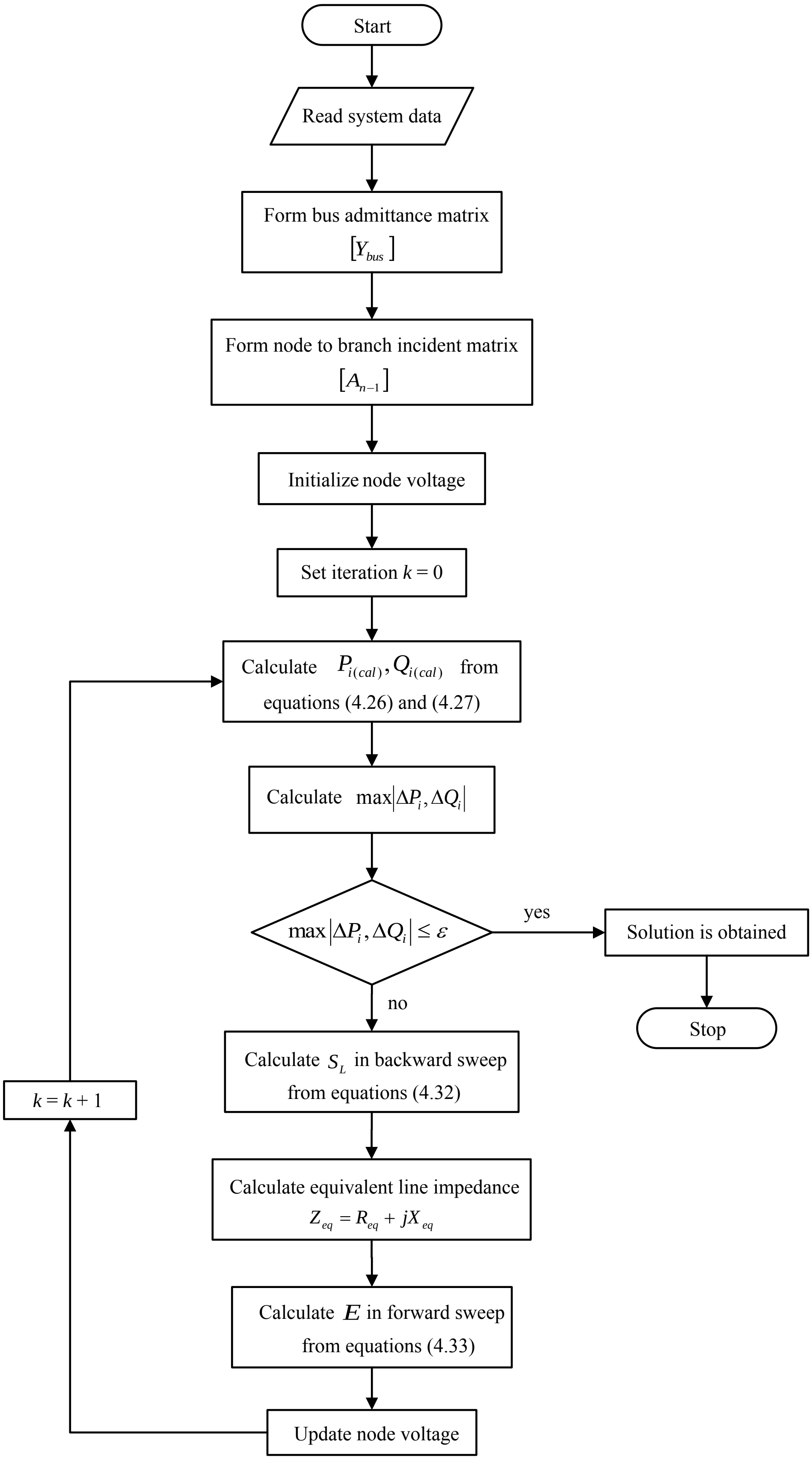

Figure 4.2 Flow chart of radial distribution system power flow calculation

4.3 Test Results of Radial Distribution System Power Flow Calculation

To demonstrate the methodology of the radial distribution system power flow calculation. The 15-bus radial distribution system from Chapter 3 is used again. Figure 4.3 shows the ordering of nodes and branches of the 15-bus radial distribution system, which node 1 is the reference node.

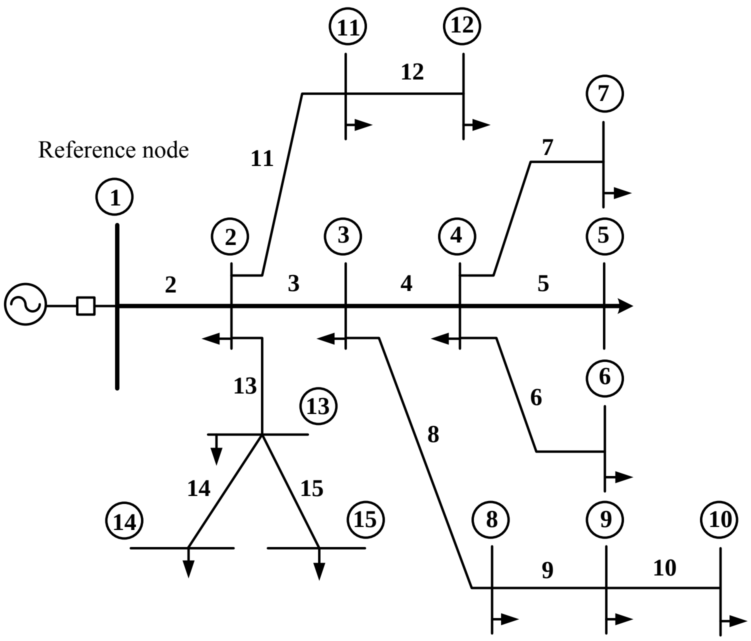

Figure 4.3 Single-line diagram of the 15-bus radial distribution system with nodes to branches ordering

From Figure 4.3, the node to branch incident matrix A_{n-1} has a dimension of (14×14) and it is given as:

$$A_{n-1} = \begin{bmatrix} 1 & 0 & -1 & 0 & 0 & 0 & 0 & 0 & 0 & 0 & -1 & 0 & -1 & 0 \\ & 1 & -1 & 0 & 0 & 0 & -1 & 0 & 0 & 0 & 0 & 0 & 0 & 0 \\ & & 1 & -1 & -1 & -1 & 0 & 0 & 0 & 0 & 0 & 0 & 0 & 0 \\ & & & 1 & 0 & 0 & 0 & 0 & 0 & 0 & 0 & 0 & 0 & 0 \\ & & & & 1 & 0 & 0 & 0 & 0 & 0 & 0 & 0 & 0 & 0 \\ & & & & & 1 & 0 & 0 & 0 & 0 & 0 & 0 & 0 & 0 \\ & & & & & & 1 & -1 & 0 & 0 & 0 & 0 & 0 & 0 \\ & & & & & & & 1 & -1 & 0 & 0 & 0 & 0 & 0 \\ & & & & & & & & 1 & 0 & 0 & 0 & 0 & 0 \\ & & & & & & & & & 1 & -1 & 0 & 0 & 0 \\ & & & & & & & & & & 1 & 0 & 0 & 0 \\ & & & & & & & & & & & 1 & -1 & -1 \\ & & & & & & & & & & & & 1 & 0 \\ & & & & & & & & & & & & & 1 \end{bmatrix}$$

For this test, the power flow results are compared with the solution obtained by a conventional Newton method as shown in Table 4.1. This table indicates that the modified Newton method offers the same solution as that obtained by the conventional Newton method, which validates its solution accuracy.

Table 4.1 Power flow solution obtained for the 15-bus radial distribution system

Node no.	***Modified Newton method***		***Conventional Newton method***	
	|V| (pu)	δ (deg)	|V| (pu)	δ (deg)
1	1.00000	0.00000	1.00000	0.00000
2	0.97130	0.03194	0.97129	0.03193
3	0.95669	0.04929	0.95668	0.04928
4	0.95093	0.05645	0.95091	0.05644
5	0.94994	0.06862	0.94993	0.06861
6	0.94846	0.08685	0.94845	0.08685
7	0.94863	0.08477	0.94862	0.08477
8	0.94997	0.13142	0.94996	0.13144
9	0.94585	0.18229	0.94584	0.18233
10	0.94454	0.19855	0.94453	0.19859
11	0.96798	0.07191	0.96797	0.07191
12	0.96691	0.08492	0.96690	0.08492
13	0.95825	0.18928	0.95824	0.18931
14	0.95603	0.21649	0.95601	0.21653
15	0.95697	0.20491	0.95696	0.20495
P_{loss} , Q_{loss}	61.74 kW , 57.25 kVar		61.78 kW , 57.28 kVar	

4.4 Harmonic Modeling

For harmonic calculation, in this dissertation, the electrical equipments in a distribution system are modeled based on CIGRE model [81], which is a balance system. Therefore, the impedance values of each model are represented in all per phase.

4.4.1 Harmonic Load Modeling

Generally, a harmonic load model is represented as a simple model for harmonic study. This model includes a connection in series or parallel of resistance (R) and inductance (L), which some physical of load is neglected. Consequence, harmonic voltage and harmonic current calculations may be incorrect.

Therefore, an effective harmonic load model is used in this dissertation. This harmonic load model can be divided into two types (CIGRE and R//L) for a different harmonic order consideration, as seen in Figure 4.4.

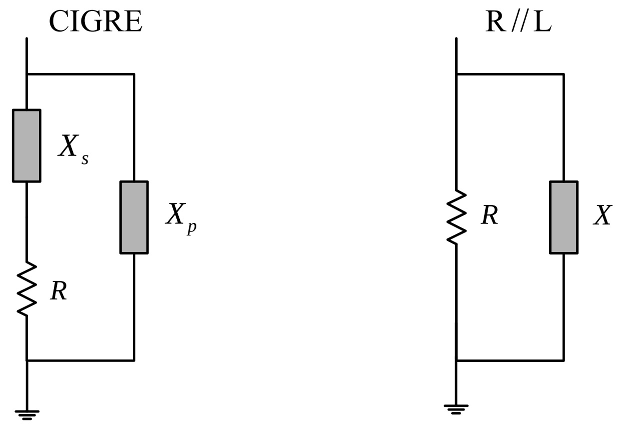

Figure 4.4 Harmonic load model of CIGRE and R//L

From Figure 4.4, the CIGRE load model is used to study for harmonic frequency order 5th to 20th. This model consists of a series reactance (X_s), a parallel reactance (X_p) and a resistance (R). The other is R//L load model, which consists of a resistance (R) and a reactance (X) in parallel connection. The R//L lode model is used to study for harmonic frequency in order more than 20th. The parameters in each model can be expressed as follows:

$$R = \frac{U_{n,net}^2}{P_1} \tag{4.44}$$

$$X_s = (0.0073) \times h \times R \tag{4.45}$$

$$X_p = \frac{h \times R}{(6.7)\tan\theta_1 - 0.74} \tag{4.46}$$

$$X = h \times \frac{U_{n,net}^2}{Q_1} \tag{4.47}$$

where $U_{n,net}$ is normal system voltage

P_1 is real power load at fundamental frequency under $U_{n,net}$

Q_1 is reactive power load at fundamental frequency under $U_{n,net}$

h is harmonic order

$\tan\theta_1 = Q_1/P_1$

4.4.2 Harmonic Capacitor Modeling

For harmonic calculation, the capacitor modeling can be represented by capacitance which depends on harmonic frequency as:

$$X_c^h = -j\frac{1}{h2\pi \; f_1 C} \tag{4.48}$$

and

$$y_c^h = -\frac{1}{X_c^h} \tag{4.49}$$

where X_c^h is capacitive reactance at harmonic frequency order h

y_c^h is capacitive admittance at harmonic frequency order h

C is capacitance of capacitor

f_1 is fundamental frequency

4.4.3 Harmonic Feeder Modeling

The equivalent circuit of feeder can be represented by a series connection of feeder resistance and reactance, which depends on harmonic frequency as shown in Figure 4.5. And its expression is given in Equation (4.50).

Figure 4.5 Equivalent circuit of harmonic feeder modeling

$$y_{line}^h = \frac{1}{R_{line} + jhX_{line}} \tag{4.50}$$

where R_{line} is line resistance

X_{line} is line reactance at fundamental frequency

y_{line}^h is line admittance at harmonic frequency order h

4.4.4 Background Harmonic Modeling

In this dissertation, existing background harmonic conditions in a distribution system are taken into account for optimal PV-DG sizing. Actually, background harmonics may occur from several nonlinear equipments such as 6-pulse and 12-pulse rectifier, arc furnaces, adjustable speed drives, etc. However, 6-pulse converters are the main harmonic sources which generate background harmonics in this study. And the background harmonics are treated as a percentage of nonlinear loads at all load buses except PV-DG buses.

4.5 Harmonic Calculation in a Distribution System

This section presents harmonic voltage and current calculations in a distribution system. Also total harmonic distortion of voltage and current are mentioned.

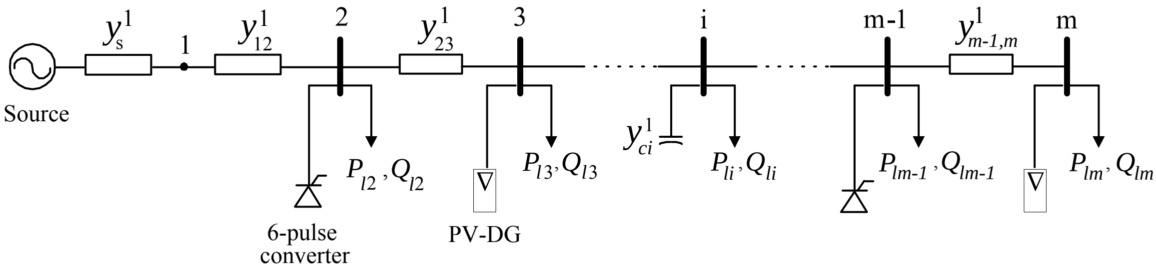

Figure 4.6 A simplified distribution system for fundamental frequency analysis

Figure 4.6 shows a simplified distribution system for fundamental frequency analysis. In this figure, 6-pulse converters are treated as background harmonic sources of the system and it can be represented by harmonic current source with the typical harmonic current spectra (I_{BH}) as shown in Table 4.2 [82]. For the PV-DGs are interconnected at any bus, they are treated as harmonic current sources with the typical harmonic current spectra based on measurements at a PV farm (I_{PV}) as mentioned in Chapter 2. The other parameter in Figure 4.6 can be defined as follows:

y_{ij}^1 is line admittance at fundamental frequency of branch i - j

y_{ci}^1 is capacitive admittance at fundamental frequency at bus i

P_{li} is real power load at bus i

Q_{li} is reactive power load at bus i

Table 4.2 Characteristic AC line harmonic currents in multi-pulse systems

Harmonic	Rectifier system pulse number				Harmonic frequency	Harmonic current in percent of fundamental	
	6	12	18	24		Theoretical	Typical
5	X				300	20.00	19.20
7	X				420	14.20	13.20
11	X	X			660	9.09	7.30
13	X	X			780	7.69	5.70
17	X		X		1020	5.88	3.50
19	X		X		1140	5.26	2.70
23	X	X		X	1380	4.36	2.00
25	X	X		X	1500	4.00	1.60
29	X				1740	3.45	1.40
31	X				1860	3.23	1.20
35	X		X		2100	2.86	1.10
37	X		X		2220	2.70	1.00

NOTE—The theoretical values are given for a 6-pulse converter with ideal characteristics (i.e., square current waves with 120° conduction). The last column gives typical values based on a commutating impedance of 0.12 pu and a firing angle of 30° and infinite dc reactor (IEEE Std 519-1992, Table 13.1). These values are on the basis of one 6-pulse converter or all converters, assuming that the harmonics are additive. Since some harmonics will be canceled, but not entirely, a small percentage value may be assumed, as explained earlier in this subclause. Note that if the dc reactor is not large, some of the harmonics can be greater than typical (or theoretical) and some smaller.

The equivalent circuit for harmonic frequency analysis corresponding to the simplified system in Figure 4.6 is shown in Figure 4.7. Note from this figure that the 6-pulse converters and the PV-DGs are modeled as harmonic current sources to inject harmonic currents into the connected bus. The load demand, shunt capacitor and feeder line are modeled as admittance of each components.

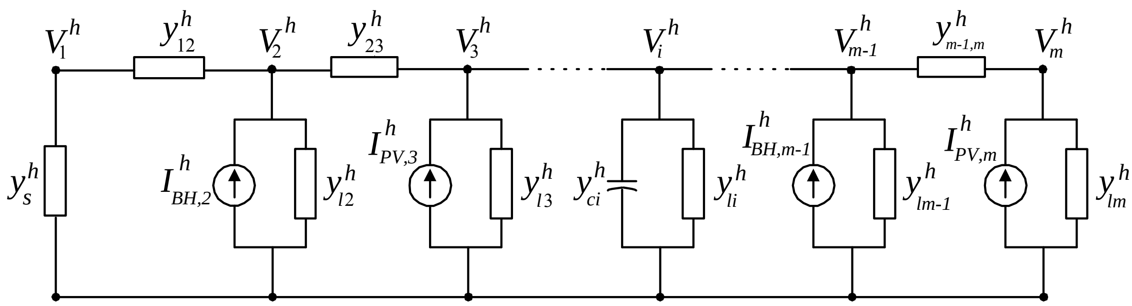

Figure 4.7 A simplified distribution system for harmonic frequency analysis

where the parameters in Figure 4.7 can be defined as follows:

y_{ij}^h is line admittance at harmonic frequency order h of branch i - j

y_{ci}^h is capacitive admittance at harmonic frequency order h at bus i

y_{li}^{h} is load admittance at harmonic frequency order h at bus i

y_{s}^{h} is source admittance at harmonic frequency order h

V_{i}^{h} is voltage at harmonic frequency order h at bus i

I_{i}^{h} is current source at harmonic frequency order h at bus i

The source impedance (Z_s) can be obtained from the given source data such as transformer voltage ratio, R/X ratio and MVA short circuit. The example for source impedance calculation can be expressed by the given source data as:

- Transformer ratio (V_{high}/V_{low}) = 22kV/416V
- R/X ratio = 10
- MVA short circuit = 100

From source data, we can calculate the short circuit current (I_{sc}) as:

$$I_{sc} = \frac{MVA_{sc} \times 10^6}{\sqrt{3} \times V_{low}} = \frac{(100 \times 10^6)}{\sqrt{3} \times 416} = 138.79 \ kA$$

And we can calculate the source impedance magnitude ($|Z_s|$) as:

$$|Z_s| = \frac{(V_{low}/\sqrt{3})}{I_{sc}} = \frac{(416/\sqrt{3})}{138.79 \ kA} = 0.00173 \ \Omega$$

Thus, we get a source resistance (R_s) and reactance (X_s) as:

$$R_s = \frac{|Z_s|}{\sqrt{(R/X \ ratio)^2 + 1}} = \frac{(0.00173)}{\sqrt{10^2 + 1}} = 0.000172 \ \Omega$$

$$X_s = (R/X \ ratio) \times R_s = 10 \times 0.000172 = 0.00172 \ \Omega$$

Therefore, we can find the source impedance and source admittance as:

$$Z_s = R_s + jX_s = 0.000172 + j0.00172 \ \Omega$$

$$y_s = \frac{1}{Z_s} = \frac{1}{0.000172 + j0.00172} = 57.563 - j575.639 \ mho$$

From Figure 4. 7, we can form bus admittance matrix at harmonic frequency order h directly from the admittance of each component in a distribution system as mentioned above. The harmonic bus admittance matrix $\left[Y_{bus}^{h}\right]$ of system with m nodes is a square matrix which its dimension is (m×m) as given by:

$$\left[Y_{bus}^{h}\right]=\begin{bmatrix} Y_{11}^{h} & Y_{12}^{h} & 0 & & & 0 \\ Y_{21}^{h} & Y_{22}^{h} & \cdot & & & \\ 0 & \cdot & \cdot & & & \\ & & & \cdot & \cdot & 0 \\ & & & \cdot & Y_{m-1,m-1}^{h} & Y_{m-1,m}^{h} \\ 0 & & & 0 & Y_{m,m-1}^{h} & Y_{mm}^{h} \end{bmatrix} \tag{4.51}$$

where
$$Y_{ij}^{h}=\begin{cases} -y_{ij}^{h} & if \quad j\neq i \\ y_{i-1,i}^{h}+y_{i,i+1}^{h}+y_{li}^{h}+y_{ci}^{h} & if \quad j=i\neq 1 \\ y_{12}^{h}+y_{s}^{h} & if \quad j=i=1 \end{cases} \tag{4.52}$$

By knowing the harmonic current source at any bus $\left[I_{i}^{h}\right]$ and also the harmonic bus admittance $\left[Y_{bus}^{h}\right]$, we can obtain the harmonic voltage at any bus $\left[V_{i}^{h}\right]$ from Equation (4.53).

$$\left[I_{i}^{h}\right]=\left[Y_{bus}^{h}\right]\left[V_{i}^{h}\right] \tag{4.53}$$

and we get

$$\begin{bmatrix} V_{1}^{h} \\ V_{2}^{h} \\ \cdot \\ \cdot \\ V_{m-1}^{h} \\ V_{m}^{h} \end{bmatrix}=\begin{bmatrix} Y_{11}^{h} & Y_{12}^{h} & 0 & & & 0 \\ Y_{21}^{h} & Y_{22}^{h} & \cdot & & & \\ 0 & \cdot & \cdot & & & \\ & & & \cdot & \cdot & 0 \\ & & & \cdot & Y_{m-1,m-1}^{h} & Y_{m-1,m}^{h} \\ 0 & & & 0 & Y_{m,m-1}^{h} & Y_{mm}^{h} \end{bmatrix}^{-1}\begin{bmatrix} I_{1}^{h} \\ I_{2}^{h} \\ \cdot \\ \cdot \\ I_{m-1}^{h} \\ I_{m}^{h} \end{bmatrix} \tag{4.54}$$

In optimal PV-DGs sizing process, the harmonic constraints i.e., total harmonic voltage distortion (THDv), and total demand distortion (TDD) at a point of common coupling (PCC) are taken into accounted. The THDv and TDD are defined with harmonic frequency from order 2nd to 33rd as given by:

$$THD_{v,i} = \frac{\sqrt{\sum_{h=2}^{33} \left|V_i^h\right|^2}}{\left|V_i^1\right|} \times 100\ \% \tag{4.55}$$

$$TDD_i = \frac{\sqrt{\sum_{h=2}^{33} \left|I_i^h\right|^2}}{\left|I_{m,i}^1\right|} \times 100\ \% \tag{4.56}$$

where V_i^1 is fundamental voltage at bus i

V_i^h is harmonic voltage order h at bus i

$THD_{V,i}$ is total harmonic distortion voltage at bus i

I_i^1 is fundamental current flow through bus i

I_i^h is harmonic current order h flow through bus i

$I_{m,i}^1$ is fundamental maximum load current flow through bus i

TDD_i is total demand distortion at bus i

From IEC 61727 standard in Photovoltaic systems-Characteristic of the utility interface, low levels of current and voltage harmonics at a connection point of PV-DG are desirable. Acceptable levels of harmonic voltage and current depend upon distribution system characteristic, type of service, connected loads/apparatus and established utility practice. The PV-DG output should have low current distortion levels to ensure that no adverse effects are caused to other equipment connected to the utility system.

To comply with IEC 61727 standard, the total harmonic current distortion shall be less than 5% at rated inverter output. Hence, in order to calculate the TDD at the connection point of PV-DG, the maximum load current in Equation (4.56) is replaced by rated current of PV inverter. And each individual harmonic current from PV inverter shall be limited to the percentages listed in Table 4.3.

Table 4.3 Current distortion limits in IEC 61727 standard

Odd harmonics	***Distortion limit***
3rd through 9th	≤ 4.0 %
11th through 15th	≤ 2.0 %
17th through 21st	≤ 1.5 %
23rd through 33rd	≤ 0.6 %
Even harmonics	***Distortion limit***
2nd through 8th	≤ 1.0 %
10th through 32nd	≤ 0.5 %
Total harmonic current distortion at rated inverter output (TDD)	≤ 5.0 %

In the IEC 61727 standard, the THDv constraint is not mentioned. However, according to the IEEE 519-1992 standard, IEEE Recommended Practices and Requirements for Harmonic Control in Electrical Power Systems, the THDv at a PCC should not exceed 5%.

CHAPTER V
ALGORITHM OF OPTIMAL PV-DG SIZING TECHNIQUE AND NUMERICAL RESULTS

5.1 Introduction

This chapter proposes the algorithm of optimal PV-DG sizing technique. Also problem formulation and constraints detail are mentioned. Furthermore, the numerical results of various study cases are investigated. An actual 51-bus radial distribution system of Provincial Electricity Authority (PEA) of Thailand and a heavy load 33-bus radial distribution system are selected as test cases. Results from study cases indicate that the optimal PV-DG size solution may be changed depend on system operating conditions. Furthermore, it demonstrates that PV-DGs may improve voltage regulation and decrease losses in distribution systems, however, the THDv may also increase. Impact of static load models and power factor control on optimal sizing of PV-DG are also addressed. Finally, effects of inverter modeling and existing DGs in a distribution system on optimal PV-DG sizing are presented.

5.2 Problem Formulation

The PV-DG installation in a distribution system has several advantages (e.g., voltage improvement, losses reduction, etc.). In the proposed technique, the main objective is to minimize the "*average*" real power losses of a distribution system by varying the size of PV-DG over N_s samples. The problem can be expressed mathematically as follows:

$$\text{Minimize} \qquad \frac{1}{N_s}\sum_{r=1}^{N_s} P_{L,r}(PV_{size}) \tag{5.1}$$

subjected to the following constraints:

- $0.95 \text{ pu} \leq V_i \leq 1.05 \text{ pu}$, at PCC
- THDv and TDD $\leq 5\%$, at PCC
- $I_h \leq$ IEC limits , at PCC

where $P_{L,r}(PV_{size})$ is the real power losses of a radial distribution system shown as a function of the size of PV-DG (PV_{size}). Note that $P_{L,r}(PV_{size})$ is calculated from the sample r and the real power losses equation can be written as

$$P_{L,r}(PV_{size}) = \sum_{i=1}^{N_b}\sum_{j=1}^{N_b}\left[\frac{R_{ij}\cos\delta_{ij}}{|V_i||V_j|}(P_iP_j + Q_iQ_j) + \frac{R_{ij}\sin\delta_{ij}}{|V_i||V_j|}(Q_iP_j - P_iQ_j)\right] \quad (5.2)$$

where R_{ij} is resistance of branch $i-j$

$|V_i|$ and δ_i are the voltage magnitude and phase angle at bus i

P_i and Q_i are the net real and reactive power at bus i

δ_{ij} is the voltage phase angle difference between buses i and j

N_b is the total number of buses in a distribution system

5.3 The Algorithm of Optimal PV-DG Sizing Technique

The algorithm for determining an optimal PV-DG size can be depicted in Figure 5.1. As mentioned in Chapter 2 on PV modeling section, the PV_{size} in Figure 5.1 is the rated size of PV-DG which based on a connection group of Sharp 80Wp PV modules. Several random variables are generated with Monte Carlo simulations i.e., solar radiations (G_a), ambient temperatures (T_a), load demands ($L_{d,i}$) and substation voltages (V_S). The maximum active power outputs of PV-DGs ($P_{mp,i}$) are obtained at each location by PV model and MPPT block.

From the report in [83], it shows that the power factor of PV grid-connected inverter is usually controlled to be 100%. However, some inverters have the capability to adjust the power factor for two main purposes. One is leading power factor operation to suppress the voltage rise in a distribution system due to the output power from PV-DGs during light-load hours in the daytime. The other is operated at the lagging power factor during heavy load to compensate for the voltage drop of the distribution lines. Therefore, various power factor operations and also proper load models are important in PV system installation planning. Then, the reactive power output of PV-DGs ($Q_{mp,i}$) in PV model block can flow in both directions to the network under lagging or leading power factor operations.

System losses and node voltages are evaluated by the distribution power flow calculation. Based on the data measured from a PV farm (540 units of 11 kW grid-connected inverters), harmonic distortions at each bus are evaluated by the harmonic flow analysis. As shown in the flow chart in Figure 5.1, the process is calculated repeatedly from a specific range of PV-DG size at each incremental step. The optimal solution of Equation (5.1) is the rated size of PV-DG with minimum the average system loss and under the constraints from 5,000 samples (N_s).

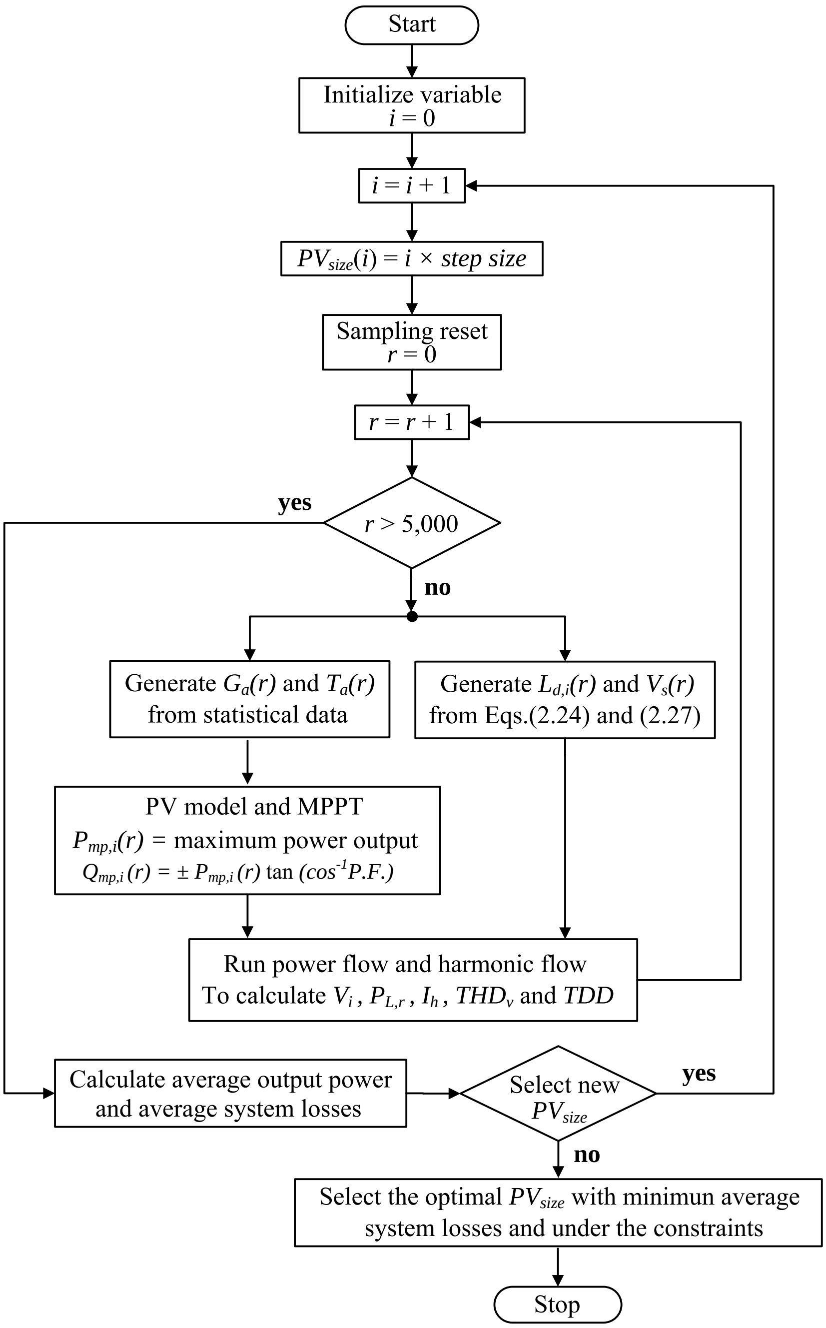

Figure 5.1 Flow chart of the optimal PV-DG sizing technique

5.4 Numerical Results and Discussion

For the purposes of this dissertation, there are three scenarios to determine the optimal PV-DGs size in the difference system operating conditions. However, the hourly solar radiation and ambient temperature based on measured from Chiang Mai province as given in Chapter 2 on section 2.2 are used for all scenarios.

5.4.1 Scenario-1: Optimal PV-DGs sizing with and without consideration of background harmonic in distribution system

An actual 22 kV radial distribution system in Thailand is employed as a test case in this scenario. All system parameter are given in Appendix C, which can be found in [84]. The test system has 51 buses with a total load of 1.92 MW, 1.06 MVar and 1 unit of 900 kVar capacitor bank at bus-13 as shown in Figure 5.2. The results of base case deterministic load flow are given in Appendix D.

This scenario shows the optimal PV-DGs sizing with and without consideration of existing background harmonic conditions in distribution system. The PV-DGs placements are obtained based on the static voltage stability index (VSI) calculations. The system operating conditions in this scenario are given as:

- Substation voltage and load demand are assumed to be random variables with normal distribution, which standard deviations (σ) of substation voltage and load models are set to 1.5% and 10% respectively.
- Power factors of PV-DGs are assumed to be 1.0 constant.
- Load model is assumed to be constant power load.
- The 6-pulse converters are main harmonic sources which generate background harmonics (the typical harmonic current spectra are given in Table 4.2 on Chapter 4).
- Three levels of background harmonics (15%, 25% and 35%) are considered.
- Other DGs are not considered in this test system.
- In this scenario, all constraints (V_i, I_h, $THDv$ and TDD) are considered with 95% confidence interval.
- Range of PV_{size} on this study is between 0.1 MWp to 2 MWp with a 0.1 MWp increment.

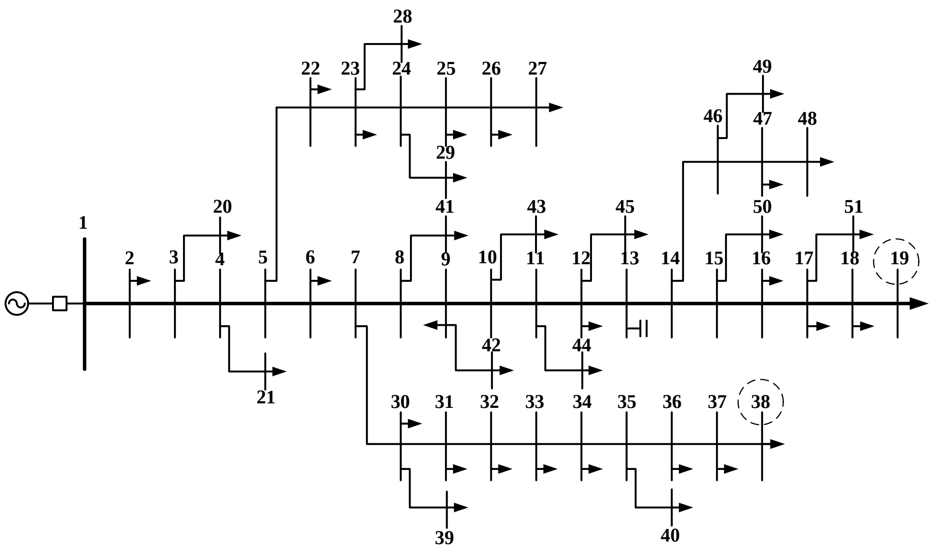

Figure 5.2 Single-line diagram of the 51-bus test system

Firstly, a voltage stability index is computed as a basis to determine proper locations of PV-DG. Buses with descending minimum VSI are selected as candidate locations to install PV-DG. A constant power load model is also assumed in VSI calculation. Table 5.1 shows three candidate locations (i.e., buses 38, 19 and 37) with various voltage levels of substation in the test system. The results in Table 5.1 also show the minimum voltage related to the critical bus with minimum VSI.

Table 5.1 Critical bus stability index values of the test system

Substation voltage (pu)	***Candidate buses with VSI min***	***VSI min***	***Voltage min (pu)***
0.95	38	0.0387	0.4436
	19	0.0392	0.4451
	37	0.0402	0.4478
1.00	38	0.0453	0.4613
	19	0.0457	0.4623
	37	0.0459	0.4630
1.05	38	0.0545	0.4831
	19	0.0554	0.4851
	37	0.0561	0.4868

After selecting proper locations of PV-DG, the proposed technique is then employed to solve the optimal PV-DG size. In this study, existing background harmonic conditions in test system are also taken into account. The background harmonics (BH) are treated as a percentage of nonlinear loads at all load bus except PV-DG bus. Three levels of background harmonics (i.e., 15%, 25% and 35% of load demands) are tested. Based on the results of the voltage stability index of the candidate buses, three study cases are investigated to determine the optimal size of PV-DG.

<u>Case-1</u>: *Single PV-DG*

The PV-DG installation is assumed to be owned by a generation company and located at the bus with minimum VSI (bus-38). This case shows the selection of PV-DG size based on the technical constraints with and without consideration of background harmonics.

Figure 5.3 presents the relationship between the average system loss and the average PV-DG active power output. As shown in Figure 5.3, the system losses vary with the size of PV-DG installed at bus-38. The average system loss without installing PV-DG is 30.1 kW. Beside, the system losses decrease when installing PV-DG less than 1.7 MWp. The minimum average system loss in this case is 23.3 kW, which is given by installing a PV-DG at 0.8 MWp. Also note that with the variation of solar radiation and operating temperature, from installing 0.8 MWp PV-DG (peak power output), the average active power output is 0.35 MW.

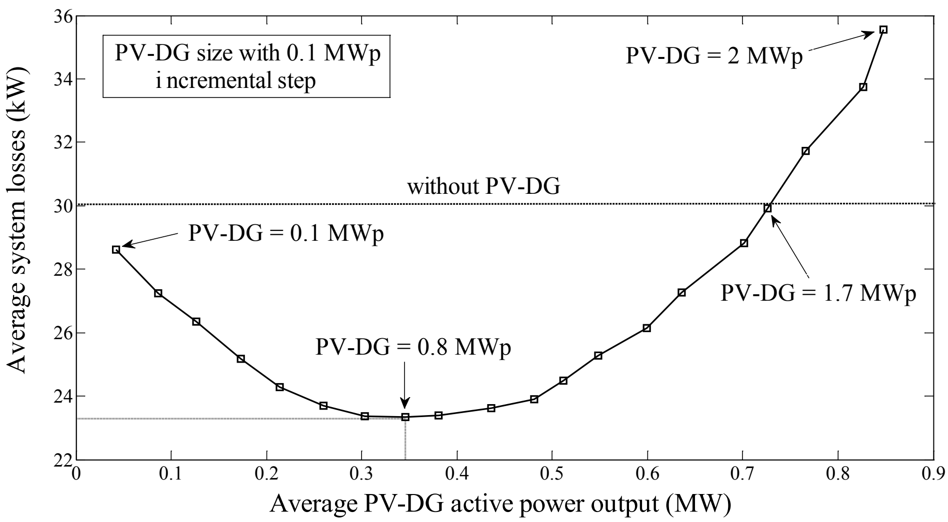

Figure 5.3 Average system losses as a function of average PV-DG power output in Case-1

The cumulative probability of voltage at bus-38 with and without installation of 0.8 MWp PV-DG is shown in Figure 5.4. Similarly, an installation of PV-DG mostly improves the voltage regulation at the PCC. Note from the figure, it shows that the voltage level at bus-38 stays within an acceptable range (i.e., 0.95 to 1.05 pu.) with 95% confidence interval.

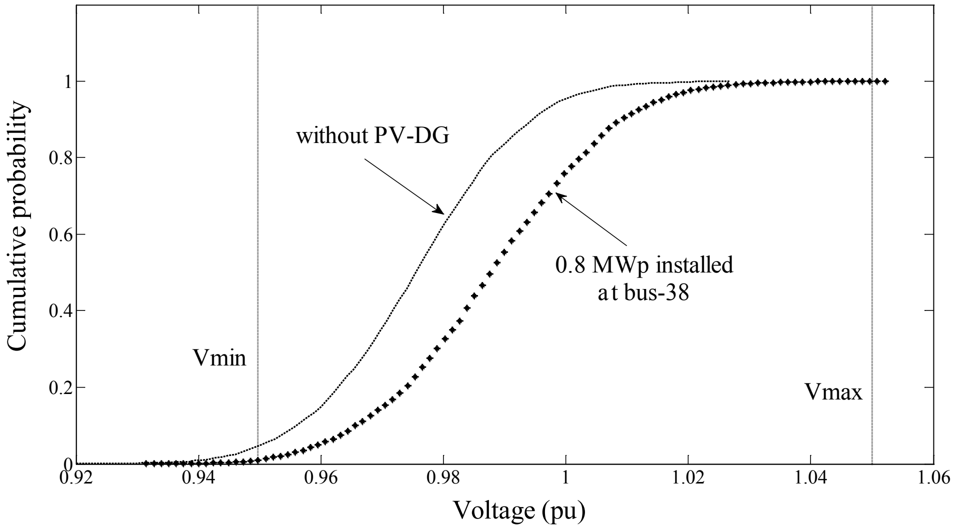

Figure 5.4 Cumulative probability of voltage at PCC with and without PV-DG in Case-1

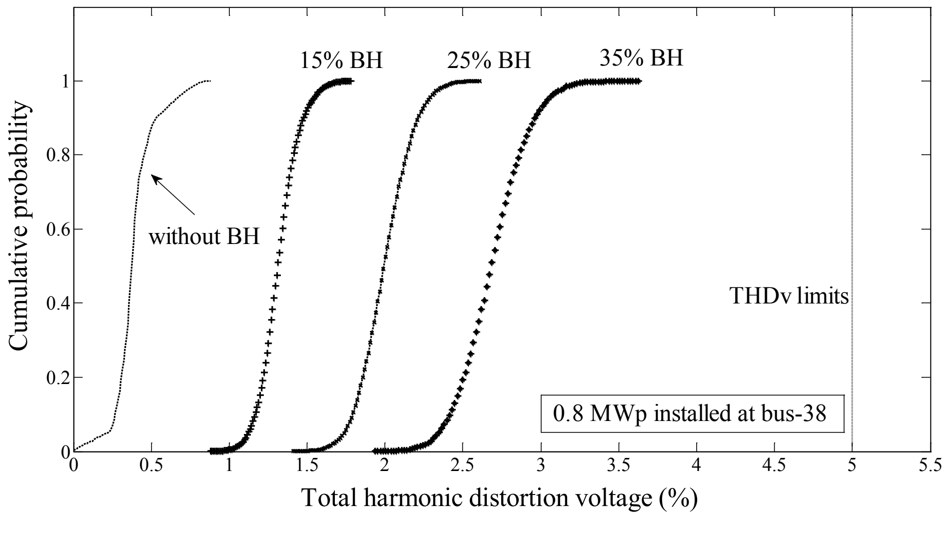

Figure 5.5 Cumulative probability of THDv at PCC with and without background harmonics in Case-1

Figure 5.5 shows the impact of background harmonics on THDv at bus-38. Results show that THDv values are less than 1% without considering background harmonics. This indicates that an individual PV-DG produces small voltage distortion waveform. On the contrary, the THDv rises when the percentage of background harmonics on the test system increases. The THDv reaches 3.5% when the level of background harmonics is 35%. In this case, the background harmonics produce more impact on THDv at PCC than PV-DG. However, all THDv values do not reach the 5% limits in Case-1.

Based on SMC-11000TL grid-connected inverter, PWM technology is employed to control the output waveform. Therefore, the harmonic current (I_h) from the inverter is less than the limits. The cumulative probability of TDD and harmonic current from inverter simulated at PCC of Case-1 are shown in Figures 5.6 to 5.11. The results show that all constraints are complied with IEC standard. Therefore, in Case-1, the optimal PV-DG size at bus-38 is 0.8 MWp for both with and without consideration of background harmonics.

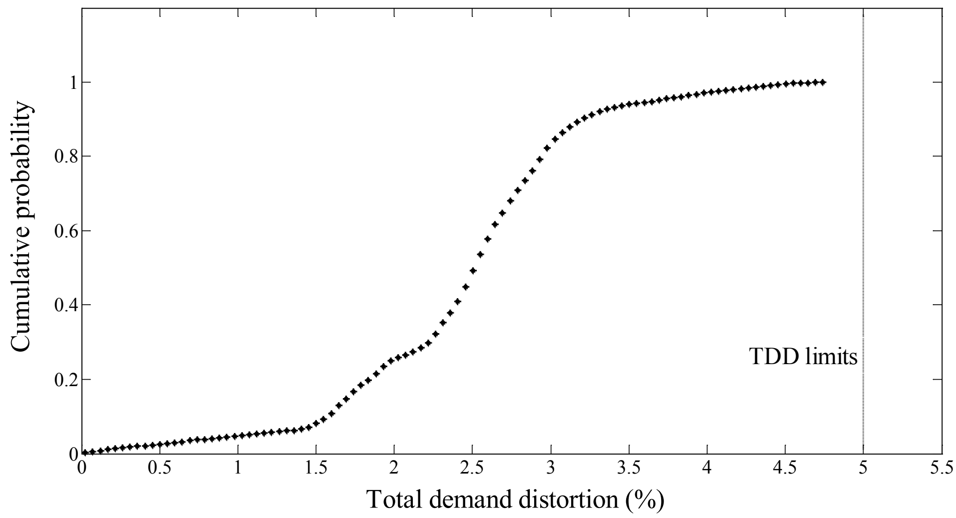

Figure 5.6 Cumulative probability of TDD at PCC of inverter

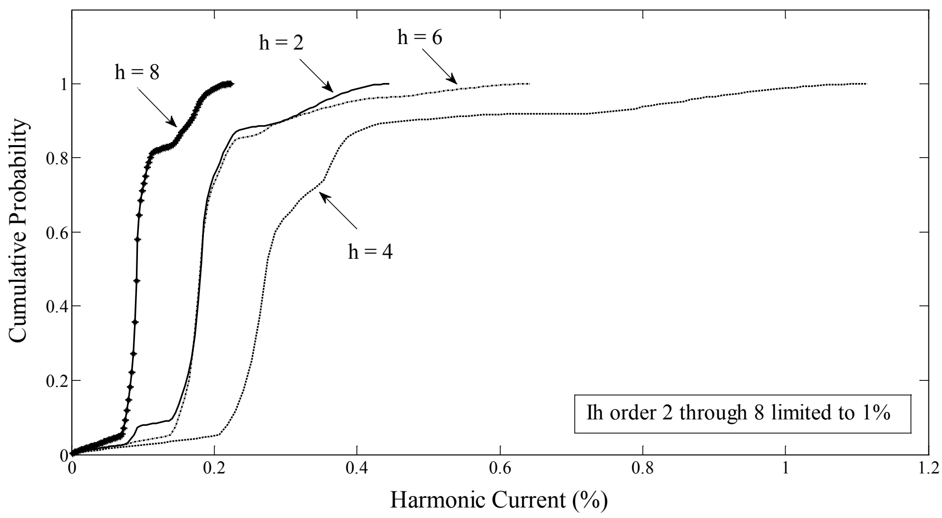

Figure 5.7 Cumulative probability of I_h (even orders 2 to 8) at PCC of inverter

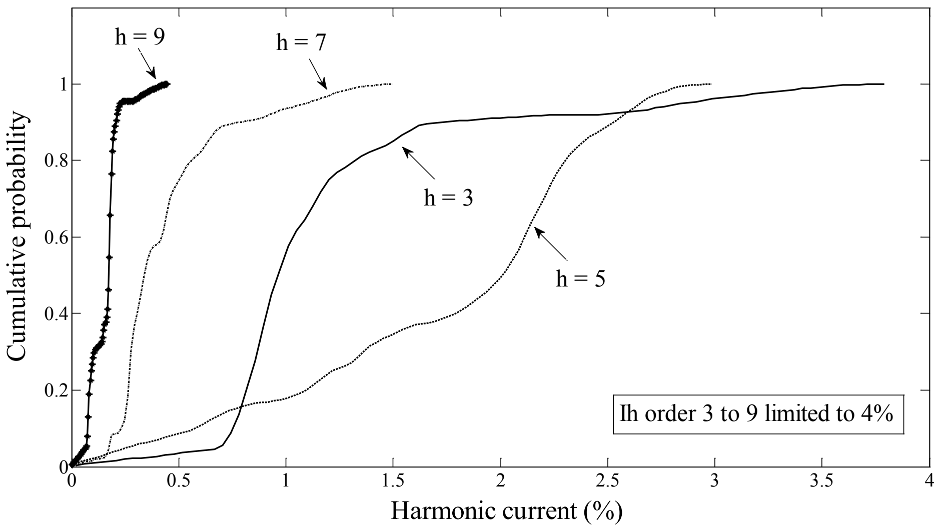

Figure 5.8 Cumulative probability of I_h (odd orders 3 to 9) at PCC of inverter

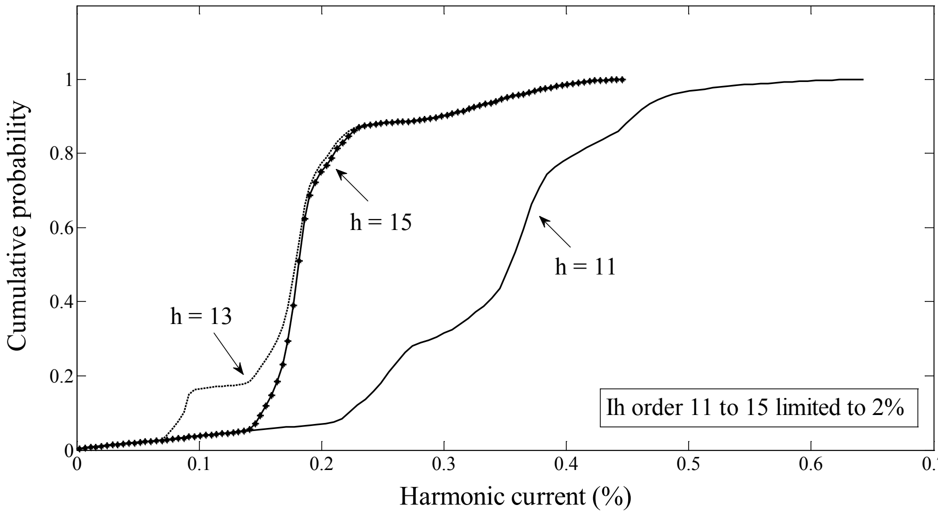

Figure 5.9 Cumulative probability of I_h (odd orders 11 to 15) at PCC of inverter

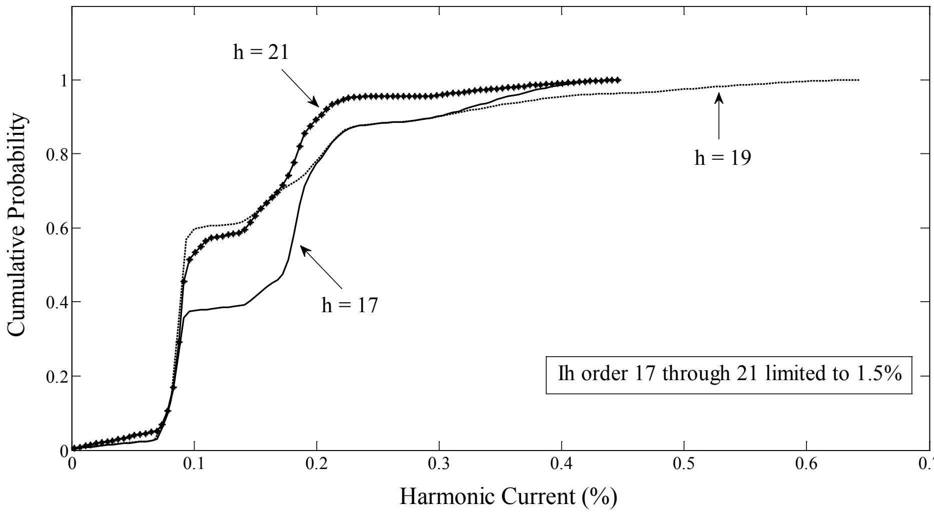

Figure 5.10 Cumulative probability of I_h (odd orders 17 to 21) at PCC of inverter

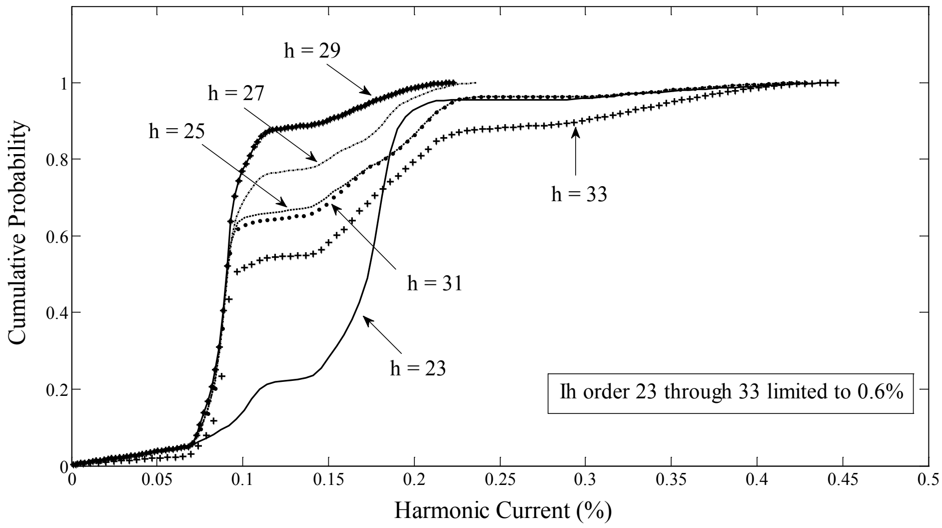

Figure 5.11 Cumulative probability of I_h (odd orders 23 to 33) at PCC of inverter

Case-2A: ***Multiple PV-DGs without consideration of background harmonics***

In this case, by considering the same constraint as in Case-1, two PV-DGs are installed at buses 38 and 19. This case shows that the proposed technique can be applied to determine the optimal size for multiple locations. Note that, the background harmonics are not considered in this case.

The system losses after installing PV-DGs at buses 38 and 19 are shown as 3-D plot in Figure 5.12. Note from the figure that the minimum average system loss occurs when installing a 0.7 MWp PV-DG at bus-38 and a 0.9 MWp at bus-19. With the variation of solar radiation and operating temperature, the total average PV-DGs output is around 0.7 MW which results in 16.86 kW of average system loss. The results in Figure 5.12 also show that, with multiple PV-DGs installations, the average system losses of Case-2A are lower than Case-1 (23.33 kW). Hence, the installations of PV-DGs reduce 56.2% of system losses comparing the case without PV-DG (30.1 kW).

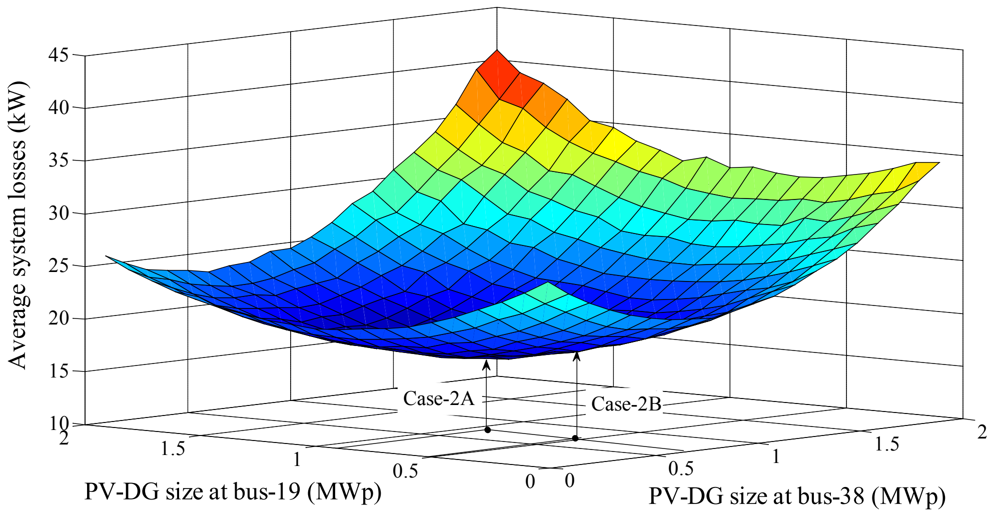

Figure 5.12 Average system losses as a function of PV-DGs size at buses 38 and 19

From installing a 0.7 MWp PV-DG at bus-38 and a 0.9 MWp at bus-19, Figure 5.13 shows the cumulative probability of voltages at buses 38 and 19 (both with and without PV-DGs). The results show that voltages at PCC are increased when the PV-DGs are presented. However, the voltages at both locations stay in an acceptable level with 95% confidence interval.

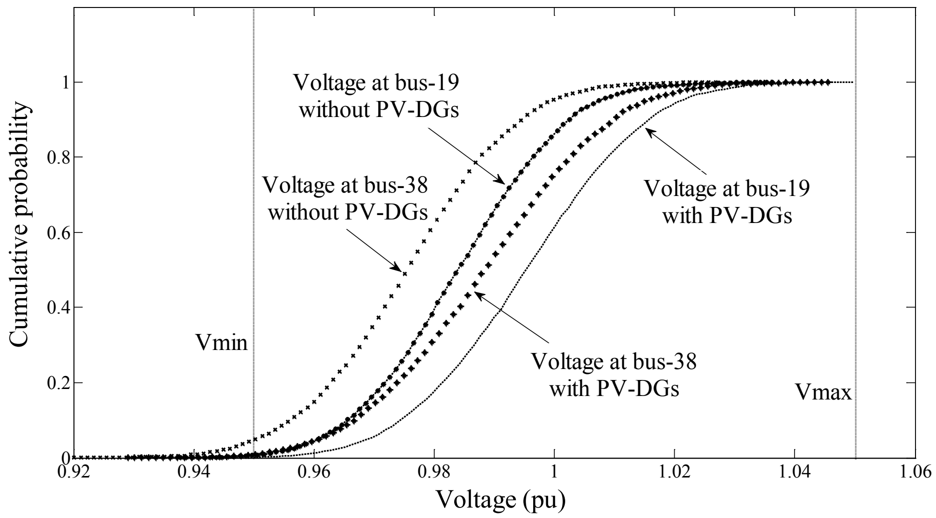

Figure 5.13 Cumulative probability of voltage at buses 38 and 19 with and without PV-DGs in Case-2A

Figure 5.14 shows the impact of background harmonics on THDv values. Note from the figure that the THDv at PCC increases and may exceed the limits when higher percentage of background harmonics occurs. The THDv at both locations does not reach the limits for 15% and 25% of background harmonics. However, when the level of background harmonics is 35%, the probability at which THDv at bus-19 violates the constraint (exceeds 5%) is 0.1.

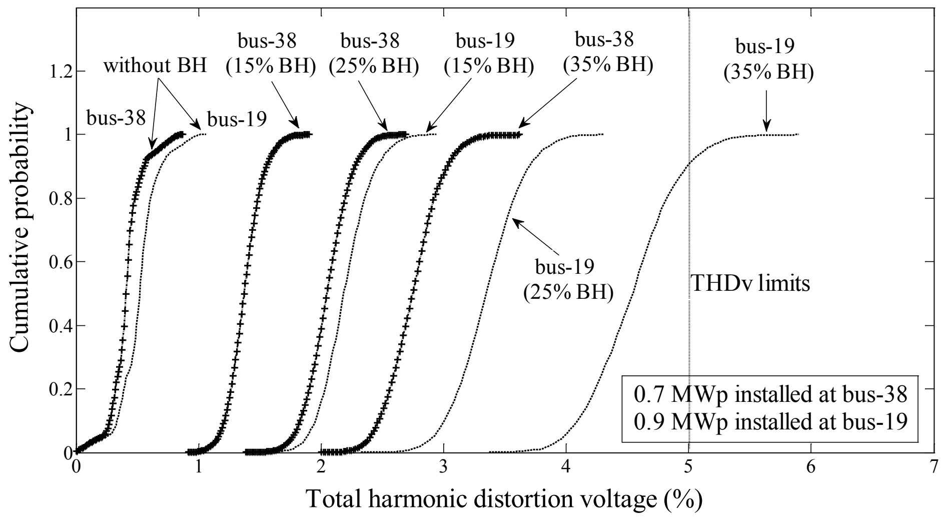

Figure 5.14 Cumulative probability of THDv at PCC with and without background harmonics in Case-2A

Although, the THDv constraint is violated in some levels of background harmonics. Fortunately, the process of optimal PV-DG sizing does not considered the background harmonics in this case.

<u>Case-2B</u>: ***Multiple PV-DGs with consideration of background harmonics***

When the level of background harmonics is 35%, as the results in Case-2A, the THDv at bus-19 violates the constraint more than 0.05 of probability of occurrences. Therefore, to comply with harmonic limits, Case-2A is considered again taking into account the background harmonics. By applying the same algorithm as shown in Figure 5.1, the minimum average system loss in Case-2B occurs when installing a 0.7 MWp PV-DG at bus-38 and a 0.5 MWp at bus-19 (see Fig.5.12). In this case, the average system loss is 18.39 kW and the total average PV-DGs output is around 0.52 MW.

Figure 5.15 shows the comparison of THDv at buses 38 and 19 between Cases-2A and 2B (with 35% of background harmonics). Note that the solution from

Case-2B guarantees the THDv constraint with 95% confidence interval. This case shows the effectiveness of the proposed technique when the background harmonics are presented in an actual distribution system.

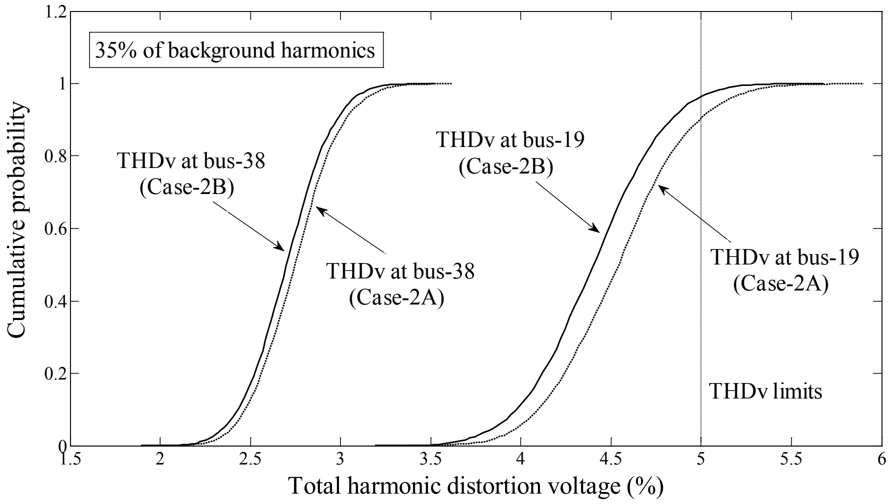

Figure 5.15 Comparison of THDv at PCC between Case-2A and Case-2B with 35% of background harmonics

As the results in Case-2B, the optimal size of PV-DG at bus-19 is reduced to 0.5 MWp from Case-2A (0.9 MWp). This guarantees the voltage constraint at buses 38 and 19 with 95% confidence interval.

Also from Figures 5.6 to 5.11, the cumulative probability of %TDD and inverter harmonic current from the same inverter in each order at PCC of Cases-2A and 2B are similar to Case-1. Therefore, the harmonic current constraints are maintained at acceptable levels in both cases.

Table 5.2 summarizes the PV-DGs installation for all cases. With various background harmonic levels, average values of %THDv at PCC are presented with the corresponding optimal sizes of PV-DGs. For all cases without background harmonics, average values of %THDv are lower than 1%. On the contrary, the average values of %THDv vary depending on the background harmonic levels. Furthermore, with higher total installed capacity of PV-DGs, the THDv at PCC may increase. This can be observed from the average of %THDv at bus-38 of all cases.

Table 5.2 Summarize the optimal size of PV-DGs installation

Location Bus	Optimal PV-DG size (MWp)	Total PV-DG Capacity (MWp)	Total average PV-DG power output (MW)	Minimum average system losses (kW)	Average of %THDv at PCC related to optimal PV-DG size with and without background harmonics (BH)			
					without BH	*15% BH*	*25% BH*	*35% BH*
38 *(Case-1)*	0.8	0.8	0.346	23.327	0.389	1.322	2.004	2.694
38 19 *(Case-2A)*	0.7 0.9	1.6	0.696	16.863	0.415 0.518	1.383 2.203	2.058 3.362	2.747 **4.537**
38 19 *(Case-2B)*	0.7 0.5	1.2	0.519	18.387	0.392 0.344	1.337 2.052	2.020 3.229	2.710 4.414

Although, the THDv at bus-19 violates the harmonic constraint in Case-2A with 35% of background harmonics. While the average of %THDv is less than 5% (4.537%) as shown by bold number in Table 5.2.

Thus, by using the average of %THDv as a criterion, the optimal sizes of PV-DGs solution in Case-2A may be acceptable with considering up to 35% of background harmonic levels. However, the solution in Case-2B indicates that the optimal size of PV-DG at bus-19 should be reduced to maintain the THDv constraint. This indicates that when the average of %THDv is used as a criterion, the optimal sizes of PV-DGs may be overestimated.

A summary of the total number of PV modules and inverters for optimal sizes of PV-DGs solution is given in Table 5.3. Note that the total number of PV modules and inverters are based on a connection group of Sharp 80Wp PV module and SMC 11 kW grid-connected inverter.

Table 5.3 Summarize the total number of PV modules and inverter units for optimal PV-DGs sizes solutions

Location Bus	***Optimal PV-DG size*** *(MWp)*	***Total number of PV modules*** *(module)*	***Total number of inverters*** *(unit)*
38 *(Case-1)*	0.8	10,000	72
38	0.7	8,750	63
19 *(Case-2A)*	0.9	11,250	81
38	0.7	8,750	63
19 *(Case-2B)*	0.5	6,250	45

The results in Scenario-1 show that the proposed technique performs well to obtain the optimal sizes of PV-DGs for multiple locations based on technical constraints. In practice, some background harmonic distortion are normally present in the network. By applying this technique, the optimal sizes of PV-DGs can be determined taking into account the background harmonics.

It has been demonstrated that the installation of PV-DGs may affect the power quality when some background harmonics are presented in a distribution system. With high background harmonics, the THDv at PCC may not satisfy the standard. As shown in Case-2A, the optimal sizes of PV-DGs are not acceptable with a 35% of background harmonic level. This is due to THDv constraint violation at bus 19. Therefore, as shown in Case-2B, the optimal sizes of PV-DGs with consideration of background harmonics are required. However, in Case-1, the optimal size of PV-DG is successfully obtained in both with and without consideration of background harmonics.

The results from several cases also indicate that PV-DGs are likely to improve the voltage regulation and decrease system losses in a distribution system. However, installing with high capacity of PV-DGs may increase THDv at PCC especially when the background harmonics are presented.

5.4.2 **Scenario-2**: Impact of load model and power factor control on optimal PV-DG sizing

The purpose of this scenario is to study an impact on optimal PV-DG sizing in a distribution system using different static load models (i.e., constant power, constant current and constant impedance) and various power factor operations.

The 51-bus radial distribution system in Scenario-1 is employed as a test case again, but the capacitor bank at bus-13 is neglected in this scenario. The system operating conditions in this scenario are given as:

- Substation voltage is set to $1.0\angle 0°$ constant.
- Load demand is assumed to be random variables with normal distribution, which standard deviations (σ) is set to 10%.
- Various power factor operations of PV-DGs are considered.
- Three static load models are considered i.e., constant power (CP), constant current (CI) and constant impedance (CZ).
- Background harmonics are not considered in this test system.
- Other DGs are not considered in this test system.
- In this scenario, only voltage and THDv constraints are considered.
- Range of PV_{size} on this study is between 50 kWp to 2.5 MWp with a 50 kWp increment.

For the purpose of this scenario, it is assumed that the PV-DG installation is located at buses 10 and 19. Two cases are studied for determining the impact of load model and various power factor operations on optimal sizing of PV-DG.

Case-1: ***Single PV-DG***

In this case, the PV-DG installation is assumed to locate at only bus-19. The impact of PV-DG connection on system losses with different load models is presented in Figure 5.16, which power factor (PF) is set to 1.0 constant. It shows that PV-DG normally decreases system losses, except when its size largely increases. Furthermore, it demonstrates that using different static load models do not impact on optimal PV-DG size, which is 1.1 MWp. Besides, the voltage and THDv constraints are satisfied for PV-DG size with minimum the average system loss as shown in Figures 5.17 and 5.18, respectively.

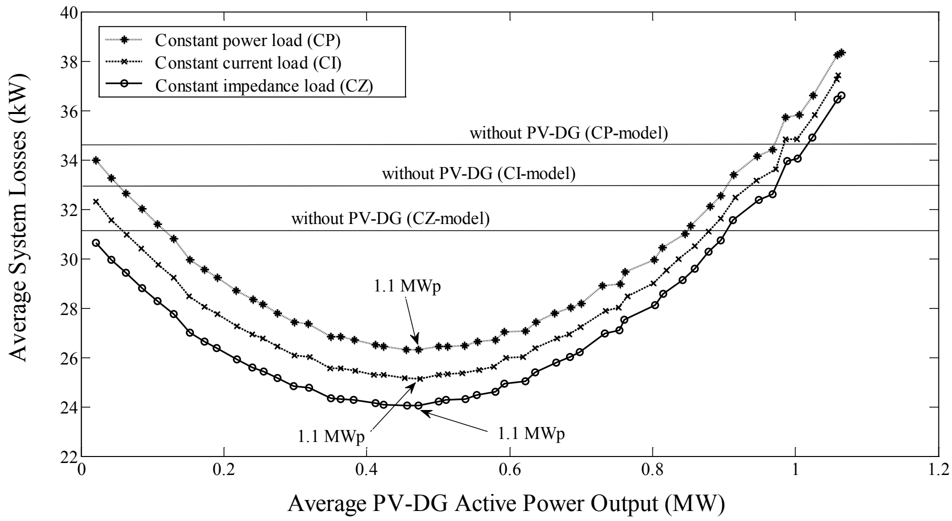

Figure 5.16 Average system losses as a function of average PV-DG power output with different load models

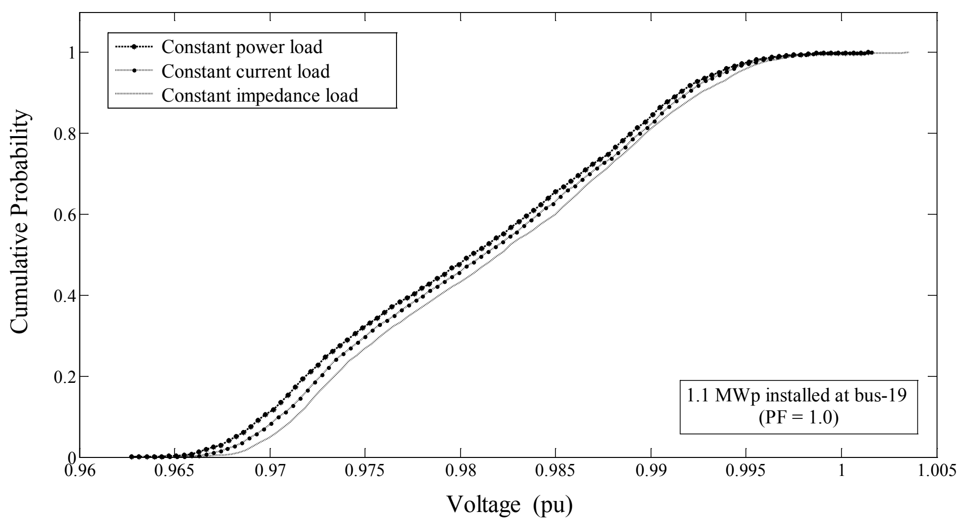

Figure 5.17 Cumulative probability of voltage at bus-19 with different load models (PF = 1.0)

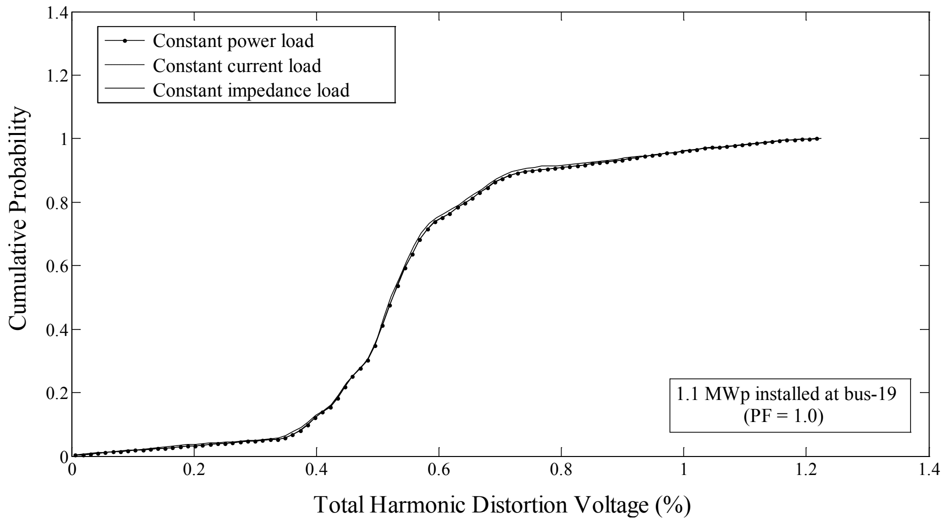

Figure 5.18 Cumulative probability of THDv at bus-19 with different load models (PF = 1.0)

Figure 5.17 shows that the voltage values depend on load models. The lowest voltage is occurred when using the CP model. However, the voltage constraints of all load models are within the limits. Figure 5.18 shows that different load models do not affect the THDv. In reality, the THDv strongly depends on PV-DG size as shown in Figure 5.22. Further, it can be observed from Figure 5.18 that THDv is small and less than 1.25%. This shows that the low harmonic distortion power can be generated based on SMC-11000TL inverter.

The impact of leading operation on system losses in Case-1 with CP load model is presented in Figure 5.19. It shows that the solution of optimal PV-DG size may be changed for wide leading power factor range. Unlike the lagging operation which has a few impact on optimal size of PV-DG as shown in Figure 5.20. Further, Figure 5.19 indicates that the system losses are rapidly increasing when PV-DG size is larger. This can be seen by comparing the curve for a given PF values with the curve obtained for lagging operation. This is due to the fact of PV-DG consumes reactive power at leading operation. Therefore, low leading PF causes voltage to reduce. As a result, the system losses are nonlinearly increasing.

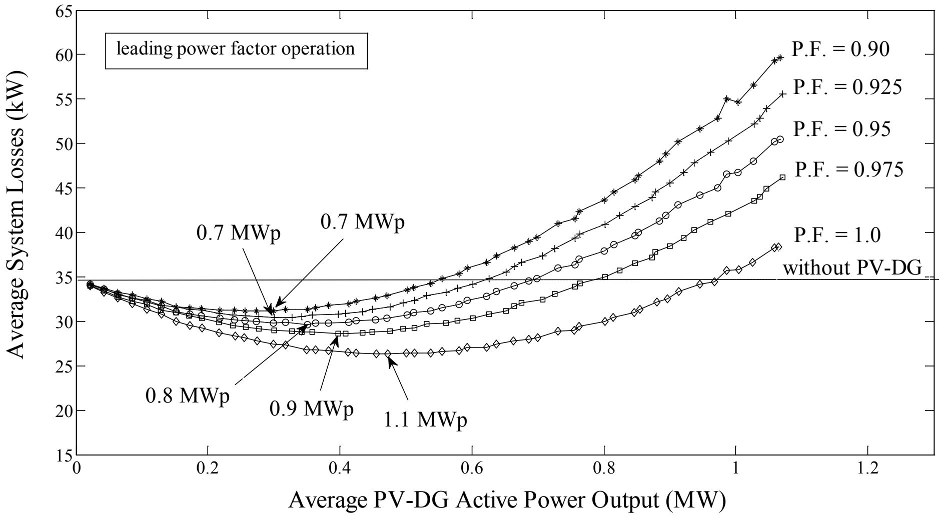

Figure 5.19 Average system losses as a function of average PV-DG power output with different leading power factor (CP-model)

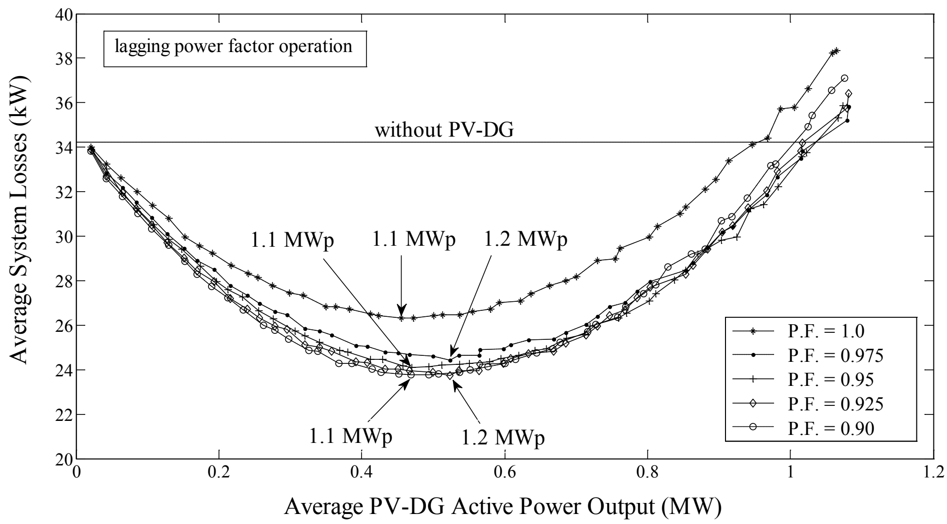

Figure 5.20 Average system losses as a function of average PV-DG power output with different lagging power factor (CP-model)

Figures 5.21 and 5.22 show cumulative probability of voltage and THDv at bus-19 corresponding to the results in Figure 5.19, with different optimal PV-DG sizes at each power factor. Figure 5.21 indicates that voltage is increasing when the size of PV-DG is larger, similar with THDv values as shown in Figure 5.22.

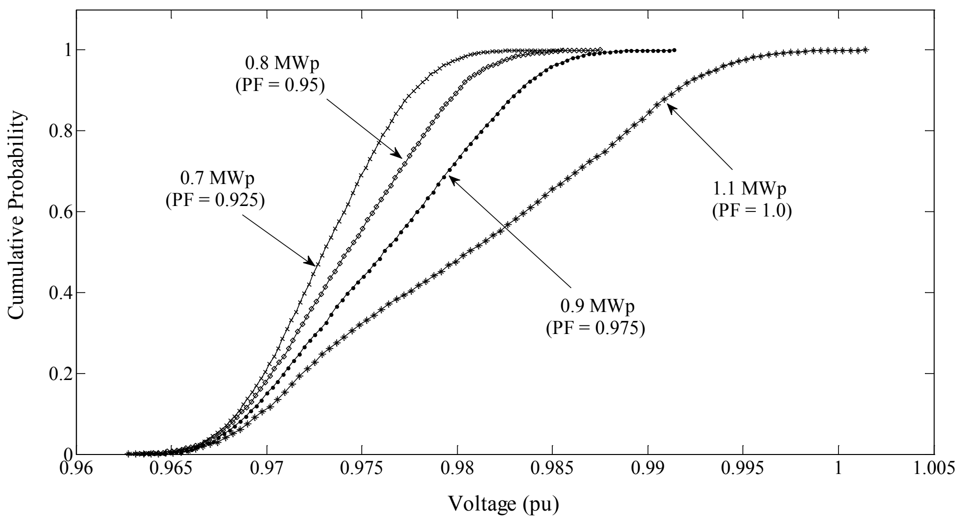

Figure 5.21 Cumulative probability of voltage at bus-19 with different PV-DG sizes corresponding to Figure 5.19

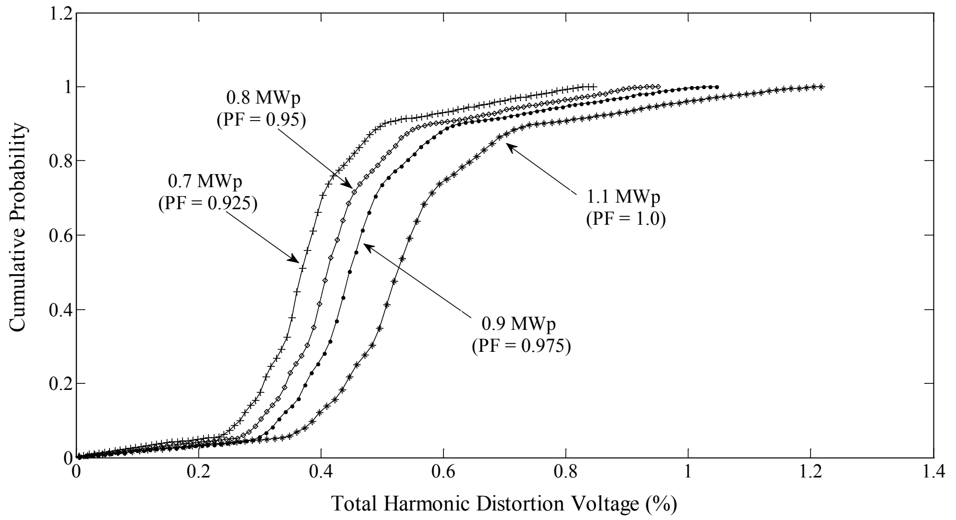

Figure 5.22 Cumulative probability of THDv at bus-19 with different PV-DG sizes corresponding to Figure 5.19

Case-2: ***Multiple PV-DG***

In this case, two PV-DGs are installed at buses 10 and 19. The impact of PV-DGs connection on system losses with different load models are shown as 3-D plot in Figures 5.23 to 5.25, which PF is set to 1.0 constant. It shows that the average system losses decrease more than Case-1 with multiple PV-DGs. It demonstrates that using different static load models do not impact on optimal PV-DGs sizes, which is

1.5 MWp at bus 10 and 0.7 MWp at bus-19. The voltage and THDv constraints at each bus related to PV-DGs sizes of constant power load model are shown in Figures 5.26 and 5.27, respectively. The results indicate that all constraints are kept within the limits.

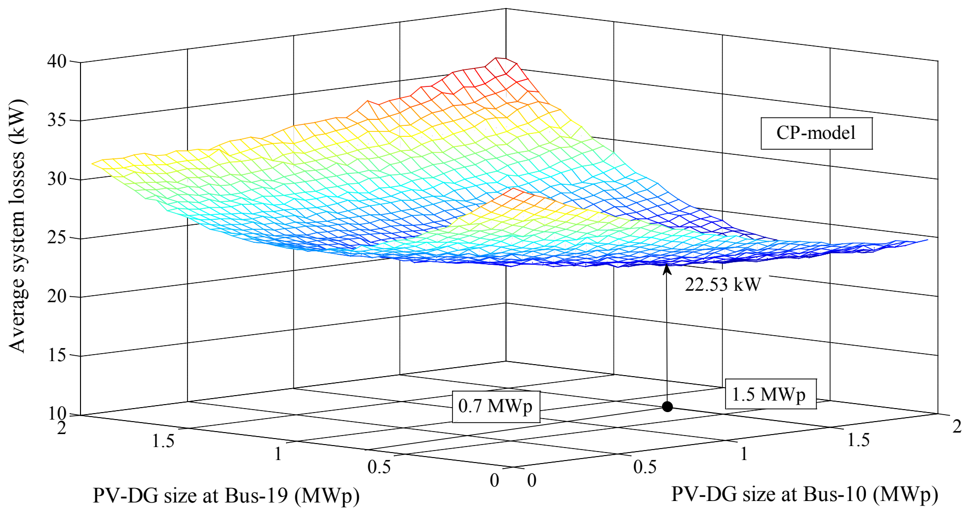

Figure 5.23 Average system losses as a function of PV-DGs capacity at buses 10 and 19 with constant power load model (PF = 1.0)

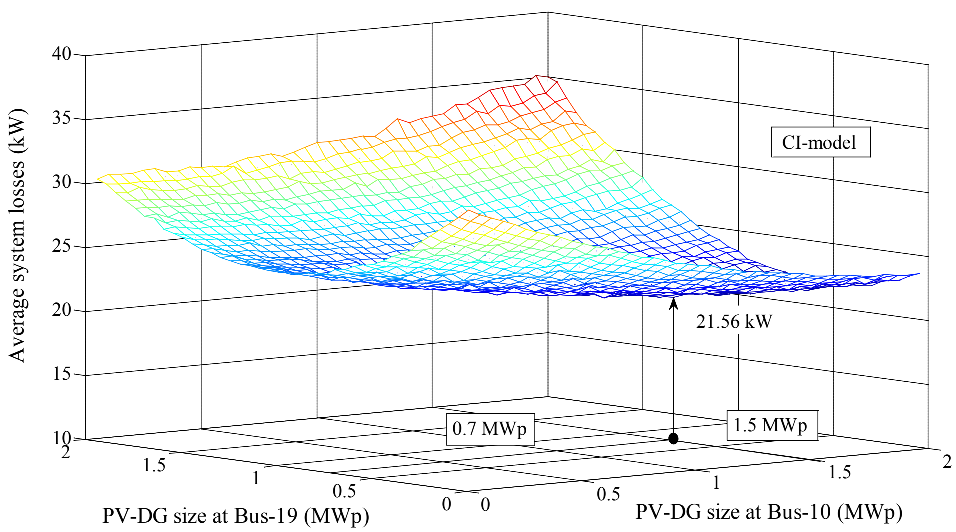

Figure 5.24 Average system losses as a function of PV-DGs capacity at buses 10 and 19 with constant current load model (PF = 1.0)

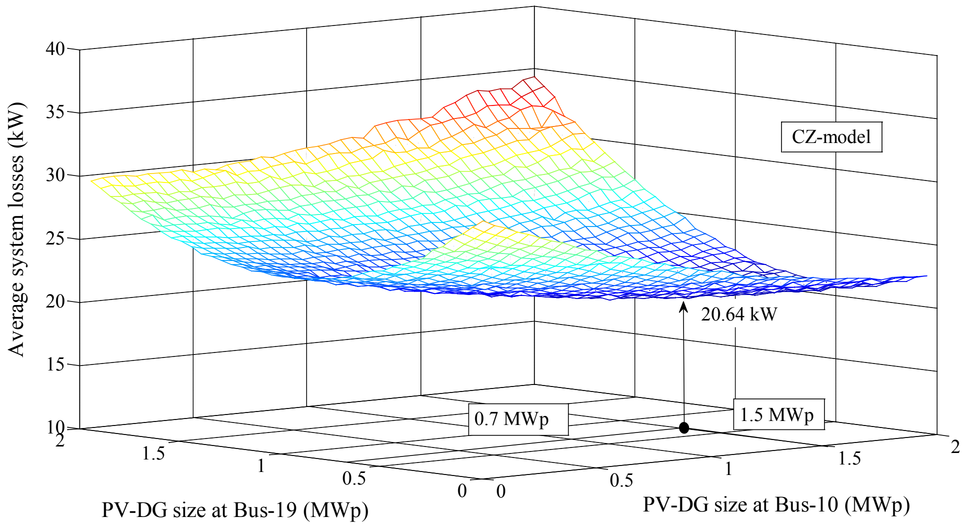

Figure 5.25 Average system losses as a function of PV-DGs capacity at buses 10 and 19 with constant impedance load model (PF = 1.0)

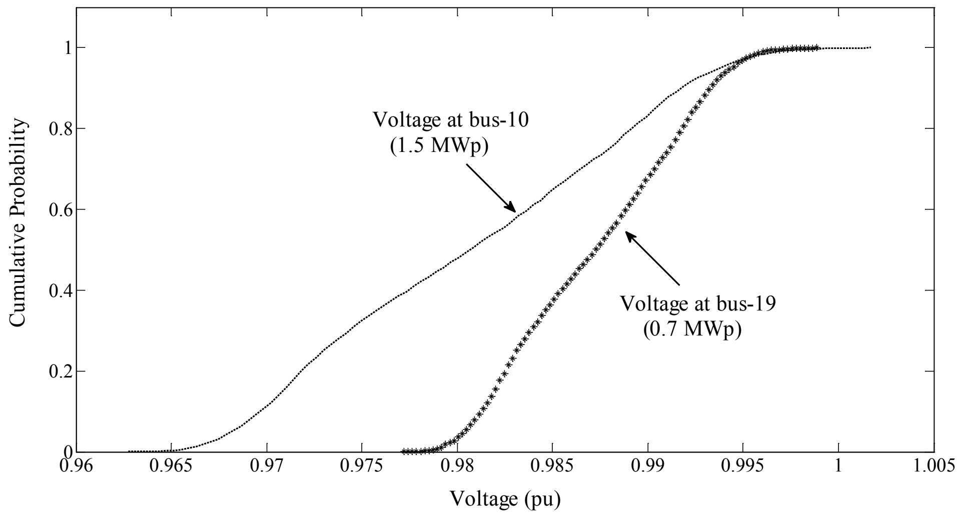

Figure 5.26 Cumulative probability of voltage at buses 10 and 19 corresponding to the result in Figure 5.23

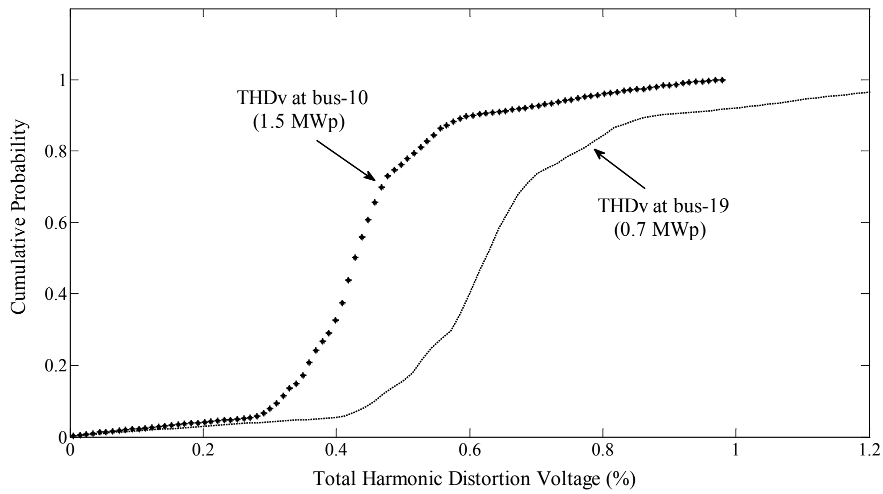

Figure 5.27 Cumulative probability of THDv at buses 10 and 19 corresponding to the result in Figure 5.23

From Figure 5.27, the THDv at bus-19 is higher than the THDv at bus-10 although the PV-DG size at bus-19 (0.7 MWp) is about 50% less compared with bus-10 (1.5 MWp). This is due to the increasing system impedance (longer distance from the substation) and also the influence from large PV-DG size at bus-10. Therefore, higher THDv can be observed at the end of the feeder. This finding is critical for PV-DG installation considering in rural areas where distribution systems are widely spread over large distances.

The impact of various power factor operations with constant power load model on multiple optimal PV-DGs sizes is presented in Table 5.4. Similarly in Case-1, the optimal sizes solution may be changed for wide leading power factor range and it has a few impact on optimal sizes in lagging power factor operation.

Table 5.4 Multiple optimal PV-DGs sizes for various PF operations with CP-model

P.F.	***Lagging type*** Bus-10 (MWp)	Bus-19 (MWp)	System losses (kW)	***Leading type*** Bus-10 (MWp)	Bus-19 (MWp)	System losses (kW)
0.9	1.7	0.8	18.56	0.95	0.4	29.33
0.925	1.7	0.65	18.57	0.95	0.45	28.35
0.95	1.7	0.65	19.21	1.0	0.6	27.29
0.975	1.7	0.8	19.71	1.3	0.65	25.69
1.0	1.5	0.7	22.53	1.5	0.7	22.53

From the results in Scenario-2, it can be summarized that different static load models do not impact on optimal sizes of PV-DGs. It demonstrates that the voltage has a significant change with both load models and PV-DG size (see Figs. 5.17 and 5.21). While the THDv values depend on PV-DG sizes more than load models (see Figs. 5.18 and 5.22). Furthermore, an impact of power factor control on optimal sizes of PV-DGs indicates that leading operation changes the optimal size of PV-DG at each power factor operation. This differs from lagging operation which has low impact on optimal PV-DG size.

In addition, fast growing technologies like PV-DGs is emerging as part of a distribution system. Therefore, it is necessary to evaluate and analyze the power quality issue due to various non-linear current. In practice, utilities cannot assign the PV-DGs installation location to be connected to the feeder because it mainly depends on customers who own the PV systems. Thus, for planning aspect, the proper load models and operating mode of inverter are required to accurately find the PV-DG size solution. However, the simulation result from Case-2 shows that the harmonic distortion voltage can be high depending on the distance away from a substation (see Fig. 5.27). Therefore, it may require the harmonic filter if the PV-DGs are located at the end of feeder, especially the large size of PV-DG.

5.4.3 **Scenario-3:** Effect of inverter modeling and existing DGs in a distribution system on optimal PV-DG sizing

The purpose of this scenario is to study an effect on optimal PV-DG sizing in a distribution system using different PV inverter models (i.e., 6-pulse, 12-pulse and PWM) and existing DGs with various operating conditions.

A heavy load 23 kV radial distribution system is employed as a test case in this scenario. All system parameter are given in Appendix C, which can be found in [85]. The test system has 33 buses with a total load of 9.29 MW, 5.75 MVar as shown in Figure 5.28. The results of base case deterministic load flow are given in Appendix D. And the system operating conditions in this scenario are given as:

- Substation voltage is set to $1.0\angle 0°$ constant.
- Load demand is assumed to be random variables with normal distribution, which standard deviations (σ) is set to 10%.

- Power factor of PV-DG is assumed to be 1.0 constant.
- Load model is assumed to be constant power load.
- Background harmonics are not considered in this test system.
- Various operating conditions of existing DGs in test system are considered.
- Only voltage and THDv constraints are considered in this scenario.
- Range of PV_{size} on this study is between 0.2 MWp to 13 MWp with a 0.2 MWp increment.

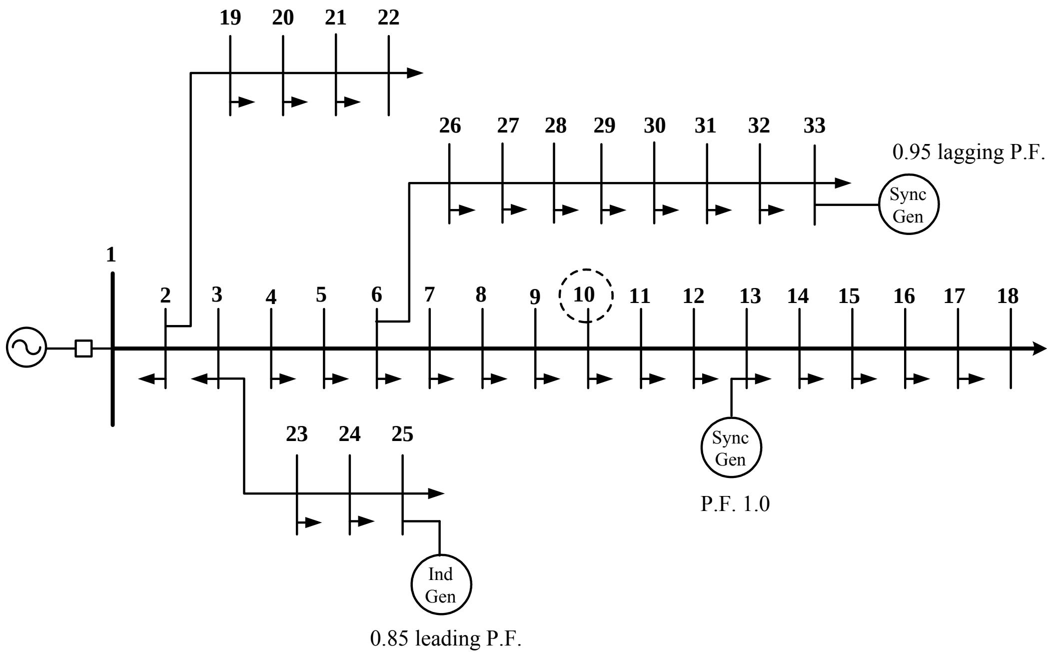

Figure 5.28 Single-line diagram of the 33-bus test system

For the purpose of this study, it is assumed that the single PV-DG installation is located at bus-10. Two cases are studied for investigating the effect of inverter models and existing DGs on optimal PV-DG sizing.

Case-1: ***Optimal PV-DG sizing without consideration of existing DGs***

This case shows the selection of optimal PV-DG size based on the technical constraints without consideration of existing DGs using different inverter models, which the typical harmonic current spectra are given by:

- Using data in Table 4.2 from chapter 4 for 6-pulse and 12 pulse inverter models.
- Using data based on measurements of grid-connected inverter (SMC-11000TL) from a PV farm for PWM inverter model.

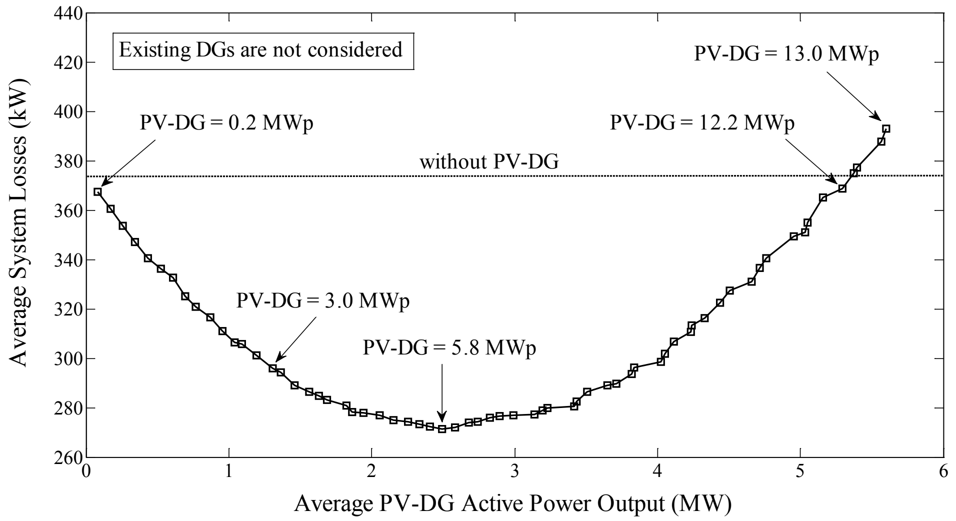

Figure 5.29 Average system losses as a function of average PV-DG power output without consideration of existing DGs

Figure 5.29 presents the relationship between the average system loss and the average PV-DG active power output. From this figure, the system losses vary with the size of PV-DG installed at bus-10. The average system loss without installing PV-DG is 375.1 kW. Besides, the system losses decrease when installing PV-DG less than 12.2 MWp. The minimum average system loss in this case is 271.3 kW, which is given by installing a PV-DG at 5.8 MWp. While the average active power output of PV-DG is around 2.5 MW.

The cumulative probability of voltage at bus-10 with and without installation of 5.8 MWp PV-DG is shown in Figure 5.30. Similarly to scenarios 1 and 2, an installation of PV-DG mostly improves the voltage regulation at the PCC. Note from the figure, it shows that the highest voltage level at bus-10 stays within an acceptable limits (i.e., 1.05 pu). Since, however, the test system in this case has heavy load and there is no any compensator elements to regulate the voltage rise up. Hence, voltage at some node before installing PV-DG is lower the limits (i.e., 0.95 pu), this can be found in base case deterministic load flow solution as given in Appendix D. By this reason, the minimum voltage at bus-10 may lower than the limits after installing PV-DG. However, the probability at which voltage at bus-10 lower than 0.95 pu is 0.1, and it can be acceptable for this system.

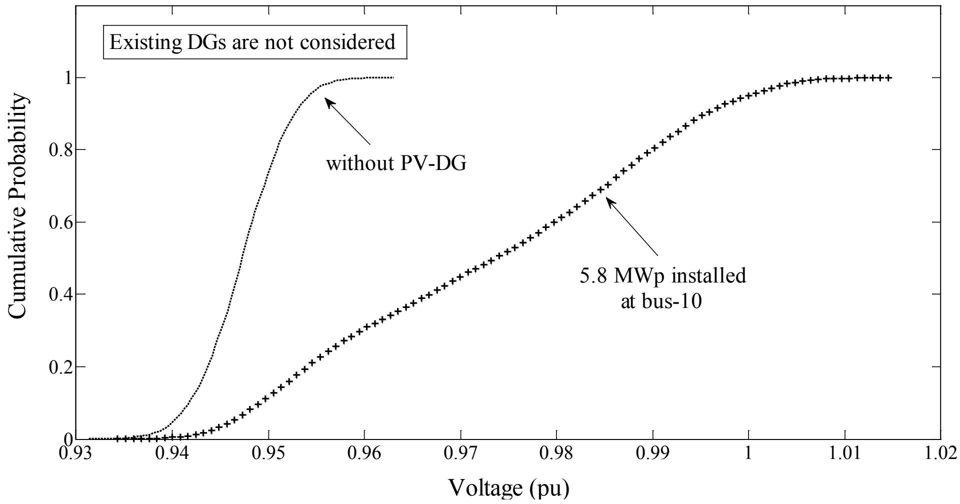

Figure 5.30 Cumulative probability of voltage at bus-10 without consideration of existing DGs

Figure 5.31 shows the comparison of THDv values at bus -10 using different PV inverter models. Since, it need to be installed high capacity of PV-DG (5.8 MWp) to minimize system loss in this case. Therefore, the THDv values can exceed the limits for 6-pulse and 12-pulse inverter models, especially the 6-pulse inverter. This differs from PWM inverter that the THDv value is less than 2%. This indicates that a PWM technology can produce small voltage distortion waveform. In present, mostly PV inverter technologies are based on PWM [83]. However, the purpose of this case needs to show the distinction of THDv values from using different PV inverter models in our study.

Furthermore, to comply with IEEE standard, PV-DG size should be reduced to 3.0 MWp for 6-pulse inverter. The average system loss is around 295 kW for this installation size, see Figure 5.29.

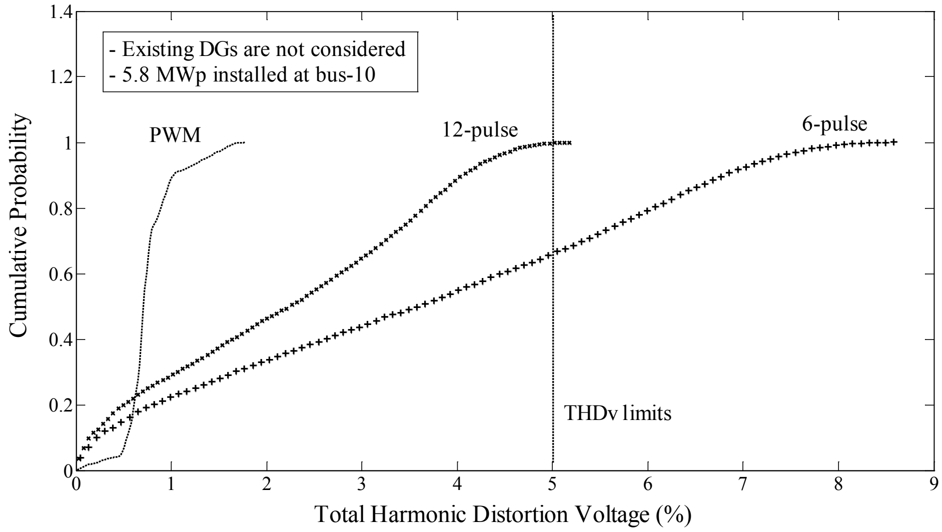

Figure 5.31 Cumulative probability of THDv at bus-10 using different inverter models without consideration of existing DGs

<u>Case-2</u>: *Optimal PV-DG sizing with consideration of existing DGs*

This case shows the effect of optimal PV-DG sizing with consideration of existing DGs in distribution system. Using different inverter models are also presented to compare THDv values with Case-1. For the purpose of study case, the locations of existing DGs as well as its operating conditions and capacity are given in Table 5.5.

Table 5.5 Existing DGs locations, capacity and its operating conditions

Location Bus	*DGs capacity (MW)*	*DG type*	*Operating mode*
13	1.5	Synchronous	PF. 1.0
25	1.0	Induction	PF. 0.85 leading
33	1.0	Synchronous	PF. 0.95 lagging

As shown in Figure 5.32, it needs to install 2.6 MWp PV-DG to minimize average system loss, which approximately reduced 50% compared with Case-1 (5.8 MWp). This is due to highly generation power of the existing DGs (3.5 MW). So, the average system loss before installing PV-DG is more decreased than Case-1 (178 kW). From the figure, the minimum average system loss is 163.6 kW in this case, while the average active power output of PV-DG is around 1.12 MW.

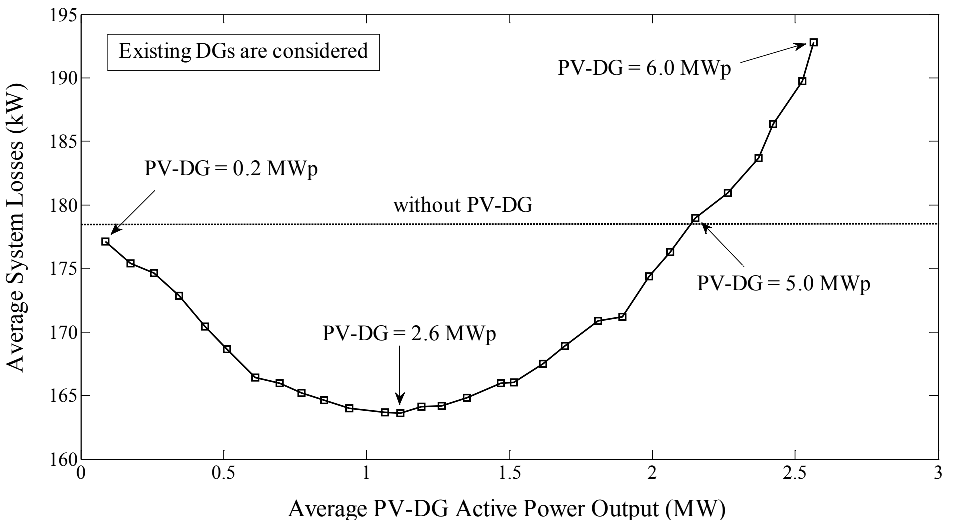

Figure 5.32 Average system losses as a function of average PV-DG power output with consideration of existing DGs

Figure 5.33 shows comparison of the voltage cumulative probability at bus-10 before and after installation of 2.6 MWp PV-DG. The voltage level at bus-10 stays within an acceptable range in this case. Note from the figure, it shows that the minimum voltage at bus-10 is higher than Case-1 and kept within the limits, when the existing DGs are presented.

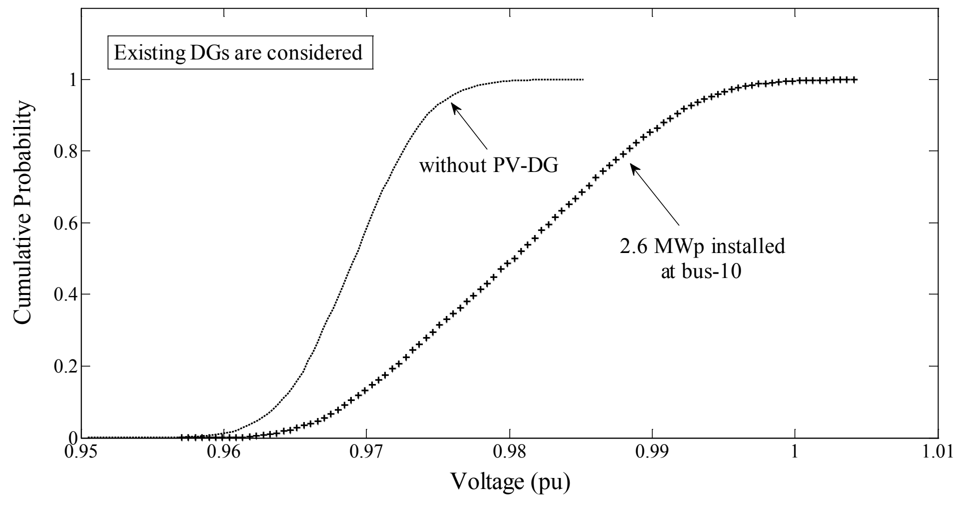

Figure 5.33 Cumulative probability of voltage at bus-10 with consideration of existing DGs

Since the reducing more of PV-DG capacity in Case-2, consequence the THDv values are within the limits for all PV inverter model as shown in Figure 5.34. Similarly to Case-1, however, it indicates that the PWM technology can produce very small voltage distortion waveform, which less than 1% in this case.

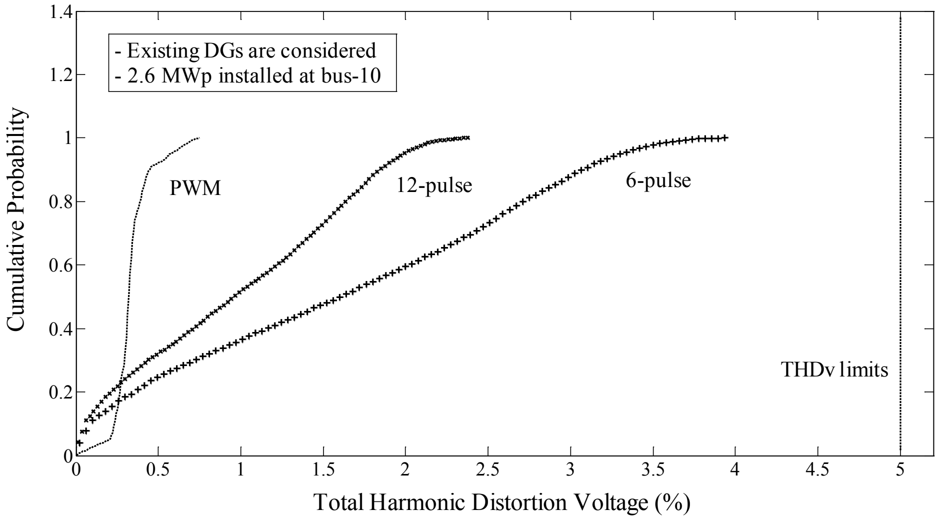

Figure 5.34 Cumulative probability of THDv at bus-10 using different inverter models with consideration of existing DGs

From the results in Scenario-3, it can be summarized that different PV inverter models have effect to optimal size of PV-DG. It demonstrates that the 6-pulse inverter modeling may produce high THDv values at PCC, while the PWM inverter modeling can produce very small THDv values. The THDv values produced from the 12-pulse inverter are in between these two, as seen in Figures 5.31 and 5.34. From these figures, it indicates that interconnection of small PV-DG may not result in violation of the power quality standard. However, the THDv values are comply with standard for PWM inverter in all case. While PV-DG size may reduced for 6-pulse and 12-pulse inverters, as shown in Case-1. Furthermore, addition other DGs in distribution system can effect is to decrease PV-DG size to minimize system losses.

CHAPTER VI

CONCLUSIONS AND FUTURE WORKS

6.1 Conclusions

This dissertation presents a probabilistic approach to calculate an optimal size of PV-DG in a distribution system. The stochastic variables of both generation and load have been considered. The proposed technique is based on actual hourly solar radiation, ambient temperature and typical harmonic currents of grid-connected inverter in Thailand. The results from all scenarios show that the proposed technique is effectively to obtain optimal sizes of PV-DGs for both single and multiple locations based on technical constraints.

From several system operating conditions, it can be summarized the optimal PV-DGs sizing based on this approach as follows:

- It need to be collected the data of hourly variations of solar radiation and ambient temperature for a site of interest.
- In practical, a validation of PV model is necessary to accurate the power output of PV-DG corresponding to solar radiation and temperature.
- In planning aspect, a measurement of harmonic current spectra of PV inverter is necessary to assess the power quality.
- By applying this technique, optimal sizes of PV-DGs can be determined taking into account background harmonics. And With high background harmonics or with high capacity of PV-DGs, %THDv at PCC may increase and not satisfy the standard.
- Different static load models do not impact on optimal PV-DGs sizes. And THDv values depend on PV-DG sizes more than load models.
- Leading power factor operation changes optimal PV-DG size but lagging operation has low impact on optimal PV-DG size.
- High distortion voltage waveform may be produced by 6-pulse and 12-pulse inverter modeling causes THDv values exceed the limits. While the PWM inverter modeling can produce very small distortion harmonic voltage and satisfied the standard.

- Additional DGs in a distribution system may lead to decrease optimal PV-DG size to minimize system losses.
- The PV-DGs are likely to improve voltage regulation and decrease system losses in a distribution system, but increase THDv values at PCC.

6.2 Future Works

In order to determine the optimal PV-DGs sizes in a distribution system for future studies. Some further issue described below may be of interest.

- It is possible for applying the proposed method to determine optimal size and location of PV-DG at the same time while satisfying the number of constraints described in this works. The Genetic Algorithm (GA) may be used for this issue.
- Other technical constraints such as distribution line current limits can also be added into the proposed algorithm.
- The impact of PV-DG on protection coordination should be studied.
- The coordination of voltage regulation equipments in distribution system may be incorporate with optimal PV-DGs sizing.

REFERENCES

[1] IEEE Standard 1547-2003, IEEE Standard for Interconnecting Distributed Resources with Electric Power Systems.

[2] Philip, P. Barder, and Robert, W. de Mello. Determining the impact of Distributed Generation on Power Systems: Part1-Radial Distribution Systems. in Power Engineering Society Summer Meeting 3 (July 2000): 1645-1656.

[3] Frede Blaabjerg, Remus Teodorescu, Marco Liserre, and Adrian, V. Timbus. Overview of Control and Grid Synchronization for Distributed Power Generation Systems. IEEE Trans. Industrial Electronics 53, 5 (October 2006): 1398-1409.

[4] International Energy Agency (IEA-PVPS). Cumulative Installed PV Power [Online]. 2010. Available from: http://www.iea-pvps.org [2011, June]

[5] M., Shahidehpour, and F., Schwartz. Don't let the sun go down on PV. IEEE Power Energy Magazine 2 (May/June 2004): 40-48.

[6] SEARCA Knowledge Center on Climate Change. Thailand's Solar Lessons for the World [Online]. 2011. Available from: http://www.beta.searca.org [2011, June]

[7] Denis Lenardic. Large-Scale Photovoltaic Power Plants Annual Review 2008 [Online]. 2009. Available from: http://www.pvresources.com [2011, June]

[8] First Solar. PV Technology Comparison [Online]. 2011. Available from: http://www.firstsolar.com [2011, June]

[9] Gilbert, M. Masters. Renewable and Efficient Electric Power Systems. A John Wiley & Sons Inc., 2004.

[10] Solar Energy Development Programmatic EIS. Solar Photovoltaic Technologies [Online]. 2011. Available from : http://www.solareis.anl.gov/guide/solar/pv/index.cfm [2011, June]

[11] Solar Energy Development Programmatic EIS. Concentrating Solar Power Technology [Online]. 2011. Available from: http://www.solareis.anl.gov [2011, June]

[12] Department of Alternative Energy Development and Efficiency (DEDE). Ministry of Energy in Thailand. Thailand Energy Situation 2010 [Online]. 2010. Available from: http://www.dede.go.th [2011, July]

[13] System Planning Division. Electricity Generating Authority of Thailand. Summary of Thailand Power Development Plan 2010-2030 Report no. 912000-5305, April 2010.

[14] Department of Alternative Energy Development and Efficiency (DEDE). Ministry of Energy in Thailand. Solar Map of Thailand [Online]. 1999. Available from: http://www.dede.go.th [2011, August]

[15] Department of Alternative Energy Development and Efficiency (DEDE). Ministry of Energy in Thailand. PV Systems Installation Status in Thailand since 1983-2010 [Online]. 2011. Available from: http://www.dede.go.th [2011, August]

[16] Victor, H. Mendez Quezada, Juan Rivier Abbad, and Tomas Gomez San Roman. Assessment of Energy Distribution Losses for Increasing Penetration of Distributed Generation. IEEE Trans. Power System 21, 2 (May 2006): 533-540.

[17] Daniel, S. Shugar. Photovoltaic in the Utility Distribution System: The Evaluation of System and Distributed Benefits. in Proc. Conference Record of the 21st IEEE Photovoltaic Specialists Conference, Kissimmee 2 (1990): 836-843.

[18] T., Ichikawa. Recent Research and Development on Power Systems with a Large Number of Distributed Generating Facilities. in Transmission and Distribution Conference and Exhibition 2002: Asia Pacific. IEEE/PES 2 (October 2002): 1367-1369.

[19] Jung Hun So, Young Seok Jung, Byung Gyu Yu, Hye Mi Hwang, and Gwon Jong Yu. Performance Results and Analysis of Large Scale PV System. in Photovoltaic Energy Conversion Conference Record of the 2006 IEEE 4th World Conference 2 (May 2006): 2375-2378.

[20] Alejandro, R. Oliva, and Juan Carlos Balda. A PV Dispersed Generator: A Power Quality Analysis Within the IEEE 519. IEEE Trans. Power Delivery 18, 2 (April 2003): 525-530.

[21] K., Tran, and M., Vaziri. Effects of Dispersed Generation (DG) on Distribution Systems. in Power Engineering Society General Meeting 3 (June 2005): 2173-2178.

[22] A., Bhowmik, A., Maitra, A. M., Halpin, and J. E., Schatz. Determination of Allowable Penetration Levels of Distributed Generation Resources Based on Harmonic Limit Consideration. IEEE Trans. Power Delivery 18, 2 (April 2003): 619-624.

[23] R., Dugan, M., McGranaghan, and H. W., Beaty. Electrical Power Systems Quality. McGraw-Hill, 1996.

[24] N., Mohan, T., Undeland, and W., Robbins. Power Electronics: Converters Applications and Design. John Wiley & Sons, 1995.

[25] Johan, H.R. Enslin, and Peter, J.M. Heskes. Harmonic Interaction Between a Large Number of Distributed Power Inverters and the Distribution Network. IEEE Trans. Power Electronics 19, 6 (November 2004): 1586-1593.

[26] M.C., Benhabib, J.M.A., Myrzik, and J.L., Duarte. Harmonic effects caused by large scale PV installations in LV network. in Electrical Power Quality and Utilisation 2007, 9th International Conference (October 2007): 1-6.

[27] Florentin Batrinu, Gianfranco Chicco, Jurgen Schlabbach, and Filippo Spertino. Impacts of grid-connected photovoltaic plant operation on the harmonic distortion. in IEEE MELECON (May 2006): 861-864.

[28] Andrew Kotsopoulos, Peter, J.M. Heskes, and Mark, J. Jansen. Zero-Crossing Distortion in Grid-Connected PV Inverters. IEEE Trans. Industrial Electronics 52, 2 (April 2005): 558-565.

[29] A.R., Oliva, J.C., Balda, D.W., McNabb, and R.D., Richardson. Power-Quality Monitoring of a PV Generator. IEEE Trans. Energy Conversion 13, 2 (June 1998): 188-193.

[30] S., Yanagawa, T., Kato, K., Wu, A., Tabata, and Y., Suzuoki. Evaluation of LFC capacity for output fluctuation of photovoltaic generation systems based on multi-point observation of insolation. in Proc. IEEE Power Engineering Society Summer Meeting (2001): 1652-1657.

[31] Walid, A. Omran, and M., Kazerani. Investigation of Methods for Reduction of Power Fluctuations Generated From Large Grid-Connected Photovoltaics Systems. IEEE Trans. Energy Conversion 26, 1 (March 2011): 318-327.

[32] Y.T., Tan, D.S., Kirschen, and N., Jenkins. A model of PV generation suitable for stability analysis. IEEE Trans. Energy Conversion 19, 4 (Dec 2004): 748-755.

[33] Achim Woyte, Vu Van Thong, Ronnie Belmans, and Johan Nijs. Voltage Fluctuations on Distribution Level Introduced by Photovoltaic Systems. IEEE Trans. Energy Conversion 21, 1 (March 2006): 202-209.

[34] P., Chen, Z., Chen, B., Bak-Jensen, R., Villafafila, and S., Sorensen. Study of Power Fluctuation from Dispersed Generations and loads and its impact on a Distribution Network through a probabilistic approach. in Electrical Power Quality and Utilisation 2007, 9th International Conference (October 2007): 1-5.

[35] Benoit BLETTERIE, and Tomaz PFAJFAR. Impact of Photovoltaic Generation on Voltage Variations-How Stochastic is PV. in 19th International Conference on Electricity Distribution (CIRED), Vienna 513 (May 2007): 1-4.

[36] T., Kinjo, T., Senjyu, N., Urasaki, and H., Fujita. Output levelling of renewable energy by electric double layer capacitor applied for energy storage system. IEEE Trans. Energy Conversion 21, 1 (March 2006): 221-227.

[37] Md., H. Rahman, and S., Yamashiro. Novel distributed power generating system of PV-ECaSS using solar energy estimation. IEEE Trans. Energy Conversion 22, 2 (June 2007): 358-367.

[38] J. P., Barton, and D. G., Infield. A probabilistic method for calculating the usefulness of a store with finite energy capacity for smoothing electricity generation from wind and solar power. Journal of Power Sources 162 (2006): 943-948.

[39] R., Wanger. Large lead/acid batteries for frequency regulation, load levelling and solar power applications. Journal of Power Sources 67 (1997): 163-172.

[40] H., Sugihara, S., Nishikawa, and Y., Kimura. Observation of the hybrid system using photovoltaic and sodium-sulphur battery. in Proc. JSES/JWEA Joint Conference (2001): 13-16.

[41] H., Miyauchi, K., Eguchi, and H., Hayashi. SEMS to power quality improvement. in Proc. IEEJ Conference of Power and Energy Society (2002): 110-115.

[42] J., Thongpron, U., Sangpanich, C., Limsakul, D., Chenvidya, K., Kirtikara, and C., Jivacate. Study of a PV-Grid Connected System on its Output Harmonics and Voltage Variation. Asian J. Energy Environ 5, 1 (2004): 59-73.

[43] D., Chenvidya, J., Thongpron, U., Sangpanich, N., Wongyao, K., Kirtikara, and C., Jivacate. A Thai National Demonstration Project on PV Grid-Interactive Systems: Power Quality Observation. in 3rd World Conference on Photovoltaic Energy Conversion, Osaka Japan (May 2003): 2152 - 2154.

[44] M.A., Kashem, An, D.T. Le, M., Negnevitsky, and G., Ledwich. Distributed Generation for Minimization of Power Losses in Distribution Systems. in Conference on Power Engineering Society General Meeting (June 2006): 1-8.

[45] L., Ramesh, S.P., Chowdhury, S., Chowdhury, Y.H., Song, and A.A., Natarajan. Voltage Stability Analysis and Real Power Loss Reduction in Distributed Distribution System. in Transmission and Distribution Conference and Exposition (IEEE/PES) (April 2008): 1-6.

[46] Yue Yuan, Kejun Qian, and Chengke Zhou. The Optimal Location and Penetration Level of Distributed Generation. in 42nd International Universities Power Engineering Conference (UPEC), Brighton University, UK (September 2007): 917-923.

[47] G., Celli, E., Ghiani, S., Mocci, and F., Pilo. A Multi-Objective Approach to Maximize the Penetration of Distributed Generation in Distribution Networks. in 9th International Conference on Probabilistic Methods Applied to Power Systems, Stockholm, Sweden (June 2006): 1-6.

[48] Hamid Falaghi, and Mahmood-Reza Haghifam. ACO Based Algorithm for Distributed Generation Sources Allocation and Sizing in Distribution Systems. in Power Tech'07 Conference, Lausanne, Switzerland (July 2007): 555-560.

[49] M.F., AlHajri, and M.E., El-Hawary. Improving the voltage profiles of Distribution Networks using multiple Distribution Generation Sources. in Conference on Power Engineering, Large Engineering Systems (October 2007): 295-299.

[50] Kai Zou, A.P., Agalgaonkar, K.M., Muttaqi, and S., Perera. Optimisation of Distributed Generation Units and Shunt Capacitors for Economic Operation of Distribution Systems. in Australasian Universities Power Engineering Conference (AUPEC), Australia (2008): P-137/1-P-137/7.

[51] Raj Kumar Singh, Nalin, B. Dev Choudhury, and S.K., Goswami. Optimal Allocation of Distributed Generation in Distribution Network with Voltage and Frequency Dependent Loads. in IEEE Region 10 Colloquium and the Third ICIIS, Kharagpur, India (December 2008): 1-5.

[52] R.K., Singh, and S.K., Goswami. Optimal Siting and Sizing of Distributed Generations in Radial and Networked Systems Considering Different Voltage Dependent Static Load Models. in 2nd IEEE International Conference on Power and Energy (PECon), Johor Bahary, Malaysia (December 2008): 1535-1540.

[53] Soo-Hyoung Lee, and Jung-Wook Park. Selection of Optimal Location and Size of Multiple Distributed Generations by Using Kalman Filter Algorithm. IEEE Trans. Power Systems 24, 3 (August 2009): 1393-1400.

[54] M.F., AlHajri, and M.E., El-Hawary. The Effect of Distributed Generation Modeling and Static Load Representation on the Optimal Integrated Sizing and Network Losses. in Canadian Conference on Electrical and Computer Engineering (CCECE) (May 2008): 1543-1548.

[55] S., Kamalinia, S., Afsharnia, M.E., Khodayar, A., Rahimikian, and M.A. Sharbafi. A Combination of MADM and Genetic Algorithm for Optimal DG Allocation in Power Systems. in 42nd International Universities Power Engineering Conference (UPEC), Brighton University, UK (September 2007): 1031-1035.

[56] M., Gandomkar, M., Vakilian, and M., Ehsan. A Combination of Genetic Algorithm and Simulated Annealing for Optimal DG Allocation in Distribution Networks. in 18th Canadian Conference on Electrical and Computer Engineering, Saskatoon, Saskatchewan Canada (May 2005): 645-648.

[57] G.B., Shrestha, and L., Goel. A Study on Optimal Sizing of Stand-Alone Photovoltaic Stations. IEEE Trans. Energy Conversion 13, 4 (December 1998): 373-378.

[58] H.A.M., Maghraby, M.H., Shwehdi, and G.K., Al-Bassam. Probabilistic Assessment of Photovoltaic (PV) Generation Systems. IEEE Trans. Power System 17, 1 (February 2002): 205-208.

[59] Eiichi Endo and Kosuke Kurokawa. Sizing Procedure for Photovoltaic Systems. in First WCPEC, Hawaii (December 1994): 1196-1199.

[60] Ferry, A. Viawan, Ferruccio Vuinovich, and Ambra Sannino. Probabilistic Approach to the Design of Photovoltaic Distributed Generation in Low Voltage Feeder. in 9th International Conference on Probabilistic Methods Applied to Power Systems. KTH, Stockholm, Sweden (June 2006): 1-7.

[61] Christoph Mayr, Roland Brundlinger, and Benoit Bletterie. Photovoltaic-inverters as Active Filters to improve Power Quality in the Grid. What can State-of-the-art Equipment Achieve. in 9th International Conference on Electrical Power Quality and Utilisation. Barcelona (October 2007): 1-5.

[62] G., Carpinelli, G., Celli, S., Mocci, F., Pilo, D., Proto, and A., Russo. Multiobjective Programming for the Optimal Sizing and Siting of Power-Electronic Interfaced Dispersed Generators. in Power Tech'07 Conference, Lausanne, Switzerland (July 2007): 443-448.

[63] International Electrotechnical Commission, IEC 61727 Photovoltaic (PV) systems – Characteristics of the Utility Interface, June 1995.

[64] IEEE Standard 519-1992, IEEE Recommended Practices and Requirements for Harmonic Control in Electrical Power Systems, 1992.

[65] Roy Billiton, and Wenyuan Li. Reliability Assessment of Electric Power Systems Using Monte Carlo Methods. Plenum Press, New York, 1994.

[66] Geoff Walker, Evaluating MPPT Converter Topologies Using A Matlab PV Model. *Journal of Electrical & Electronics Engineering*, Australia, vol. 21, 2001, pp. 49-55.

[67] J.A., Gow, and C. D., Manning. Development of a photovoltaic array model for use in power electronics simulation studies. IEEE Proceedings on Electric Power Applications 146, 2 (March 1999): 193-200.

[68] Eduardo Lorenzo. Solar Electricity Engineering of Photovoltaic Systems. Progensa, Spain, 1994.

[69] Anca, D. Hansen, Poul Sorensen, Lars, H. Hansen, and Henrik Bindner. Models for a Stand-Alone PV system. A stand-alone PV system modeling and simulation report. Riso National Laboratory, Roskilde, Denmark (December 2000): 1-78.

[70] R., Faranda, S., Leva, and V., Maugeri. MPPT techniques for PV System: energetic and cost comparison. in Power and Energy Society General Meeting - Conversion and Delivery of Electrical Energy in the 21st Century (July 2008): 1-6.

[71] Trishan Esram, and Patrick, L. Comparison of Photovoltaic Array Maximum Power Point Tracking Techniques. IEEE Transactions on Energy Conversion 22, 2 (June 2007): 439-449.

[72] Hanifi Guldemir. Sliding Mode Control of Dc-Dc Boost Converter. Journal of Applied Sciences 5, 3 (2005): 588-592.

[73] N., Mithulananthan, and C. A., Canizares. Effect of Static Load Models on Hopf Bifurcation Point and Critical Modes of Power Systems. Thammasat International Journal Science and Technology 9, 4 (October 2004): 69-76.

[74] U., Eminoglu, and M. H., Hocaoglu. A Voltage Stability Index for Radial Distribution Networks. in International Universities Power Engineering Conference (UPEC) (2007): 408-413.

[75] M., Charkravorty, and D., Das. Voltage Stability Analysis of Radial Distribution Networks. International Journal of Electrical Power & Energy Systems, Elsevier 23, 2 (2001): 129-135.

[76] D., Das, D. P., Kothari, and A., Kalam. Simple and efficient method for load flow solution of radial distribution networks. International Journal of Electrical Power & Energy Systems, Elsevier 17, 5 (1995): 335-346.

[77] Ashokkumar, R., and Aravindhababu, P. An Improved Power flow Technique for Distribution Systems. Journal of Computer Science, Informatics & Electrical Engineering 3, 1 (2009): 1-8.

[78] Fan Zhang, and Carol, S. Cheng. A Modified Newton Method for Radial Distribution System Power Flow Analysis. IEEE Trans. Power System 12, 1 (February 1997): 389-397.

[79] W.F., Tinney, and C.E., Hart. Power Flow Solution by Newton's Method. IEEE Trans. Power App. System PAS-86 (November 1967): 1449-1460.

[80] Behic, R. Gungor, Power Systems. Harcourt Brace Jovanovich, Publishers, Florida, 1988.

[81] Robert, A., Deflandre, T., and Working Group CC02, ELECTRA No. 16: Guide for Assessing the Network Harmonic Impedance, 1996.

[82] Nick Jenkins, Ron Allan, Peter Crossley, David Kirschen, and Goran Strbac. Embedded Generation. The Institution of Electrical Engineers, 2000.

[83] IEA. Grid-connected PV power systems: Survey of inverter and related protection equipments. Task V report IEA-PVPS (December 2002).

[84] Pradit Fuangfoo. The Impact of Distributed Generation on The Thailand's Electric Power System. Doctoral dissertation, Faculty of the Graduate School of The University of Texas at Arlington, 2006.

[85] Vichakorn Hengsritawat. Optimal Shunt Capacitor Sizing and Location on the Radial Distribution System. Master's Thesis, Department of Electrical Engineering, Chulalongkorn University, 1998.

[86] Department of Alternative Energy Development and Efficiency (DEDE), Ministry of Energy in Thailand.

[87] Thai Meteorological Department, Ministry of Information and Communication Technology of Thailand.

APPENDICES

Appendix A

Hourly Variations of Solar Radiation and Ambient Temperature of Chiang Mai Province

(During 6.00 to 18.00 on Jan-Dec 2007)

A1. Hourly and daily solar radiation (MJ/m^2) [86]

January

Date/Time	6-7	7-8	8-9	9-10	10-11	11-12	12-13	13-14	14-15	15-16	16-17	17-18	Total
1													
2													
3	0.000	0.000	0.000	0.000	0.000	0.000	0.000	0.000	0.000	0.000	0.842	0.265	1.108
4	0.000	0.090	0.540	1.482	2.168	2.561	2.735	2.673	2.265	1.658	0.966	0.251	17.388
5	0.000	0.086	0.527	1.445	2.076	2.475	2.679	2.622	2.232	1.661	0.960	0.231	16.995
6	0.000	0.142	0.632	1.030	2.023	2.389	2.500	2.581	2.203	1.689	1.002	0.264	16.454
7	0.000	0.100	0.527	0.938	2.059	2.602	2.781	2.733	2.153	1.561	0.428	0.155	16.038
8	0.000	0.080	0.551	0.755	1.428	2.390	2.792	2.671	2.394	1.788	1.056	0.326	16.232
9	0.000	0.088	0.584	1.529	2.160	2.586	2.759	2.679	2.317	1.773	1.093	0.315	17.883
10	0.000	0.092	0.573	1.436	1.994	2.502	2.669	2.591	2.265	1.681	0.969	0.264	17.036
11	0.000	0.088	0.573	1.459	2.070	2.479	2.685	2.576	2.181	1.655	0.957	0.242	16.966
12	0.000	0.096	0.532	1.368	1.978	2.391	2.679	2.555	2.198	1.798	1.028	0.256	16.879
13	0.000	0.088	0.528	1.402	2.007	2.443	2.674	2.474	2.171	1.552	0.953	0.277	16.571
14	0.000	0.110	0.517	1.384	1.928	2.437	2.594	2.583	2.211	1.682	1.053	0.335	16.832
15	0.000	0.091	0.533	1.526	2.147	2.581	2.796	2.714	2.343	1.789	1.082	0.366	17.968
16	0.000	0.076	0.526	1.570	2.189	2.587	2.810	2.732	2.391	1.883	1.155	0.374	18.294
17	0.000	0.089	0.497	1.464	2.056	2.469	2.692	2.611	2.297	1.751	1.065	0.331	17.322
18	0.000	0.082	0.476	1.515	2.185	2.639	2.853	2.796	2.449	1.858	1.184	0.398	18.434
19	0.000	0.085	0.482	1.458	2.088	2.529	2.740	2.679	2.348	1.784	1.116	0.387	17.698
20	0.000	0.080	0.506	1.631	2.232	2.685	2.878	2.817	2.465	1.889	1.165	0.385	18.735
21	0.000	0.083	0.511	1.588	2.216	2.656	2.864	2.803	2.528	1.936	1.205	0.411	18.803
22	0.000	0.089	0.510	1.535	2.160	2.595	2.844	2.819	2.480	1.942	1.218	0.432	18.631
23	0.000	0.082	0.486	1.470	2.057	2.458	2.653	2.545	2.244	1.720	1.081	0.346	17.145
24	0.000	0.110	0.430	0.863	1.024	1.784	2.315	2.439	2.090	1.538	0.986	0.303	13.886
25	0.000	0.111	0.498	1.105	1.016	2.183	2.354	2.396	2.191	1.704	0.997	0.315	14.876
26	0.000	0.101	0.482	1.364	2.015	2.460	2.637	2.567	2.275	1.703	1.053	0.380	17.042
27	0.000	0.086	0.473	1.286	1.911	2.306	2.556	2.421	2.247	1.530	0.683	0.299	15.804
28	0.000	0.045	0.346	0.717	1.104	1.224	1.194	1.069	0.414	0.284	0.364	0.080	6.841
29	0.000	0.115	0.529	1.364	2.020	2.486	2.662	2.671	2.349	1.795	1.067	0.344	17.414
30	0.000	0.086	0.472	1.165	1.645	2.140	2.491	2.444	2.045	1.665	0.988	0.342	15.493
31	0.000	0.094	0.461	0.843	1.687	1.984	1.905	1.880	1.317	1.206	0.845	0.375	12.612
Average	**0.000**	**0.088**	**0.493**	**1.265**	**1.850**	**2.311**	**2.510**	**2.453**	**2.106**	**1.603**	**0.985**	**0.312**	**15.979**

February

Date/Time	6-7	7-8	8-9	9-10	10-11	11-12	12-13	13-14	14-15	15-16	16-17	17-18	Total
1	0.000	0.090	0.489	1.229	1.863	2.329	2.561	2.475	2.189	1.660	0.958	0.295	16.156
2	0.000	0.108	0.604	0.989	1.697	1.969	2.006	2.143	1.826	1.440	0.826	0.340	13.964
3	0.000	0.120	0.408	1.097	1.650	2.124	2.306	2.141	2.017	1.593	0.944	0.299	14.710
4	0.000	0.105	0.450	1.003	1.540	1.968	2.178	2.136	1.938	1.424	0.796	0.265	13.810
5	0.000	0.085	0.453	1.017	1.627	2.115	2.394	2.443	2.109	1.581	0.918	0.314	15.063
6	0.000	0.092	0.514	1.137	1.709	2.132	2.389	2.396	2.097	1.533	0.919	0.313	15.243
7	0.000	0.095	0.488	1.048	1.606	2.003	2.211	1.789	1.806	1.544	0.846	0.291	13.738
8	0.000	0.091	0.439	0.910	1.296	1.726	1.888	2.326	2.000	1.542	0.935	0.318	13.480
9	0.000	0.088	0.559	1.224	1.858	2.304	2.559	2.495	2.192	1.745	1.083	0.369	16.487
10	0.000	0.092	0.646	1.387	2.037	2.488	2.725	2.669	2.344	1.767	1.083	0.404	17.662
11	0.000	0.140	0.562	1.143	1.787	2.245	2.478	2.530	2.244	1.704	1.021	0.355	16.227
12	0.000	0.097	0.600	1.325	1.979	2.430	2.658	2.612	2.293	1.738	0.825	0.368	16.944
13	0.000	0.100	0.663	1.468	2.136	2.567	2.754	2.704	2.382	1.739	1.065	0.494	18.100
14	0.000	0.088	0.634	1.488	2.163	2.629	2.889	2.848	2.494	1.772	1.219	0.443	18.685
15	0.000	0.124	0.506	1.617	1.787	2.825	1.563	1.826	1.390	0.818	0.565	0.679	13.745
16	0.000	0.091	0.694	1.620	2.266	2.744	2.915	2.713	2.389	1.555	0.874	0.258	18.152
17	0.000	0.099	0.692	1.555	2.205	2.680	2.917	2.861	2.570	2.017	1.261	0.517	19.408
18	0.000	0.096	0.643	1.537	2.232	2.695	2.884	2.847	2.592	1.992	1.290	0.493	19.339
19	0.000	0.099	0.598	1.401	2.028	2.473	2.858	2.732	2.460	1.917	1.235	0.526	18.357
20	0.000	0.090	0.585	1.408	2.069	2.547	2.720	2.686	2.410	1.866	1.170	0.501	18.082
21	0.000	0.095	0.615	1.490	2.159	2.601	2.748	2.710	2.514	1.891	1.218	0.506	18.591
22	0.000	0.097	0.652	1.516	2.199	2.792	3.028	2.853	2.383	1.852	1.157	0.473	19.034
23	0.000	0.110	0.584	1.414	2.051	2.570	2.742	2.596	2.236	1.740	1.110	0.437	17.624
24	0.000	0.106	0.555	1.313	1.942	2.391	2.596	2.501	2.175	1.599	0.983	0.380	16.582
25	0.000	0.107	0.635	1.493	2.165	2.597	2.848	2.684	2.311	1.655	1.055	0.532	18.133
26	0.001	0.108	0.654	1.625	2.213	2.697	2.898	2.765	1.762	1.867	1.296	0.650	18.606
27	0.001	0.151	0.672	1.613	2.210	2.708	2.867	2.819	2.217	1.244	1.072	0.421	18.040
28	0.000	0.112	0.610	1.476	2.082	2.631	2.793	2.656	2.305	1.759	1.058	0.414	17.927
Average	**0.000**	**0.103**	**0.579**	**1.341**	**1.948**	**2.428**	**2.585**	**2.534**	**2.202**	**1.663**	**1.028**	**0.416**	**16.853**

March

Date/Time	6-7	7-8	8-9	9-10	10-11	11-12	12-13	13-14	14-15	15-16	16-17	17-18	Total
1	0.000	0.103	0.551	1.338	1.947	2.385	2.531	2.479	2.219	1.614	0.968	0.358	16.519
2	0.000	0.108	0.514	1.261	1.884	2.518	2.670	2.780	2.312	1.676	1.081	0.469	17.314
3	0.001	0.124	0.605	1.480	2.075	2.499	2.677	2.402	2.114	1.544	0.963	0.375	16.890
4	0.001	0.111	0.529	1.216	1.791	2.266	2.202	2.197	1.958	1.533	0.910	0.277	15.013
5	0.000	0.094	0.501	1.170	1.669	2.054	1.767	1.636	1.154	1.404	0.711	0.191	12.386
6	0.000	0.073	0.599	1.174	1.530	1.846	2.216	2.283	2.298	1.671	1.017	0.409	15.155
7	0.001	0.146	0.988	1.755	2.199	2.695	3.044	2.995	2.622	2.018	1.223	0.492	20.226
8	0.004	0.145	0.837	1.570	2.294	2.740	2.843	2.922	2.530	1.933	1.267	0.460	19.583
9	0.002	0.166	1.015	1.776	2.413	3.063	3.222	3.056	2.556	2.046	1.364	0.562	21.291
10	0.002	0.148	0.667	1.219	1.774	2.227	2.410	2.507	2.214	1.563	0.959	0.354	16.078
11	0.002	0.125	0.641	1.217	1.711	2.185	2.413	2.389	2.164	1.408	0.955	0.343	15.582
12	0.002	0.125	0.553	1.084	1.554	2.017	2.216	2.181	1.961	1.385	0.794	0.305	14.208
13	0.002	0.125	0.517	0.983	1.426	1.796	1.832	1.734	1.437	1.020	0.572	0.217	11.688
14	0.004	0.142	0.596	1.160	1.717	2.217	2.399	2.182	1.833	1.344	0.879	0.301	14.802
15	0.005	0.174	0.753	1.462	2.036	2.563	2.736	2.624	2.267	1.690	1.000	0.428	17.779
16	0.005	0.176	0.723	1.339	1.818	2.394	2.584	2.131	2.065	1.677	0.952	0.310	16.222
17	0.006	0.197	0.539	1.356	1.860	1.487	1.468	1.631	1.523	0.849	0.615	0.432	12.022
18	0.007	0.200	0.727	1.341	1.838	2.191	2.423	2.387	2.052	1.585	0.985	0.421	16.194
19	0.006	0.192	0.579	1.261	1.941	2.435	2.545	2.574	2.308	1.871	1.232	0.535	17.512
20	0.007	0.211	0.690	1.258	1.863	2.328	2.517	2.575	2.318	1.834	1.146	0.455	17.259
21	0.013	0.297	0.996	1.754	2.422	2.822	3.022	2.990	2.665	2.053	1.252	0.387	20.737
22	0.013	0.284	0.958	1.634	2.323	2.833	3.032	2.972	2.626	1.981	0.983	0.497	20.191
23	0.013	0.307	1.114	1.912	2.686	3.253	3.414	3.262	2.892	2.234	1.451	0.630	23.232
24	0.011	0.252	0.840	1.546	2.247	2.718	3.045	2.951	2.484	1.807	1.033	0.417	19.394
25	0.010	0.252	0.837	1.551	2.247	2.804	3.066	2.921	2.485	1.778	1.064	0.469	19.535
26	0.013	0.281	0.919	1.619	2.284	2.836	3.033	3.023	2.518	1.967	1.256	0.548	20.349
27	0.017	0.292	0.919	1.625	2.280	2.787	3.069	3.120	2.772	2.318	1.467	0.624	21.363
28	0.016	0.307	0.980	1.723	2.435	2.963	3.201	3.232	2.910	2.104	1.339	0.512	21.787
29	0.017	0.314	0.953	1.675	2.328	2.788	3.004	2.990	2.642	2.049	1.311	0.518	20.646
30	0.013	0.215	0.778	1.577	2.254	2.793	3.038	2.034	0.382	1.333	0.500	0.325	15.400
31	0.021	0.357	1.126	1.935	2.623	3.082	3.259	2.960	1.436	1.722	1.149	0.587	20.316
Average	**0.007**	**0.195**	**0.759**	**1.451**	**2.047**	**2.503**	**2.674**	**2.585**	**2.184**	**1.710**	**1.045**	**0.426**	**17.635**

April

Date/Time	6-7	7-8	8-9	9-10	10-11	11-12	12-13	13-14	14-15	15-16	16-17	17-18	Total
1	0.024	0.389	1.184	2.032	2.770	3.192	3.352	3.214	2.950	2.359	1.243	0.563	23.351
2	0.026	0.475	1.363	2.170	2.888	3.343	3.504	3.461	3.096	2.467	1.617	0.711	25.200
3	0.023	0.324	0.909	1.597	2.267	2.794	3.082	3.068	2.800	2.166	1.221	0.459	20.800
4	0.029	0.411	1.133	1.907	2.613	3.127	3.241	3.248	2.794	2.192	1.330	0.543	22.637
5	0.030	0.364	1.019	1.723	2.371	2.752	2.904	2.959	2.547	2.052	1.330	0.598	20.726
6	0.026	0.330	0.908	1.604	2.036	2.564	2.659	2.400	1.992	1.564	0.936	0.406	17.467
7	0.033	0.354	0.952	1.661	2.144	2.669	2.834	2.861	2.070	1.516	0.718	0.297	18.161
8	0.030	0.337	0.912	1.613	2.241	2.652	2.822	2.561	2.444	1.872	1.106	0.437	19.070
9	0.035	0.415	1.103	1.847	2.465	2.864	3.047	2.994	2.660	2.002	1.244	0.476	21.235
10	0.034	0.397	1.067	1.816	2.446	2.856	2.933	2.853	2.604	1.463	0.798	0.595	19.939
11	0.040	0.388	0.991	1.677	2.370	2.828	3.047	2.935	1.252	1.615	1.342	0.590	19.163
12	0.058	0.424	1.239	2.065	2.817	3.224	3.376	1.244	1.873	2.301	0.999	0.208	19.908
13	0.065	0.413	1.409	2.091	2.844	2.842	2.556	1.839	2.029	1.075	1.050	0.357	18.628
14	0.046	0.275	0.887	1.222	1.376	1.156	2.138	2.198	1.996	0.434	0.480	0.385	12.633
15	0.034	0.248	0.881	1.525	2.496	2.983	3.038	2.461	1.812	0.736	0.270	0.111	16.620
16	0.054	0.430	1.112	1.732	1.975	3.151	3.623	2.562	1.229	0.993	0.476	0.204	17.583
17	0.058	0.458	0.899	2.183	2.592	2.491	2.508	3.189	1.608	1.154	1.374	0.318	18.933
18	0.074	0.637	1.443	2.214	2.705	3.335	3.207	0.570	1.664	2.628	1.302	0.172	19.975
19	0.056	0.377	0.411	0.675	1.793	3.312	3.201	3.434	3.061	2.418	1.620	0.806	21.287
20	0.083	0.700	1.571	2.381	3.041	3.489	3.658	3.532	3.124	2.401	1.718	0.839	26.669
21	0.086	0.731	1.583	2.404	3.089	3.495	3.619	3.469	2.974	2.473	1.467	0.853	26.382
22	0.094	0.755	1.587	2.387	3.024	3.437	3.551	3.462	3.174	2.561	1.757	0.747	26.675
23	0.092	0.725	1.587	2.419	3.088	3.533	3.624	3.534	3.089	2.430	1.150	0.695	26.153
24	0.097	0.719	1.541	2.322	2.967	3.410	3.542	3.421	3.016	2.370	1.559	0.755	25.791
25	0.097	0.691	1.484	2.228	2.859	3.304	3.495	3.313	2.247	2.231	1.366	0.654	24.110
26	0.024	0.178	0.537	1.544	1.442	2.154	3.557	3.279	2.950	2.271	0.849	0.372	19.380
27	0.047	0.714	1.628	2.449	3.100	3.489	3.661	2.926	2.434	1.665	1.833	0.307	24.371
28	0.051	0.167	0.459	1.776	2.780	3.655	3.845	3.533	2.953	1.643	1.798	0.791	23.562
29	0.073	0.396	1.555	2.391	3.055	3.549	2.119	0.774	2.006	1.024	0.848	0.985	18.867
30	0.094	0.784	1.621	2.450	2.970	3.577	3.837	2.413	1.877	0.813	1.570	0.935	23.070
Average	**0.054**	**0.467**	**1.166**	**1.937**	**2.554**	**3.041**	**3.186**	**2.790**	**2.411**	**1.830**	**1.212**	**0.539**	**21.278**

May

Date/Time	6-7	7-8	8-9	9-10	10-11	11-12	12-13	13-14	14-15	15-16	16-17	17-18	Total
1	0.133	0.579	1.424	2.311	2.617	3.052	3.406	3.545	3.101	2.594	1.761	0.960	25.720
2	0.090	0.733	0.938	1.807	2.275	3.074	2.912	1.656	2.321	1.486	1.084	0.537	18.969
3	0.046	0.161	0.251	0.534	0.742	1.512	1.944	1.906	1.520	1.749	0.683	0.263	11.379
4	0.029	0.147	0.333	0.741	0.764	0.926	0.420	0.780	0.745	0.679	0.385	0.207	6.200
5	0.028	0.067	0.146	0.336	0.666	1.342	1.892	1.311	1.031	1.064	0.492	0.130	8.534
6	0.052	0.258	0.340	0.378	0.955	0.910	1.296	1.541	2.017	1.961	1.162	0.581	11.562
7	0.091	0.476	0.673	1.538	2.043	1.832	1.486	2.198	2.272	2.637	0.898	0.417	16.620
8	0.024	0.181	0.503	1.211	2.555	2.994	2.748	3.359	3.072	2.500	0.628	0.427	20.271
9	0.130	0.641	1.353	1.733	2.685	2.491	2.216	3.593	2.917	2.630	1.761	0.643	22.852
10	0.113	0.167	0.668	1.036	2.903	3.537	3.297	2.429	2.914	2.612	1.863	0.942	22.504
11	0.043	0.241	0.665	0.965	1.196	1.972	2.861	3.209	2.159	1.600	0.689	0.415	16.139
12	0.054	0.460	1.226	2.142	1.805	1.979	1.394	0.325	0.252	0.047	0.117	0.333	10.285
13	0.050	0.181	0.287	0.963	0.554	1.101	1.785	1.570	0.989	0.791	1.185	0.609	10.178
14	0.065	0.224	0.577	1.490	0.484	2.158	1.111	1.930	2.606	2.205	1.383	0.342	14.595
15	0.074	0.511	1.578	1.861	1.398	1.363	2.893	3.420	2.540	0.252	0.974	0.853	17.772
16	0.119	0.511	1.734	2.546	3.247	3.129	3.727	3.486	3.268	2.604	1.327	0.770	26.584
17	0.085	0.355	1.369	2.076	2.559	3.099	3.624	2.270	2.940	2.119	1.447	1.168	23.209
18	0.118	0.408	1.185	2.514	1.188	3.007	2.518	2.446	1.329	0.823	2.131	0.912	18.739
19	0.178	0.371	0.820	1.880	2.460	2.995	1.837	1.643	0.712	1.059	1.639	0.807	16.591
20	0.023	0.128	0.353	0.685	1.631	2.374	2.488	1.464	1.394	0.968	0.856	0.432	12.860
21	0.153	0.668	0.622	1.330	1.303	1.641	1.948	1.575	1.159	1.317	0.787	0.380	12.975
22	0.107	0.577	1.142	0.581	1.497	1.890	2.343	2.091	2.000	1.572	0.946	0.346	15.179
23	0.150	0.658	0.907	1.759	2.009	2.205	2.686	2.675	2.996	1.924	1.492	0.908	20.551
24	0.119	0.874	1.716	2.519	2.697	3.340	3.520	3.305	3.189	2.219	1.828	0.954	26.512
25	0.099	0.822	1.720	2.368	3.041	3.421	3.527	3.443	2.960	0.181	0.180	0.381	22.278
26	0.103	0.858	1.709	2.506	3.117	3.499	3.655	3.459	0.860	0.314	0.946	0.918	22.114
27	0.129	0.708	1.633	2.449	3.080	3.473	3.627	3.527	3.198	2.591	1.867	0.919	27.490
28	0.189	0.908	1.641	2.410	2.839	3.235	2.978	2.342	2.440	1.606	2.013	0.388	23.110
29	0.155	0.736	1.671	2.383	2.993	3.213	2.978	2.804	3.030	1.735	0.712	0.459	22.950
30	0.119	0.635	0.949	1.425	1.731	2.955	3.408	3.590	2.388	2.149	1.307	0.504	21.228
31	0.112	0.495	0.885	1.919	2.516	3.174	3.714	3.420	3.627	1.215	0.275	0.041	21.414
Average	**0.096**	**0.476**	**1.001**	**1.626**	**1.986**	**2.480**	**2.588**	**2.462**	**2.192**	**1.587**	**1.123**	**0.579**	**18.302**

June

Date/Time	6-7	7-8	8-9	9-10	10-11	11-12	12-13	13-14	14-15	15-16	16-17	17-18	Total
1	0.106	0.484	0.570	1.456	2.137	2.653	2.636	3.292	2.523	1.514	0.996	0.338	18.843
2	0.105	0.775	1.585	2.458	3.000	2.799	3.096	3.500	3.191	1.987	0.572	0.563	23.777
3	0.148	0.769	1.790	2.518	3.131	3.525	3.583	3.236	1.979	1.750	0.394	0.335	23.294
4	0.108	0.504	1.273	2.250	2.748	3.343	3.783	0.954	1.795	2.876	1.906	1.146	22.894
5	0.131	0.417	0.977	2.338	2.849	3.299	3.197	1.841	2.457	2.635	1.776	0.258	22.313
6	0.062	0.382	1.234	1.681	2.172	2.705	2.216	3.259	3.135	2.014	0.839	0.116	19.877
7	0.128	0.786	1.692	2.264	3.112	3.599	3.198	2.143	1.817	1.765	1.173	0.952	22.789
8	0.127	0.613	1.779	2.281	2.713	2.869	3.560	2.993	2.814	2.707	1.966	1.188	25.805
9	0.147	0.523	0.656	1.638	2.220	3.071	3.208	3.281	3.249	1.947	1.210	1.056	22.353
10	0.134	0.852	1.737	2.531	3.195	3.342	2.976	2.990	1.211	2.786	2.096	1.171	25.250
11	0.146	0.804	1.294	1.816	2.462	2.772	1.654	0.969	2.988	2.497	1.028	0.178	18.787
12	0.176	0.848	1.538	1.557	2.527	1.798	1.749	3.427	1.819	0.703	1.518	0.340	18.040
13	0.082	0.291	0.786	0.936	1.750	2.298	2.065	2.243	1.984	1.200	0.933	0.333	15.058
14	0.130	0.431	0.936	1.956	2.871	3.466	3.265	1.020	0.413	0.385	0.937	0.901	17.034
15	0.141	0.504	0.845	1.675	2.406	3.672	3.549	1.970	2.642	1.559	1.852	1.308	22.541
16	0.069	0.338	1.229	2.405	2.556	2.002	1.948	2.828	1.897	2.202	1.652	0.890	20.205
17	0.122	0.521	1.300	1.874	1.547	2.092	1.605	2.623	2.478	2.646	1.829	0.527	19.249
18	0.153	0.654	1.092	1.139	1.653	2.758	2.552	3.085	1.790	0.730	0.335	0.409	16.591
19	0.131	0.646	0.840	2.036	1.986	2.681	1.826	2.953	1.888	1.811	0.823	0.167	17.869
20	0.112	0.650	0.841	1.414	1.587	1.930	2.513	2.668	3.214	2.527	2.110	1.299	21.262
21	0.135	0.706	1.010	2.294	3.260	3.419	3.792	3.287	2.759	1.841	0.951	0.589	24.190
22	0.097	0.762	1.647	2.488	3.110	3.453	3.609	3.527	3.225	2.781	1.997	1.182	28.228
23	0.106	0.758	1.698	2.500	3.140	3.484	3.722	3.801	3.208	2.752	2.028	1.168	28.705
24	0.101	0.756	2.031	2.221	3.057	3.505	3.649	3.747	2.733	1.062	1.171	1.275	25.552
25	0.140	0.613	1.376	1.582	1.596	3.046	3.304	2.573	2.400	1.585	0.756	0.459	19.593
26	0.069	0.414	0.792	1.288	2.149	2.623	3.092	3.660	2.910	0.993	0.370	0.063	18.439
27	0.105	0.546	0.747	1.684	1.737	2.109	1.213	0.270	0.176	0.454	0.652	0.360	10.142
28	0.040	0.247	1.368	2.125	1.482	2.287	2.203	1.532	1.004	0.612	0.780	0.534	14.365
29	0.168	0.466	0.672	0.718	2.140	1.981	1.840	1.765	1.615	1.521	0.628	0.198	13.905
30	0.082	0.623	1.205	2.018	1.529	2.186	2.870	1.615	1.507	2.370	1.468	1.162	18.856
Average	**0.117**	**0.590**	**1.218**	**1.905**	**2.394**	**2.826**	**2.782**	**2.568**	**2.227**	**1.807**	**1.225**	**0.682**	**20.527**

July

Date/Time	6-7	7-8	8-9	9-10	10-11	11-12	12-13	13-14	14-15	15-16	16-17	17-18	Total
1	0.102	0.408	0.789	2.280	2.759	3.129	2.437	1.891	3.127	1.542	0.505	0.460	19.617
2	0.077	0.424	0.834	1.527	0.915	2.625	1.047	3.662	3.342	1.819	1.850	0.775	19.154
3	0.131	0.490	1.740	1.706	1.900	1.790	1.459	1.428	1.751	2.875	1.292	0.619	17.255
4	0.095	0.560	1.677	1.588	0.824	2.230	1.695	2.292	1.795	2.243	1.358	0.527	17.064
5	0.056	0.386	0.807	1.794	1.361	1.568	1.552	2.399	3.021	1.277	0.921	0.522	15.822
6	0.046	0.298	0.422	0.808	0.540	1.166	1.094	1.016	0.752	0.617	0.692	0.309	7.855
7	0.094	0.517	1.246	1.695	1.906	3.139	3.447	2.731	2.517	2.316	1.280	0.330	21.393
8	0.086	0.665	1.507	2.130	2.703	3.455	3.546	3.617	2.781	1.218	0.880	0.472	23.210
9	0.063	0.682	1.662	2.428	3.074	3.369	3.828	3.355	2.552	2.284	2.073	0.778	26.328
10	0.099	0.448	1.228	2.777	2.914	2.760	2.562	2.486	2.144	2.149	1.908	0.813	22.645
11	0.074	0.459	1.425	2.322	3.097	2.861	2.234	0.712	0.924	1.886	1.104	0.649	17.931
12	0.107	0.717	1.039	1.062	2.097	2.004	2.390	1.716	1.882	1.300	1.330	0.792	16.851
13	0.080	0.490	1.543	1.841	1.397	2.253	2.747	2.301	0.734	0.246	0.600	0.387	14.843
14	0.113	0.668	1.212	1.903	2.884	1.503	1.237	1.403	1.280	1.819	0.744	0.422	15.330
15	0.107	0.389	0.920	1.383	1.788	1.327	1.945	1.983	1.897	2.081	1.491	0.924	16.389
16	0.041	0.386	0.937	1.291	0.854	1.112	1.369	2.101	2.659	2.558	0.542	1.247	15.498
17	0.100	0.682	1.316	1.443	2.247	2.903	2.194	1.771	1.700	1.389	1.235	0.571	17.820
18	0.050	0.316	0.968	1.843	2.003	2.271	3.155	3.230	1.845	1.425	0.859	0.567	18.628
19	0.078	0.453	0.843	1.378	2.040	1.925	1.793	1.135	1.952	1.344	0.359	0.061	13.392
20	0.062	0.354	0.919	1.182	1.273	1.050	0.998	1.160	1.199	0.823	0.498	0.253	9.848
21	0.043	0.192	0.427	0.476	0.747	0.735	0.735	0.584	0.770	0.938	1.056	0.509	7.386
22	0.082	0.386	0.798	1.370	2.444	3.174	2.548	2.182	2.270	1.862	1.083	0.366	18.686
23	0.058	0.405	1.260	2.329	2.579	3.727	3.707	2.154	2.569	0.458	0.416	0.938	20.775
24	0.022	0.168	0.358	0.808	1.174	1.275	1.117	0.772	0.935	0.755	0.489	0.240	8.191
25	0.019	0.360	0.525	1.442	1.874	1.680	2.226	2.446	2.338	1.966	2.158	1.024	18.329
26	0.078	0.769	1.768	2.465	2.668	2.631	2.926	2.744	0.727	1.058	1.318	0.930	20.161
27	0.038	0.304	0.665	1.244	1.563	1.983	2.535	2.452	1.882	1.252	0.999	0.751	15.801
28	0.083	0.610	1.611	2.428	3.089	3.529	3.753	2.608	1.439	2.973	1.366	0.836	24.466
29	0.029	0.183	0.566	1.774	2.410	3.181	2.042	2.054	1.819	2.091	1.745	0.559	18.549
30	0.050	0.411	0.842	0.992	2.670	2.191	3.534	2.292	1.575	1.675	1.237	0.372	17.899
31	0.058	0.352	0.520	0.700	1.325	3.228	2.238	1.582	2.118	2.068	2.041	1.381	17.800
Average	**0.072**	**0.449**	**1.044**	**1.626**	**1.972**	**2.315**	**2.261**	**2.073**	**1.880**	**1.623**	**1.143**	**0.625**	**17.255**

August

Date/Time	6-7	7-8	8-9	9-10	10-11	11-12	12-13	13-14	14-15	15-16	16-17	17-18	Total
1	0.044	0.319	0.774	1.219	1.282	1.622	1.467	1.844	1.672	1.636	1.163	0.531	13.699
2	0.024	0.372	0.251	1.171	2.194	1.475	1.468	1.984	1.902	1.589	1.015	0.371	13.878
3	0.022	0.254	0.863	2.028	1.617	2.354	2.855	1.706	1.480	1.341	0.764	0.598	16.160
4	0.055	0.347	0.969	1.709	3.270	3.471	2.698	2.482	3.021	2.143	1.135	0.784	22.134
5	0.091	0.450	1.022	1.835	2.183	2.519	2.465	3.220	3.288	2.305	1.929	1.170	22.617
6	0.083	0.520	1.307	2.269	2.938	3.195	3.746	2.682	3.105	2.752	1.963	0.767	25.447
7	0.055	0.649	1.531	2.169	2.814	3.005	2.618	3.442	2.898	2.483	1.531	0.796	24.235
8	0.022	0.157	0.531	1.011	1.549	2.816	2.322	1.849	1.849	1.856	0.127	0.123	14.245
9	0.027	0.129	0.539	0.972	1.581	1.451	0.615	0.550	0.875	1.286	0.835	0.498	9.515
10	0.041	0.422	1.215	1.625	2.002	3.148	2.757	1.305	1.418	1.571	1.049	0.267	16.951
11	0.057	0.336	0.795	0.781	1.247	1.015	2.310	2.591	1.492	1.880	0.641	0.327	13.498
12	0.022	0.158	0.303	0.994	1.617	2.129	1.703	2.035	1.355	0.612	0.618	0.455	12.100
13	0.058	0.378	0.943	2.447	2.489	3.492	2.288	2.232	2.737	1.862	1.833	0.623	21.666
14	0.005	0.285	0.796	0.677	1.849	3.419	2.782	3.263	3.030	1.454	0.913	0.277	18.931
15	0.026	0.156	0.415	0.931	1.407	1.409	2.477	3.084	2.715	2.248	1.330	0.443	16.777
16	0.007	0.044	0.134	0.269	0.326	1.370	2.909	2.578	3.078	0.751	0.079	0.035	11.592
17	0.037	0.398	1.106	1.880	1.538	2.928	2.948	3.112	3.001	2.597	1.622	0.701	22.071
18	0.056	0.545	1.328	2.517	2.505	3.173	3.856	3.675	2.892	1.714	2.046	0.668	25.235
19	0.044	0.594	1.580	2.412	3.084	3.544	3.392	3.252	3.344	2.968	1.658	0.571	26.562
20	0.075	0.722	1.574	2.238	2.776	3.377	3.727	3.348	0.561	0.588	1.508	0.786	21.470
21	0.044	0.331	1.144	1.916	2.333	3.465	3.736	2.517	2.163	0.759	0.329	0.533	19.420
22	0.022	0.241	0.532	1.593	1.946	2.513	3.563	3.562	2.396	1.535	1.059	0.381	19.374
23	0.038	0.347	1.106	1.487	2.082	2.099	1.436	2.309	2.551	2.713	1.593	0.083	17.864
24	0.041	0.226	0.360	0.628	0.615	1.061	1.568	1.945	2.424	1.379	0.728	0.346	11.394
25	0.009	0.123	0.509	0.918	0.957	1.228	1.509	1.391	1.603	1.742	1.154	0.561	11.803
26	0.044	0.348	1.240	2.245	2.085	3.351	3.265	2.949	1.362	2.003	1.212	0.445	20.631
27	0.044	0.506	1.619	1.652	3.111	2.848	3.527	3.685	3.058	2.524	1.732	1.054	25.552
28	0.039	0.414	0.908	2.317	2.859	2.534	1.485	0.487	0.490	1.000	0.590	0.528	13.721
29	0.044	0.302	0.845	1.658	2.580	3.351	3.083	2.871	2.813	1.750	1.052	0.951	21.464
30	0.041	0.273	0.867	0.981	1.447	2.276	2.658	3.480	3.413	2.073	0.711	0.156	18.439
31	0.019	0.276	0.824	1.812	2.710	2.656	3.408	2.904	3.251	2.146	1.571	0.587	22.221
Average	**0.040**	**0.343**	**0.901**	**1.560**	**2.032**	**2.526**	**2.601**	**2.527**	**2.298**	**1.783**	**1.145**	**0.529**	**18.409**

September

Date/Time	6-7	7-8	8-9	9-10	10-11	11-12	12-13	13-14	14-15	15-16	16-17	17-18	Total
1	0.065	0.338	0.881	1.883	2.489	3.489	3.360	3.565	2.862	1.951	1.204	0.495	22.650
2	0.045	0.386	1.125	1.217	1.843	2.407	3.355	3.398	3.192	2.120	1.530	0.690	21.371
3	0.052	0.559	1.471	2.592	2.566	2.051	2.720	3.893	2.337	0.538	0.241	0.277	19.340
4	0.050	0.307	0.628	1.031	1.649	3.122	2.479	2.758	1.436	1.574	0.857	0.375	16.333
5	0.015	0.129	0.476	1.110	1.087	1.846	2.587	3.353	2.429	1.727	0.323	0.181	15.327
6	0.022	0.329	0.831	1.386	1.632	2.126	3.105	2.990	1.773	1.611	0.213	0.179	16.257
7	0.033	0.235	0.921	1.143	1.303	1.738	3.265	2.675	2.433	1.963	1.521	0.470	17.748
8	0.029	0.455	1.235	2.359	2.940	3.288	3.441	3.539	3.084	2.757	1.841	0.756	25.900
9	0.044	0.559	1.514	2.387	2.484	3.179	3.308	3.018	2.191	2.794	1.045	0.635	23.261
10	0.029	0.269	0.582	1.801	2.287	2.426	2.131	2.932	2.503	1.659	1.207	0.689	18.621
11	0.001	0.029	0.142	0.324	0.851	1.300	1.873	2.108	2.152	1.637	1.189	0.475	12.170
12	0.015	0.241	0.895	1.897	2.937	3.133	2.410	2.271	3.372	2.598	1.957	0.699	22.490
13	0.041	0.304	0.555	2.497	2.893	3.239	3.583	2.679	2.780	2.486	0.887	0.189	22.165
14	0.024	0.425	0.572	2.725	2.676	3.481	2.280	2.237	2.713	0.895	0.688	0.430	19.195
15	0.049	0.416	0.662	0.846	1.671	2.496	2.803	1.708	3.016	2.395	1.378	0.420	17.928
16	0.017	0.408	0.933	1.805	2.492	2.981	2.309	2.957	2.998	2.398	1.606	0.817	21.807
17	0.035	0.380	1.473	2.127	2.288	2.144	3.370	3.088	3.054	2.382	1.559	0.840	22.804
18	0.044	0.557	0.985	1.512	1.828	1.916	1.502	1.624	1.217	1.581	0.441	0.344	13.622
19	0.038	0.559	1.002	1.009	2.782	2.680	3.406	1.519	2.368	0.383	1.077	0.224	17.062
20	0.009	0.061	0.511	0.759	1.053	0.824	1.560	1.642	1.131	1.873	1.598	0.504	11.548
21	0.071	0.443	0.835	1.883	1.896	2.682	3.187	3.402	2.895	2.163	0.800	0.376	20.673
22	0.022	0.602	1.482	2.137	2.323	2.766	2.542	2.922	1.986	1.415	0.684	0.308	19.223
23	0.052	0.493	1.313	2.202	2.901	3.249	3.400	3.284	2.953	2.131	1.160	0.201	23.359
24	0.030	0.344	1.266	2.170	2.800	3.320	3.123	3.136	2.859	2.310	1.069	0.189	22.631
25	0.023	0.424	1.202	1.880	1.790	2.553	2.321	2.590	2.444	2.091	1.261	0.448	19.048
26	0.026	0.230	0.626	1.149	1.557	2.185	1.750	2.003	2.220	2.060	0.862	0.305	14.994
27	0.019	0.144	0.269	0.772	1.720	1.324	1.760	1.950	1.352	1.448	1.251	0.318	12.337
28	0.028	0.447	1.284	1.424	1.983	2.867	3.490	0.975	1.033	0.947	0.484	0.286	15.279
29	0.037	0.351	1.011	1.502	1.890	2.101	2.011	2.654	2.597	2.456	1.361	0.303	18.288
30	0.028	0.130	0.702	1.998	2.673	2.917	3.596	2.827	3.011	2.445	1.535	0.606	22.490
Average	**0.033**	**0.352**	**0.913**	**1.651**	**2.109**	**2.528**	**2.734**	**2.657**	**2.413**	**1.893**	**1.094**	**0.434**	**18.864**

October

Date/Time	6-7	7-8	8-9	9-10	10-11	11-12	12-13	13-14	14-15	15-16	16-17	17-18	Total
1	0.032	0.326	0.918	2.047	2.517	3.610	2.699	2.746	2.749	1.962	0.972	0.378	20.983
2	0.029	0.394	1.246	2.039	2.777	3.245	3.327	2.095	2.518	1.708	0.647	0.274	20.334
3	0.023	0.338	0.756	1.097	1.873	2.183	1.700	1.621	1.782	1.813	0.834	0.347	14.378
4	0.037	0.348	0.736	1.502	1.380	1.445	1.352	2.328	1.286	1.324	0.811	0.285	12.853
5	0.011	0.196	0.755	1.038	1.495	1.083	1.234	1.235	0.758	0.136	0.044	0.032	8.018
6	0.012	0.263	0.680	0.722	0.972	1.424	1.423	1.978	1.861	1.796	0.234	0.133	11.501
7	0.024	0.296	0.815	0.960	0.808	1.044	0.753	1.045	1.153	0.723	0.477	0.159	8.271
8	0.018	0.288	0.691	1.787	2.506	3.303	3.054	3.349	2.091	2.248	1.172	0.480	20.995
9	0.019	0.329	0.692	0.787	1.785	1.447	3.092	1.291	0.357	0.369	0.198	0.062	10.435
10	0.012	0.208	0.940	1.959	2.463	1.845	1.261	2.695	2.830	2.547	0.487	0.111	17.365
11	0.022	0.225	0.700	1.765	1.845	2.698	3.425	1.653	1.032	1.659	1.112	0.454	16.594
12	0.017	0.247	0.852	1.673	2.170	2.359	1.985	1.178	1.383	2.170	1.317	0.456	15.817
13	0.015	0.138	0.843	1.149	1.653	1.923	1.092	1.069	1.467	0.865	0.559	0.239	11.023
14	0.027	0.376	0.618	1.992	2.518	2.830	2.776	2.595	2.373	0.506	0.486	0.128	17.228
15	0.016	0.142	0.290	0.482	0.789	2.469	2.959	2.559	0.703	0.431	0.712	0.326	11.899
16	0.017	0.217	0.357	1.020	1.430	2.387	2.231	2.275	2.013	1.290	0.271	0.203	13.715
17	0.010	0.275	1.137	1.485	2.070	2.370	2.981	1.548	0.705	0.813	0.415	0.271	14.085
18	0.013	0.176	0.643	2.227	2.837	3.016	3.388	3.039	2.581	2.191	1.137	0.335	21.585
19	0.019	0.295	0.981	1.903	2.730	2.665	3.016	2.994	2.622	1.660	1.058	0.376	20.320
20	0.027	0.262	1.153	1.942	2.656	3.082	3.169	1.609	1.055	0.748	0.296	0.092	16.090
21	0.016	0.202	0.555	1.647	2.540	2.973	3.148	2.965	2.510	1.553	1.006	0.285	19.404
22	0.018	0.290	1.020	1.828	2.557	2.929	3.404	2.738	2.282	1.760	1.002	0.198	20.029
23	0.011	0.252	0.869	1.807	2.176	2.979	3.150	3.051	2.602	1.875	1.120	0.305	20.199
24	0.019	0.242	0.840	1.822	2.629	2.972	2.232	1.896	2.615	1.798	0.818	0.153	18.040
25	0.023	0.268	1.065	1.910	2.660	3.069	2.624	2.417	2.053	1.840	1.114	0.263	19.308
26	0.011	0.243	0.849	1.585	2.343	2.981	3.241	3.049	2.534	1.537	0.832	0.179	19.385
27	0.016	0.355	1.084	1.676	2.325	2.906	2.815	2.811	2.534	1.683	0.781	0.214	19.201
28	0.016	0.260	0.612	1.727	2.517	2.956	3.122	2.954	2.551	1.877	1.053	0.260	19.905
29	0.016	0.253	1.021	1.824	2.520	2.922	3.118	2.880	2.568	1.665	1.054	0.230	20.071
30	0.005	0.080	0.683	1.227	2.208	2.146	1.252	2.182	1.959	1.748	1.148	0.279	14.916
31	0.023	0.173	0.559	1.559	2.093	2.000	1.569	2.311	1.385	0.688	0.374	0.051	12.785
Average	**0.019**	**0.257**	**0.805**	**1.554**	**2.124**	**2.492**	**2.471**	**2.263**	**1.900**	**1.451**	**0.759**	**0.244**	**16.346**

November

Date/Time	6-7	7-8	8-9	9-10	10-11	11-12	12-13	13-14	14-15	15-16	16-17	17-18	Total
1	0.007	0.086	0.349	0.489	1.037	1.972	1.589	2.153	1.799	0.808	0.430	0.256	10.975
2	0.005	0.164	0.455	0.661	1.252	2.097	2.040	1.172	0.972	0.685	0.263	0.082	9.848
3	0.001	0.045	0.079	0.196	0.259	0.417	0.568	0.417	0.399	0.284	0.120	0.051	2.838
4	0.002	0.075	0.125	0.275	0.583	1.032	0.858	0.484	0.498	0.644	0.282	0.129	4.991
5	0.002	0.089	0.352	0.842	1.519	2.236	1.940	1.362	1.404	0.941	0.466	0.246	11.399
6	0.005	0.130	0.458	1.234	2.641	3.032	2.899	1.817	1.353	0.960	0.565	0.150	15.243
7	0.010	0.168	0.924	1.927	2.576	2.985	3.141	3.051	2.662	1.089	1.111	0.127	19.771
8	0.012	0.248	0.940	1.934	2.563	2.959	3.075	2.901	2.477	1.844	1.056	0.258	20.267
9	0.007	0.156	0.920	1.924	2.548	2.932	3.056	2.931	2.520	1.880	1.067	0.259	20.202
10	0.006	0.156	0.909	1.877	2.512	2.910	3.018	2.858	2.421	1.737	0.966	0.237	19.606
11	0.007	0.191	0.933	1.699	2.409	2.691	2.768	2.602	2.492	1.852	1.054	0.200	18.898
12	0.005	0.168	0.577	1.734	1.589	2.084	1.818	1.508	1.291	1.773	0.646	0.090	13.284
13	0.005	0.119	0.419	0.800	1.288	2.025	1.599	1.570	1.929	1.899	0.902	0.184	12.738
14	0.002	0.071	0.256	0.750	1.056	1.538	1.424	1.137	1.244	0.806	0.380	0.099	8.761
15	0.004	0.090	0.385	0.755	1.294	1.255	0.898	1.536	1.953	2.028	1.086	0.192	11.474
16	0.005	0.187	0.824	1.381	2.451	1.464	2.394	2.614	2.485	1.817	0.637	0.229	16.488
17	0.006	0.230	0.891	1.888	2.517	2.922	3.045	2.893	2.491	1.841	1.026	0.224	19.974
18	0.004	0.124	0.773	1.863	2.474	2.876	3.009	2.960	2.455	1.817	0.994	0.096	19.445
19	0.001	0.118	0.576	1.163	1.992	2.095	3.022	2.116	1.020	0.680	0.417	0.082	13.283
20	0.002	0.117	0.974	1.396	2.382	1.916	1.177	1.110	0.957	1.456	0.912	0.080	12.477
21	0.001	0.032	0.144	0.532	0.697	1.058	1.301	1.852	1.065	0.246	0.068	0.022	7.017
22	0.001	0.153	0.668	1.469	1.383	2.322	1.938	1.187	1.627	1.038	0.769	0.152	12.707
23	0.001	0.190	0.562	1.692	2.211	2.676	1.995	1.366	1.431	0.891	0.585	0.130	13.731
24	0.004	0.103	0.321	1.065	1.794	1.916	2.196	2.178	1.480	0.745	0.482	0.082	12.365
25	0.001	0.156	0.599	1.484	2.123	2.563	2.721	2.578	2.219	1.602	0.835	0.175	17.054
26	0.001	0.153	0.606	1.574	2.209	2.619	2.757	2.622	2.211	1.588	0.837	0.185	17.362
27	0.001	0.150	0.598	1.498	2.119	2.558	2.704	2.602	2.248	1.632	0.863	0.181	17.154
28	0.001	0.148	0.604	1.423	2.052	2.472	2.636	2.540	2.149	1.501	0.854	0.189	16.569
29	0.001	0.152	0.600	1.441	2.063	2.474	2.630	2.514	2.029	1.348	0.770	0.164	16.188
30	0.001	0.145	0.602	1.611	2.277	2.654	2.520	2.651	2.286	1.613	0.791	0.179	17.331
Average	**0.004**	**0.137**	**0.581**	**1.286**	**1.862**	**2.225**	**2.225**	**2.043**	**1.786**	**1.301**	**0.708**	**0.158**	**14.315**

December

Date/Time	6-7	7-8	8-9	9-10	10-11	11-12	12-13	13-14	14-15	15-16	16-17	17-18	Total
1	0.000	0.134	0.542	1.467	2.131	2.538	2.695	2.586	2.233	1.516	0.761	0.153	16.755
2	0.000	0.127	0.518	1.467	2.170	2.598	2.768	2.648	2.284	1.642	0.769	0.164	17.155
3	0.001	0.147	0.466	1.398	2.196	2.619	2.785	2.729	2.349	1.712	0.916	0.167	17.485
4	0.000	0.123	0.508	0.937	1.549	2.462	2.789	2.721	2.305	1.673	0.712	0.068	15.848
5	0.000	0.127	0.493	1.154	1.939	2.556	2.659	2.882	2.424	1.418	0.604	0.230	16.485
6	0.000	0.131	0.503	1.487	2.160	2.623	2.755	2.461	2.332	1.763	0.993	0.185	17.394
7	0.000	0.131	0.465	1.302	2.154	2.372	2.685	2.641	2.305	1.687	0.944	0.151	16.838
8	0.000	0.120	0.459	1.244	2.079	2.510	2.732	2.659	1.918	1.559	0.891	0.153	16.324
9	0.000	0.140	0.445	1.246	2.079	2.501	2.658	2.611	2.248	1.638	0.912	0.151	16.628
10	0.000	0.101	0.414	0.978	1.609	2.231	2.680	2.660	2.249	1.669	0.663	0.100	15.354
11	0.000	0.100	0.400	1.218	2.076	2.548	2.738	2.657	2.304	1.682	0.671	0.136	16.531
12	0.000	0.212	0.549	0.918	1.754	2.092	2.822	2.757	2.474	1.766	0.556	0.146	16.045
13	0.000	0.101	0.376	1.262	2.226	2.642	2.843	2.804	2.430	1.796	0.662	0.100	17.243
14	0.000	0.102	0.391	1.230	2.222	2.673	2.826	2.732	2.475	1.873	0.706	0.101	17.332
15	0.000	0.086	0.347	1.174	2.127	2.542	2.721	2.606	2.093	1.689	0.662	0.130	16.179
16	0.000	0.067	0.381	0.877	1.785	2.433	2.542	2.583	2.225	1.669	0.635	0.148	15.346
17	0.000	0.080	0.392	1.251	1.974	2.433	2.647	2.640	2.272	1.665	0.667	0.114	16.135
18	0.000	0.096	0.371	1.083	2.053	2.310	2.637	2.614	2.261	1.726	0.699	0.110	15.960
19	0.000	0.089	0.366	1.055	2.003	2.398	2.589	2.567	2.241	1.683	0.699	0.117	15.806
20	0.000	0.101	0.374	1.047	2.002	2.426	2.603	2.528	2.197	1.653	0.669	0.139	15.738
21	0.000	0.095	0.352	1.066	2.124	2.516	2.709	2.662	2.301	1.755	0.712	0.106	16.397
22	0.000	0.110	0.372	1.092	2.152	2.595	2.758	2.692	2.356	1.839	0.738	0.090	16.793
23	0.000	0.086	0.348	1.075	2.191	2.628	2.766	2.703	2.343	1.802	0.757	0.116	16.814
24	0.000	0.083	0.354	1.049	2.136	2.592	2.759	2.708	2.390	1.837	0.769	0.123	16.800
25	0.000	0.080	0.358	1.027	2.081	2.505	2.696	2.657	2.357	1.818	0.790	0.120	16.490
26	0.000	0.086	0.432	1.016	1.983	2.440	2.651	2.555	2.276	1.725	0.766	0.144	16.073
27	0.000	0.072	0.361	1.005	1.981	2.402	2.619	2.573	2.287	1.715	0.768	0.140	15.926
28	0.000	0.073	0.370	0.873	1.854	2.488	2.578	2.494	2.095	1.605	0.730	0.173	15.332
29	0.000	0.069	0.382	0.986	1.952	2.446	2.677	2.603	2.277	1.727	0.794	0.215	16.134
30	0.000	0.077	0.380	0.895	1.914	2.391	2.624	2.591	2.264	1.744	0.795	0.159	15.836
31	0.000	0.072	0.377	0.947	1.908	2.359	2.581	2.508	2.267	1.753	1.003	0.203	15.981
Average	**0.000**	**0.104**	**0.414**	**1.123**	**2.018**	**2.480**	**2.697**	**2.640**	**2.285**	**1.703**	**0.755**	**0.140**	**16.360**

A2. Hourly and daily ambient temperature (celsius) [87]

January

Date/Time	6.00	7.00	8.00	09.00	10.00	11.00	12.00	13.00	14.00	15.00	16.00	17.00	18.00
1	13.3	13.2	15	17.4	19.8	23.7	24.1	26.2	27.6	27.8	27.4	27.4	23.7
2	13.9	13.5	14.5	17.1	20.2	22.4	24.1	26.1	27.3	26.7	27.8	26.6	23.6
3	13.6	12.9	14.8	16.7	19.5	22.1	23.6	25.6	26.4	27.9	27.6	27.4	23.1
4	13.9	12.3	14.5	17	19.7	21.8	24.4	26.2	27.3	28.3	28.6	28.3	24.8
5	14.5	13.8	15.7	18.2	21.7	25	26.9	27.5	29.1	29.5	29.3	28.8	24.7
6	15.8	15.4	16.3	19	22.8	25.5	28.9	28.6	30.4	29	31.3	29.5	25.6
7	15.5	14.9	16.7	18.1	21.2	25.4	26.5	27.8	27.7	27.9	28.2	27.4	25.2
8	17.6	17.1	17.8	19.7	21.7	24.8	25.9	26.8	26.8	28.7	28.7	27.4	24.8
9	14	13.5	15.7	19.2	22.3	24.7	25.8	26.8	26.9	27.8	27.5	27.2	24
10	14.7	14.3	15.4	18.3	21.5	25.3	26.3	27.3	27.3	28.5	28.3	27.6	24.5
11	15	14.6	15.3	18.4	22.4	23.6	26.3	27.1	29	29	28.9	28.4	25.1
12	14.7	15	16.2	19.5	22.2	24.4	26.4	27.5	28.5	29.5	29.2	28.9	24.9
13	14.4	14.6	15.8	19.6	21.3	24.7	26.6	28.4	28.7	29.2	29.6	29.5	25.8
14	15.6	15.3	16.7	19.3	21.1	24.3	26.9	28.8	29.2	30.5	30.3	30.8	26.4
15	15	14.6	16.8	19.2	21.7	24.5	27	28.4	29.5	29.9	31.3	31	26.6
16	14.1	13.8	16.7	21	22.4	24.5	26	28.5	29.4	30.4	31.1	30.7	26.1
17	13.7	13.7	15	18.4	21.1	23.7	25.8	28.7	29.7	30.7	31.7	30.7	26.6
18	13.9	13.4	16.4	19.6	21.8	24.1	26.7	29.3	30	31.4	32	30.9	25.5
19	12.1	12.2	14	17.7	20.4	25.1	25.8	27.8	29.1	30.5	31.5	30.9	26.6
20	13.1	12.8	14.1	18.6	21.9	25.2	27	28.8	30.5	30.1	30.8	30.9	25.6
21	13	11.8	13.8	17.5	21.1	23.7	26.3	28.6	29.6	29.8	31	30	28.5
22	12	12	14.2	16.6	19.1	23.4	26.3	27.7	29.3	29.9	30.2	31.3	25.2
23	12.1	12.3	13.8	17.2	20.6	24.1	26.9	27.5	29.3	29.9	30.3	29.8	26.6
24	17.6	17.7	18.1	20.2	22.3	26.9	27.4	29	30.6	30	31	30.1	29.1
25	20.3	20.6	21.3	23.8	24.1	26.1	27.6	28.9	30	30.2	30.2	30.6	27.8
26	18.7	17.9	19	20.9	23.8	27	28	29.1	30.6	30.5	31.4	31.2	28.5
27	19.3	19.6	20.4	22.4	25.2	26.9	28.1	28.9	29.7	30.5	29.7	29.3	28.3
28	20.5	18.5	19.7	21.6	22.5	23.9	24.5	23.7	24.6	24.1	23.8	22.7	21.6
29	17.6	17.2	17.9	19.5	22	23.8	24.4	24	25.6	25.3	26.2	25.4	24
30	13.8	13	14.3	16.6	19.6	23.4	25.6	25.6	28	28.4	28.3	27.5	24.5
31	13.1	13.7	14.1	16.6	19.2	22.8	24.1	25.4	27.5	27	27.3	25.8	23.6

February

Date/Time	6.00	7.00	8.00	09.00	10.00	11.00	12.00	13.00	14.00	15.00	16.00	17.00	18.00
1	12.7	12.7	13.5	16	18.8	22.5	24.9	25.5	26.4	26.9	27.1	26.6	23.9
2	14.9	15.3	16.1	19	20.6	23.9	24.1	24.6	27.3	25.4	25.6	24.8	22.5
3	13.4	13.3	13.6	15.7	19	22.7	23.7	23.2	24.5	25.4	25.4	24.7	22.4
4	12	12.9	13.1	15.1	17.7	21.4	22.8	23.8	25.7	26.5	27.2	26.8	23.2
5	13.4	12.6	13.8	16.7	19.1	22.4	23.9	25.8	27.7	28.4	29.1	27.6	24.5
6	13.5	12.4	13.5	16.9	19.6	22.8	25.1	26.2	27.9	29.1	28.8	28.7	25.4
7	14	13.7	14.7	17.2	19.5	22.2	25.9	27.1	28	29.4	29.4	28.7	25.7
8	14.4	14.3	14.8	18.7	19.6	23	25.6	27.7	29.2	29.8	29.5	29.4	25.6
9	17.1	16.1	16.6	19.4	22.4	24.7	27.3	29.6	31.3	32.7	32.8	30.4	28.2
10	15.1	15.5	16.7	19.5	23.1	26.8	30.8	31.6	32.4	32.3	33.2	31.3	28.9
11	16.2	16	17.2	21.8	24.8	26.7	28.6	29.4	31.3	32	32.1	31.7	29
12	16.2	16	17.8	21	23.9	26.6	28.4	30.8	32	33.1	32.8	32.7	29.4
13	16.8	16.9	20	22.6	25.4	28.6	29.8	30.7	32.1	32.7	33.3	32.8	30.9
14	16.6	15.1	17.5	21.7	24.4	26.7	29.2	30.4	31.9	33.3	33.6	34	30.4
15	18.2	17.9	20.4	25	26.4	28.7	30.1	32.5	32.6	32.3	32.1	31.2	30.8
16	17.9	17.2	20	25.2	26.3	27.8	29	30.2	31.5	30.6	30.9	32.6	30.8
17	18.3	18.1	20.5	24.5	27.2	28.2	31.6	32.4	32.1	31.9	32.4	31.9	27.5
18	17.2	16.1	18.6	21.8	25.6	29.1	30.4	29.9	32.5	32.1	32.2	31.8	30.5
19	16.2	16.1	18	22.9	25.6	28.9	31	31.5	33	32.8	33.3	32.4	30.2
20	14.3	14.6	17.3	19.8	23.3	26.3	29.6	31.3	32	32.8	32.9	32.8	29.7
21	16	14.2	17.1	20.7	24.8	28.5	30.7	31.4	33.4	34.2	34.5	33.8	31.1
22	16.4	14.8	17.6	23.4	26.9	29.6	32.2	32.4	33	33.5	33.9	33.3	29.9
23	15.9	15	18.4	22.1	25.1	28.1	32	32.8	34.3	34.1	34.3	34.6	30.6
24	18.6	17.4	20.4	23.5	26.7	30.8	32.5	33.8	34.3	34.8	36.1	35.1	33.3
25	19.2	18.8	20.6	24.4	27.1	30.4	32.2	33.7	35.1	35.2	36.5	35.7	33.4
26	21.2	19.7	23.3	27.1	29.4	31.3	33	34.4	35.2	34.7	36	36.3	34.1
27	20.8	20.1	24.8	27.9	29.3	31.1	32.3	34	35.2	34.2	35.6	36	33.6
28	20.3	18.5	21.1	24.6	28.7	31.4	33.1	33.4	33.7	33.7	33.4	33.3	30.6

March

Date/Time	6.00	7.00	8.00	09.00	10.00	11.00	12.00	13.00	14.00	15.00	16.00	17.00	18.00
1	17.3	16.8	18.3	21.2	26.3	29.8	31.6	33.3	34.5	34.2	34.1	34	29.9
2	16.6	15.8	18.1	21.1	26	27.9	30.5	32.5	33.9	34.7	35.6	35.1	31.5
3	16.2	16.1	18.3	21.3	26	28.2	31.2	32.7	33.3	34.1	34.6	34	30.8
4	16.5	17.4	17.8	20.3	24.3	28.1	30.4	33.7	33.4	33.8	33.9	33.9	30
5	17.1	16.8	18.1	21.4	23.9	27.2	29.3	30.8	32.6	34.2	34.8	34.1	30.5
6	17.9	16.8	17.4	21.1	23.5	26	28.1	31	32.8	33.9	34.1	33.7	30.7
7	17	15	19	23.8	25.5	28.6	30.8	32.5	34.3	35.1	35	35.2	32.1
8	15.8	15.5	19.1	23.3	26.5	30	30.6	31.7	33.3	34.7	34.9	34.3	32.5
9	16.1	15.2	18.9	23.4	26.3	29.4	31.5	32.4	33.2	34.2	34.5	34.2	32.3
10	16.2	15.7	17.7	20.5	22.8	26.5	28.6	31.8	32.9	33.5	33.6	33.3	30.5
11	15.2	14.7	16.2	20.1	23.5	26.6	28.8	31.4	32.8	33.6	34.5	34.4	30.6
12	15.7	15.8	17.4	20.6	23.2	26.7	29.6	31.9	34	35	35.3	35.1	30.1
13	17.9	17	18.3	21.3	24.3	28.3	30.7	32.4	33.5	33.8	33.4	32	30.5
14	17.7	17.3	19.3	22	25.1	29	31.8	33.5	35.2	35.8	36	35.7	31.2
15	19.3	19.4	20.6	25.7	28.3	31	33.3	34.8	36.7	36.9	37	36.3	33.3
16	19.1	18.7	21.1	25.7	27.4	30.8	32.3	34	34.8	35.8	36	35.8	32.9
17	21.8	20.8	23.6	26.2	28.4	29.8	31.5	33.3	33.8	33.8	33.4	33.2	31.8
18	19.4	18.7	21.5	23.6	27	29.1	32	34.8	35.5	36.1	35.6	34.8	31.5
19	19	19.5	21.1	23.4	27.1	30.5	31.8	33	33.7	35.1	35.8	34.8	33.4
20	22.7	23.1	24.9	28.9	29.5	31.2	33.1	34.1	34.6	36.1	35	34.6	33.5
21	20.5	20.1	22.4	25.1	26.2	28.3	29.8	30.7	32	32.4	33.5	32.5	31.6
22	21.5	20.7	23.8	26.3	28.8	29.5	32.1	32.4	34.1	35	33.2	33.2	32.4
23	20.7	20.4	23.6	27.4	28.9	30.7	32.9	33.9	35.1	35.4	35.3	34.9	34
24	20.4	19.8	22.3	24.5	26.9	29.7	31.7	33	34.4	35.4	35.4	35.1	33.3
25	20	20.6	23.1	26.5	27.9	29.9	32.3	33.9	36.1	37.6	36.5	36.6	34.5
26	21.7	22.1	25.1	27.2	29.2	31.7	33.8	34.7	36.7	36.5	37.3	36.9	35.9
27	22.1	21.4	24.7	28.6	30.5	32.3	35.9	36.3	37.5	38.5	38.3	37.7	36.4
28	21.5	22.8	24.9	27.5	29.8	32.3	34.6	36.2	37.6	37.5	38	37.2	35.7
29	22.9	21.5	24.4	27	30.2	33.2	35.5	37.2	37.2	38.2	38.5	37.5	36.7
30	26.3	25.7	28	30.4	31.5	33.9	36.2	35.3	37.7	32.6	31.4	34.3	33.1
31	22.9	23	25.9	28.2	30.4	32.2	34.4	36.3	37.7	37.8	37.6	37	36.2

April

Date/Time	6.00	7.00	8.00	09.00	10.00	11.00	12.00	13.00	14.00	15.00	16.00	17.00	18.00
1	24	24.7	29.1	31.3	33.2	34.7	35.8	36.8	38.1	39.1	39.8	38.4	37
2	23.5	23.6	27.7	30.6	31.7	34	35.9	37	38.1	38.9	39	37.8	35.4
3	21.6	21.1	23.9	28.2	30.3	32.3	34	35.5	37.7	37	37.5	37.1	34.7
4	20.1	21.2	23.4	28.5	31.5	33.5	34.2	36	36.1	36.9	36.6	36.2	34.9
5	23.9	23.2	26.3	30	31	32.6	33.5	34.6	35.7	36.5	36.9	36.6	35
6	23.6	23.6	26.5	28.8	31	32	32.9	34	34.5	35.5	35.9	35.5	34.2
7	24.4	24.1	26.5	28.2	30.9	31.6	33	34.6	35.4	36.3	36.6	36	33.3
8	23.9	23.8	26.6	28.5	30.6	31.6	33.2	34.2	34.9	35.8	36.4	36.5	35.1
9	24.3	23.6	28	29	30.4	31.9	33.6	34.5	35.6	36.3	36.6	36.3	34.9
10	23.4	24.9	27.6	29.7	30.3	31.7	33.4	34.7	35.4	36.1	36.3	36.5	35.2
11	22.2	23	26.9	29.1	30.9	31.1	32.1	32.1	33.4	29.4	32.3	32.7	29.9
12	24.2	24.2	26.8	28.1	30	30.7	32.7	32.9	31.8	34.1	35.8	30.7	27.5
13	23.5	23.5	26.1	28	28.8	30.8	32.1	33.7	35	35	31.7	33.1	31.9
14	24.5	24.2	25.5	28.2	30.1	30.2	30.7	32.5	32.2	31.3	31.7	30.8	28.6
15	24.4	24.5	25.8	28.1	29.1	32.7	33.3	34.4	34.6	34.1	33.4	29.6	27.8
16	23.8	24.2	26.1	27.4	29.3	31.2	31.4	33.9	33.3	33.8	33.1	33	31.5
17	24.7	24.9	27.1	29.8	31.8	33.1	34.4	35.2	34.3	34.5	36.3	34	34.1
18	23.5	24.8	28.4	29.9	31.4	33.8	35.3	36.1	38.6	37.1	37.1	24.3	25.6
19	24.9	25.6	26.4	27.4	28	30.9	31.6	32.8	33.6	34.3	34.6	35	34.3
20	23.3	24	27.1	30.2	31.2	32.4	34.8	35.5	35.6	36.4	35.8	37.5	36.6
21	24.3	25	28.8	31.3	33.3	34.6	35.6	37	37.4	38.3	38.4	39.5	38.6
22	25.7	26.6	30.8	32.4	33.1	34.4	36	37.7	38.3	39.1	38.4	38.9	38.5
23	25.8	26.2	30.1	32.3	34.6	34.6	36.2	36.7	37.5	38.2	38.5	38.6	37.3
24	24.4	26.6	29.4	31.4	33.8	36.4	36.6	37.2	38.2	38.5	38.9	38.2	37.8
25	24.4	26.4	28.8	31.3	33.7	35.2	37.2	38	40.3	39.3	38.9	38.7	37.9
26	23.7	22.2	22.5	23.4	26.1	26.8	30.3	32.1	33.5	34.3	32.6	31.9	31.2
27	21.1	21.6	24.5	26.5	29.1	30.5	30.9	33.6	33.9	35.3	35.4	33.6	33
28	21.6	21.5	21.6	22.9	24.8	28.2	28.7	30.6	29.7	30.3	30.1	30.7	29.9
29	24.8	25.5	27.3	29.4	30.7	32.5	32.4	32.9	35.9	32.7	30.6	32.4	31.5
30	23.2	23.9	27	29.1	31	32.3	33.3	34.4	36.2	32.2	31.3	32.3	32.3

May

Date/Time	6.00	7.00	8.00	09.00	10.00	11.00	12.00	13.00	14.00	15.00	16.00	17.00	18.00
1	23.5	24.2	25.8	27.8	30.8	33.1	33	34.3	34.7	36.3	35.9	36.3	35.3
2	25.6	26.4	27	28.1	29.5	29.8	31.1	29.9	30.8	30.9	30.4	28.8	27.9
3	24.2	24.3	23.9	24	24.4	25.6	26.5	31.5	29.4	31	26.5	24.7	24.8
4	23.5	23.3	23.5	24.3	24.3	25.3	24.4	24.6	24.8	24.4	24.5	24.1	24.2
5	22.3	22.3	22.4	22.4	22.7	23.2	24.5	24.7	26.7	26.2	23.7	24	23.7
6	22.6	22.3	22.5	22.3	22.8	23	22.9	23.2	23	23.3	24.4	25.2	24.9
7	23.2	23.5	24.1	24.5	24.7	26.2	26.7	25.9	26.9	28.9	29.2	28.4	27.8
8	22.5	22.6	22.9	23.4	25.2	25.7	27.8	29.5	28.5	30.1	29.8	30	27.4
9	23.7	23.8	25	25.8	27.2	28.6	29.2	29.6	30.3	31.5	32	31.7	31.2
10	24.8	24.5	25	26.1	27.9	28.3	30.5	28.8	31.7	32.1	32.2	32.2	31.5
11	21.4	23.5	23.1	24.3	25.5	26.5	28.4	29.5	30.7	29.3	26.7	27.7	27.2
12	23.5	23.6	24.8	26.3	27.9	27.9	28.7	30	27.2	25.1	23.5	24.5	24.7
13	23.8	23.8	24.2	24.2	24	24.4	26.3	27.1	26.6	26.1	26.2	27.6	27.5
14	23	23.1	23.6	25.6	25.4	26.8	27.7	27.8	29.9	29.2	29.2	29	24.2
15	23.6	23.7	25.6	26.3	26.8	27.7	28.7	29.9	31.2	23.7	24.9	27.4	26.1
16	22.6	23	25.7	27.1	27.4	28.3	29.4	30.4	31.5	31.7	32.2	31.7	31.2
17	23.5	23.9	24.9	26.6	28	29.2	30.6	30.4	30.2	31.3	30.6	30.9	30.8
18	24	24.4	24.9	26.9	26.9	28.7	30	31.1	31.1	29.4	30.2	29.2	29.2
19	24.4	24.4	25.3	27	27.6	28.9	29.1	29.5	29.8	31.2	31.6	31.7	30.4
20	24.1	23.1	23	23.4	24.3	25.4	26.4	27.3	28.1	27.8	28.3	27.8	27.2
21	24	24.1	26	26	26.7	27.1	27.9	29.3	28.7	29.3	28.3	28.6	27.5
22	24.2	24.3	25.9	26.7	28.1	28.8	29.2	29.8	30.3	30.2	31.1	30.6	29.4
23	22.9	24	25.9	26.5	28	29.9	31	32.6	31.5	32.5	32.2	31.4	31.1
24	22.9	24.4	26.3	27.8	29.5	30.6	31.6	32.8	33.3	33.8	34.6	34.3	33.8
25	24.2	25.2	27.7	29.7	30.3	32.8	32.4	33.2	34.2	34.2	31.2	30.8	30.5
26	23.9	25.3	27.9	29.3	29.5	30.9	32.1	33.3	34	33.8	28.4	28.4	28.5
27	24	24.8	27.4	28.3	30	32.4	33.4	33.5	36	34.9	35.5	34.2	31.9
28	24.5	26.2	29	29.7	30.9	33.6	34.2	33.7	33.3	30.9	30.8	32.8	29.6
29	24.2	25	27.4	29	30.5	30.6	32.1	33.4	33.8	34.6	30.8	29.6	27.5
30	23.5	23.8	24.9	26.1	26.5	28.1	30.4	30.5	32.2	32.4	33.5	29.6	28.9
31	24.3	24.5	25.4	25.7	27.5	29.6	30.2	31.5	32.9	33.8	32.9	27.6	22.9

June

Date/Time	6.00	7.00	8.00	09.00	10.00	11.00	12.00	13.00	14.00	15.00	16.00	17.00	18.00
1	23.7	23.7	24.3	25.3	26.2	27.2	28.2	29.2	30.2	30.9	31.4	30.7	29.5
2	24.4	25.3	27.5	27.5	29	29.9	31.3	29.4	31.2	32.2	32.8	31.1	30.4
3	23.4	24.6	26.9	27.6	29.1	31.1	31.8	32.6	32	31.2	30.7	29.5	28.6
4	24	24	25.6	27.4	28.5	29.8	31.3	32.5	31	31	31.4	30.1	29.5
5	23.6	23.5	24.4	26.9	27.1	28.3	29.8	30.8	29.4	32.4	32.6	29.1	27.3
6	23.9	24.3	25.6	26.8	27	28.2	29.5	30.6	31.5	31.8	32.3	28.8	27.3
7	24.3	25.1	26.5	27.3	28.1	30.1	31.2	31.7	31.2	31.6	32.4	32.4	30.7
8	24.5	25.9	26.4	28.3	29.5	30.9	31.8	32.1	31.8	33.1	33.5	32.4	31
9	24.7	25.3	26.4	27.5	29.7	31.6	32.3	31.7	32.3	32.9	33.1	33.9	32.1
10	25.1	26.1	28.4	29.3	30.5	32.1	32.4	32	32.7	33.4	34.3	33.4	33
11	25	26.3	28	29.2	30.4	32.1	31.5	29.8	32.2	33.1	32.4	31.3	29.2
12	25.2	25.4	27.5	28	29.1	31	29.6	29.8	31.7	31	32.6	31.2	24.7
13	24.3	24.5	25.7	26.9	27.6	28.1	29.9	29.5	30.2	31.1	31.5	30.6	29.6
14	24.7	25.1	26.2	27.7	29.8	30.3	31.6	32.2	33.3	32.2	28.3	27.9	27.4
15	24.6	25.3	26.7	27.7	28.8	30.1	30.9	31.9	32.6	33	32.6	33.1	32
16	26.4	25.7	26.5	27.9	29.5	30.5	31.4	32.6	29.2	26.1	28.3	30	30.3
17	24.7	25.2	26.9	27.8	28.2	29	30.2	31.1	31.4	31.7	32.2	32.4	32.1
18	25.3	26.7	27.9	28.9	29.3	31.6	30.8	32.1	32.3	31.9	31.9	31	30.9
19	24.8	24.9	25.9	27.3	28.3	28.8	30.5	31.3	31.7	32.3	30.8	29.3	29
20	24.6	24.4	25.5	27.8	27.7	29.1	30.3	31	31.6	32.9	32.5	32.5	32.2
21	23.9	24.6	26	27	30.6	30.4	32.3	33.2	33.5	33.5	33.9	30.5	30.2
22	25.3	25.9	28.8	30	31.2	33.9	34.7	34.1	35.1	35.3	35.3	35.1	34.1
23	25.2	25.6	27.3	28.9	31.1	33.4	33.8	35	35.9	36	36.7	36.7	35.6
24	26.2	27.1	28.1	29.6	31	32.3	33.8	35.6	35.3	31.2	31.1	31.4	30.8
25	26.4	25.9	26.7	28.7	29.6	29.9	31.5	32.3	33.7	33.9	27.5	28.9	27.2
26	25.5	25.5	25.9	27	27.5	28.7	30.9	31.9	33	31.8	31.3	25.3	26
27	24.6	24.9	25.4	26.2	27.4	28.5	29.5	27.4	25	25.2	26.7	25.8	25.8
28	24	22.5	23.2	24.5	25.8	26.5	27.7	27.8	28.8	26.6	27.5	27.5	27.6
29	24.2	24.9	25.6	26.6	26.7	27.8	28.3	28.6	29.1	29.8	29.3	26.8	26.9
30	23.9	24	26.2	26.8	28	29.7	31.2	32.2	32.6	32.5	31	31.4	31.3

July

Date/Time	6.00	7.00	8.00	09.00	10.00	11.00	12.00	13.00	14.00	15.00	16.00	17.00	18.00
1	24.8	25.4	26.6	27.7	29.3	29.8	31.2	31.1	28.6	27.4	29.6	28.3	28.9
2	24.7	25.5	26.7	28.2	28.7	29.3	29.1	29.6	31.4	32	32.8	32.7	31.8
3	24.9	26.1	27.4	28	28.5	29.4	29.7	29.7	28.8	30.8	30	30.3	26
4	24.3	25	26.2	26.8	27.9	28.7	29.9	30.3	30.6	31.5	30.9	30.9	29.7
5	25.4	25.3	25.7	27	27.4	28.3	29.3	29.9	31.4	31.4	31.1	29.8	29.3
6	25.1	25.5	25.9	26.6	23.8	24.3	24.4	24.7	25	25.1	24.9	24.9	25.3
7	24.1	24.3	26.2	26.6	26.9	28.6	29.5	30.6	31.3	32	29.1	26.9	27.4
8	22.9	23.4	24.7	26.2	28.8	29.9	30.7	31.7	31.9	32.2	25.7	25.5	26.2
9	23.2	23.9	25.6	27	28.1	30.6	31.1	32.7	32.6	32.8	33	32.6	32.1
10	24.9	25.4	26.5	27.5	28.8	29.8	30.3	30.8	32	32.6	32.9	32.6	33.7
11	25.1	25.3	26.4	27.8	29	30.5	31	31.2	31.7	32.4	31.9	30.7	30.7
12	25.3	25.5	26.7	27.3	27.8	29	29.6	30.4	32.3	31.5	31.3	30.9	29.9
13	24.9	25.7	26.5	27.7	29.2	29.2	30.9	31.7	31.6	29.3	29	29.7	29.2
14	24.6	25.7	26.4	27.4	28.6	29.8	30.2	30.4	29.6	31.3	30.8	30.5	29.6
15	26.3	26.3	26.9	27.4	28.2	28.7	29.1	29.6	29.4	30.1	30.3	30.9	30
16	25.7	25.8	27.4	27.8	28.1	28.4	28.2	30.6	31	32.4	32	30.2	26.9
17	25.1	25.4	26.6	27.7	28.9	31.2	31.6	32.7	31.9	32.7	33.4	33.1	31
18	25.3	25.9	26.8	28.1	30.1	30.5	31	31	32.1	33.1	32.3	32.6	30.9
19	24.3	24.6	26.3	27.3	28.4	29.7	29.9	30	32.3	27.1	30	25.9	25
20	23.9	24.2	25.3	26.1	26.6	26.9	26.9	26.8	27	26.7	26.6	25.9	25.6
21	23.3	23.5	23.7	24	24.3	24.5	24.6	24.1	24.2	23.6	24	24.6	24.7
22	22.7	22.8	23.7	24.7	25.8	27.8	27.7	29	29.3	29.9	29.1	29.4	28.8
23	23.2	23.7	24.9	27.1	28.2	29.9	31	32.1	32.3	32.1	30.3	28.8	28.1
24	23.2	23.2	23.5	23.6	23.9	24.9	26	26.4	26.1	26	25.7	24.9	24.5
25	21.3	21.4	21.9	22.7	24	24.9	26.3	27.5	28.7	29.3	29.8	30.2	29.7
26	23.3	24.3	26.2	26.7	28.5	29.4	30.3	31.4	30.8	24.6	28	30.5	29.3
27	24.1	24	25.5	26.7	27.5	28	28.4	29.2	30.2	30.4	30.6	30.3	29.5
28	23.2	24.6	26.4	27.9	28.8	29.9	30.9	32.9	32.3	33	33.2	33.5	31.4
29	24	24.3	24.6	25.6	26.8	29.7	30.6	32.6	32.4	32.3	29.7	29.4	27.8
30	24.3	24.5	25.5	25.9	27.4	30.2	30.1	33.1	31.3	32.6	33.3	32.6	31
31	24.3	25.4	25.7	26.9	28.1	31.7	31.6	30.1	27.5	25.5	27.2	29.9	29.8

August

Date/Time	6.00	7.00	8.00	09.00	10.00	11.00	12.00	13.00	14.00	15.00	16.00	17.00	18.00
1	24.4	24.6	25.7	28	28.5	29.5	30.5	31	29.5	29.8	29.7	29.5	29.3
2	24.5	24.5	25	24	24.4	25.4	26.7	27.6	28.9	28.8	29.7	30	28.8
3	23.8	23.9	24.4	25.8	26.5	28.2	28.6	28.6	29.6	29	29	29	28.3
4	24.2	24.7	26.2	27.4	27.7	29.4	29.7	30.6	31.1	31.9	32.9	29.5	27.3
5	23.7	23.9	25.1	26.1	27.7	28.6	29.4	30.6	31.3	31.7	31.3	32.3	31.6
6	24.3	24.9	25.8	27.3	27.7	29.8	30.8	30.7	32.1	32.6	32.7	31.4	30.1
7	24	24.3	26.5	27.6	29.6	31.3	32.8	32.4	31.1	32.2	31.5	31.4	31.6
8	24.9	25	25.5	26.7	27.6	29	30.3	31.4	31.5	31.6	32	26.1	24.6
9	24.5	24.6	24.7	26	27.2	29.3	29.5	25.6	26	27.9	28.5	27.2	26.4
10	24.1	24.6	25.6	26.5	27.4	28.7	28.7	29.4	28	27.8	27.4	27.9	27.3
11	24.9	25.1	25.1	26.4	26.8	26.8	27.8	28.3	29.8	29.7	30	29.1	28.4
12	24.2	24.7	25.1	25.6	26.5	28	29	28.8	30	30.3	29.3	29.2	28.6
13	24.6	24.8	26.2	26.9	28.4	29.5	31.1	30.9	31.8	32.5	33.1	32.8	31.8
14	25.2	25.3	26.3	27.8	28	29.8	30.4	31.9	32.1	32.8	31.7	32.6	31.1
15	25.1	24.9	26	26.7	28.1	28.4	29.3	30.3	31	31.9	31.6	31.6	31.2
16	25.6	25.4	25.7	25.3	25.6	26.3	29.7	29.1	27.1	28.7	27.8	24.8	24.4
17	23.6	23.7	24.6	25.2	26	26.9	28	29.5	30.5	31.3	31.3	31.1	29.9
18	23.1	23.2	25.4	26.7	27.1	28.6	29.5	29.8	30.9	31.9	32.1	32.1	32
19	23.4	24.1	25.7	27.5	28.5	29.8	30.1	30.8	29.8	29.4	31	31.9	30.4
20	23.3	23.8	25.9	27.1	28.7	29.9	31.3	32.5	32.3	32.3	30.7	30.9	30.1
21	25.2	24.8	25.6	28	28.8	29.7	31.2	32.4	33.1	31.3	25.2	28.2	27.4
22	24.6	24.8	25.7	26.8	27.8	30.1	30.4	31.4	30.7	31	30.7	30.8	26.5
23	24.1	24.3	25.1	25.9	27.2	28.5	30.2	28.6	30	31.6	30.8	27.3	24.3
24	24	24.1	24.7	25.4	25.9	26.4	26.4	27.2	28.1	28.9	28.7	28.1	26.7
25	23.5	23.8	24.2	25.3	25.9	26.2	26.8	27.6	28.3	29.3	28.9	26.6	25.3
26	23.7	23.5	24.1	26.1	26.9	29.6	29.8	30.4	31.4	32	31.9	30.2	29.7
27	24.1	24.5	25.6	26.7	28.1	30.5	31.8	31.3	32.5	33	33.2	32.9	32.6
28	25.1	24.7	26	27.8	29.4	30.4	31.5	31.1	30.2	28.1	27.5	27.2	27.8
29	24	23.9	24.9	27	29.2	30.8	31.8	31	32.4	31.9	28.2	28.9	30
30	23.7	24.2	24.5	25.6	26.1	26.9	28	30	30.5	31.8	27.4	24.9	25.9
31	23.2	23.6	24.2	25.9	26.5	28.2	29.3	30.2	30.7	30.9	30	29.3	28.1

September

Date/Time	6.00	7.00	8.00	09.00	10.00	11.00	12.00	13.00	14.00	15.00	16.00	17.00	18.00
1	24.2	24.2	24.8	26.6	27.1	28.8	29.8	30.7	31.7	32.1	31.8	31.4	28.6
2	25.2	25	25.8	28.4	27.9	28.6	29.8	31.2	32	32.2	32	32.3	31
3	24.1	24.4	26.1	26.9	28	29	29.7	30.1	31.7	31.2	31	27.1	27.3
4	24.9	24.8	26	26.5	27.4	29	29.8	31	31.5	31.6	30.6	30.8	28.9
5	23.7	23.6	24.4	25.5	26.8	27.5	29.2	31.6	32	31.1	28.7	27.8	27.4
6	24.1	24.1	24.7	25.9	26.4	27.1	28.2	29.9	30.7	29.8	28.8	27.9	27.3
7	24.2	24.5	25	26.4	26.6	27.1	28.2	30.1	29.5	30.9	30.4	30.4	29
8	24.4	24.6	25.6	26.8	28	30.5	32.6	32.3	32.9	34	28.1	28.7	27.2
9	24.5	24.4	27	28.6	29.3	30.4	31.1	32.2	31.7	25.1	25.8	28.4	28
10	24.5	24.3	25.4	27	28.5	30.3	30.4	30.7	31.2	31.9	31.8	31.7	31
11	25.2	25.2	24.6	24.9	25.8	26	27.8	28.1	28	28.5	29	28.2	28
12	24.3	24.5	24.8	26.8	27.8	29.4	30.4	30.6	32.3	33	32.8	32.7	26.4
13	24.6	24.7	25.9	27.4	28.5	30	30.9	31.8	32.6	32.3	32.1	27	27.4
14	24.3	24.6	25.8	27.4	29.1	29.5	31	31.9	31.5	32.3	29.3	27.2	27.5
15	24.3	24.4	24.7	25.6	26.9	28.8	29.9	30.8	30.5	30.3	32.2	30.1	28.9
16	24.8	25.4	25.2	28	30	31.2	25.2	28.6	30	30.8	31.4	31.5	30.9
17	24.9	24.6	26.6	27.6	28	29.7	31.8	31.4	32.7	33.5	33.5	31.9	30.8
18	25.2	25.5	27.4	28.2	30.4	29.5	32	31.3	25.8	27.2	27.8	27.6	27.4
19	23.9	24.2	25	26.9	28.8	30.1	30.4	31	30.2	28.7	27	30.4	26.5
20	23.3	23.9	24.6	26.8	24.3	24.4	25.5	26.3	27.3	27.8	28.5	28.1	27
21	22.3	22.7	23.3	24.5	25.4	26.8	28.1	28.2	29.4	29.3	29.8	29	27
22	22.3	22.2	24.5	26.3	28.5	28.7	29.6	29.9	30.3	30.4	30.2	29.2	28.3
23	22.5	23.1	24.7	26.1	27.6	29.6	31.1	31.4	31.5	31.3	31.4	30.5	29.9
24	22.7	23.4	24.6	27.1	29.2	29.1	30.9	33.4	32.6	32.8	33.8	29.5	29
25	22.7	23	25.2	27.3	28.3	29.3	30.7	31.3	32	32.4	32	31.6	30.4
26	22.8	23.2	22.9	24	25.6	26.9	27.5	28.1	28.7	29.7	29.9	30.4	29.1
27	23.8	24.3	23.9	25.1	26.4	27.3	27.9	28.7	29.8	29.9	30.9	30.3	28.8
28	24.3	24.3	24.4	26.2	27.8	28.9	29.6	29.4	29.9	29.8	29.8	28.7	27.9
29	23	23.6	24.7	27.1	26.6	28.6	28.8	29.6	30.9	29.9	29.9	29.3	28.8
30	23.6	23.6	24.6	25.9	28.1	29.2	30.4	31	30.7	31.6	30.4	31	29.3

October

Date/Time	6.00	7.00	8.00	09.00	10.00	11.00	12.00	13.00	14.00	15.00	16.00	17.00	18.00
1	22.9	23.1	24.5	26.4	27.7	29.6	30.7	30.9	30.8	31.7	32.1	30	29.2
2	23	23.3	24.1	26.1	28.9	30.8	32.9	33.8	33.2	29.5	31.1	31.4	29.7
3	24.4	24.7	25.8	26.2	27.3	30.2	31	31.8	33.5	34	34.1	32	29.9
4	24.1	24.4	25.6	26.3	29.3	29.8	30.9	29.9	32.9	32.6	32.8	32	31.2
5	24.8	24.6	24.9	25.9	27.8	30.1	30	30.9	28.8	24.8	24.3	24.3	24.2
6	23.9	24	24.6	25.1	24.5	25.7	26.9	27.2	28	28.4	25.8	26.2	24.6
7	23.7	23.8	24.6	24.1	24.2	25.2	25.3	24.7	25.4	24.9	25	25	24.8
8	22.6	22.7	23.5	24.7	26.2	27.9	28.6	29.8	30.1	30.4	31.1	30.4	28.3
9	24.4	24.4	25	25.8	27.4	29.5	30	30.9	27.2	25.6	25.9	26.2	24.7
10	22.7	22.8	23.4	25.7	27.4	28.8	30.3	28.6	30.2	30	30.4	28.6	27.7
11	23.6	23.4	23.9	26.8	27.8	29.1	29.2	30.3	29.3	28	29	28.2	27.4
12	22.7	22.8	23.7	26.9	28.2	29.1	28.3	28.9	29.6	28.1	30	29.5	27
13	23.4	23.5	23.8	25.9	26.6	27.3	26.7	24.9	24.6	25.2	25.3	25.6	25.1
14	22.2	22.4	22.9	24.1	28.1	28.6	29.1	29.6	28	29.3	25.9	27.6	26.1
15	23	23.2	23.7	24.2	26	26.6	27.3	27	29.8	28.6	26	25	24.2
16	22.4	22.2	23.1	25.5	26.4	27.9	28.5	28.3	28.3	28.6	28.2	27.3	26.8
17	23.3	23.4	24.4	25.5	27.7	28.9	28.7	28.5	28.5	28.7	28.9	27.6	26.2
18	22.4	22.5	24.4	26.2	27.2	28.7	29.7	30.7	30.3	30.2	31.6	30.2	28.6
19	22.3	22.5	24.8	26.4	28.9	29.9	30.3	31.8	32.3	31.6	31.8	30.6	28.1
20	21.8	21.5	23.2	25.4	26.8	28.2	29.4	29.9	29	29.2	28.3	28	27
21	20.9	21.1	22.8	24.9	27.5	28.7	29.1	28.6	29.5	29.5	29.9	29	26.6
22	20.9	21	22.2	24.4	25.8	27.7	30.3	29.3	30.3	30.8	30.3	29.7	28
23	20.9	21	21.5	24.8	26.9	28.4	29.8	30.7	30.7	31.6	31.4	31	27.9
24	21.3	21.5	22.3	24.4	27.9	30.3	30.4	31.6	31.4	32	32.3	31.2	28.3
25	21.2	21.6	22.9	26	28.1	29.2	30	29.5	30.8	30.8	31	30	27.4
26	20.5	20.2	21.4	23.8	26.2	27.7	29.9	30.6	31.1	31	30.6	28.6	26.4
27	20.4	20.8	21.8	24.7	26.7	28.6	29.9	30.7	31.1	30.9	30.9	29.3	26.2
28	19.9	20.1	22.3	24.5	26.5	28.4	30.2	31	31.6	31.5	31.2	30.6	27.9
29	21.3	21.5	24.2	25.4	28.1	29.7	30.8	31.3	31.7	31.7	32.4	31.5	30
30	22.4	22.4	22.7	24.3	28	30.3	30.6	30.7	31.5	32	32	30.8	27.9
31	20.3	19.7	20.3	22.1	23.6	25.8	28.4	30.4	30.2	29.9	29.4	24.6	22.9

November

Date/Time	6.00	7.00	8.00	09.00	10.00	11.00	12.00	13.00	14.00	15.00	16.00	17.00	18.00
1	21.1	21.8	22	22.7	23	23.9	25.1	26	26.5	27.1	26.9	25.9	25.2
2	22.3	22.2	23	23.8	24.7	27.1	27.5	28.8	29.8	29.2	28.6	28.2	27.1
3	22.5	22.3	22.2	21.6	21.8	21.8	21.7	21.4	21.1	21.2	20.8	20.4	20.9
4	19.8	19.5	19.7	20.4	20.5	21.3	22.7	22.8	22.7	23.4	23.2	23.1	22.3
5	21.6	21.8	21.8	21.9	22.5	24.6	26.2	26.5	25.9	25.2	25	24.2	23.4
6	20.8	20.8	21.5	23.9	25.5	26.9	28	28.7	28.1	27.7	27.5	27.1	25.1
7	19.1	19.3	19.5	22.3	26	27.8	28.5	28.3	30.2	30.7	30	28.4	26.7
8	19.1	19.8	21	22.9	26.3	28.1	28.8	29.7	30	30.1	30.2	28.8	25.3
9	16.2	16.2	18.7	20	22.8	27.4	28.6	29.6	29.2	29.6	29.3	26.7	24.5
10	17.4	16.7	18.5	21.8	22.5	26.8	28.5	29.5	30.2	30	29.9	28.3	24.3
11	18.3	20.6	20	22.9	23.3	26.8	26.9	28.9	30	29.9	30.6	29.1	26.3
12	20.4	20.5	22.8	24.3	26	28.3	29.5	30.5	30	29.7	30.3	28.7	27.7
13	21.2	21.4	22.8	23.7	25.1	27.2	28.5	28.9	30.4	30.4	30.2	28.3	26.2
14	22.4	22.6	23.1	24.1	25.7	27.9	27.5	28.3	28.3	28.5	25.5	25.7	25
15	22.6	22.9	23.6	24.9	26.9	26.4	26.4	26.8	27.5	28.4	28.5	27.4	25.8
16	20.8	22.7	21.9	23.7	25.2	27.9	30.6	29.2	29.9	31	30.4	30.1	27
17	20.5	20.3	21.4	24.5	26.2	27.9	29.1	31	31.8	31.8	31.9	30.4	27
18	19.1	19.1	19.6	22.4	24.8	28.1	29.7	31.1	31.7	32	31.6	30.6	28.2
19	23.5	23.2	23.8	24.6	28.2	29.1	30.6	29.2	29.8	29.3	28.8	27.3	26.2
20	23.1	23.1	23.8	26.3	27.2	28	29.8	29.9	29.9	27.1	25.7	26	24.3
21	21.4	21.5	22	22.4	22.9	24.1	24.6	25.9	27	26.2	24.7	21.8	20.9
22	20.3	20	21	22.4	23.4	24.2	27	26.9	28.4	28.2	28.8	27.1	24.8
23	19.7	19.3	19.5	21.4	25.1	26.1	26.7	26.6	26.8	26.7	27.9	25.4	24.8
24	18.6	18.9	19.4	20.2	24.5	25.7	26.4	27.4	26.9	25.9	25.6	24.9	24.1
25	17.1	16.5	18.1	19.5	23.1	25.4	26.7	27.5	27.9	28.1	27.9	26.2	23.2
26	15.7	15.5	16.3	18.4	20.3	23	26.2	27.9	28.4	28.4	28.3	26.5	24.1
27	15.6	15.5	16.4	18.2	20.6	24.3	26.6	27.5	27.5	27.9	27.7	26	22
28	15.2	14.7	15.6	17.5	20.2	22.6	24	24.5	26.5	25.9	26.1	25.2	21.3
29	14.5	14.4	15.8	18.3	19.3	21.9	23.2	24.8	25.7	26.6	25.9	25.1	21.9
30	14.7	14.2	15.5	17.4	20.6	23.5	23.5	23.3	23.8	24.4	24.7	23.6	20.2

December

Date/Time	6.00	7.00	8.00	09.00	10.00	11.00	12.00	13.00	14.00	15.00	16.00	17.00	18.00
1	13.1	12.9	13.8	16	18	21.7	22.6	24	24.5	24.7	25	24.3	20.2
2	12.6	12.6	14	15.6	18.3	21.4	22.5	24.2	26.2	27.1	26	25.4	21.7
3	14.3	14.5	15.4	17.3	20.4	22.4	24.3	26.6	26.8	27.6	27.1	26.4	24.5
4	15.7	15.6	16.4	18	21.2	23.5	25.6	26.1	26.6	27.1	26	25.4	23.1
5	17	17.3	17.7	19.3	21.3	24.8	27	27.7	27.4	28.6	28.2	26	23.3
6	16	15.6	16.8	18.7	21.5	25.1	26.9	28.1	28.6	29.3	28.8	27.4	23.9
7	16.1	16.5	17.8	19.7	22	24.7	26.7	27.7	28.8	28.7	28.6	28.4	24.4
8	17.3	17.1	18.5	20.4	22	24.4	26.5	27.9	28.5	29.4	28.9	28.1	24.3
9	17.1	17.7	19	21.4	22.2	24.5	26.5	27.8	28.8	29	29.2	28.3	24.5
10	17.8	17.4	18.2	20.1	22.7	25.1	27	28.1	28.3	28.8	29.2	28.7	24
11	16.9	16.4	18.4	21.1	23.8	26.2	29.8	29.4	30.1	30.3	30	29.3	24.8
12	16.3	16.4	19.1	20.2	20.8	22.5	26.2	28.6	28.5	28.9	28.3	26.2	22.3
13	14.9	15.2	16.5	19.7	22.7	24.8	26	26.8	28.7	29.2	29.6	29.1	23.8
14	14.4	14	16.4	19.8	21.3	24.6	26.8	27.8	29.1	30.3	30.6	28.6	23.3
15	14.7	14.4	16.5	18.7	22.2	24.6	26.7	27.7	28.9	29.5	29.6	28.8	24.5
16	17.2	17.3	18.9	19.9	21.9	25.6	27.4	27.6	28.8	29.4	29.6	29.1	26.1
17	19.6	19.3	20.7	24	25.7	27.4	28.6	30.1	30.3	30.6	31.1	30.6	26.9
18	19.9	19.4	21.2	24.2	24.7	26.8	29	30.2	30.8	31.1	31.6	31.2	27.5
19	20.1	20.1	20.7	22.2	24.6	27.3	29.2	30	31	31.5	31.8	31.1	27.7
20	20.5	20.1	21.4	24.1	25.4	27.7	29.2	30.1	31.3	31.7	31.9	31.4	28.6
21	20.1	19.7	21.6	23.8	25.4	27.1	29.7	30.4	31.5	31.8	32.5	32.5	28.3
22	18.2	17.6	20.3	22.9	24.6	26.1	28.5	29	30.8	31.7	32.2	31.6	26.4
23	16.4	15.5	17.2	19.8	24	25.4	27.4	28.3	28.9	28.6	29.4	28.3	23.9
24	14.2	13.9	16	17.8	20	22.5	24.6	26.2	27.7	28.7	28.8	28.7	23.3
25	14.3	13.8	15.7	17.3	19.8	22.8	24.5	25.8	27.5	28.6	28.9	28.6	24.5
26	15.4	15.3	15.8	18.5	21	24.6	27.2	27.9	28.9	28.8	29.1	28.5	24.9
27	17	16.8	17.3	19.9	22.1	26.3	27.9	28.2	28.5	29.2	29.3	28.8	25.5
28	16	15.8	16	18.1	20.3	23.4	26.6	26.8	28	28.4	28.5	27.4	24.3
29	16	15.9	16.8	18.9	21.8	24.3	26.4	28.4	28.6	29	29.2	28.9	25.7
30	16.3	16.2	16.7	19.4	22.8	25.2	26.6	28.2	28.7	28.8	29.3	28.7	25.7
31	17.2	17	18.1	20.1	22.3	25.3	26.2	27.4	28	28.9	29.6	28.8	25.6

Appendix B

Specification Sheets of Sharp 80 Wp NE-80E2E Photovoltaic Module

80 WATT

DESIGNED FOR
LARGE ELECTRICAL
POWER REQUIREMENTS

FEATURES

- High-power module (80W) using 125.5mm square polycrystalline silicon solar cells with 12.60% module conversion efficiency
- Photovoltaic module with bypass diode minimises the power drop caused by shade
- Anti reflection coating and BSF (Back Surface Field) structure to improve cell conversion efficiency: 14.0%
- White tempered glass, EVA resin and a weatherproof film, plus aluminum frame for extended outdoor use
- Nominal 12 volt output for battery charging applications
- Output terminal: Lead wire with waterproof connector
- Certifications: IEC 61215
- SHARP modules are manufactured in ISO 9001 certified factories

POLYCRYSTALLINE SILICON PHOTOVOLTAIC MODULE WITH 80W MAXIMUM POWER

A safe, clean, reliable source of energy, Sharp's **NE-80E2E** photovoltaic module is designed for a variety of electrical power requirements. Based on the technology of crystal silicon solar cells developed over 45 years, this module has superb durability to withstand rigorous operating conditions and is suitable for use in most solar systems.

Common applications for the Sharp NE-80E2E include office buildings, private residences, RVs, cabins, vacation homes, solar power stations, pumps, beacons and lighting equipment. As the world's leading manufacturer of photovoltaic modules, Sharp produces an extensive line of high power modules for every electrical power requirement.

SHARP

NE-80E2E – MULTI-PURPOSE MODULE

ELECTRICAL CHARACTERISTICS

Cell	polycrystalline silicon, 125.5mm
No. of Cells and Connections	36 in series
Open Circuit Voltage (Voc)	21.3 V
Maximum Power Voltage (Vpm)	17.1 V
Short Circuit Current (Isc)	5.31 A
Maximum Power Current (Ipm)	4.67 A
Maximum Power (Minimum Power) (Pm) [1]	80 W (76W)
Encapsulated Solar Cell Efficiency (ηc)	14.0 %
Module Efficiency (ηm)	12.60 %
Maximum System Voltage	DC 540V
Series Fuse Rating	10A
Type of Output Terminal	Lead wire with connector

Specifications are subject to change without notice
[1] (STC Standard Test Conditions: 25°C, 1 kW/m², AM 1.5

MECHANICAL CHARACTERISTICS

Dimensions	1200 x 530 x 35 mm
Weight	8.5 kg
Packing Condition	1 pcs per Carton
Size of Carton	1350 x 700 x 110 mm

ABSOLUTE MAXIMUM RATINGS

Parameters	Rating	Unit
Operating Temperature	-40 to +90	°C
Storage Temperature	-40 to +90	°C
Dielectric Voltage Withstood	2200 V DC max.	V-DC

IV CURVES

Open Circuit Voltage, Short Circuit Current vs. Irradiance Characteristics (Module temperature: 25°C)

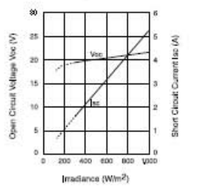

Normalised Isc, Voc, Pm vs, Module Temperature Characteristics

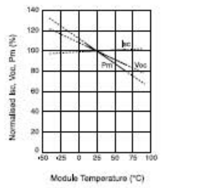

Current, Power vs. Voltage Characteristics (Module temperature: 25°C)

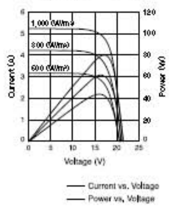

Specifications are subject to change without notice

DIMENSIONS

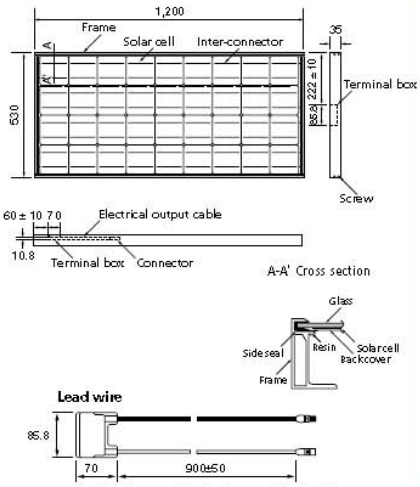

Specifications are subject to change without notice

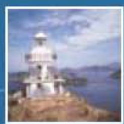

In the absence of confirmation by device specifications sheets, Sharp takes no responsibility for any defects that may occur in equipment using any Sharp devices shown in catalogues, data books, etc. Contact Sharp in order to obtain the latest device specification sheets before using any Sharp device.

SHARP ······· be sharp

Sharp Corporation of Australia
1 Huntingwood Drive, Huntingwood, NSW 2148.
Phone: (02) 9830 4600 E-mail: sales@sharp.net.au
www.sharp.net.au

SHARP Solar

Appendix C

Radial Distribution Test System Parameters

C1. Data for 51-Bus Base Case Radial Distribution Test System

Branch	***Line impedance (ohm)***		***Load demand at bus-j***	
i - j	***R***	***X***	P_L ***(kW)***	Q_L ***(kVar)***
1-2	0.4214	0.7334	0	0
2-3	0.4214	0.7334	14.58	8.07
3-4	0.2107	0.3667	0	0
4-5	0.4214	0.7334	0	0
5-6	0.2107	0.3667	0	0
6-7	0.2107	0.3667	14.58	8.07
7-8	0.4214	0.7334	0	0
8-9	0.4214	0.7334	0	0
9-10	0.3996	0.67215	58.33	32.27
10-11	0.5328	0.8962	0	0
11-12	0.2664	0.4481	0	0
12-13	0.7992	1.3443	20	15
13-14	0.5328	0.8962	0	0
14-15	1.66675	1.102	0	0
15-16	2.0001	1.3224	0	0
16-17	0.6667	0.4408	29.17	16.14
17-18	1.3334	0.8816	72.92	40.34
18-19	0.6667	0.4408	20	15
3-20	5.3336	3.5264	145.67	80.69
4-21	1.3334	0.8816	62.88	33.33
5-22	3.3335	2.204	14.58	8.07
22-23	2.6668	1.7632	94.79	52.45
23-24	0.6667	0.4408	14.58	8.07
24-25	6.667	4.408	0	0
25-26	1.3334	0.8816	14.58	8.07
26-27	2.0001	1.3224	35	19.36
23-28	5.3336	3.5264	29.17	16.14
24-29	1.3334	0.8816	29.17	16.14
7-30	5.00025	3.306	91.88	50.83
30-31	0.6667	0.4408	85.9	36.83
31-32	1.3334	0.8816	29.17	16.14
32-33	1.3334	0.8816	14.58	8.07
33-34	1.00005	0.6612	43.75	24.21
34-35	1.3334	0.8816	43.75	24.21
35-36	2.33345	1.5428	0	0
36-37	1.3334	0.8816	145.83	80.69
37-38	1.00005	0.6612	91.88	50.83
30-39	2.0001	1.3224	29.17	16.14
35-40	1.3334	0.8816	58.33	32.27
8-41	1.00005	0.6612	14.58	8.07
9-42	1.3334	0.8816	29.17	16.14
10-43	4.0002	2.6448	29.17	16.14
11-44	1.3334	0.8816	29.17	16.14
12-45	4.6669	3.0856	148.75	82.3
14-46	0.6667	0.4408	29.17	16.14
46-47	2.0001	1.3224	0	0
47-48	2.0001	1.3224	29.17	16.14
46-49	0.13334	0.08816	58.33	32.27
15-50	4.6669	3.0856	43.75	24.21
17-51	2.6668	1.7632	116.67	64.55

Note. 900 kVar shunt capacitor bank installed at bus-13

C2. Data for 33-Bus Base Case Radial Distribution Test System

Branch	***Line impedance (ohm)***		***Load demand at bus-j***	
i - j	***R***	***X***	P_L ***(MW)***	Q_L ***(MVar)***
1 -2	0.0922	0.047	0.25	0.15
2 - 3	0.493	0.2511	0.225	0.1
3 - 4	0.366	0.1864	0.3	0.2
4 - 5	0.3811	0.1941	0.15	0.075
5 - 6	0.819	0.707	0.15	0.05
6 - 7	0.1872	0.6188	0.5	0.25
7 - 8	0.7114	0.2351	0.5	0.25
8 - 9	1.03	0.74	0.15	0.05
9 - 10	1.044	0.74	0.15	0.05
10 - 11	0.1966	0.065	0.1125	0.075
11 - 12	0.3744	0.1238	0.15	0.0875
12 - 13	1.468	1.155	0.15	0.0875
13 - 14	0.5416	0.7129	0.3	0.2
14 - 15	0.591	0.526	0.15	0.025
15 - 16	0.7463	0.545	0.15	0.05
16 - 17	1.289	1.721	0.15	0.05
17 - 18	0.732	0.574	0.225	0.1
2 - 19	0.164	0.1565	0.225	0.1
19 - 20	1.5042	1.3554	0.225	0.1
20 - 21	0.4095	0.4784	0.225	0.1
21 - 22	0.7089	0.9373	0.225	0.1
3 - 23	0.4512	0.3083	0.225	0.125
23 - 24	0.898	0.7091	1.05	0.5
24 - 25	0.896	0.7011	1.05	0.5
6 - 26	0.203	0.1034	0.15	0.0625
26 - 27	0.2842	0.1447	0.15	0.0625
27 - 28	1.059	0.9337	0.15	0.05
28 - 29	0.8042	0.7006	0.3	0.175
29 - 30	0.5075	0.2585	0.5	1.5
30 - 31	0.9744	0.963	0.375	0.175
31 - 32	0.3105	0.3619	0.525	0.25
32 - 33	0.341	0.5302	0.15	0.1

Appendix D

Deterministic Load Flow Solutions of Test Systems

D1. Load Flow Results for 51-Bus Base Case System

Bus no.	*|V| (pu)*	*δ (deg)*
1	1.00000	0.00000
2	0.99800	-0.15996
3	0.99603	-0.31970
4	0.99510	-0.39788
5	0.99328	-0.55380
6	0.99263	-0.62263
7	0.99201	-0.69112
8	0.99171	-0.79377
9	0.99146	-0.89472
10	0.99135	-0.98312
11	0.99128	-1.09890
12	0.99140	-1.15139
13	0.99194	-1.30381
14	0.99062	-1.34773
15	0.98834	-1.35728
16	0.98627	-1.36573
17	0.98563	-1.36830
18	0.98499	-1.37055
19	0.98471	-1.37182
20	0.99509	-0.32495
21	0.99505	-0.39813
22	0.99033	-0.56718
23	0.98870	-0.57464
24	0.98838	-0.57613
25	0.98687	-0.58300
26	0.98663	-0.58413
27	0.98646	-0.58489
28	0.98826	-0.57668
29	0.98803	-0.57773
30	0.98405	-0.73403
31	0.98326	-0.73766
32	0.98178	-0.74443
33	0.98036	-0.75095
34	0.97942	-0.75528
35	0.97834	-0.76028
36	0.97654	-0.76861
37	0.97607	-0.77077
38	0.97599	-0.77116
39	0.98372	-0.73557
40	0.97828	-0.76054
41	0.99162	-0.79415
42	0.99135	-0.89522
43	0.99102	-0.98464
44	0.99071	-1.10148
45	0.99101	-1.15316
46	0.99037	-1.34887
47	0.98987	-1.35115
48	0.98954	-1.35267
49	0.99035	-1.34895
50	0.98678	-1.36441
51	0.98493	-1.37153

Note. P_{loss} = 29.83 kW and Q_{loss} = 39.93 kVar

D2. Load Flow Results for 33-Bus Base Case System

Bus no.	***|V| (pu)***	***δ (deg)***
1	1.00000	0.00000
2	0.99778	0.01074
3	0.98728	0.07103
4	0.98172	0.11937
5	0.97623	0.16824
6	0.96258	0.09844
7	0.95999	-0.07043
8	0.95640	-0.04425
9	0.95176	-0.09780
10	0.94745	-0.14346
11	0.94681	-0.13822
12	0.94570	-0.12994
13	0.94118	-0.19632
14	0.93950	-0.25330
15	0.93846	-0.28057
16	0.93745	-0.29739
17	0.93595	-0.35319
18	0.93550	-0.36011
19	0.99738	0.00255
20	0.99468	-0.04805
21	0.99415	-0.06266
22	0.99367	-0.07801
23	0.98458	0.04779
24	0.97957	-0.01860
25	0.97707	-0.05120
26	0.96115	0.12738
27	0.95925	0.16852
28	0.95078	0.22943
29	0.94469	0.28628
30	0.94205	0.36268
31	0.93898	0.30154
32	0.93830	0.28487
33	0.93809	0.27928

Note. P_{loss} = 369.76 kW and Q_{loss} = 246.41 kVar

BIOGRAPHY

Vichakorn Hengsritawat received the B.E. degree in electrical engineering from University of the Thai Chamber of Commerce, Bangkok, Thailand, in 1995. And he received the M.E. degree in electrical engineering from Chulalongkorn University, Bangkok, Thailand, in 1998. He has joined with the Sripatum University in 1998 as the instructor in the department of electrical engineering to present. His research interests include distributed generation, power quality, renewable energy, energy saving and power system simulation.